"THE PREPARATION AND CHARACTERISATION OF

POLY (BUTYL 2-CYANOACRYLATE) NANOPARTICLES"

by

Stephen John Douglas

B.Pharm.(Hons.), MPS.

A thesis submitted to the

University of Nottingham

for the degree of

Doctor of Philosophy

October, 1985

CONTENTS

CHAPTER FIVE – COVALENT ATTACHMENT OF AMINES TO NANOPARTICLES

CHAPTER SIX – RADIOLABELLING OF NANOPARTICLES

ABSTRACT

Poly (butyl 2-cyanoacrylate) nanoparticles have been prepared with a range of particle sizes by varying the nature and concentration of stabiliser added to the polymerisation medium. Particle size analysis was performed by photon correlation spectroscopy. The range of diameters produced using dextran stabilisers was found to be approximately 100 to 800nm. This could be extended to 3μm using β-cyclodextrin and to 20nm using polysorbate 20. The results infer that the nanoparticles are sterically stabilised.

The molecular weight of the cyanoacrylate polymer formed during nanoparticle production was found to be dependent on the type of stabiliser used together with the polymerisation pH and monomer concentration. The bulk of the polymer had a relatively low molecular weight (<2000) which indicates that nanoparticles are formed by an aggregative mechanism.

Dextran was found to copolymerise with the monomer to give an interfacial layer of the polysaccharide attached by covalent linkages. By using dextrans bearing charged functional groups it was possible to alter the electrophoretic behaviour of the resulting nanoparticles.

Partial oxidation of the surface dextran introduced aldehyde groups which were capable of covalently binding a simple amine, aniline, thereby enhancing the uptake and decreasing the release rate of this compound. This technique may be applicable to the

covalent coupling of antibodies or cytotoxic agents to the nanoparticle surface.

Nanoparticles were radiolabelled with a technetium-99m-dextran complex and the biodistribution of this colloid determined in rabbits by gamma scintigraphy following intravenous injection. Most of the nanoparticle suspension (approximately 50%) was cleared by the liver and spleen. Coating the nanoparticles with non-ionic surfactants (poloxamer 338 or Tetronic 908) failed to alter significantly this distribution pattern.

ACKNOWLEDGEMENTS

Within the Department of Pharmacy, University of Nottingham, I would like to thank my supervisor Professor S.S. Davis, other members of staff and friends and colleagues for their contributions throughout the past three years. My thanks also go to Dr. L. Illum of the Royal Danish School of Pharmacy, Copenhagen, for her help during and after her sabbatical term here in Nottingham.

Concerning my 6 weeks spent at the Institute of Pharmacy, ETH, Zurich, I would like to thank Professor P. Speiser, Dr. M. Muller and especially Dr. J. Kreuter for their advice and typical hospitality.

I am also grateful to Dr. S. Holding and his staff at the Rubber and Plastics Research Association, Shawbury, for analysing the many polymer samples and subsequent helpful discussions.

With regard to the in vivo studies, I would like to thank the staff of the Animal Unit and Medical Physics Department of the Queens Medical Centre, Nottingham, and in particular Dr. M. Frier for his willing help with the radiolabelling work.

My thanks also go to Professor R.W. Baldwin and the staff of the Cancer Research Campaign Laboratories, Nottingham, for help and advice, not least from Dr. P.D.E. Jones, now of the Pharmacy Department.

Concerning the use of PCS I wish to fully acknowledge the expert tuition of Dr. A.J. Pearce regarding the principles and use of this imposing instrument, together with the advice from Dr. M.J. Hey, both of the Chemistry Department, University of Nottingham.

Finally, my thanks go to the many people with whom I have worked and studied during the past 10 years for their inspiration, encouragement and occasional wisdom. In this respect I am particularly indebted to Dr. G. Burton of Beecham Pharmaceuticals, Brockham Park. My special thanks and appreciation go to Angela for her unselfish support throughout the course of this work and for proof reading this thesis, which I dedicate to my parents.

ABBREVIATIONS

ACA	Alkyl 2-cyanoacrylate
APP	4-aminopyrazolo (3,4-d) pyrimidine
BCA	Butyl 2-cyanoacrylate
BSA	Bovine serum albumin
DEAE	Diethylaminoethyl
dn	Number average diameter
dz	z-average diameter
EPM	Electrophoretic mobility
eV	Electron volt
Fd	Doppler frequency
FoB	Formycin B
GA	Gum arabic
GPC	Gel permeation chromatography
HLB	Hydrophile-lipophile balance
Ig	Immunoglobulin
IR	Infrared
iv	Intravenous
LDA	Laser doppler anemometry
MBq	Mega-Bequerel
MCA	Monoclonal antibody
Mn	Number average molecular weight
Mp	Peak molecular weight
Mw	Weight average molecular weight
NMR	Nuclear magnetic resonance
NZW	New Zealand White

p(ACA)	Poly (alkyl 2-cyanoacrylate)
p(BCA)	Poly (butyl 2-cyanoacrylate)
p(ECA)	Poly (ethyl 2-cyanoacrylate)
p(HCA)	Poly (hexyl 2-cyanoacrylate)
p(iBCA)	Poly (isobutyl 2-cyanoacrylate)
p(MeCA)	Poly (methyl 2-cyanoacrylate)
PBS	Phosphate buffered saline
PCS	Photon correlation spectroscopy
PEG	Polyethylene glycol
PLG	Polylysyl gelatin
PM	Photomultiplier
POE	Polyethyleneoxide
POP	Polypropyleneoxide
PSD	Particle size distribution
Q	Polydispersity index
RE	Reticulo-endothelial
RES	Reticulo-endothelial system
ROI	Region of interest
SEM	Scanning electron microscopy
TEM	Transmission electron microscopy
THF	Tetrahydrofuran
UV	Ultraviolet
ZP	Zeta potential

CHAPTER ONE

GENERAL INTRODUCTION

1.1. CONCEPT OF DRUG TARGETING

The ability to target pharmaceutically active molecules to specific sites in the body has been actively pursued ever since Ehrlich (1906) first envisaged the use of "magic bullets" for the eradication of disease. Interest in this concept has increased significantly in recent years with the advent of new technology and a greater understanding of the processes involved in drug delivery both at a cellular and sub-cellular level. Despite these advances and the vast literature which has been generated (e.g. Gregoriadis et al, 1982 and 1985; Goldberg, 1983; Juliano, 1980) site specific drug targeting remains an elusive goal.

The aim of this introduction will be to present a balanced view of the potential of drug targeting through an understanding of the problems involved, and the possibilities for resolving them. Particular emphasis will be placed on the use of carrier systems. Other approaches such as prodrug design have been reviewed elsewhere (Stella et al, 1980).

1.2. PROBLEMS WITH CONVENTIONAL DRUG DELIVERY

Following the administration of a drug, either by the oral route or by injection, the drug substance will distribute throughout the body as a function of the intrinsic properties of its molecular

structure. The final amount of drug reaching its target site may only be a small fraction of the administered dose, as represented diagramatically in figure 1.1. Accumulation at non-target sites may lead to adverse reactions and unwanted side effects.

One way of circumventing this problem is to apply the drug in a region local to its intended site of action. The range of conventional formulations for local administration, such as sprays, inhalers, creams, eye drops, etc., have been augmented in recent years by several more sophisticated systems. These have included the Ocusert system for pilocarpine delivery to the eye (Armaly and Rao, 1973) and the Progestasert intrauterine device for contraceptive use (Tatum, 1977). Further examples are still under investigation such as colloidal carriers for intra-articular injection in arthritis (Ratcliffe et al, 1984). However, this approach of 'targeting' via a locally applied controlled release device is of limited use in treating disseminated disease states or when the target tissue is inaccessible. In such cases systemic drug administration is necessary.

One such example of the need for systemic drug targeting is in cancer chemotherapy where the severe adverse reactions due to cytotoxic agents are a major limiting factor. The lack of anti-tumour specificity displayed by cytotoxic agents results from the low level of biochemical differentiation between host and tumour cells which, together with the heterogeneous nature of tumour cell populations, limits the effectiveness of current therapeutic approaches (Poste, 1985). Although progress has been made in reducing the severity of cytotoxic induced side effects by multiple

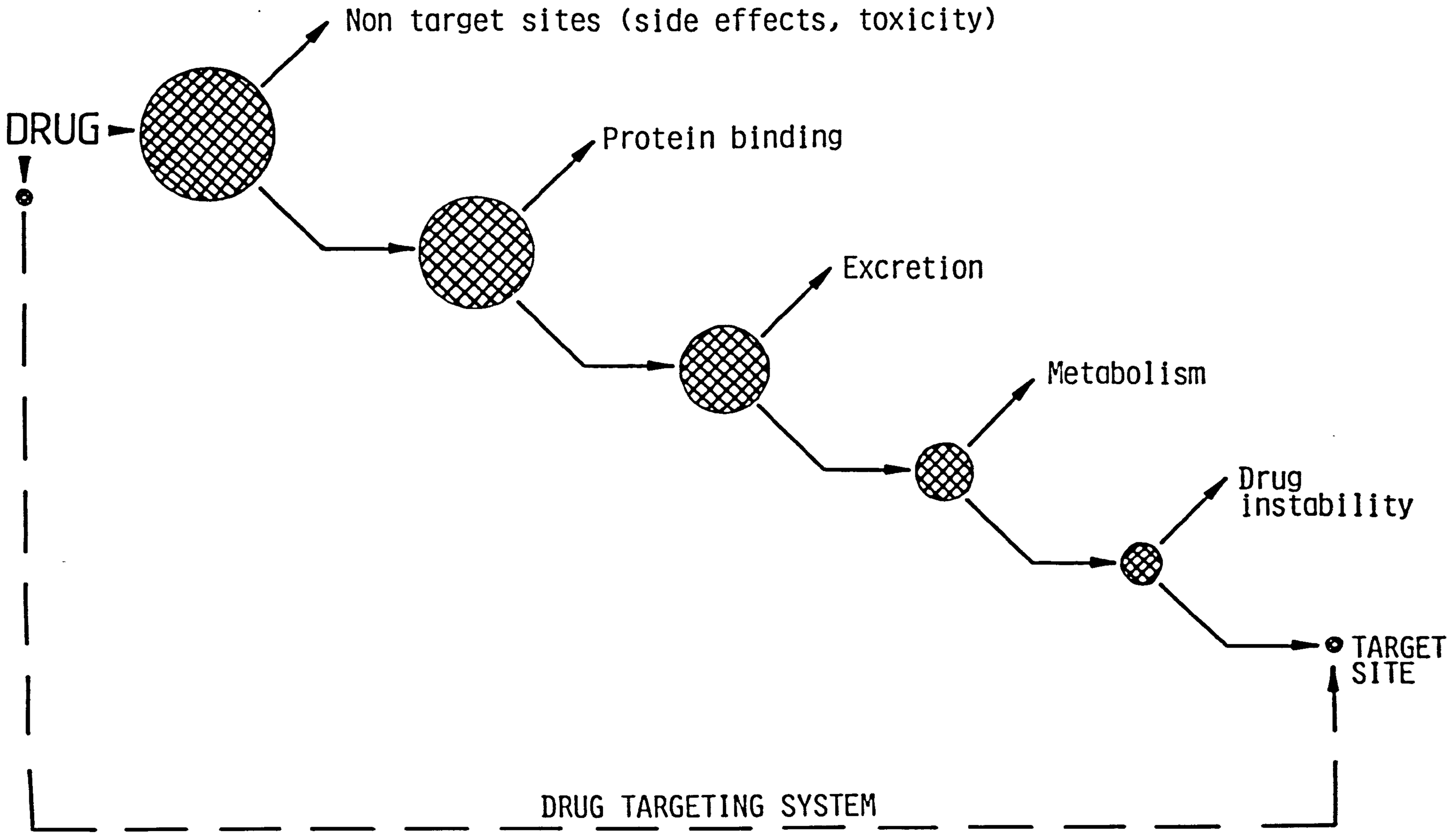

Figure 1.1. Problems in drug delivery

administration schedules and kinetic dosage regimens (Price et al, 1981), there is a limit to their effectiveness. Selective drug targeting to tumour sites not only would lead to a reduction in adverse reactions but also open the possibilities of using highly potent toxins (Jansen et al, 1982).

The systems available for achieving site specific delivery range from direct chemical modification of the drug molecule, prodrug design, to the use of carriers such as colloids and macromolecules (Juliano, 1980). These carrier systems will be discussed in later sections (1.6 and 1.7) after first examining the general aspects of targeting in relation to physiological factors.

1.3. FACTORS AFFECTING DRUG CARRIER BIODISTRIBUTION

The physico-chemical properties of an injected carrier system will effect its in vivo distribution and ultimately influence its ability to reach the target site. The role of these properties is particularly well illustrated in the case of particulate systems (Davis, 1981; Illum and Davis, 1982a). Particle size, shape and number, together with surface charge and surface characteristics all influence the biofate of colloids upon injection. These properties are particularly important in relation to particle sequestration by the reticulo-endothelial system (RES) (Frier, 1981). The RES is a collective name for a group of highly phagocytic mononuclear cells derived from the bone marrow (Bradfield, 1984). These cells are found throughout the body, either at fixed sites or free in the circulation. The RES is alternatively known as the mononuclear phagocyte system (MPS). Large concentrations of reticulo-endothelial

(RE) cells are found in the liver (fixed macrophages called Kupffer cells), spleen and bone marrow. RES mediated clearance is a major factor in determining the biodistribution of colloidal systems.

1.3.1. Effect of Particle Size and Shape

The fate of an intravenously (i.v.) injected colloid can be related to various physiological processes as a function of particle size (Poste, 1985; Tomlinson, 1983). This is shown diagrammatically in figure 1.2. Particles with a mean diameter greater than approximately 7μm become entrapped in the capillary bed of the lungs due to mechanical filtration (Illum and Davis, 1982a and b; Kanke et al, 1980). However, the situation is complicated by the influence of particle shape which can result in lung entrapment of small fibres (Illum et al, 1982) and the gradual clearance and relocation elsewhere of spherical particles 7-12μm in diameter (Slack et al, 1981). In addition, for particles less than 7μm which are aggregated, positively charged or very hydrophilic, lung deposition can still be significant (Wilkins and Myers, 1966).

Normally, smaller particles (<7μm), following i.v. injection, are deposited in the liver, spleen and bone marrow by RES mediated uptake (Illum and Davis, 1982a; Singer et al, 1969). The partitioning between these three sites depends on their relative blood flow, capacity and kinetics of uptake. This results in a normally predominant hepatic clearance by Kupffer cells.

Although most particles in the size range 0.0025-10μm accumulate in the RES, particle size does have an effect on clearance rate (Juliano and Stamp, 1975; Senior et al, 1985) and

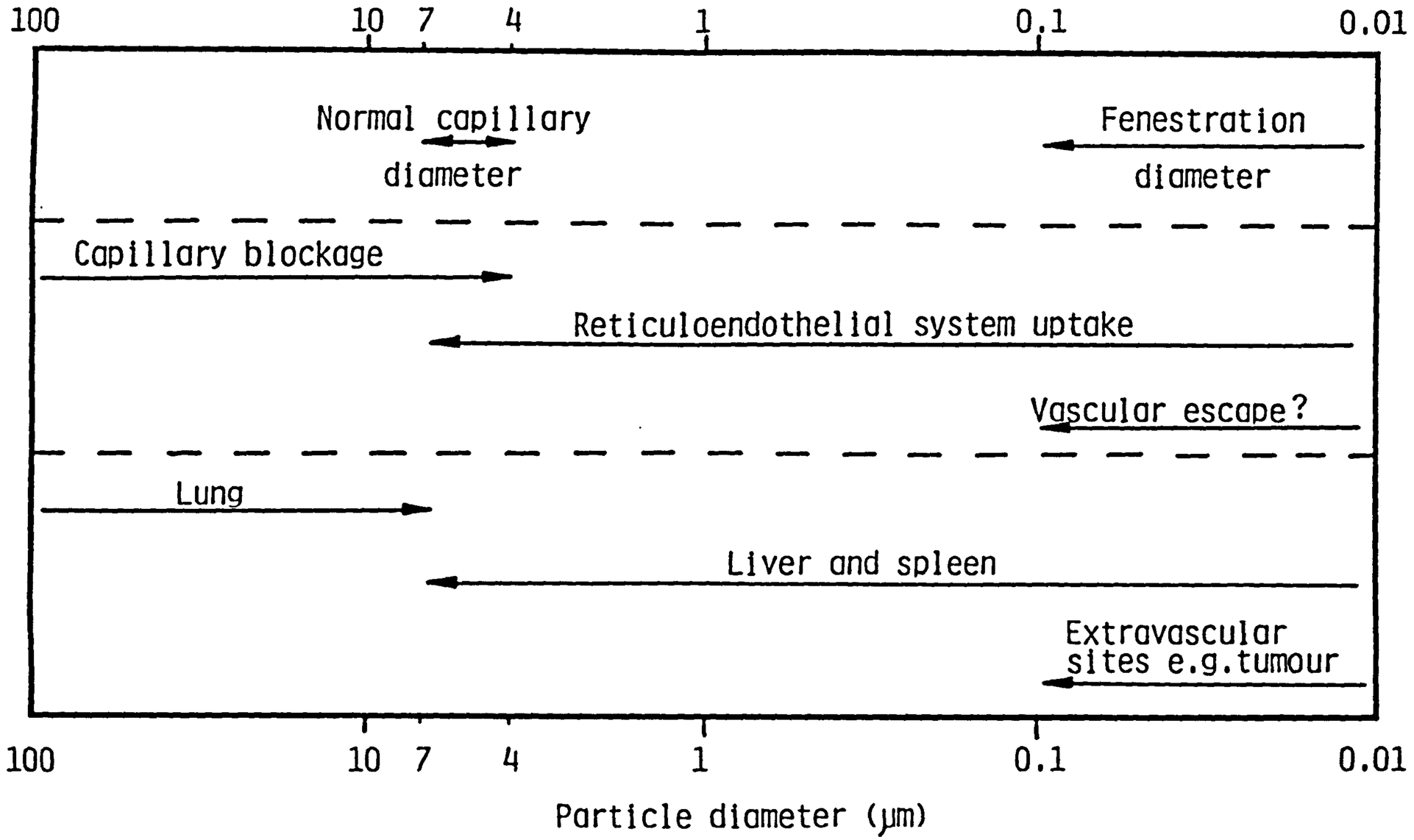

Figure 1.2. Relationship between particle size, physiological processes and biodistribution of intravenously injected colloids.

distribution within the RES (Frier, 1981). Large particles, in general, are rapidly removed by the liver and spleen whereas small particles are cleared more slowly and show a greater tendency to concentrate in bone marrow. This has been shown, for example, by Frier (1981) with antimony sulphide colloid of sizes 200-400nm (rapid hepatic clearance) and <10nm (slower bone marrow accumulation).

Reducing particle size below approximately 100nm introduces the possibility of vascular escape via fenestrations, or openings, in the lining of blood vessels. There are three major classifications of blood capillaries; continuous capillaries; fenestrated capillaries; and discontinuous or sinusoidal capillaries (Weiss and Greep, 1977). Extravasation of particles via continuous capillaries is highly unlikely since these have endothelial cells joined by tight junctions and an uninterrupted subendothelial basement membrane. Escape via fenestrated capillaries is theoretically possible via the fenestrae in the endothelial cells. These fenestrae, however, are spanned by a thin membranous diaphragm which, together with the continuous subendothelial membrane of these capillaries, makes particle penetration seem unlikely. In contrast, sinusoidal capillaries of the liver have no basement membrane and those of the spleen and bone marrow only have an interrupted membrane. The fenestrae of these capillaries are particularly large (approximately 100nm). Extravasation of colloids via this route is feasible and probably accounts for the observed accumulation of small liposomes in liver parenchymal cells (Poste, 1983).

The possibilities of targeting sites outside the vascular system appear to be severely limited except for areas possessing sinusoidal capillaries. The microvascular structure of certain tumours, however, is known to be defective (Peterson, 1979) and it has been proposed (Grislain et al, 1983) that it may be possible to target 'leaky' tumours in this way. In contrast, Poste (1983) has raised doubts about such an approach since the proportion of tumour capillaries allowing extravasation may well be low and not all tumours possess a defective microvasculature.

1.3.2. Effects of Surface Characteristics (Hydrophobicity/ Hydrophilicity)

Immediately upon injection into the blood stream colloidal particles become coated with various blood components (opsonisation). The nature of this adsorbed layer can have marked effects on the distribution of colloids, particularly in connection with RES mediated clearance. Antibodies act directly as opsonins for macrophages by specifically coating a wide range of particles (Boxer and Stossel, 1974) and also activating the complement pathway (Gigli and Nelson, 1968). RES macrophages possess membrane receptors for the Fc region of immunoglobulins and for the C3 component of the complement sequence (Bradfield, 1984). Macrophages can recognise also particulate material through the nature of the particle surface (Frier, 1981).

The uptake of blood components onto bacteria has been studied by Van Oss (1978), who suggested that surface hydrophobicity is a critical determinant in the opsonisation process. Particles with

hydrophilic surfaces are rendered more hydrophobic by adsorption of immunoglobulin G (IgG). In contrast, hydrophobic particles are taken up by macrophages without the necessity of opsonisation.

Alteration of particle surface characteristics which affect opsonisation and/or particle hydrophobicity/hydrophilicity would be expected to bring about changes in RES uptake. This has been shown in rabbits by Illum and Davis (1984a and b) with ^{131}I labelled polystyrene particles coated with various polymers. Following i.v. injection the liver and spleen uptake of the latex was reduced from 90% to 46% by adsorption of poloxamer 338 (figure 1.3). Liver and spleen accumulation were reduced as well using poloxamer 188, but this surfactant was less effective. The kinetics of uptake, however, were relatively unaffected except for IgM coated particles (table 1.1). Of the various coating materials used only poloxamer 338 produced any prolonged (8 days) alteration in distribution (table 1.1). Similar studies in rats by Leu et al (1984) with poloxamer 188 coated poly methyl methacrylate particles resulted in a reduction of liver uptake from 85% to 38%, 30 minutes after injection. This was accompanied, however, by an increase in spleen uptake (4% uncoated, 21% coated) so that total RES clearance was still high. In addition, liver uptake gradually increased over a period of 24 hours for the coated particles indicating possible displacement of the surfactant and particle opsonisation. Reductions in macrophage uptake have been reported also for emulsion systems prepared with poloxamer 338 (Davis and Hansrani, 1985), and poloxamers 338, 188, and polysorbate 20 (Stossel et al, 1972).

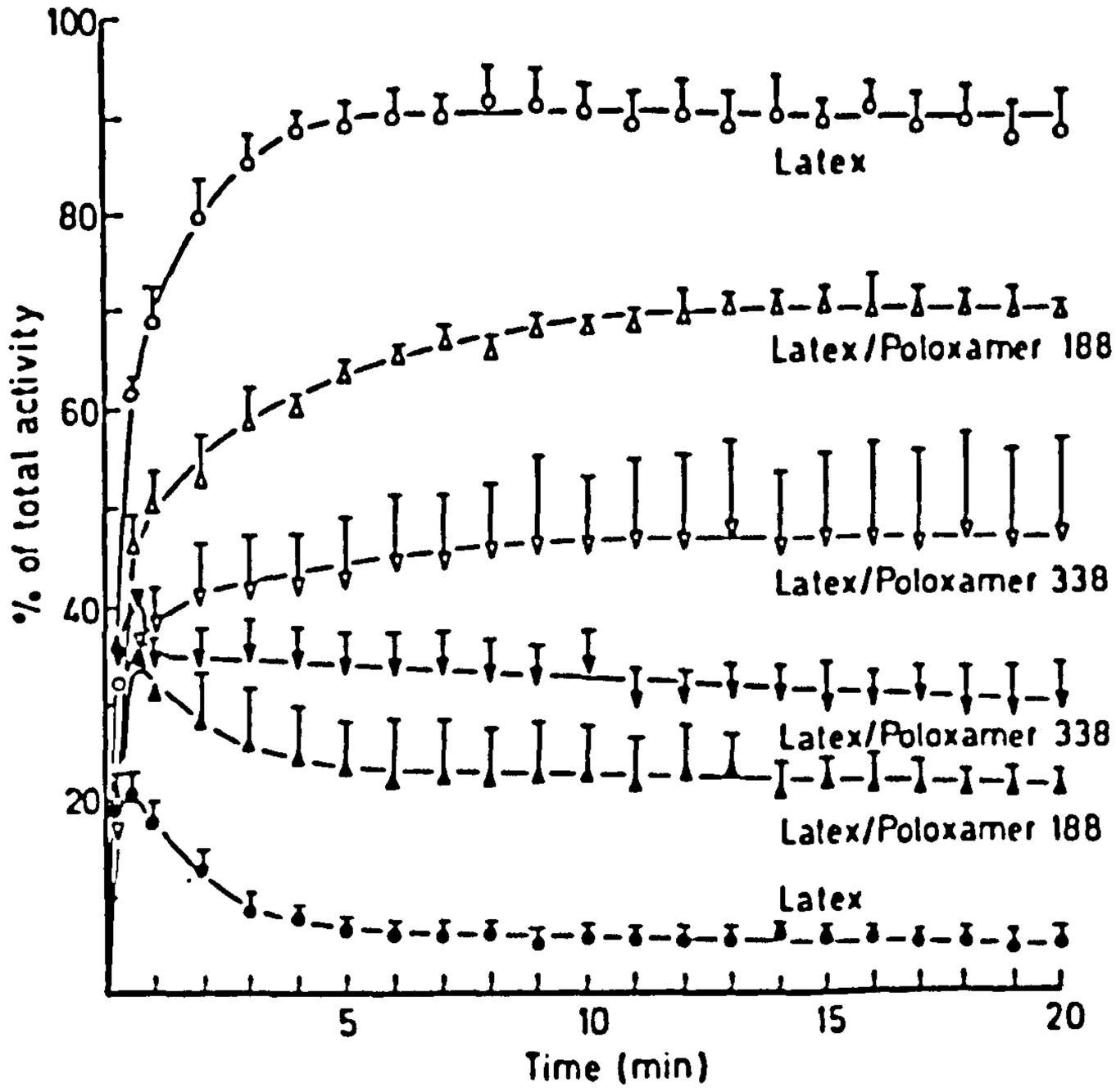

Figure 1.3. Effects of coating with poloxamers on the distribution of polystyrene latex in rabbits. Activity-time profiles for different body regions after administration of uncoated, poloxamer 188 coated and poloxamer 338 coated latex particles. Uncoated: liver/spleen (o); lung/heart (•). Poloxamer 188 coated: liver/spleen (Δ); lung/heart (▲). Poloxamer 338 coated:liver/spleen (▽); lung/heart (▼). (n=3, mean ± standard error).
Illum and Davis, 1984b.

TABLE 1.1. The kinetics of uptake and organ distribution of uncoated and coated polystyrene latex particles (Illum and Davis, 1984b).

System	Rate of uptake in the liver ($T_{50\%}$)	Extent of uptake in the liver after 20 mins	Tissue distribution after 8 days	
			Liver	Lung
Uncoated latex	50.3 sec	90%	59.5%	0.2%
Latex coated with lecithin	50.3 sec	76%	55.7%	2.3%
Latex coated with IgA	66.1 sec*	88%	61.7%	0.2%
Latex coated with poloxamer 388	55.0 sec	46%	30.0%	0.5%
Latex coated with poloxamer 188	65.6 sec	70%	60.8%	1.6%

* significant difference from latex.

The mechanisms involved in reducing RES sequestration are obviously complex. Surface coatings alter not only particle hydrophobicity but also affect surface charge (Ottewill, 1967). In addition, the increase in particle steric stabilisation imparted by the surface polymer probably decreases particle-cell (macrophage) adhesion together with the uptake of opsonic factors (Davis et al, 1985).

1.3.3. Effect of Surface Charge

Particle surface charge can have marked effects on the clearance and deposition of colloids. Wilkins and Meyers (1966) altered the electrophoretic mobility (EPM) of 1.305μm polystyrene latex with coatings of either gum arabic (GA) to provide a negative charge, or polylysyl gelatin (PLG) to give a positive charge; mixtures of GA and PLG gave intermediate charges. Following injection of these various colloids into rats, the mobility was seen to affect both the rate of clearance and site of deposition. Negatively charged particles were taken up by the liver and this distribution maintained, while positively charged colloids showed an initial (15 minutes) appreciable accumulation in the lungs and subsequent (72 hours) relocation to the liver and spleen. Although these particles displayed various EPM's in buffer, in rat serum the mobilities for all particles were essentially identical. The differences in organ distribution, therefore, cannot be attributed to surface charge alone.

Surface charge also affects the phagocytosis of paraffin oil emulsions by polymorphonuclear leukocytes (Stossel et al, 1972).

Emulsions prepared with emulsifiers giving a strong net negative charge (e.g. acetylated albumin) or a strong net positive charge (e.g. diethylaminoethyl-dextran) showed a higher rate of ingestion compared with weakly negative emulsifiers (e.g. gelatin). In contrast, Davis and Hansrani (1985) found no clear correlation between zeta potential and in vitro macrophage phagocytosis for soybean oil emulsion systems prepared with a range of phosphatide emulsifiers.

Similar work with liposomes has shown that increasing the negative surface potential by altering phosphatide content has a strong suppressive effect on ingestion of liposomes by mouse peritoneal macrophages when the liposomes are opsonised by complement (Roerdink et al, 1983). It was concluded that opsonisation and strong negative surface charge can be opposing forces that work actively against each other. These findings correlate with those of Hnatowich and Clancy (1980) who determined the distribution of liposomes two hours after injection in mice. Increasing the negative liposome charge by replacing lecithin with cardiolipin decreased liver and spleen accumulation by 5- and 20-fold respectively. However, there was an increase in bone accumulation (presumably RES mediated) such that most of the liposomes were found in RES tissues. In contrast, other workers have found that negative liposomes, in comparison with neutral or positive liposomes, show a faster rate of clearance (Juliano and Stamp, 1975; Senior et al, 1985) and higher liver and spleen uptake (Richardson et al, 1978).

Clearly the connection between phagocytosis, RES uptake and surface potential is far from simple and concomitant changes in other surface properties may override any effects produced by variations in surface charge.

1.3.4. Effect of Particle Number

Initial clearance rate by the RES can be affected by the presence of large numbers of particles occupying available RES receptors or exhausting opsonising factors (Saba, 1970). Although clearance rate may be affected by large doses of colloidal material, the distribution within the RES does not seem to be altered (Benacereff et al, 1975). It is possible, however, to overload the RES either by single large doses or repeated administration. Subsequent injections remain in the circulation and this is discussed as a means of affecting distribution patterns in section 1.4.3.1.

1.4. MODES OF DRUG TARGETING

Site specific drug delivery systems can be classified according to the methods employed for achieving target site localisation. These are termed either passive, physical (external) or active targeting (Poste and Kirsh, 1983).

1.4.1. Passive Targeting

Passive targeting refers to the natural distribution pattern of the carrier in vivo. The fate of particulate systems will be

determined largely by the factors discussed in section 1.3. Therefore it is possible to target passively the lungs and RES with relative ease.

1.4.1.1. Passive lung targeting

Entrapment of large particles (>7μm) in the capillary bed of the lungs has been exploited in radiodiagnostic imaging as well as for the delivery of anticancer agents to the lungs (Yoshioka et al, 1981). Illum and Davis (1982b) have shown the potential of attaining sustained release of acidic drugs in lung capillaries using diethylaminoethyl-cellulose microspheres. However, this material is not biodegradable and therefore is unsuitable as such for potential clinical use.

1.4.1.2. Passive RES targeting

RES mediated clearance of drug targeting systems is normally a major disadvantage. Sequestration by RE cells not only decreases targeting effiency, but can also result in damage to the RES, particularly if the carrier payload is a highly cytotoxic agent (Poste, 1983). This can have serious consequences in cancer patients since mononuclear phagocytes are active in preventing the spread of metestases (Poste, 1983; Fidler, 1977). Despite these drawbacks RES clearance can be exploited to gain benefit (Alving, 1983).

Macrophages form an important part of the host defence mechanism against tumour cells. When activated, these cells are capable of killing tumour cells via an immunologically non-specific

mechanism that is unaffected by tumour cell cycle phase or anti-tumour drug resistance (Poste et al, 1982). Macrophages may be activated by lymphokines, such as macrophage activating factor (MAF) or synthetic compounds such as muramyl dipeptide (MDP). These have been incorporated into liposomes and used to activate alveolar macrophages in mice, thereby augmenting host defences and resulting in a significant reduction in the metastatic burden of tumour bearing animals (Fidler et al, 1981 and 1982). However, it has been emphasised (Poste et al, 1982) that macrophage mediated destruction of large tumour burdens may not be feasible and this approach is limited to the erradication of micro-metastases and residual tumour cells remaining after surgery or chemotherapy.

Liposomes have been used to target infections of the RES such as leishmaniasis (Alving et al, 1978; Alving, 1983), crypto-coccosis (Graybill et al, 1982), candidiasis (Lopez-Berestein et al, 1983) and histoplasmosis (Taylor et al, 1982). In all cases liposomal entrapment of the anti-parasitic drugs increased their therapeutic index. Such approaches may be of benefit for the control of disseminated fungal infections which are a major problem associated with the use of cytotoxic agents (Poste, 1985).

Soluble carriers are also taken up by the RES and this too has been investigated. Conjugates of rabbit serum albumin with two DNA synthesis inhibitors, 5-fluorodeoxyuridine and cytosine arabinoside, are ingested mainly by Kupffer cells. This has been used successfully to treat mice infected with Ectromelia virus which replicates initially in Kupffer cells (Fiume et al, 1982).

1.4.1.3. Passive intra-arterial targeting

Intra-arterial injection of large particles results in filtration by the first capillary bed encountered. Injection into arteries supplying tumour sites would result, therefore, in significant accumulation in the locality of the malignancy before RES clearance could take effect. This technique has been investigated with various microspheres composed of ethylcellulose (Kato et al, 1980), albumin (Tomlinson et al, 1984) and starch (Lindberg et al, 1984). With this latter system the microspheres (40μm diameter) are co-injected with cytotoxic agents. The resultant blockage of the tumour arterioles induces localised hypoxia and high concentrations of drug. Although now undergoing clinical trial (Russell, 1983) this type of approach is only useful for well defined malignancies, being of little value in treating disseminated tumours or metastases.

1.4.2. Physical Targeting

In physical targeting some characteristic of the environment is used either to direct the carrier to a specific location or to cause selective release of its contents there. This is normally achieved through some external targeting mechanism such as induced local hyperthermia or a localised magnetic field.

1.4.2.1. Localised drug release through induced hyperthermia

In the presence of certain serum proteins, principally lipo-proteins, unilamellar liposomes can be designed to release their

payload rapidly at their liquid crystalline phase transition temperature (Weinstein and Leserman, 1984). Liposomes with phase transition temperatures of about 42°C can be made to release their drug preferentially in a capillary bed subjected to moderate local hyperthermia. In this way increased tumour uptake of methotrexate has been achieved resulting in moderate effects on tumour growth (Weinstein et al, 1980). Nevertheless, liver accumulation is still significant and this approach does not address the problem of metastatic lesions (Yatvin et al, 1984).

1.4.2.2. Localised drug release through pH sensitive carriers

In an attempt to exploit pH differences between normal and tumour tissues, Yatvin et al (1980) proposed the use of pH sensitive liposomes. The in vitro release of the model drug carboxyfluoroscein can be enhanced 5-fold at pH 6, compared with pH 7.4, by incorporating the pH sensitive lipid N-palmitoyl L-homo- cysteine into liposomes (Yatvin et al, 1984). It is unlikely, however, that pH differences will be so marked in vivo and hepatic clearance again will be limiting.

1.4.2.3. Localised targeting by an applied magnetic field

Widder et al (1978) first reported the use of magnetically responsive microspheres for localised site specific drug delivery. Albumin microspheres (approximately 1μm diameter) were prepared containing small particles of magnetite (Fe_3O_4) and following intra-arterial injection in rats made to localise in the tail at the

site of an applied magnetic field. In this way more than 50% of the carrier was targeted to the magnetised tail segment. Subsequent studies investigated the anti-tumour activity of doxorubicin containing magnetic microspheres against a tail implanted Yoshida rat sarcoma (Widder et al, 1981). With a single magnetically localised doxorubicin dose of 0.5 mg/kg, 90-100% regression was obtained compared to 0% regression for a 10-fold higher dose of non-targeted drug. Localisation of the carrier in this way results in high levels of drug in the immediate tumour environment. In addition, after localisation, albumin microspheres are able to migrate out of the vasculature (Widder et al, 1983) probably as a result of an endocytic response secondary to mechanical pushing against endothelial cells (Widder and Senyei, 1983). Studies with magnetically targeted biological response modifiers, poly IC (an interferon inducer) and protein A (an interferon inducer and T- and B-cell mitogen), also have yielded promising results (Widder and Senyei, 1983).

Other magnetically responsive carriers such as nanoparticles (Ibrahim et al, 1983), erythrocytes (Zimmerman, 1983) and emulsions (Akimoto and Morimoto, 1983) have been prepared.

Although the results with magnetically responsive albumin microspheres seem promising, they are obtained using the highly favourable model of tail implanted tumours, i.e. the tumour site is readily accessible to the applied magnetic field. For deep seated tumours, microsphere localisation would be more difficult to attain. Encouraging results from targeting to the kidneys (Ibrahim et al, 1983; Kato et al,1979) and lungs (Morimoto et al, 1981), although

offering a greater challenge, do not address this problem entirely. In addition, this method would not be applicable in treating metastases.

1.4.3. Active Targeting

Active targeting refers to a deliberate modification of the carrier in order to alter its natural disposition pattern, directing it to specific organs, tissues or cells. Several of these modifications, such as coating with surfactants to suppress macrophage capture, and alteration of particle size and charge, have been discussed in section 1.3. Other approaches include blockade of liver Kupffer cells or attachment of cell specific ligands and monoclonal antibodies.

1.4.3.1. Reticulo-endothelial system blockade

One approach in preventing the capture of drug carriers by cells of the RES is to pre-block the RES with placebo colloid. Subsequent injections of drug carrier in treated animals are not subjected to RES clearance. Blockade can be achieved with substances such as carbon, methyl palmitate, latex particles, dextran sulphate, heat aggregated albumin and liposomes (Bradfield, 1984). By using liposomes to block the RES of mice bearing EMT6 tumours, Profitt *et al* (1983) were able to increase by 50% the tumour targeting ability of ^{111}In loaded liposomes. Illum and Davis (1984b) have used latex particles and dextran sulphate to block the RES of rabbits. Subsequent injections of radiolabelled polystyrene particles

resulted in only 30% of the injected dose accumulating in the liver and spleen compared with 90% for unblocked animals. In both studies clearance from the circulation was greatly reduced.

The clinical potential of this technique is doubtful since impairment of RES function can have serious consequences, particularly in cancer patients (Poste, 1983; Poste and Kirsh, 1983). Indeed, any drug targeting system accumulating in the RES would need to be readily degradable so that RES overload does not occur with repeated dosing.

1.4.3.2. The use of cell specific ligands

The binding by cell-surface receptors of certain molecules, such as sugars, lectins, peptide hormones and small haptens, can be utilised to target carrier systems to specific cell types.

Removal of sialic acid from glycoproteins exposes galactosyl residues which can bind specifically to receptors on the surface of hepatocytes. Desialyted fetuin has been used to transport a variety of DNA synthesis inhibitors to mouse hepatocytes infected with Ectromelia virus (Fiume et al, 1982). Results indicated a higher incorporation of drug into hepatocytes resulting in increased efficacy. It was proposed that this system may be applicable to treating hepatitis infections. Asialofetuin has also been used successfully as a carrier of primaquine in treating Plasmodium berghei infected mice (Trouet et al, 1982). Alternatively, carrier molecules can be galactosylated and used to deliver cytotoxics to hepatoma cells (Schneider et al, 1985).

Similar approaches may be applied to target a number of other sites (Gregoriadis et al, 1985). Examples of the use of glycolipids or glycoproteins with liposomes are given by Weinstein and Leserman (1984) and Widder et al (1982). In contrast to monoclonal antibodies, many of these substances are readily available and complications with target recognition are less likely to occur in vivo. However, they lack the breadth of target choice of immunoglobulins as a group and will be limited to a small number of tumour types (Gregoriadis, 1977).

1.4.3.3. The use of monoclonal antibodies

Ever since Kohler and Milstein (1975) first reported the production and isolation of antibodies displaying specificity for single antigenic determinants, the concept of a monoclonal antibody (MCA) targeted cytotoxic modality has been rigorously explored.

Several approaches have been investigated concerning the design of such a system (Sikora et al, 1984). Direct covalent attachment of cytotoxic molecules to MCA's is not very efficient, resulting in only approximately 10 drug moleclues per antibody and diminishing the antigen binding capacity (Kulkarni et al, 1981). Conjugation via intermediate carrier molecules such as poly L-glutamic acid (Rowland et al, 1975) or dextran (Pimm et al, 1982) substantially increases the drug-antibody ratio and retains a higher degree of antibody activity. Also, this approach is more versatile chemically in terms of conjugation and drug release (Trouet et al, 1981).

MCA's have been used to target high energy beta-emitters such as ^{131}I and ^{32}P, although with disappointing results (Schneinberg

and Strand, 1982). However, radiolabelling with gamma-emitters has been used successfully in tumour localisation and diagnosis (Midoux et al, 1984).

Much interest has been shown in the use of MCA's for the tumour targeting of powerful toxins such as diphtheria toxin, ricin and abrin. These toxins consist of two polypeptide chains, A and B, which are linked via a disulphide bond. The B chain, which acts as the cell recognition and binding moiety, can be cleaved from the A chain, which is highly cytotoxic. Coupling of the isolated A chain to MCA then produces, in theory, a highly cytotoxic agent or immunotoxin (Jansen et al, 1982). Although extremely potent in vitro, these immunotoxins have proved disappointing in vivo. Other powerful toxic molecules such as venom phospholipases and bacterial cytolysins could be coupled to MCA's in a similar way (Sikora et al, 1984).

MCA mediated targeting of particulate carriers offers a distinct advantage in terms of payload capacity compared with MCA-carrier-drug conjugates (Couvreur, 1984). MCA can be linked to liposomes either by adsorption or covalent coupling (Weinstein and Leserman, 1984). The targeting capability of these liposomes in certain circumstances is very efficient; for example, liposomes conjugated with antibody to L929 murine fibroblasts, associated with these cells in 6- to 20-fold greater amounts compared with non-specific liposomes (Heath et al, 1983). Also, the ability of methotrexate-gamma-aspartate to inhibit L929 growth was increased nearly 7-fold. Although no studies have been published using MCA to

target microspheres loaded with drug, the coupling of antibodies to microspheres has been reviewed by Illum and Jones (1985).

In addition to problems encountered with the use of drug carriers alone, as already discussed, there are inherent drawbacks associated with the application of MCA mediated targeting. These have been considered by Poste and Kirsh (1983) and are outlined below.

a) **Antigen specificity.** Apart from antigen idiotypes on B-cell tumours, totally tumour specific antigens still have to be isolated. The binding of anti-tumour MCA to non-target cells displaying tumour related antigens is a potentially serious problem for targeted immunotoxins.

b) **Tumour cell heterogeneity.** Differences in tumour cell antigen phenotype occur between cells of the same primary tumour, between primary and metastatic cells, and between metastatic cells from the same primary tumour. A mixture of MCA's which recognise different antigenic determinants would be needed to target the entire neoplastic cell population and different mixtures would be required to treat the same tumour type in different patients.

c) **Anti-idiotypic antibodies.** Most MCA's currently used are murine immunoglobulins, which can elicit production of anti-idiotypic antibodies. This blocks MCA activity and can cause hypersensitivity reactions. The administration in low doses of immunosuppresive agents, such as cyclophosphamide, could alleviate this problem, or antibody immunogenicity could be reduced by removal of the Fc portion to leave $F(ab')_2$ fragments. Alternatively, human MCA could be used (provided production difficulties can be overcome).

d) **Release of free antigen.** Natural shedding of tumour antigen or large scale release induced by tumour cell destruction could block effectively antibody mediated targeting. Consequent RES uptake of antigen blocked antibody complexes could be hazardous, especially with immunotoxins. RES uptake, however, may be utilised for removal of free antigen by pre-treatment with non-therapeutic MCA coated liposomes.

e) **Antigenic modulation.** Loss of tumour cell antigenicity or immunoselection of antigen negative tumour cells following initial treatment will negate the effectiveness of subsequent treatment cycles. Employing two MCA's recognising the same antigen, but different epitopes, or recognising different antigens, are possible solutions.

Far from solving the difficulties of site specific targeting, the problems introduced by the use of MCA are daunting. This approach, however, still holds potential, particularly for targeting neoplastic lymphoid subsets (Poste and Kirsh, 1983) and in ex vivo treatment of leukaemic bone marrow (Muirhead et al, 1983).

1.5. TARGET SITE SPECIFICITY

The degree of specificity achieved by drug targeting can be classified according to the level of selectivity of the delivery system (Poste and Kirsh, 1983: Widder et al, 1979). First order delivery is described as targeting to individual organs or tissues (organ targeting); second order refers to targeting to a specific cell type(s) within a tissue (cellular targeting); and third order targeting involves delivery to selected intracellular compartments

in target cells (sub-cellular targeting). Although it is possible to attain each level of targeting with various delivery systems, no single system exists which can achieve all three levels.

The order of targeting may be of particular importance in cancer chemotherapy since solid malignancies usually consist of a heterogeneous collection of tumour cells which vary in their response to anti-neoplastic *agents. This is probably the factor most* responsible for the current lack *of success in* cancer chemotherapy and necessitates the use of multiple-drug regimens (Poste and Kirsh, 1983). Therefore, not only would any potential drug targeting system be required to deliver its payload to a range of tumour cell sub-populations, but also be capable of accommodating an array of drugs. Furthermore, because cytotoxic agents act at a variety of sub-cellular sites, a degree of third order targeting may be necessary to ensure maximum therapeutic efficiency if the survival of drug resistant tumour cells is not to remain a major cause of treatment failure.

1.6. SYNTHETIC DRUG CARRIER SYSTEMS

From the vast array of drug carriers studied in recent years no single device has emerged as being clearly superior or fulfilling all the requirements of an ideal system. This may be understood in considering the criteria of an ideal carrier (Widder and Senyei, 1983; Tomlinson, 1984) which, briefly, require that it should;

1) be easy to prepare in a sterile form,

2) be easy to store and to administer,

3) be non-toxic and non-allergenic,

4) have a high capacity for a range of drugs,

5) not release its payload prematurely,

6) protect the payload from degradation,

7) accumulate and remain at the desired site of action,

8) release the drug(s) in an active form at a suitable rate and in therapeutic amounts to the target cell(s),

9) be biodegradable with minimal toxicity.

In attempting to meet these requirements two main types of carrier systems have been developed; soluble macromolecular drug carriers and particulate carriers.

1.6.1. Soluble Macromolecular Drug Carriers

The concept of a target specific macromolecular drug carrier is shown by figure 1.4 (Ringsdorf, 1975). In this representation the polymer backbone is modified by three functional moieties. One area is used to fix the 'pharmacon' or therapeutic agent. This is done via covalent bonds which may be permanent or temporary depending on whether the therapeutic agent can exert its effect whilst bound to the carrier. Target specificity is achieved by the attachment of a 'homing device' such as an antibody, lectin or hormone. The third part of the conjugate can be used for controlling physico-chemical properties such as molecular weight, solubility, electrical charge and hydrophilic/lipophilic balance.

Several polymeric materials have been utilised as carrier molecules. The choice of polymer is important in determining the biodistribution of injected carrier systems. In particular, RES uptake and glomerular filtration are highly dependant upon molecular

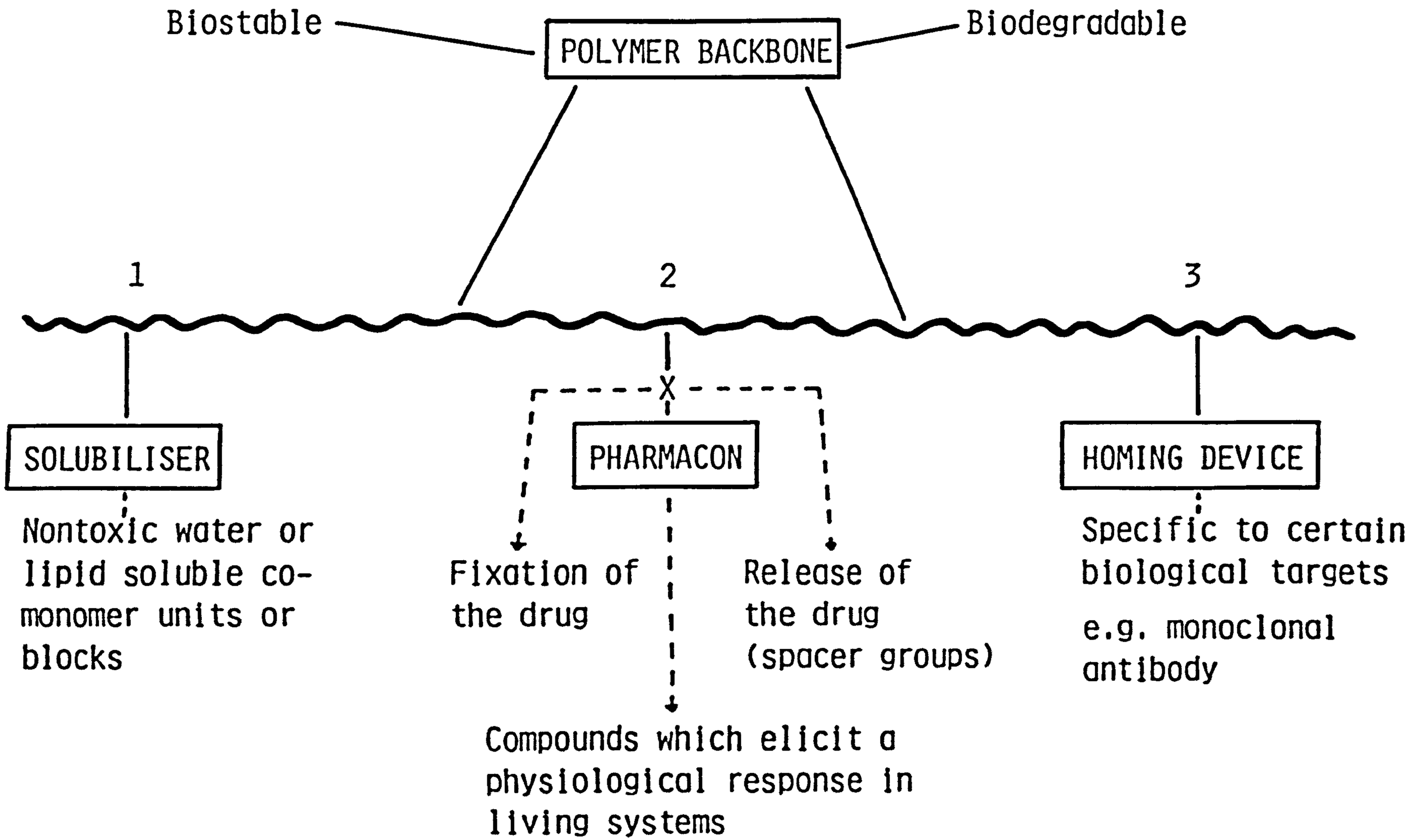

Figure 1.4. Design of a macromolecular drug carrier (Ringsdorf, 1975).

weight. Albumin has been used extensively, being readily available, well defined and chemically versatile due to large numbers of free carboxyl and amino groups. Dextrans too have attracted much attention due to their high water solubility, range of well defined molecular weights, low toxicity and ability to conjugate a wide range of drugs. Other molecules such as polylysine, polyglutamic acid and pyran also have been proposed as carriers and examples of the use of all these polymers are given by Sezaki and Hashida (1985). Results, however, in treating neoplastic cells in vivo are disappointing due to a lack of target specificity.

For selective targeting of tumour cells a homing device needs to be attached to the cytotoxic agent, either by direct conjugation or through a carrier molecule. The use of MCA's in this respect has been dealt with already (section 1.4.3.3.) and further examples are given elsewhere (Sezaki and Hashida, 1985). Apart from MCA's, lectins such as concanavalin A (Kitao and Hattori, 1977) and hormones (Cikes, 1978) have been proposed as targeting agents.

Although in theory soluble drug carriers have a greater potential for extravasation and accumulation at target sites than particulate carriers, their overall effective dimensions are still sufficiently large, in many cases, to limit vascular escape (Pouton, 1985). Decreasing molecular size, however, introduces the problem of rapid glomerular filtration. Also, the chemical modifications involved in preparing these carriers predispose them to clearance by the RES (Poste and Kirsh, 1983). Together with their low payload capacity these problems combine to offer little or no advantage over particulate carriers.

1.6.2. Particulate Drug Carriers

The term 'particulate carrier' is used to describe systems which, by definition, are thermodynamically unstable and irreversible, as distinct from true solutions of macromolecular carriers (Shaw, 1970). Both types of systems are colloidal by nature and separation on grounds of molecular dimensions is not possible. Thus, particulate carriers can range in size from a few nanometres, such as small liposomes, to several micrometres as with ethyl-cellulose microspheres. Comprehensive reviews on a range of systems are available elsewhere (Davis, 1981; Oppenheim, 1981; Tomlinson, 1983) while this section will be limited to discussing biodegradable carriers suitable for systemic administration.

1.6.2.1. Liposomes

Liposomes are composed of one or more concentric lipid bilayers enclosing an equal number of aqueous spaces. Three major types of liposomes can be formed depending on the preparative technique (Weinstein and Leserman, 1984). Multilamellar vesicles (MLV) are easy to prepare and relatively stable but are highly polydisperse (80nm to 10μm). Small unilamellar vesicles (SUV) are much less polydisperse but suffer from poor stability and low payload capacity. The third type of liposome, large unilamellar vesicles (LUV), are the most efficient with respect to drug encapsulation but they are difficult to prepare.

Phosphatidylcholines (such as lecithin) are usually the major liposome constituents (40-70%) together with cholesterol and a

negatively charged lipid such as phosphatidylserine. Positively charged liposomes are normally formed by incorporating stearylamine. Drug loading is achieved by incorporating water soluble drugs into the internal aqueous compartment(s). The preparation and handling of liposomes has been discussed by Szoka and Papahadjopoulos (1980).

The particulate nature of liposomes largely determines their biofate according to the factors already discussed. In addition, the composition of the lipid bilayer also seems to influence their distribution pattern (Senior and Gregoriadis, 1982). This is probably due to the fluid nature of these vesicles allowing exchange between liposome lipids and circulating lipoproteins (Scherphof et al, 1978). This, eventually, can lead to the disruption of liposome integrity and release of encapsulated drug. Attempts at stabilising the lipid membrane by incorporation of cholesterol, although successful in this respect, may increase liver uptake due to enhanced association of apoprotein E with the liposome surface (Widder et al, 1982).

Several of the versatile properties of liposomes have been highlighted already (e.g. temperature and pH sensitivity). In addition to these, particle size can be controlled over the range 25nm to 10μm, site specific ligands are readily incorporated and liposomal charge may be easily altered (Gregoriadis and Allison, 1980). Doubts, however, have been raised concerning size heterogeneity, stability, drug incorporation and production difficulties (Poste and Kirsh, 1983). Thus, the great attention paid to liposomes may be disproportionate to their potential in comparison with other drug targeting systems for use in cancer chemotherapy.

1.6.2.2. Polymeric nano- and microspheres

The preparation, properties and uses of polymeric microspheres have been reviewed in a series of articles by Kreuter (1983a,b and c) and by Davis et al (1984). The materials used to form the particle matrix may be classified broadlly into two groups; synthetic polymers and natural macromolecules. Within this latter group serum albumin has been studied extensively. First suggested as drug carriers by Kramer (1974), albumin microspheres have been used in combination with many therapeutic classes of drugs (Tomlinson, 1983; Yapel, 1979). Albumin microspheres can be prepared in a number of ways (Yapel, 1979), allowing control of particle size over a wide range (Tomlinson, 1983). One method involves heating a water-in-oil emulsion of the protein plus drug to give aggregates of drug loaded albumin. The microspheres are isolated by evaporating the water and removing the oil by washing with solvents. This method, however, is limited by degradation of heat-labile drugs and partitioning of lipophilic drugs into the oil phase. Alternatively, a chemical cross linking agent such as formaldehyde, glutaraldehyde or 2,3-butadione can be used without the need for heating (Kreuter, 1983a). Cross linking agents may be used also to harden particles produced by the desolvation of albumin solutions (Oppenheim, 1981). These reagents, however, can react with amino groups of drug molecules thereby interfering with their incorporation. Normally drug loading is very efficient for water soluble compounds and up to 35% by weight of the carrier can be drug (Tomlinson, 1984).

Gelatin too has been examined extensively for use in the preparation of particulate carriers. Yoshioka et al (1981) were able

to form nano- or micro-spheres of gelatin depending on the preparative technique. Small nanospheres (280nm diameter) were formed by cross linking a sonicated gelatin emulsion, whereas larger microspheres (14.9μm) were formed with a vigorously shaken emulsion. The same authors could then target mitomycin C either to the liver (280nm particles) or lung (14.9μm particles).

Usually, microspheres composed of synthetic molecules are prepared from acrylate polymers composed of either methyl meth-acrylate, acrylamide, N,N'-bis acrylamide, alkyl 2-cyanoacrylate (ACA) or copolymers of 2-hydroxyethyl methacrylate, methacrylic acid and acrylamide (Kreuter, 1983a). Other materials may be used such as 4-vinyl pyridine and glutaraldehyde. Most particles formed from these monomers are not biodegradable and, therefore, are not suitable for drug targeting. However, particles composed of poly (alkyl 2-cyanoacrylate) (Couvreur et al, 1979a) and co-polymers of acrylamide and dextran, termed polyacryldextran microspheres, (Edman et al, 1980) are biodegradable.

Poly (alkyl 2-cyanoacrylate) (p(ACA)) nanoparticles have attracted much attention for use in cancer chemotherapy. The next section will deal with this system in greater detail and will serve as an example of the considerations needed in the design of a suitable drug carrier.

1.7. POLY (ALKYL 2-CYANOACRYLATE) NANOPARTICLES

Initial attempts at producing a novel particulate lysosomo-tropic carrier (Couvreur et al, 1977) identified the need for a biodegradable system that would avoid prolonged overloading of

lysosomes. This work with polyacrylamide nanocapsules led to the development of p(ACA) nanoparticles, first reported by Couvreur et al (1979a). By varying the size of the alkyl ester group (generally methyl to hexyl) a range of nanoparticles with different properties can be produced.

1.7.1. Preparation

In the general method of preparation, the monomer is added to a rapidly stirred aqueous solution (pH 2-4) of a stabiliser such as a dextran or non-ionic surfactant (Couvreur et al, 1982a; Maincent, 1982), although the formation of nanoparticles without the addition of polymeric stabilisers has been reported (Ibrahim et al, 1982; Van Snick et al, 1985). Anionic polymerisation of the monomer gives the corresponding p(ACA) which forms the nanoparticle matrix. Once polymerisation is complete the suspension is filtered to remove large particles and neutralised ready for use or lyophilisation.

1.7.2. Physico-chemical Properties

1.7.2.1. Morphology

Nanoparticle morphology has been studied by both scanning and transmission electron microscopy (SEM and TEM) and shows these systems to consist of discrete spheres bearing a smooth surface (Kreuter, 1983d; El-Samaligy and Rohdewald, 1982; Couvreur et al, 1982a). Analysis of freeze-fracture replicas of nanoparticles by Kante et al (1980) also showed the presence of irregular profiles which where approximate ellipses with a maximum axial ratio of 1.5.

TEM studies have indicated these particles consist of a highly porous interior (Kreuter, 1983d) producing a large surface area for drug sorption. Although no continuous limiting envelope surrounding poly (methyl 2-cyanoacrylate) (p(MeCA)) nanoparticles could be identified by Couvreur et al (1979a), the same workers later proposed poly (butyl 2-cyanoacrylate) (p(BCA)) nanoparticles to possess a more homogeneous outer ring (Kante et al, 1980). This was not observed for all particles, however, and may be an artifact produced by the preparation technique.

1.7.2.2. Particle size

From the reports of various workers (Kreuter, 1983d; Couvreur et al, 1982a) the particle size of these systems appears to be in the range of approximately 30-500nm, although no detailed study on the control of nanoparticle size was available prior to commencing this project. Detailed discussions concerning nanoparticle size are given in chapter 2.

1.7.2.3. Polymer molecular weight

Molecular weight analysis by gel permeation chromatography indicates nanoparticles are composed mostly of short polymer chains with a polystyrene equivalent number average molecular weight of the order 2000 (El-Egakey et al, 1983). The molecular weight was found to increase slightly with ester chain length, polymerisation pH, and stabiliser (polysorbate 20) concentration. Marked differences have been found, however, between nanoparticles produced with or without

poloxamer 188 stabiliser (Couvreur et al, 1984; Van Snick et al, 1985). Nanoparticles produced in the presence of this surfactant possessed a high molecular weight component not seen in polysorbate 20 systems. In addition, the polymer molecular weight was found to be affected by the polymerisation pH, ester size, and the addition of certain drugs to the polymerisation medium (Van Snick et al, 1985). These effects, due to the stabiliser and incorporated drug, may be of importance when considering drug release from the carrier. Further aspects of nanoparticle molecular weight and composition are discussed in chapter 3.

1.7.2.4. Electrophoretic mobility and surface charge

The electrophoretic mobility of aggregated nanoparticles has been determined by Kreuter (1983d). The particles were found to have a negative surface charge which was substantially reduced in the presence of human serum indicating a significant interaction of serum components with the nanoparticles. The electrophoretic mobilities in water of nanoparticles composed of the methyl, ethyl and butyl esters were found to be -2.33, -2.18 and -2.01 $\mu m.cm.s^{-1}.V^{-1}$ respectively. These values correspondingly decreased to -0.23, -0.23, and -0.19 $\mu m.cm.s^{-1}.V^{-1}$ after the samples were incubated in serum overnight.

1.7.2.5. Surface Hydrophobicity

This property has been investigated by compressing nanoparticles composed of different cyanoacrylate esters into tablets

and determining their water contact angles, giving an order of decreasing hydrophobicity of butyl> ethyl> methyl (Kreuter, 1983d). The surface hydrophobicity was reduced greatly by incubating the nanoparticles with human serum indicating, again, a strong interaction with plasma proteins. Such an interaction could lead to particle opsonisation and rapid uptake by the RES.

1.7.3. Nanoparticle Degradation

The in vitro degradation mechanism of p(ACA) was identified first by Leonard et al (1966) who proposed a reverse Knoevenagel reaction resulting in polymer chain hydrolysis and formation of an alkyl 2-cyanoacetate and formaldehyde. The degradation rate was found to be a function of the ester chain length and pH, such that the rate decreased as the homologous series was ascended and as the pH decreased. This was confirmed by Vezin and Florence (1980) who, in addition, found the rates of degradation to vary with particle specific surface, particle size, polymer molecular weight and molecular weight distribution. A modified reaction mechanism was proposed in which degradation occurs only at chain ends. Lenaerts et al (1984a), however, dispute these findings when examining the degradation of poly (isobutyl 2-cyanoacrylate) (p(IBCA)) nanoparticles. These workers found that at pH 7 only 5% of the polymer degraded via the formaldehyde pathway after 24 hours, and at pH 12 the value reached only 7%. Conversely, after 24 hours at pH 12, between 85 and 94% of the polymer was found to have degraded via an alternative mechanism involving isobutanol production due to ester hydrolysis.

Wade and Leonard (1972) first postulated that ester hydrolysis may be involved in the degradation of these polymers *in vivo*. Although it has been stated that polymer degradation is independent of any added esterase (Vezin and Florence, 1978) other studies have shown nanoparticles to undergo enzymatic ester hydrolysis yielding a primary alcohol and water soluble poly (2-cyanoacrylic acid) (Lenaerts *et al*, 1982; Grislain *et al*, 1983). This enzymatic pathway would augment the chemical ester hydrolysis which is unlikely to be significant at pH 7.4 or below.

The degradation of nanoparticles *in vivo*, therefore, will be highly complex involving at least two pathways dependent upon such parameters as the ester group, pH, molecular weight, particle size, enzyme activity, etc..The choice of monomer does offer, however, some degree of control over nanoparticle degradation (Couvreur *et al*, 1979b).

1.7.4. Drug Loading

Drug uptake may be achieved either by incorporation during the polymerisation stage or by adsorption once the nanoparticles are isolated. Addition of drug to the reaction medium, however, can interfere with nanoparticle formation (Maincent, 1982). In addition, drugs possessing the weakly nucleophilic moieties hydroxyl, amino or carboxylate, may copolymerise with the monomer (Leonard *et al*, 1966; Schmeissner, 1970). This may reduce the payload of free active drug, although at the low pH of nanoparticle formation protonation of amino and carboxylate functions should render such compounds unreactive. Whilst nanoparticle formation does not require an

initiating energy input, such as chemical, thermal or electro-magnetic, which could have detrimental effects on drug payload as experienced with other systems (Oppenheim, 1981), the high reactivity of the monomer can pose problems if drug uptake is achieved by incorporation. Most of the payload, however, appears to be adsorbed at the particle surface as indicated by the similarities in uptake of triamcinolone diacetate achieved either by incorporation or adsorption (El-Samaligy and Rohdewald, 1982). There would appear to be little advantage, therefore, in adding the drug to the polymerisation medium.

A wide range of drugs have been loaded into nanoparticles as shown by the examples in table 1.2. This table gives the drug uptake in terms of the amount of drug per unit weight of carrier, which is much more important when considering the payload of the system than quoting percentage uptake alone (Oppenheim, 1981). Generally, the uptake is greatest for hydrophobic unionised molecules and is enhanced by nanoparticles composed of longer chain esters. Therefore fluorescein, which is strongly sorbed at low pH's in its non-ionised form, rapidly desorbs as the pH is raised due to anion formation, and shows a higher loading with nanoparticles composed of poly (ethyl 2-cyanoacrylate) (p(ECA)) compared with the p(MeCA) (Couvreur et al, 1979a). The sorptive behaviour of p(BCA) nanoparticles has been studied in detail using the model drug verapamil which displayed Langmuir type adsorption (El-Egakey and Speiser, 1982a). As expected, temperature rise, surfactants, and dispersing agents decreased adsorption, while increase in electrolyte concentration and pH increased adsorption.

TABLE 1.2 Uptake of various drugs by poly (alkyl 2-cyanoacrylate) nanoparticles either by incorporation (Inc.) or adsorption (Ads.). Results obtained at pH 7 unless otherwise stated.

Drug	Concentration		% Uptake	Loading[a] (mg/g)	Class	Ester
	Drug (μg/ml)	Monomer (mg/ml)				
Actinomycin D	20	18.3	90	1.0	Inc.	Methyl
Actinomycin D	20	17.4	86	1.0	Inc.	Ethyl
Actinomycin D	5	4.6	66	0.7	Ads.	Methyl
Daunorubicin[b]	50	3.3	85	13	Inc.	Methyl
Doxorubicin	1000	10	94	94	Inc.	Isobutyl
Insulin[c]	5	17.4	75	216	Ads.	Ethyl
Levamisole	800	16.6	25	12	Inc.	Methyl
Methotrexate	80	14.7	25	1.4	Inc.	Methyl
Penicillin V	1000	17.7	50	28.2	Inc.	Methyl
Triamcinolone	100	3.3	79	24	Inc.	Methyl
Triamcinolone	100	3.3	69	21	Ads.	Methyl
Vincamine[d]	2000	9.7	44	91	Inc.	Hexyl

[a] loading is expressed as milligrams of drug per gram of nanoparticles, assuming 1g of monomer yields 1g of nanoparticles.

[b] final pH = 9.

[c] concentration expressed as international units of activity.

[d] final pH = 5.8.

1.7.5. Drug Release

The rate of drug release from p(ACA) nanoparticles closely follows the rate of nanoparticle degradation (Couvreur et al, 1979b; Lenaerts et al, 1984a). By the choice of monomer it is possible to control drug release rates (figure 1.5) although the influence of other factors affecting nanoparticle degradation need to be considered. These results imply that the drug is dispersed throughout the nanoparticle matrix. This is in contrast to the findings of El-Samaligy and Rohdewald (1982) who proposed that drug release is mainly an estimation of drug desorption which is only partially augmented by polymer degradation. As long as a polymer surface exists an adsorption/desorption equilibrium is still present, so that drug release is complete only after final nanoparticle degradation. Diffusion of the drug through the p(ACA) matrix can also occur (El-Egakey and Speiser, 1982b), thereby complicating the release characteristics further. In vivo, the situation is probably much more complex with protein surface interactions and macrophage uptake possibly leading to a much faster release.

1.7.6. Toxicity of the Carrier

Much of the data concerning p(ACA) toxicity are derived from their use as surgical tissue adhesives. The decrease in histotoxicity of these compounds as the homologous series is ascended (Leonard et al, 1967) is related to the degradation rate of the polymer. The more toxic faster degrading esters (e.g. methyl)

Figure 1.5. Evolution of actinomycin D from nanoparticles composed of various cyanoacrylate esters.

(▽) p(MeCA)

(●) p(MeCA) and p(ECA) mixture (2:1)

(△) p(MeCA) and p(ECA) mixture (1:1)

(▲) p(MeCA) and p(ECA) mixture (1:2)

(o) p(ECA)

Couvreur et al, 1979b.

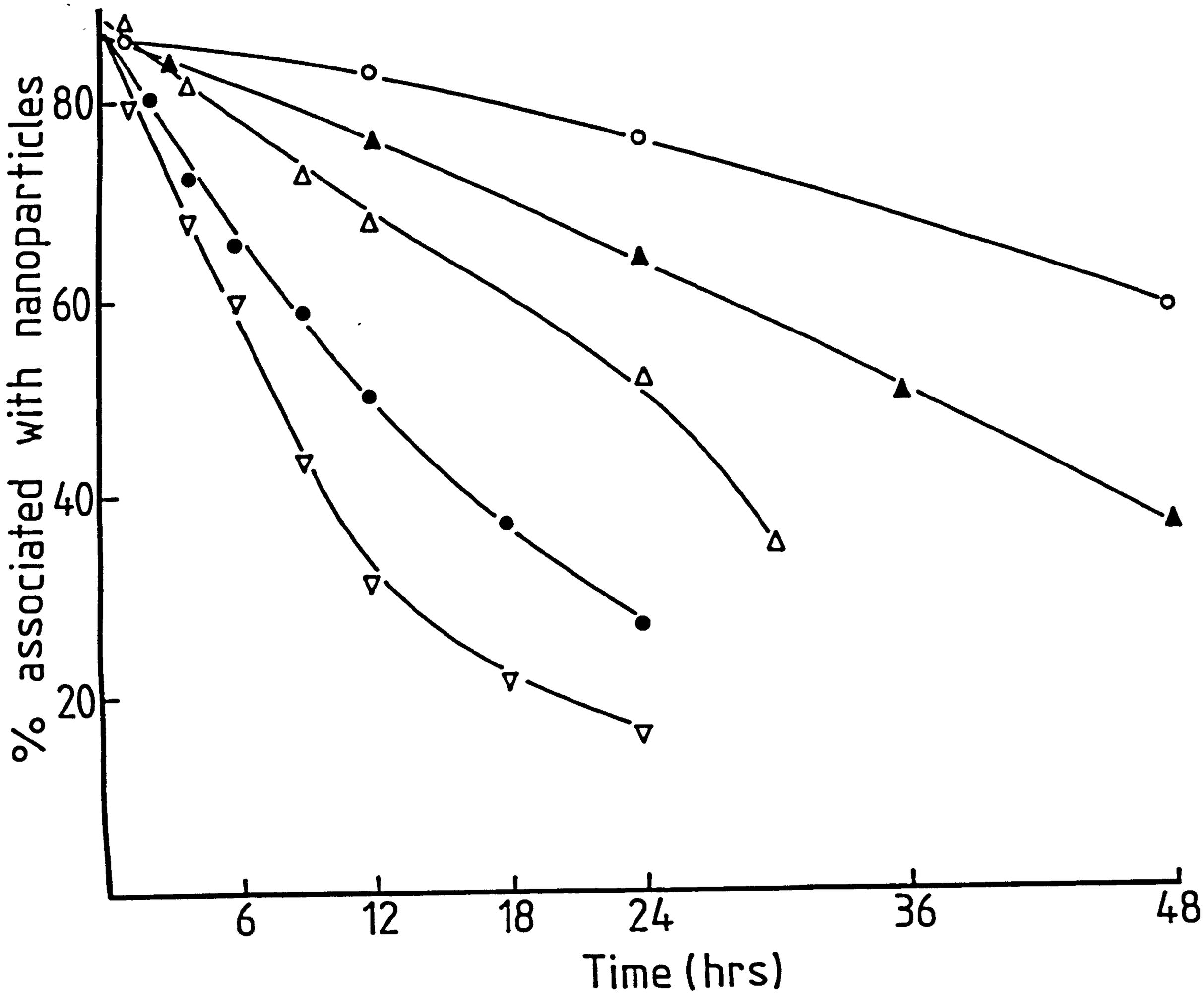
% associated with nanoparticles
80
60
40
20
6
12
18
24
36
48
Time (hrs)

lead to a rapid local accumulation of toxic metabolites believed to be formaldehyde and alkyl 2-cyanoacetates (Leonard et al, 1966). Mori et al (1967), however, found little difference between the ethyl, propyl and butyl esters. The route of administration and site of deposition also appear to be important since p(BCA) implanted subcutaneously was found to display little histotoxicity (Houston et al, 1970) whereas intra-articular injection of the same compound produced severe tissue inflammation (Ratcliffe et al, 1984).

Nanoparticle toxicity has been investigated both in vitro and in vivo by Kante et al (1982). The LD_{50} values for p(iBCA) and p(BCA) nanoparticles were found to be 196 and 230 mg/kg respectively, following intravenous injection of 9.2 mg/ml suspensions in mice, although the injection medium alone was not free of toxicity (LD_{50} = 33.4 ml/kg). Incubation of p(MeCA) nanoparticles with mouse peritoneal macrophages in vitro produced marked histotoxicity whereas p(iBCA) nanoparticles at the same concentration showed no signs of toxicity. Also, nanoparticles of the butyl ester only produced cellular damage of hepatocytes at high concentrations ($2x10^4$ particles per cell). Neither intact nanoparticles nor their degradation products were found to be mutagenic by the Ames test. In addition, no carcinogenic action has been associated with the use of these polymers in surgery (Collins et al, 1969).

These results indicate that nanoparticles composed of the higher esters of the series have a low toxicity although the production of formaldehyde in the degradation pathway will have to be carefully considered. One possibility of reducing toxicity

involves the formation of nanoparticles using alkyl 2-phosphonyl-acrylates currently under development (Hastings, 1984). In these compounds the cyano group has been replaced by a phosphonate moiety which should be less toxic.

1.7.7. Considerations for Targeting With Nanoparticles

1.7.7.1. Fate of the carrier following injection

Intravenous injection of ^{14}C-labelled p(iBCA) nanoparticles in mice resulted in 78% of the injected dose being localised in the liver after only 5 minutes (Grislain et al, 1983). This behaviour is indicative of uptake by liver Kupffer cells which was shown by determining the intra-liver distribution of nanoparticles in rats (Lenaerts et al, 1982 and 1984b). After rapid uptake the Kupffer cell concentration was found to decrease with time, while in contrast liver endothelial cell nanoparticle concentration reached a maximum after 30 minutes indicating a slower capture mechanism. Particle size was found to have no effect on the liver distribution of nanoparticles.

Studies in mice bearing a subcutaneous grafted Lewis Lung Carcinoma showed a different nanoparticle distribution compared with healthy mice (Grislain et al, 1983). Significant levels of radioactivity were found in the tumour and in the metastatic lungs of cancerous animals, with no lung accumulation in healthy animals. This was attributed to passage of the carrier through the vascular endothelium and uptake by endocytic tumour cells. However, no histological studies were performed so it is not possible to

determine whether intact nanoparticles localised in the tumour or if the increase in radioactivity was due to the uptake of nanoparticle degradation products formed elsewhere. Alternatively, the localised radioactivity could be attributed to blood pooling since the Lewis Lung Carcinoma is a haemorrhagic tumour. In contrast Illum et al (1984) did not observe any tumour localisation of nanoparticles in mice bearing an osteogenic sarcoma.

Subcutaneous or intramuscular injection of ^{14}C-labelled nanoparticles produced a slow release of radioactivity which concentrated in the gut wall with no activity detectable in the liver (Grislain et al, 1983). This would imply that lymphatic transport of the carrier did not occur or that the nanoparticles degraded at the injection site slowly releasing soluble radioactive degradation products.

1.7.7.2. Effects of nanoparticles on drug distribution, toxicity and anti-tumour activity

When considering the fate of p(ACA) nanoparticles in vivo it is not surprising that drugs administered with these carriers tend to localise in tissues rich in RE cells. Rats injected with actinomyin D incorporated into p(BCA) nanoparticles showed, after 24 hours, concentrations 64- and 44-fold higher for the liver and spleen respectively compared with the free drug (Kante et al, 1980). In addition, higher levels were observed in the muscle tissues and lungs. Similar findings have been obtained with vinblastine (Couvreur et al, 1980a). In comparison, enhanced liver and spleen uptake were not so pronounced with actinomycin D incorporated into

p(MeCA) or p(ECA) nanoparticles although levels of this drug in the lungs and small intestine were significantly higher in nanoparticle injected animals (Kante et al, 1980). The distribution of actinomycin D, therefore, appears to be affected by the nature of the carrier. This may be altered further by administering the drug with magnetically responsive p(iBCA) nanoparticles (Ibrahim et al, 1983). Ten minutes after injection of these particles loaded with ^{3}H-actinomycin D, an approximately three times higher radioactive concentration was found in the kidneys of mice bearing a magnet compared with a control. Also, the liver uptake in these animals was reduced by one third. Other drugs such as 5-fluorouracil (Kreuter and Hartmann, 1983), doxorubicin (Couvreur et al, 1982b) and ^{75}Se-norcholestenol (Kreuter et al, 1983) also display an altered biodistribution when administered in nanoparticle form.

These effects on drug biodistribution may be expected to alter the toxicity profiles of cytotoxics when administered with nanoparticles. The adsorption of doxorubicin onto p(iBCA) nanoparticles produced a significant reduction in mortality and weight loss in mice under various dosage and administration schedules compared with free drug (Couvreur et al, 1982b). In addition, lower levels of the drug were found in the myocardium of animals given the nanoparticle preparation, which may be of importance considering the high cardiotoxicity of doxorubicin. Kreuter and Hartmann (1983), however, found the toxicity of 5-fluorouracil in mice, as measured by leukopenia, weight loss and premature death, to be enhanced when given with p(BCA) nanoparticles. This was proposed to result from increased

accumulation in the bone marrow since this organ belongs to the RES and myelosuppression is the dose limiting factor for 5-fluorouracil. Similarly, actinomycin D adsorbed onto p(MeCA) nanoparticles was found to have a higher mortality compared with free drug when injected into rats bearing a soft tissue sarcoma (Brasseur et al, 1980).

Initial studies indicate that the antitumour effect of cytotoxics may be enhanced by administration with nanoparticles. An enhanced reduction in the growth of mouse Crocker Sarkoma S180 was seen with 5-fluorouracil bound to p(BCA) nanoparticles compared with free drug, although this was also associated with increased toxicity (Kreuter and Hartmann, 1983). Similarly, Brasseur et al (1980) reported a considerable decrease in the growth of a rat soft tissue sarcoma (S250) with actinomycin D adsorbed onto p(MeCA) nanoparticles (figure 1.6). The carrier alone did not demonstrate any significant antitumour activity. Clinical trials in humans are now in progress although no conclusive data are yet available (Couvreur et al, 1985).

1.7.7.3. Nanoparticle targeting mediated via monoclonal antibodies

Monoclonal antibodies may be attached to nanoparticles either via a protein spacer (Couvreur, 1984) or directly by adsorption (Illum et al, 1983). In the latter case each poly (hexyl 2-cyanoacrylate) (p(HCA)) nanoparticle was found to take up on average 2000 antibodies (791T/36 antitumour osteogenic sarcoma). These particles interacted specifically with antigenic tumour cells

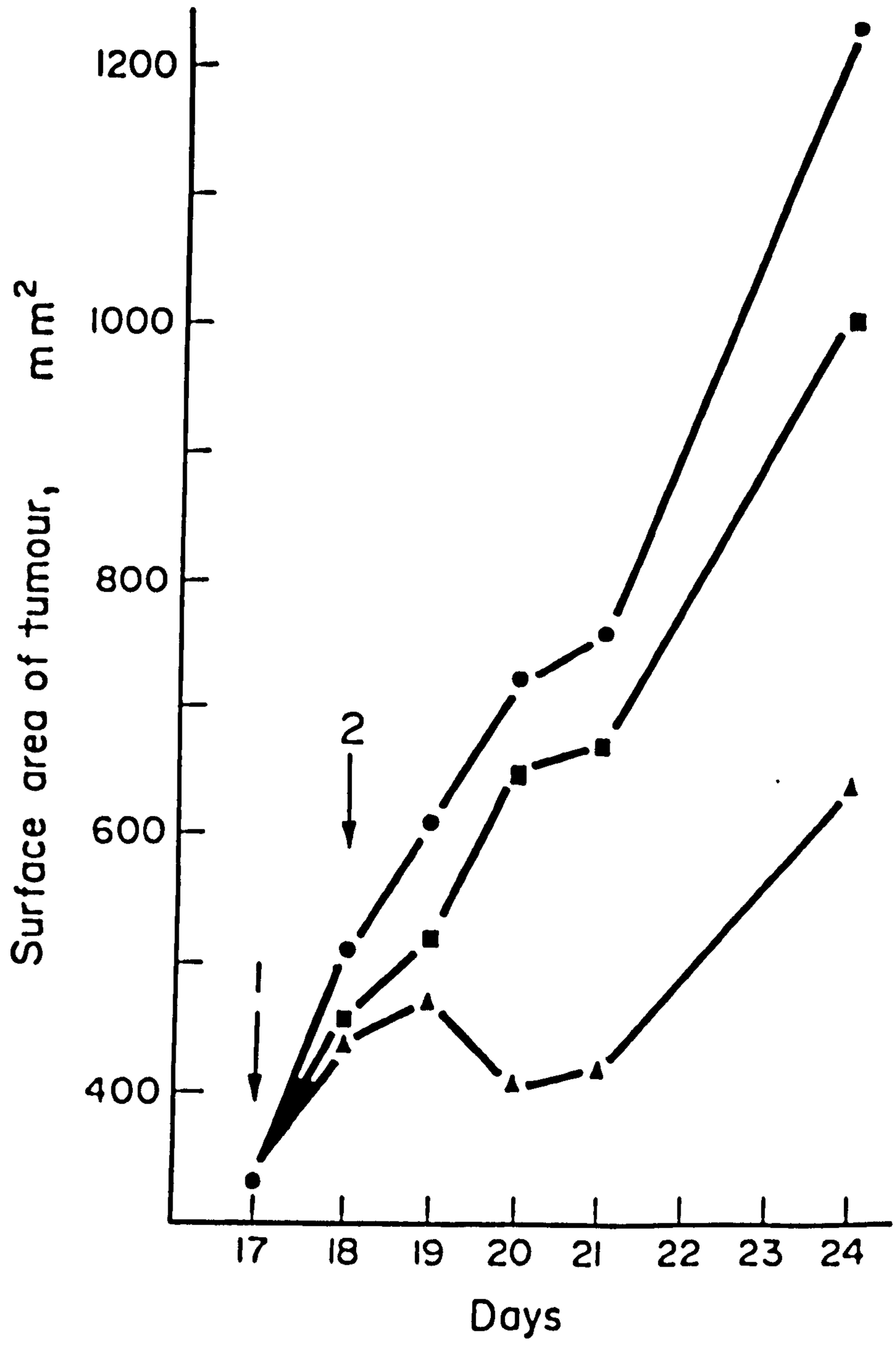

Figure 1.6. Tumour size of S250 sarcoma in mice treated with free actinomycin D (■) or with actinomycin D adsorbed onto p(MeCA) nanoparticles (▲). Dosage: two i.v. injections (arrows) of 111μg actinomycin D (free or sorbed) per kg. Controls (●).

Brasseur et al, 1980.

in vitro with the antibody retaining its immunospecificity for at least four days at 4°C.

When this system was tested in mice bearing 788T osteogenic sarcoma no specific tumour uptake was detected and the nanoparticles localised mainly in the liver and spleen (Illum *et al*, 1984). Obviously, *in vivo* the situation is much more complex and many problems such as antibody displacement, particle opsonisation and removal by the RES must be overcome before nanoparticle tumour specific targeting can be achieved using monoclonal antibodies.

1.7.8. Other Applications of Nanoparticles

The rapid uptake of nanoparticles by Kupffer cells of the liver and the high accumulation of nanoparticle associated drugs in this organ could be utilised for the treatment of hepatic diseases. Avila (1983) assessed the activity of two nanoparticle adsorbed drugs, formycin B (FoB) and 4-aminopyrazolo (3,4-d) pyrimidine (APP) in *Trypanosoma cruzi* infected mice. A significant increase in anti-trypanosomal activity was observed when FoB and APP were fixed to p(iBCA) nanoparticles, corresponding to a diminution in mortality and parasitaemia.

The release rate of subcutaneously injected insulin in mice may be controlled by incorporation of insulin into nanoparticles composed of different esters, with the slower degrading nanoparticles provoking a longer hypoglycaemic response (Couvreur *et al*, 1980b). Attempts at delivering insulin orally in nanoparticle form failed to produce any hypoglycaemic action. Either the

nanoparticles did not protect the insulin against proteolytic degradation or they were not absorbed.

1.8. SUMMARY AND AIMS

It has been shown that site specific drug delivery is a highly complex area. Before any further progress can be made a greater understanding of the basic physiological and biochemical parameters is required. The same can be argued for a more detailed analysis of drug carrier systems in terms of physico-chemical properties. Of the systems available p(ACA) nanoparticles represent a highly versatile drug delivery system being easy to prepare, biodegradable and having low toxicity. The choice of monomer determines the rate of nanoparticle degradation and affects surface hydrophobicity and drug loading. These particles are capable of sorbing and modifying the tissue distribution of a wide range of drugs and can enhance the activity of cytotoxic agents against experimental tumours in animals. There is evidence to suggest that nanoparticles may localise in certain tumours and nanoparticles coated with monoclonal antibody specifically target tumour cells in vitro, although this could not be demonstrated in vivo. Despite this, there is little detailed knowledge of nanoparticle formation, composition, physico-chemical properties and fate in vivo. The aim of this project will be to answer some of these questions via a systematic study of nanoparticle preparation and in vivo behaviour. Particular emphasis will be placed on the control of particle size, surface charge, molecular weight, and surface interactions, all of which have been shown to affect the behaviour of colloidal drug targeting systems.

CHAPTER TWO

CONTROL OF NANOPARTICLE SIZE

2.1 INTRODUCTION

The importance of particle size in determining the fate of an injected colloidal drug carrier has already been illustrated (section 1.3.1). Varying the size of p(ACA) nanoparticles would allow, therefore, some degree of control over the biodistribution of the carrier and its payload. In particular, the formation of small monodisperse nanoparticles may be important when regarding possible extravasation of the carrier (Poste, 1985). The control of nanoparticle size would not only increase the versatility of the system as a drug carrier but also yield valuable information concerning the mechanism of particle formation.

Parallel studies with other polymer colloids such as polystyrene (Fitch, 1971 and 1980; Hearn et al, 1981), have resulted in a thorough understanding of particle formation and in the control of latex particle size over a wide size range. Goodwin et al (1978) were able to regulate accurately the particle size of polystyrene particles by varying the reaction conditions during an emulsifier free polymerisation process. From these results it was possible to derive an equation to predict particle size given as

$$\log D = 0.238 \left[\log \frac{[I][M]^{1.723}}{[P]} + \frac{4929}{T} \right] - 0.827 \qquad [2.1]$$

where the final particle diameter, D(μm), in the size range 0.1 to 1μm is dependent on the absolute temperature, T, the ionic strength

of the aqueous phase, I, the initiator concentration, P, and monomer concentration, M.

These results may be related to the mechanism of particle formation (Goodwin et al, 1973). Polystyrene particles are stabilised by electrostatic forces which are affected by changes in the surface charge density and electrical double layer. The free radical polymerisation mechanism results in the charged initiator being incorporated in the polystyrene polymer as an end group. Increasing initiator concentration, or increasing temperature which increases the rate of initiator formation, leads to an increase in the number of charged end groups and a higher surface charge. This enhances particle stability and is reflected in a decrease in size. Adding more monomer to the system is equivalent to decreasing the initiator concentration, thereby resulting in an increase in particle size. If the ionic strength of the aqueous phase is increased, the electrical double layer is compressed, resulting in a decrease in the effective surface charge, or zeta potential, as seen by an increase in particle size.

The findings of these workers will serve as a suitable basis for the investigation of the control of p(ACA) nanoparticle size. In addition, the requirement of a stabilising agent for the preparation of a stable colloidal system offers an alternative means of controlling nanoparticle size. The choice of stabilisers for nanoparticle preparation will be influenced by the requirement of low toxicity. Although this problem can be overcome to some degree by removal of any free toxic material in the polymerisation medium, the methods available for purifying colloidal dispersions are often

time consuming and not totally effective (Hearn et al, 1981). Also, removal of the stabilising polymer may result in particle flocculation (Kreuter, 1983a). Consequently dextrans, non-ionic surface active agents (poloxamers and polysorbates) and β-cyclodextrin have been employed.

2.2. EXPERIMENTAL METHODS AND MATERIALS

2.2.1 Nanoparticle Preparation

A standard polymerisation formulation was used throughout and altered as necessary to study the effect of each variable on p(BCA) nanoparticle size. All chemicals were of standard laboratory grade unless otherwise stated. Glassware was thoroughly cleaned and rinsed with filtered (0.2μm membrane filter, Whatman, UK) distilled water.

Standard preparation. To 24.75ml of a filtered (0.2μm membrane filter) stirred aqueous solution of 0.5% w/v dextran 70 (molecular weight 70300; Sigma, UK) in approximately 0.01N hydrochloric acid (pH 2.25) was added 0.25ml of butyl 2-cyanoacrylate (BCA) (Sichel Werke, FRG). Stirring was achieved by means of a glass-covered magnetic stirrer bar and the stirring rate adjusted to disperse fully the monomer (approximately 1000 rpm). Reactions were carried out in a stoppered 25ml Quickfit conical flask at ambient temperature (20^{o}C). After polymerisation was complete (normally 2hours) the suspension was filtered through a sintered glass funnel (grade 4, pore size 11-16μm) to remove any large particle agglomerates. The polymerisation end point was determined by adding 0.5ml acetone to a 1.0ml sample of the reaction mixture, followed by

2 drops of a freshly prepared solution of potassium permanganate (0.1% w/v) at the same pH as the polymerisation medium; rapid discharge (within 5 seconds) of the pink colour indicated the presence of monomer and stirring was continued until all monomer was consumed. Each preparation was carried out in duplicate to ensure the results were reproducible. A formulation was only regarded as acceptable if the bulk of the monomer formed discrete particles.

Effect of stirring speed and ultrasonication. The effect of stirring rate on particle size was determined by stirring the reaction medium mechanically with a glass paddle. Stirring rate was measured with an optical digital tachometer (Compact Dot-1, Compact Instruments, UK). The minimum and maximum stirring rates were restricted by the need to fully disperse the monomer in the aqueous phase and by the upper speed limit of the stirrer, respectively.

To determine whether ultrasonication could be used as an alternative method for monomer dispersion the reaction vessel was either placed in an ultrasonic bath (Decon FS100, Decon Ultrasonics, UK) or an ultrasonic probe (Dawe Soniprobe 7532B, Dawe Instruments, UK), at power setting 4, was immersed in the reaction medium.

Effect of monomer concentration. The monomer concentration was varied over the range 0.25 to 7% v/v by adding various volumes of monomer to the polymerisation medium such that the final reaction volume was always 25ml. Suspensions above 7% v/v were not free flowing and therefore not examined.

Effect of acidifying agent. Dextran 70 solutions (0.5% w/v) were prepared at pH 2.25 using the following acids: acetic, ascorbic, citric, hydrochloric, nitric, phosphoric and sulphuric.

Effect of pH. The pH of the polymerisation medium was adjusted over the range 1.0 to 3.5, as determined by a calibrated pH meter, by varying the hydrochloric acid concentration.

Effect of temperature. The reaction temperature was varied over the range 4 to 80^{o}C by either cooling the reaction flask with ice or immersing it in a thermostatically controlled water bath ($\pm$ 1^{o}C).

Effect of ionic strength. Sodium chloride or calcium chloride over the concentration range 0.01 to 0.25 mole dm^{-3} were added to the polymerisation medium prior to monomer addition. With calcium chloride, the dextran 70 solution was prepared in distilled water and the final pH adjusted to 2.25 with hydrochloric acid after addition of the electrolyte.

Effect of dextran concentration and molecular weight. The dextran 70 concentration was varied over the range 0.05 to 2.5% w/v. This was repeated with dextran 40 (molecular weight 40000; Sigma) and dextran 10 (molecular weight 10300; Sigma).

Effect of β-cyclodextrin concentration. Dextran 70 in the standard formulation was replaced with β-cyclodextrin (Chinoin Pharmaceuticals, Hungary) and the concentration varied over the range 0.75 to 1.75% w/v. This range was limited by the production of grossly flocculated systems at a concentration less than 0.75% w/v and the

low water solubility of β-cyclodextrin (maximum 1.87% w/v at 25°C) (Szejtli, 1982).

Effect of poloxamer type and concentration. Dextran 70 in the standard formulation was replaced with poloxamer 188 (Pechiney Ugine Kuhlmann, UK) and the concentration of this surfactant varied over the range 0.1 to 2.5% w/v. Poloxamers 184, 237, 238 and 338 (Pechiney Ugine Kuhlmann) were examined at a concentration of 0.5% w/v.

Effect of polysorbate type and concentration. Dextran 70 in the standard formulation was replaced with polysorbate (Tween) 20 (Koch-Light Laboratories, UK) and the concentration of this surfactant varied over the range 0.3 to 2.5% w/v. Polysorbates 40 and 60 (Koch-Light Laboratories) were examined at a concentration of 0.5% w/v.

Effect of Brij 96. Brij 96 (Honeywell-Atlas, UK) was used to replace dextran 70 in the standard preparation at a concentration of 0.5% w/v.

Other stabilisers. In addition to the polysaccharides and surfactants listed above various other stabilisers were used in place of dextran 70. These were polyethylene glycols (PEG's) 400, 600, 1000, 1500 and 6000 (BDH, UK) at concentrations up to 5.0% w/v, polyvinyl- pyrrolidone (BDH) at concentrations up to 5.0% w/v, and glucose (BDH) at 5.0% w/v. With these stabilisers, however, most of the monomer formed an amorphous polymer mass with little or no discrete nanoparticle formation.

The use of the poly-ionic stabilisers dextran sulphate and diethylaminoethyl-dextran is discussed in chapter 4.

2.2.2. Particle Size Analysis

The majority of the nanoparticle samples were analysed by photon correlation spectroscopy (PCS) which offers many advantages over more classical particle sizing techniques such as electron microscopy (McConnell, 1981). The rapid analysis time, minimal sample preparation, and wide applicable size range (5 to 2000nm) are particularly important considering the large number and range of samples under investigation. Examples of the use of PCS in pharmaceutical analysis are available in the literature (Fairbrother, 1979; Roe and Barry, 1983).

Electron microscopy (SEM) was used to validate PCS measurements and to obtain a particle size distribution (PSD). For particles prepared using β-cyclodextrin as the stabiliser, size analysis was performed using a Coulter Counter.

Polystyrene latex standards of diameter 166 and 450nm were obtained from Polysciences (USA) and a standard of diameter 390nm was kindly donated by Dr.J. Hearn (Trent Polytechnic). These were all sonicated for 20 minutes prior to use.

2.2.2.1. Photon correlation spectroscopy

The instrument used was based on a commercially available Malvern system (Malvern Instruments, UK) and is represented diagrammatically in figure 2.1. This consisted of a 14mW, 441.6nm,

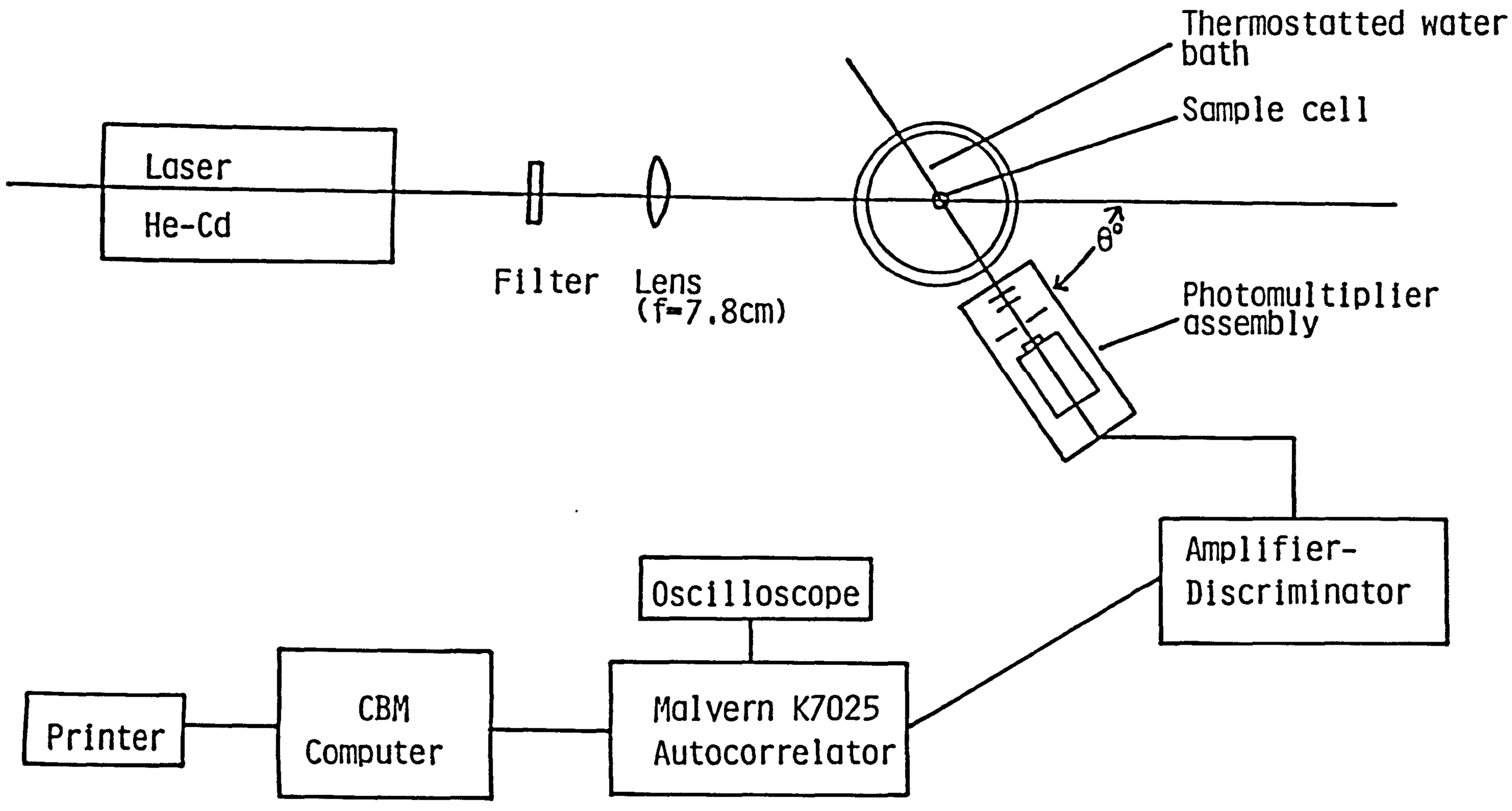

Figure 2.1. Diagrammatic representation of the PCS apparatus.

helium-cadmium laser (Liconex, USA) irradiating the scattering cell held in a thermostatted water bath at 25 ± 0.05°C. The resulting scattered light was detected at 90° by a variable angle photon detection system which transmitted the signal to a Malvern K7025, 64-channel, multibit correlator (Malvern Instruments). This was interfaced with a Commodore PET 2001-32N microprocessor (Commodore Business Machines, USA) and the correlation data were analysed by a Malvern Applications Program (7025 Spect.I.VI; Malvern Instruments). Details concerning the adjustment and maintenance of this instrument have been given by Pearce (1984).

Samples were diluted before measurement with distilled water freshly filtered through a 0.2μm membrane filter (Whatman). The optimum correlation sample time was determined for each nanoparticle suspension since both the calculated diameter and polydispersity index vary according to the sample time employed (Derderian and MacRury, 1981) and this in turn depends upon the size and PSD of each suspension. This is shown for a polystyrene latex sample in figure 2.2. Each sample was then analysed a total of 15 times to give an average value for the particle diameter and polydispersity index. The coefficient of variation for the diameter measurements was less than 3.0% and the measurement standard deviation of the polydispersity index typically 0.02.

2.2.2.2. Scanning electron microscopy

The nanoparticle suspensions were applied to a hydrophilic copper plate and freeze-dried before coating with a platinum/carbon film. Samples were examined in a Hitachi S-700 FE-SEM (Hitachi

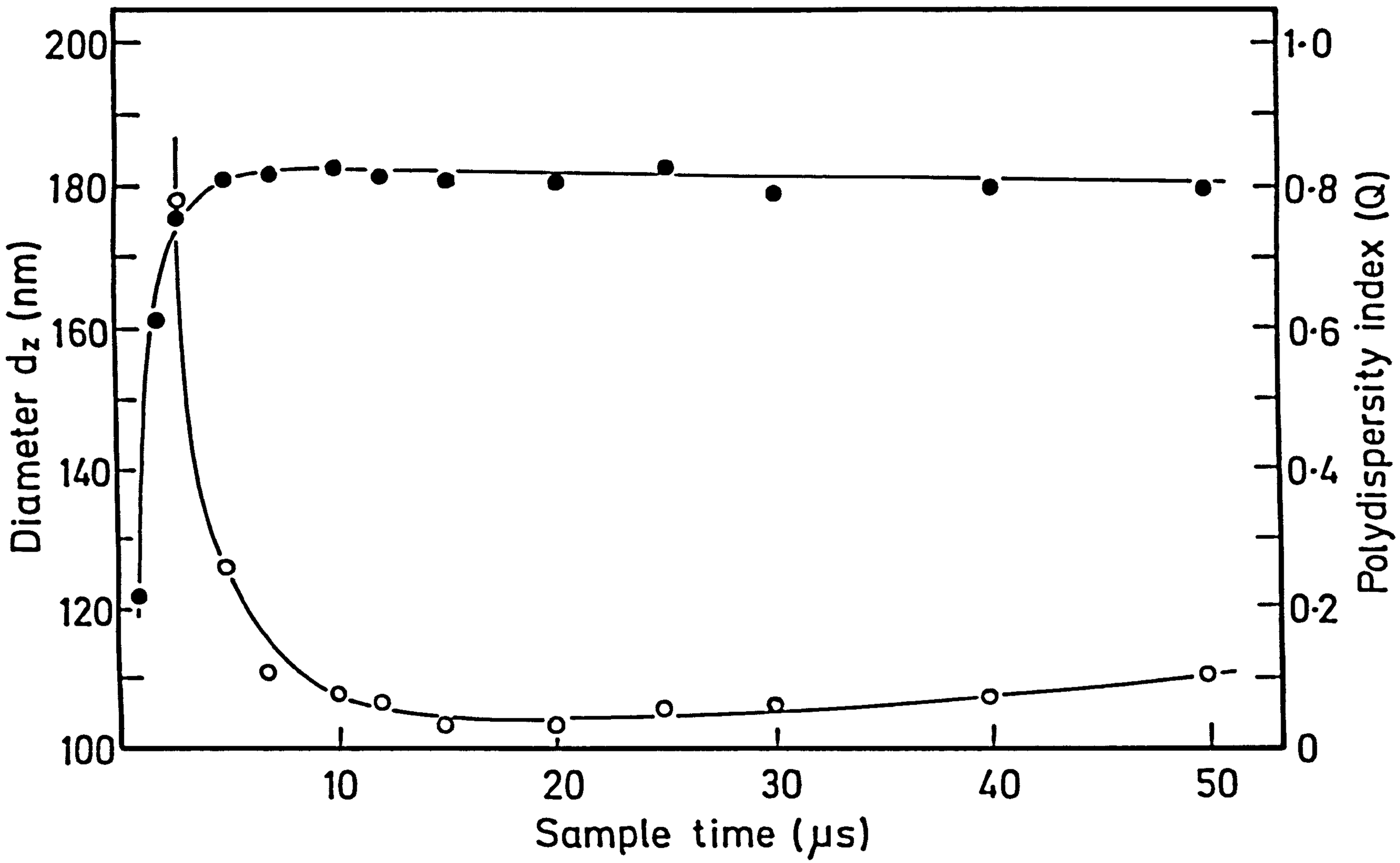

Figure 2.2. Variation of PCS measured particle size and polydispersity index with correlator sample time (sample 166nm polystyrene latex).

Electronics, Japan), fitted with a field emission electron source, at an excitation energy of 20kV and magnifications of either 20000, 45000 or 90000. Photographic prints of the electron micrographs were then examined with a particle size analyser (Model TGZ3, Carl Zeiss, FRG). A minimum of 300 individual particles were analysed for each sample.

2.2.2.3. Coulter Counter

For nanoparticle systems with an average diameter larger than 2μm the particle size analysis was performed using a Coulter Counter (Model TA, Coulter Electronics, UK). The apparatus was fitted with a 30μm-orifice tube previously calibrated with polystyrene latices or pollens of known diameter. Samples were diluted with a suitable electrolyte (Isoton II, Coulter Electronics).

2.3. RESULTS AND DISCUSSION

2.3.1. PCS Theory and Interpretation of Results

Measurement of particle size by PCS is based on the theory that the observed time dependence of the fluctuations in intensity of scattered light from a colloidal dispersion, is a function of the size of the scattering particles (Chu, 1974). When a colloidal system is illuminated by a laser light source the relative phases of the scattered light waves from different particles vary as the particles undergo Brownian motion, causing the intensity of scattered light at the detector to fluctuate with time. Although fluctuations for individual particles occur randomly there is a well

defined lifetime for the build up and decay of scattered light intensity as shown in figure 2.3 (Pusey et al, 1974).

The particle size of the system is found through the technique of photocount autocorrelation (Pusey et al, 1974). To understand this process consider the intensity curve of figure 2.3 as being divided into time intervals of length T, which in practice is the correlator sample time. During any sample time the scattering intensity is proportional to the number of detected photons which for a typical PCS experiment gives approximately one million individual sample intervals, i, each containing a photocount, n. The number of photons detected in sampling interval i, centred on time t_i, is then defined as $n(t_i)$. The autocorrelator then constructs the sum of products

$$\sum_{i=1}^{i=(N-M)} n(t_i).n(t_{i+m}) \qquad [2.2]$$

for a range of delay times, mT (also given as τ), where m = 1,2,3,..,M, and M is the number of channels built into the autocorrelator. N is the number of sampling intervals of length T in the experimental run. As the experiment proceeds the second order autocorrelation function, $G_2(\tau)$, accumulates in the correlator channels until time NT. The resulting $G_2(\tau)$ is normalised by dividing by the square of the mean scattering intensity to give the normalised second order autocorrelation function, $g_2(\tau)$.

Through the Siegert relation (Goodall et al, 1980) $g_2(\tau)$ may be given in terms of the normalised first order autocorrelation function, $|g_1(\tau)|$, by

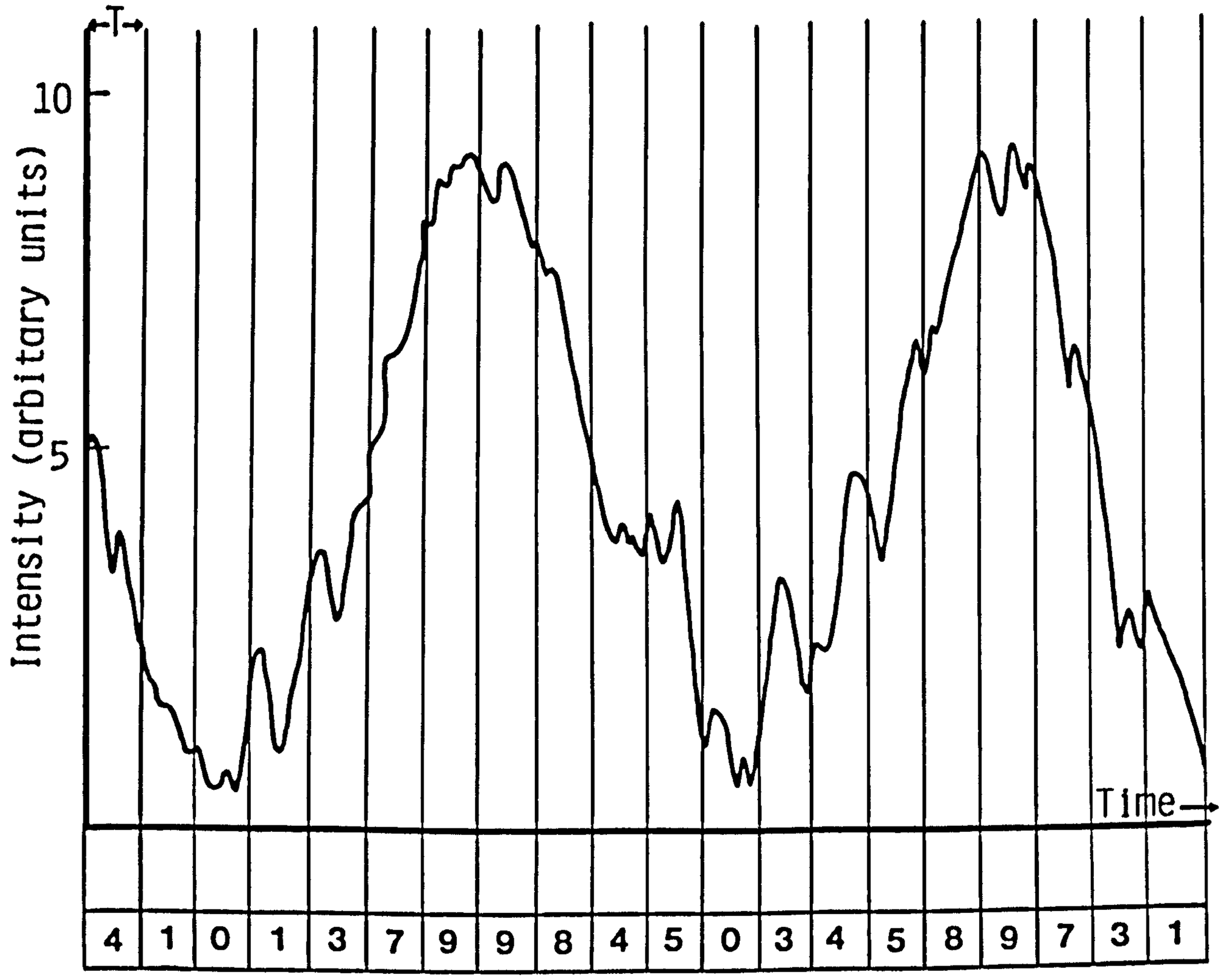

Figure 2.3. Typical trace of fluctuating scattered light intensity from a colloidal dispersion and the corresponding distribution of photocounts (Pusey et al, 1974).

Assigning the the photocount (n) in the first time interval (t_1) as nt_1 and the total number of intervals as N, then the channel contents for a 64 channel auto-correlator would contain the following sums of products:

Channel 1 = $(nt_1.nt_2) + (nt_2.nt_3) + (nt_3.nt_4) + \ldots\ldots\ldots\ldots\ldots(nt_{N-64}.nt_{N-63})$.

Channel 2 = $(nt_1.nt_3) + (nt_2.nt_4) + (nt_3.nt_5) + \ldots\ldots\ldots\ldots\ldots(nt_{N-64}.nt_{N-62})$.

Channel 64 = $(nt_1.nt_{65}) + (nt_2.nt_{66}) + (nt_3.nt_{67}) + \ldots\ldots\ldots\ldots\ldots(nt_{N-64}.nt_N)$.

$$g_2(\tau) = 1 + |g_1(\tau)|^2 \qquad [2.3]$$

The translational diffusion coefficient, D, of the particles can now be obtained since

$$|g_1(\tau)| = \exp(-\Gamma\tau) \qquad [2.4]$$

where Γ, the decay constant, is related to the scattering vector, K, and D by

$$\Gamma = DK^2 \qquad [2.5]$$

and

$$K = \frac{4\,\Pi\, n \sin(\theta/2)}{\lambda} \qquad [2.6]$$

in which n is the index of refraction of the scattering medium, θ is the scattering angle and λ the incident laser light wavelength.

Combining equations [2.3] and [2.4] gives

$$g_2(\tau) = 1 + \exp(-2\Gamma\tau) \qquad [2.7]$$

or

$$\ln[\, g_2(\tau)-1\,] = -2\Gamma\tau \qquad [2.8]$$

A plot of $\ln[\, g_2(\tau)-1\,]$ vs τ, therefore, gives a straight line of slope -2Γ. D is then calculated from equation [2.5] and used to obtain the equivalent spherical hydrodynamic diameter, d_h, by recourse to the Stokes-Einstein equation

$$d_h = \frac{k\,T}{3\,\Pi\,\eta\,D} \qquad [2.9]$$

where k is Boltzmann's constant, T is the absolute temperature and η the solvent viscosity.

The above treatment only applies strictly for a monodisperse system of non-interacting particles that are small compared with the incident light wavelength. However, for a polydisperse system

$|g_1(\tau)|$ consists of a sum of exponentials (Pusey et al, 1974) given as

$$|g_1(\tau)| = \int_0^\infty G(\Gamma)\, \exp(-\Gamma\tau)\, d\Gamma \qquad [2.10]$$

where $G(\Gamma)$ is the normalised distribution of decay rates.

The complete solution to equation [2.10] can be obtained by Laplace inversion. This is impossible, however, given the precision of the experimental data and an alternative method has to be used. One approach is Koppel's (1972) method of cumulants which involves expanding $\exp(-\Gamma\tau)$ about $\exp(-\bar{\Gamma}\tau)$, where $\bar{\Gamma}$ is the mean decay rate, giving the expression (Brown et al, 1975)

$$\ln[\, C^{0.5}.|g_1(\tau)|\,] = \ln(C^{0.5}) - \bar{\Gamma}\tau + \frac{1}{2!}\left|\frac{\mu_2}{\bar{\Gamma}^2}\right|(\bar{\Gamma}\tau)^2 - \frac{1}{3!}\left|\frac{\mu_3}{\bar{\Gamma}^3}\right|(\bar{\Gamma}\tau)^3 + \ldots., \qquad [2.11]$$

where μ_r is the rth moment about the mean of $G(\Gamma)$ and the parameter C is a constant depending on the optical design (Brown et al, 1975).

Although this equation is only exact when all terms are considered, the data can usually be adequately described by the first few terms. Data analysis then involves a curve fitting procedure to the first two terms of equation [2.11], giving the mean and variance of $G(\Gamma)$. The z-average diffusion coefficient and the equivalent z-average particle diameter, dz, (Green et al, 1976) may be calculated from $\bar{\Gamma}$ and the z-average variance of the distribution is given by

$$Q = \mu_2 / \bar{\Gamma}^2 \qquad [2.12]$$

where Q is known as the quality parameter or polydispersity index (Pusey et al, 1974). For a monodisperse system Q should be zero theoretically although this is difficult to achieve in practice (for example, we found for a monodisperse latex Q≈0.03). Values of Q < 0.02 suggest approximate monodispersity whereas values of Q < 0.2 suggest relatively narrow distributions (Pearce, 1984). If Q is larger than 0.2 it can only be considered as a qualitative guide to polydispersity because the mathematical approach to calculating Q becomes invalid at these distribution bandwidths (Pearce, 1984).

PCS data can alternatively be analysed by a number of other mathematical techniques (Chu et al, 1979) to yield a PSD, although these treatments are highly involved and require very precise data which are susceptible to experimental error. Provided the PSD is log-normal, however, it is possible to derive a relationship describing the distribution of sizes (Pearce, 1984) by utilising the second moment about the mean of the size distribution (Hearden, 1960) and relating this to the polydispersity index as given by

$$G(d) = [2\pi \ln(1+Q)]^{-0.5} \times \exp -\frac{\{\ln d - \ln[\, dz/(1+Q)^{2.5}\,]\}^2}{2\ln(1+Q)} \qquad [2.13]$$

where G(d) is the relative number population of particle size d.

By solving this equation over the appropriate size range the PSD may be obtained in terms of particle number. A computer program has been written to do this and details are given in appendix I. Equation [2.13] is based on the equation for a log-normal PSD which may be accurately defined in terms of its geometric mean diameter,

dg, and geometric standard deviation, σ g (Hearden, 1960). These two terms can be obtained by reference to equation [2.13] as

$$dg = dz/(1 + Q)^{2.5} \qquad [2.14]$$

and

$$\sigma g = \exp\{[\ln(1 + Q)]^{0.5}\} \qquad [2.15]$$

Using dg and σg it is possible to calculate any of the classical average particle diameters (Hatch and Choate, 1929; Hatch, 1933). For example, the number average diameter, dn, is given by

$$dn = \exp(\ln dg + 0.5 \ln^2 \sigma g) \qquad [2.16]$$

Calculation of dn is particularly important since this can be compared directly with dn obtained by electron microscopy.

Although this theory is relatively simple and easy to apply, it is subject to several constraints; mainly that the PSD must be log-normal and unimodal, and for highly polydisperse samples the mean size should be small compared with the wavelength of the laser. Sample contamination with dust must be avoided since this would adversely increase values of dz and Q.

This theory was tested by comparing PCS and SEM measurements of colloidal dispersions, as shown in table 2.1. In each case although the diameter calculated from SEM is less than the corresponding PCS diameter, as observed by other workers (Munro and Randle, 1976), the values of dn calculated from dz and Q, according to equation [2.16], are in good agreement with those obtained by SEM. Figure 2.4 gives a typical particle size histogram from scanning electron micrograghs of p(BCA) nanoparticles and shows the system to be log-normally distributed ($r = 0.9977$ for the corresponding log-probability plot) and unimodal as required by the constraints to equation [2.13].

TABLE 2.1 Comparison of dn calculated from dz and Q values obtained by PCS with dn obtained from electron microscopy (EM).

Sample	dz (nm)	Q	dn from dz and Q (nm)	dn determined by EM (nm)
Nanoparticle	203	0.079	174	165
Nanoparticle	160	0.103	131	122
Nanoparticle	159	0.150	120	130
Latex	180	0.037	168	166
Latex	417	0.044	383	390
Latex	469	0.033	440	450

Polystyrene latex EM size was determined by the supplier.

Nanoparticles composed of p(BCA).

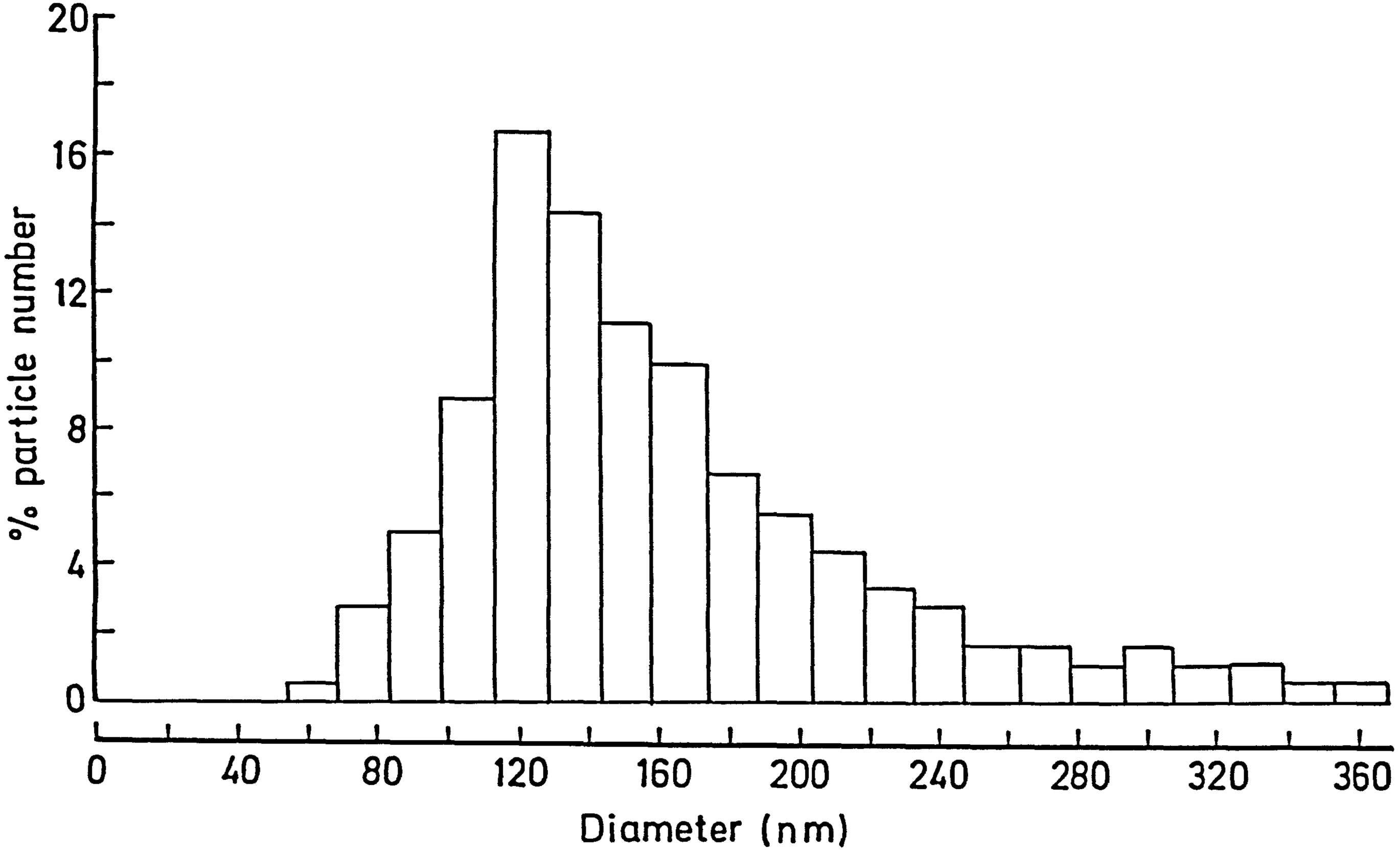

Figure 2.4. Particle size histogram of p(BCA) nanoparticles determined by electron microscopy. The distribution is log-normal and unimodal.

Figure 2.5 compares the theoretical PSD's calculated from PCS data and the log-probability plot of the histogram and shows a reasonable agreement between the two. Thus, while recognising the limitations to the use of this theory, it does provide a useful means of estimating the theoretical nanoparticle PSD and obtaining a range of average particle diameters.

2.3.2 Influence of Physico-chemical Factors on Nanoparticle Size

2.3.2.1 Influence of stirring rate and ultrasonication

The variation of nanoparticle diameter and polydispersity index with stirring rate is shown in table 2.2. Although dz was found to increase approximately linearly with stirring rate this was accompanied by a general increase in Q, thereby resulting in no significant change in dn with speed. It appears that the mean diameter of the system remains constant but the width of the distribution increases with stirring rate. Therefore, over the range investigated, stirring rate does not significantly affect the mean size of the resulting nanoparticles.

As an alternative method for dispersing the monomer throughout the polymerisation medium, ultrasonication was investigated by employing either an ultrasonic bath or probe. The ultrasonic bath was found to be unsuitable due to incomplete dispersion of the monomer in the aqueous phase. The use of an ultrasonic probe resulted in formation of nanoparticles with a dz of 409nm and an unacceptably high polydispersity index of 0.22. Ultrasonication is

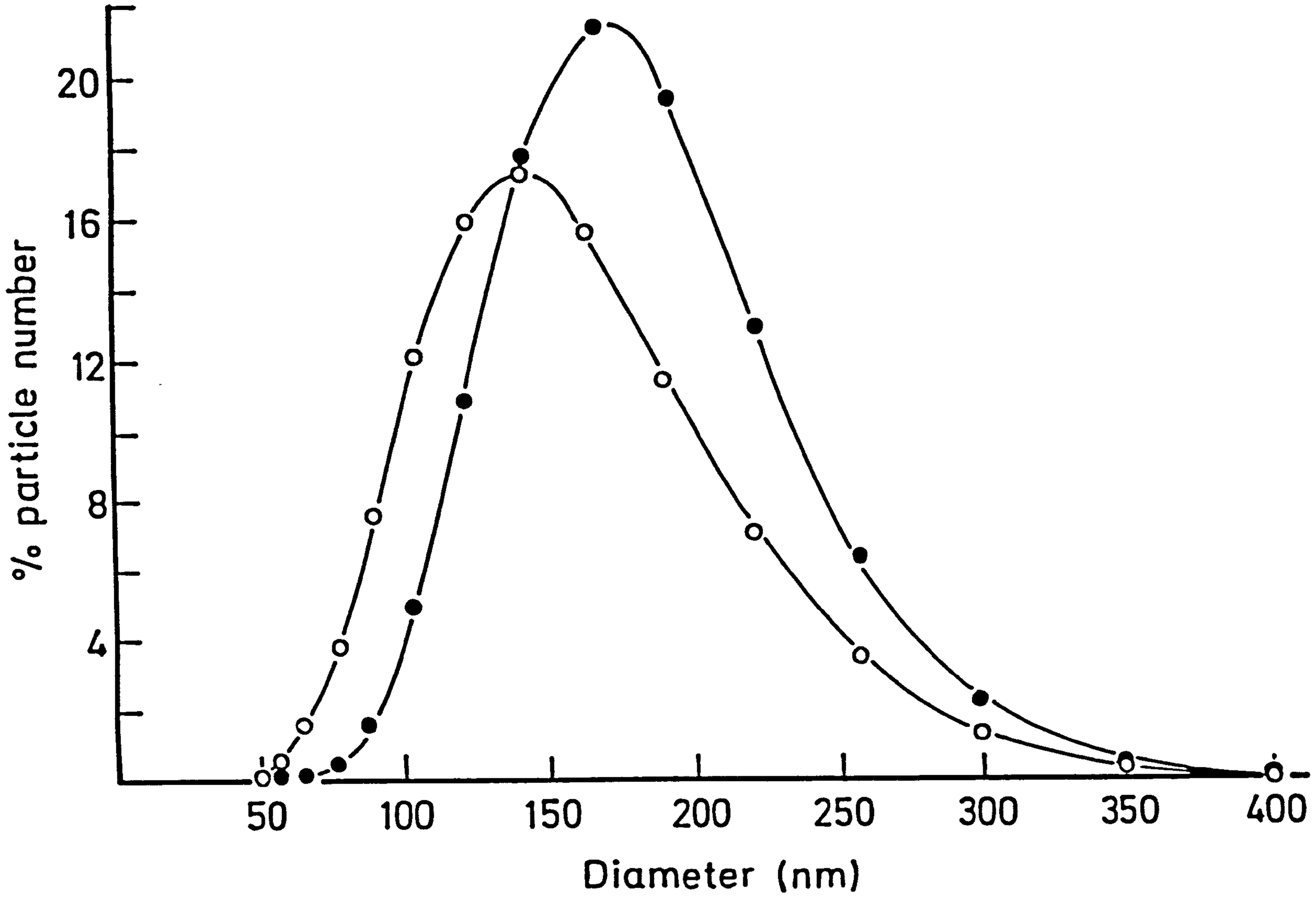

Figure 2.5. Theoretical particle size distributions calculated from PCS data according to equation 2.13 (●) and the log-probaility plot of the particle size histogram (o).

TABLE 2.2 Influence of stirring rate on the average particle diameter and polydispersity index of p(BCA) nanoparticles.

Stirrer speed (rpm)	dz (nm)	Q	dn (nm)
600	126	0.070	110
750	131	0.087	111
1000	136	0.099	113
1500	137	0.071	119
2000	142	0.140	109
2500	148	0.121	118
3000	161	0.149	122

therefore considered an unsuitable method for nanoparticle production.

2.3.2.2. Influence of monomer concentration

The variation in particle diameter and polydispersity index for p(BCA) nanoparticles as a function of the initial monomer concentration is given in figure 2.6. Although it was possible to change the nanoparticle size by varying the initial monomer concentration, the pattern is complex and limited by the importance of a low polydispersity index and the maximum monomer concentration of 7% v/v for a free flowing suspension. At low monomer concentrations, below 1% v/v, Q was found to be high, but decreased rapidly with increasing monomer concentration. Both dz and dn show increases for monomer concentrations up to 1% v/v, a subsequent fall over the range of 1 to 2.5% v/v, and a final increase at higher concentrations. This complex pattern is unexpected. A monotonic increase in size with monomer concentration would have been expected from the results of other workers (Goodwin et al, 1978; Rembaum et al, 1979) who found the particle size of various latex systems to increase with monomer concentration as shown, for example, by equation [2.1].

2.3.2.3. Influence of acidifying agent

The results obtained with the various acids investigated are shown in table 2.3. Hydrochloric, sulphuric, nitric and citric acids were all found to be suitable agents for nanoparticle production

Figure 2.6. The influence of monomer concentration on the particle size and polydispersity index of p(BCA) nanoparticles.

(●) polydispersity index, Ω

(o) dz

(Δ) dn

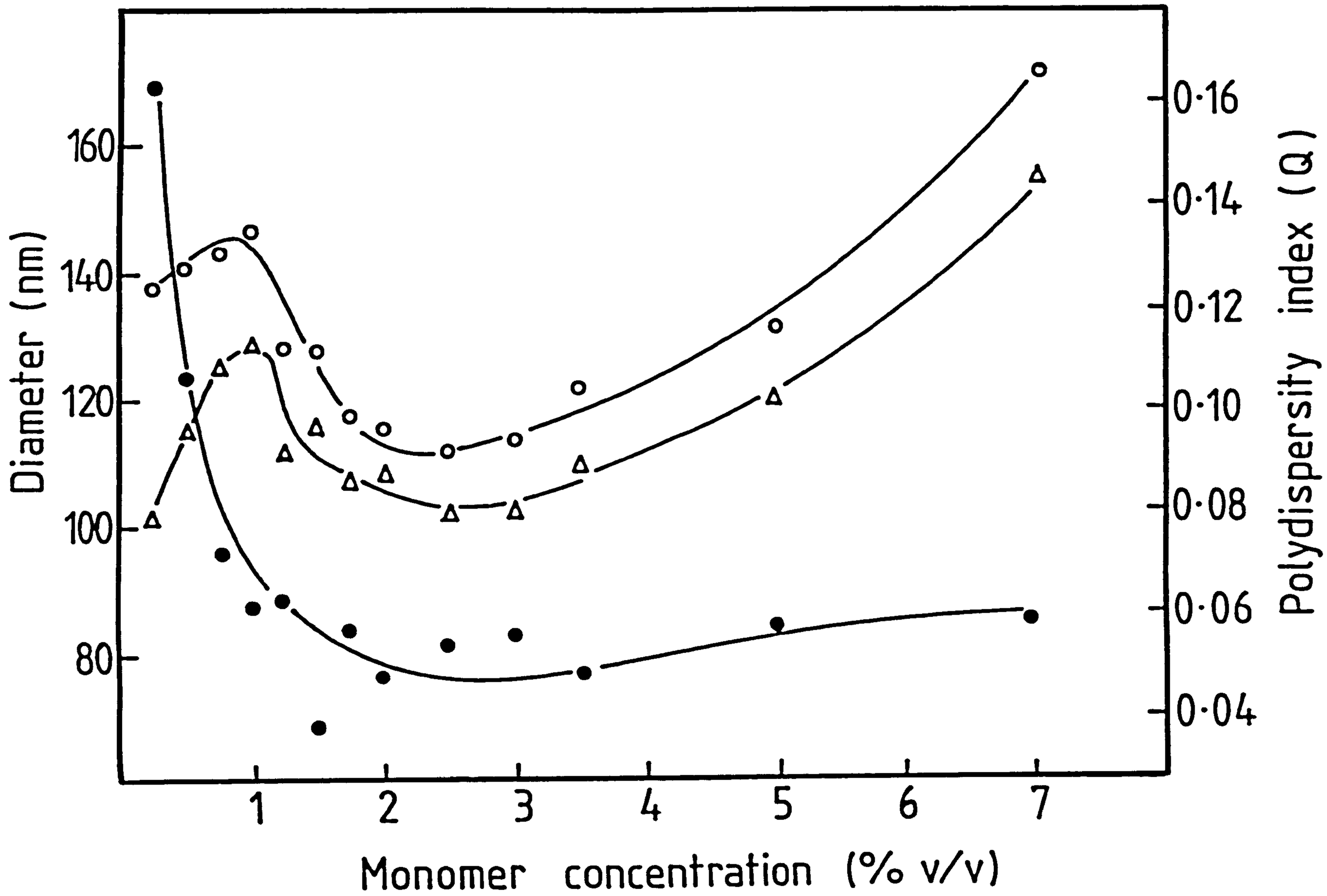
160
140
120
100
80
Diameter (nm)
0·16
0·14
0·12
0·10
0·08
0·06
0·04
Polydispersity index (Q)
1
2
3
4
5
6
7
Monomer concentration (% v/v)

TABLE 2.3 Influence of acidifying agent at pH 2.25 on the particle size and polydispersity index of p(BCA) nanoparticles.

Acid	dz (nm)	Q	dn (nm)
Hydrochloric	148	0.062	131
Citric	131	0.066	115
Sulphuric	176	0.048	160
Nitric	158	0.081	135
Acetic	811	0.201	562
Ascorbic*			

* failed to yield discrete particles.

with little difference in the resultant nanoparticle diameter or polydispersity index. The phosphoric acid system, however, produced particles with a wide PSD as indicated by the high value of Q. Acetic acid is not suitable since high concentrations were required to give the correct pH for polymerisation and the resultant nanoparticles had a high polydispersity index. The large average particle size obtained with acetic acid is probably due to swelling of the nanoparticles caused by incorporation of the acid within the polymer matrix of the particles. Attempts at nanoparticle formation employing ascorbic acid as the acidifying agent failed to yield any discrete particles. No advantage, therefore, is to be gained by using an acid other than dilute hydrochloric acid as the acidifying agent.

2.3.2.4. Influence of pH

The effects of pH on dz, dn, and Q are given in figure 2.7. The particle size shows a minimum at pH 2 for dz and, due to the changing value of Q, a slightly lower minimum for dn. The polydispersity index falls with increasing pH and reaches a plateau at pH 2.5. At pH greater than 3.5 polymerisation was too rapid to allow discrete particle formation and at pH less than 1 too slow to be applicable in practice; at pH 0.5 the polymerisation process was incomplete after 2 days at room temperature.

These results may be explained by reference to the polymerisation mechanism outlined in scheme 2.1. Polymerisation occurs via an anionic mechanism (Coover and McIntire, 1979) involving initial nucleophilic attack on the β-carbon of BCA. The

Figure 2.7. The influence of polymerisation pH on particle diameter and polydispersity index for p(BCA) nanoparticles.

(●) polydispersity index, Q

(o) dz

(▵) dn

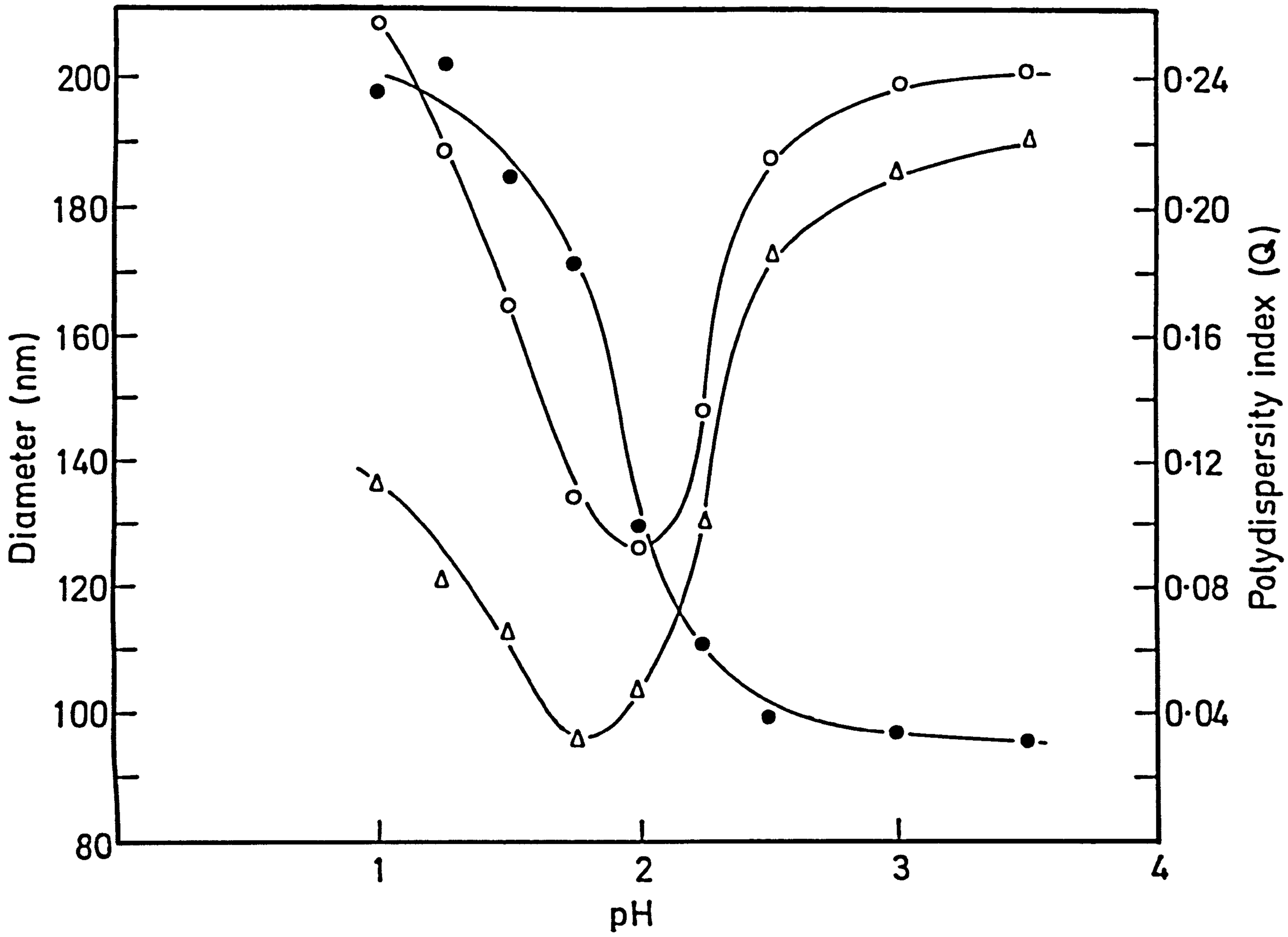
200
180
160
140
120
100
80
Diameter (nm)
0·24
0·20
0·16
0·12
0·08
0·04
Polydispersity index (Q)
1
2
3
4
pH

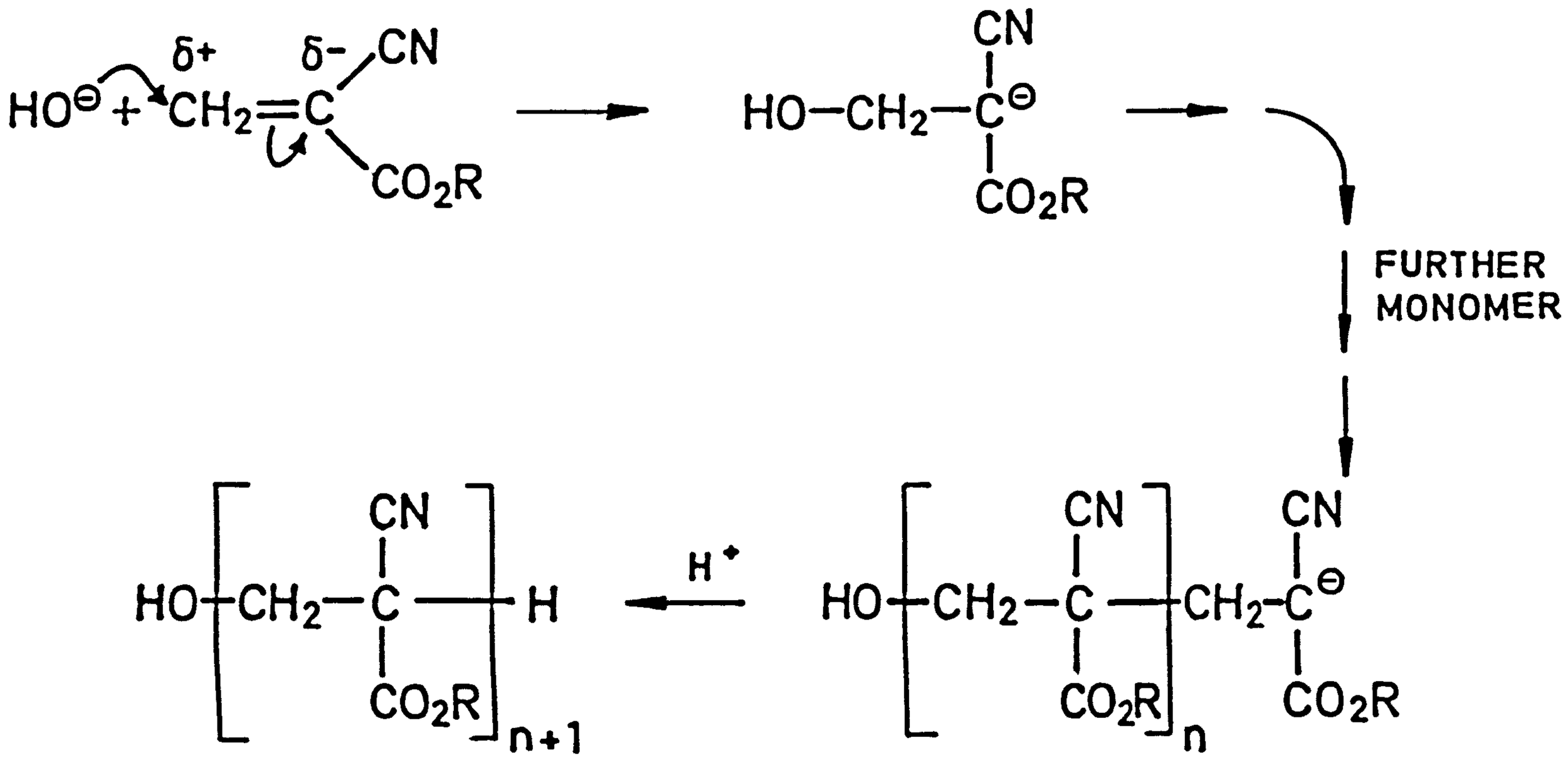

Scheme 2.1. Polymerisation mechanism of alkyl 2-cyanoacrylates under aqueous conditions (R= alkyl).

resulting carbanion reacts with further monomer to give oligomeric chains which nucleate leading to the formation of nanoparticles. The major initiating nucleophile under aqueous conditions is OH^-, the concentration of which will vary with pH. At high pH and hence high hydroxyl ion concentration, the polymerisation rate is too rapid to allow particle formation and leads to the direct polymerisation of monomer droplets producing an amorphous polymer mass. As pH decreases the decrease in reaction rate allows discrete nanoparticle formation to occur. If the pH is too low, however, the polymerisation period is greatly extended and nanoparticles in this system become swollen with monomer. Coagulation of these semi-fluid particles is not reversible and produces a polydisperse system of larger particles. Hence, a minimum size is observed in the pH profile when polymerisation is slow enough to give discrete nanoparticles but not too slow to allow excessive particle coagulation.

Control of nanoparticle size by varying the polymerisation pH may be achieved to a small degree within the range pH 2 to 3.5. The use of pH values below 2 is precluded by slow rates of reaction and the formation of systems with a broad particle size distribution.

2.3.2.5. Influence of temperature

Although altering the reaction temperature would be expected to change the rate of polymerisation its effect is obviously not as critical as the influence of pH on reaction rate and consequent particle size, as shown by the results in table 2.4. The slight increase in dz and Q with temperature is probably due to an increase

TABLE 2.4 Influence of polymerisation temperature on the particle size and polydispersity index of p(BCA) nanoparticles.

Temperature (^{o}C)	dz (nm)	Q	dn (nm)
4	152	0.062	135
20	148	0.062	131
35	156	0.070	136
50	157	0.072	137
65	163	0.073	142
80	171	0.097	142

in particle coagulation caused by the rise in kinetic energy of the system producing a broader particle size distribution; dn, however, remains fairly constant indicating that the mean particle size is unaffected.

Temperature, therefore, does not constitute a suitable variable for the control of nanoparticle size and there is no advantage to be gained by working at other than ambient temperature.

2.3.2.6. Influence of added electrolytes

Table 2.5 shows the addition of sodium chloride or calcium chloride to the polymerisation medium, over the concentration range 0.01 to 0.25 mole dm^{-3}, had no effect on nanoparticle size or PSD. These results imply that the surface charge of p(BCA) nanoparticles is not important with respect to particle size or maintenance of colloidal stability and indicates that the system is sterically stabilised. If particle surface charge was responsible for maintaining stability, the final nanoparticle size would be highly dependent upon the ionic strength of the polymerisation medium as found by Goodwin et al (1978) (see section 2.1).

2.3.3. Influence of Stabilisers on Nanoparticle Size

2.3.3.1 Influence of concentration and molecular weight of dextran

Dextrans are a homologous series of polysaccharides composed of D-glucopyranose units with predominantly α-(1-6) linkages. They are available in a wide range of molecular weights, produced by the controlled degradation of high molecular weight dextrans to yield

TABLE 2.5 Influence of added electrolyte concentration and valency on the particle size and polydispersity index of p(BCA) nanoparticles.

Concentration (mole dm^{-3})	Sodium chloride			Calcium chloride		
	dz (nm)	Q	dn (nm)	dz (nm)	Q	dn (nm)
0.01	147	0.069	129	146	0.072	127
0.02	152	0.072	132	151	0.052	136
0.05	149	0.062	132	145	0.054	131
0.10	144	0.058	129	144	0.061	128
0.15	150	0.064	133	147	0.073	128
0.25	146	0.068	128	145	0.057	130

smaller dextrans with essentially the same structure but of considerably lower molecular weight.

The influence of concentration and molecular weight of dextran on nanoparticle size and polydispersity index is given in table 2.6. It was found that at concentrations less than 0.5% w/v an increase in dextran concentration resulted in a marked decrease in particle size with all three molecular weights of dextran; the lowest (dextran 10) showing the largest variation with concentration. This concentration effect, however, was much less pronounced over the concentration range 0.5 to 2.5% w/v. The variation in polydispersity index showed a general increase with stabiliser concentration for dextrans 40 and 70 concentration but a decrease with dextran 10. Similar findings concerning the variation of particle size with stabiliser concentration have been reported for the formation of poly (methyl methacrylate) particles in the presence of graft copolymer dispersants (Walbridge, 1975).

A simple linear relationship between nanoparticle size and dextran concentration can be found for the concentration range investigated according to

$$D = \frac{m}{\log c} + i \qquad [2.17]$$

where D is the particle diameter (dz or dn), c is the corresponding dextran concentration, and m and i are constants specific to the dextran molecular weight and average diameter utilised. This relationship is shown graphically in figure 2.8.

The effect of dextran concentration on nanoparticle size can be explained by reference to the theory of particle formation in

TABLE 2.6 Variation of dz, dn and Q with dextran concentration and molecular weight.

Conc. (% w/v)	Dextran 70			Dextran 40			Dextran 10		
	dz (nm)	Q	dn (nm)	dz (nm)	Q	dn (nm)	dz (nm)	Q	dn (nm)
0.05	212	0.049	193	243	0.027	230	770	0.147	585
0.10	181	0.060	161	196	0.036	182	575	0.108	469
0.25	156	0.051	141	158	0.039	146	247	0.079	212
0.50	148	0.062	131	145	0.050	132	168	0.056	150
1.00	138	0.056	123	134	0.086	114	139	0.051	126
2.50	126	0.094	105	131	0.116	105	109	0.058	97

Figure 2.8. Graphical representation of the linear relationship between dz and the reciprocal log concentration of dextran as defined by equation 2.17 over the concentration range 0.05 to 2.50% w/v.

Linear regression analysis of the data gives the following results where m is the slope of the line, i is the intercept and r is the correlation coefficient.

(o) dextran 10 (m = 707, i = -213, r = 0.9845)

(●) dextran 40 (m = 115, i = 79, r = 0.9979)

(▵) dextran 70 (m = 82, i = 96, r = 0.9957)

Similar results can be obtained for dn.

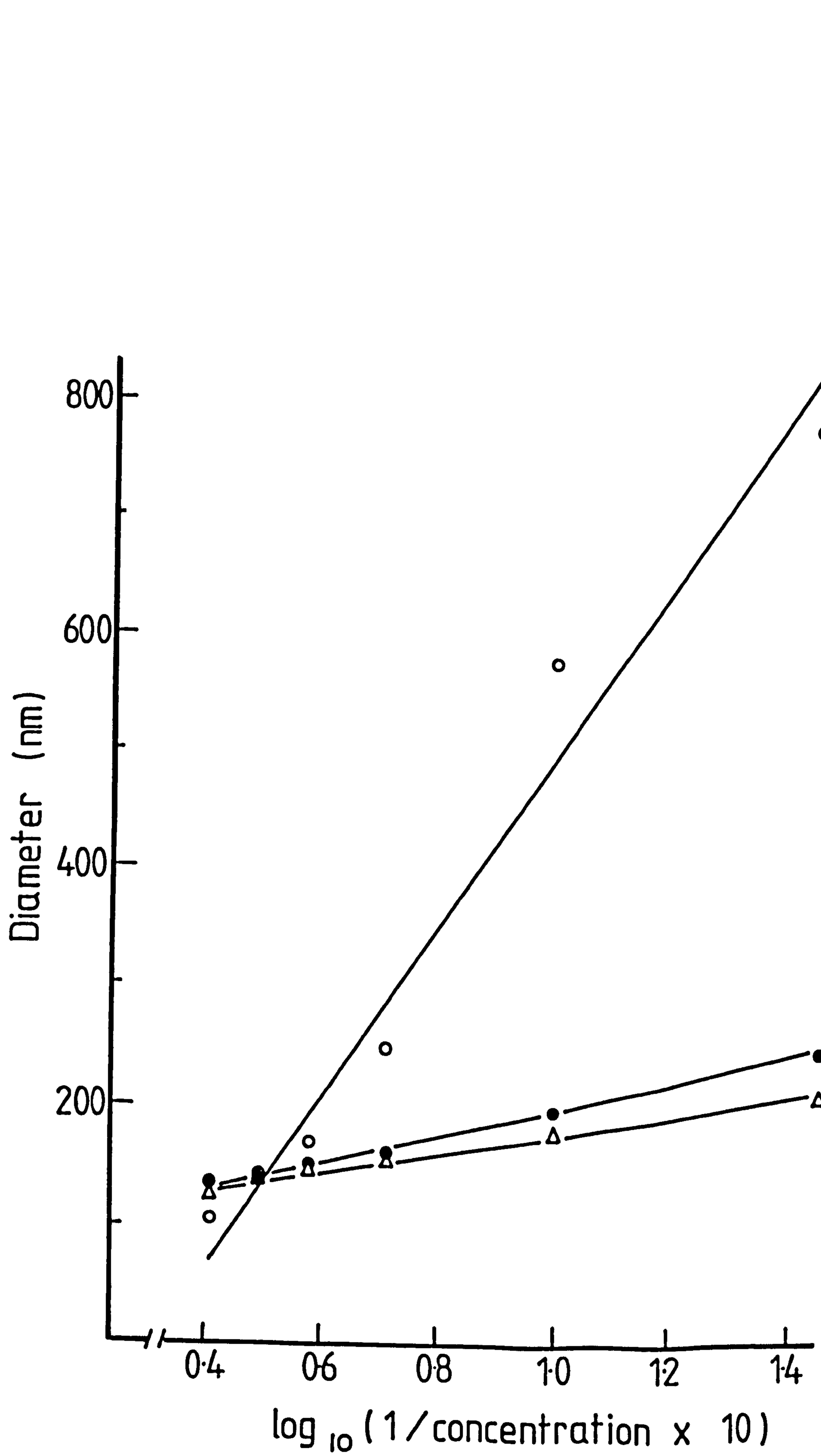
800
600
400
200
Diameter (nm)
0·4
0·6
0·8
1·0
1·2
1·4
log 10 (1/concentration x 10)

dispersion polymerisation (Barrett and Thomas, 1975). Nanoparticle formation is believed to occur via a nucleation mechanism in an analogous manner to other polymer colloids (Fitch, 1971 and 1973). Initiation of polymerisation in the aqueous phase results in the formation of oligomeric chains which grow in solution until they reach a critical molecular weight which is dependent upon the solubility of the oligomer in the reaction medium. The chains then either collapse upon themselves producing particle nuclei (self-nucleation) or several growing oligomeric chains may associate with each other to form an aggregate which, above a certain critical size, precipitates forming a new stable nucleus (aggregative nucleation). In either case the nuclei can grow by capture of further oligomers from solution or by absorption of monomer which subsequently polymerises within the particle matrix. The stability of the resultant colloidal system is achieved by uptake of polymeric stabilisers, i.e. dextrans, from solution.

The initial high number of particle nuclei and their small particle size results in a very large total surface area. At low dextran concentrations the amount of stabiliser is insufficient to cover the available surface effectively, resulting in an unstable colloidal system. These small particles therefore agglomerate until the total particle surface area has decreased to a point such that the amount of dextran available is sufficient to produce a stable suspension. Normally this process leads to a grossly flocculated system with a wide particle size distribution. However, as seen in this study (table 2.6), controlled agglomeration and the growth of a narrowly disperse particle population is possible. This effect is

indicative of a process whereby the stabilising polymer is irreversibly attached to the particle surface, as has been reported (Barrett and Thomas, 1975) for poly (methyl methacrylate) particles produced using a dispersant which anchors irreversibly to the particle surface through copolymerisable groups.

At increased dextran concentrations it is possible to stabilise effectively a larger total particle surface area, resulting in the formation of stable nanoparticles of a lower size. Above a certain dextran concentration, however, nanoparticle size was found to remain fairly constant in each system. This constancy indicates the presence of an additional limiting mechanism at high dextran concentrations, which determines a final particle size.

The differences in particle size between nanoparticle systems prepared with the same concentration of the three molecular weights of dextran over the range 0.05 to 0.5% w/v, as seen in table 2.6, can be explained by considering the theoretical aspects of steric stabilisation. Although a full treatment of this complex subject is not presented here, comprehensive reviews are available (Vincent, 1974; Sato and Ruch, 1980).

The total interactive energy, V_t, produced by the approach of two polymer coated particles is given by

$$V_t = V_a + V_{rE} + V_{rS} \qquad [2.18]$$

where V_a is the van der Waals' attractive potential energy, V_{rE} is the electrical repulsive energy and V_{rS} is the steric repulsive energy of the polymer overlap interaction. If V_t is negative upon close approach of the two particles, flocculation or coagulation will occur, whereas if it is positive, colloidal stability will be

maintained. In the case of particles with low surface charge, i.e. small V_{rE}, the sign of V_t will be determined largely by the magnitude of V_{rS} in a sterically stabilised system. V_{rS}, which is equivalent to ΔG_s, the Gibbs free energy change of the steric interaction, can be expressed in terms of the enthalpy change, ΔH_s, and entropy change, ΔS_s, of the interaction by

$$\Delta G_s = \Delta H_s - T\Delta S_s \qquad [2.19]$$

Initial attempts at calculating the repulsive potential energy in steric stabilisation by Mackor (1951) considered only the entropic term, ΔS. By a statistical method analysing the approach of two flat plates, one bearing an adsorbed molecule of length 1, the repulsive energy, ΔG_e, due to the entropy change at a given distance, H, was found to be dependent on 1 and the number of adsorbed molecules in a unit surface area at the interface. This derived relationship was used by Sato (1971) to develop an equation describing the stability of iron oxide dispersions in cyclohexane stabilised by fatty polyamides. This was given as

$$\Delta G_e = -T\Delta S = \frac{Ns\ k\ T\ \theta_\infty\ \Pi}{\delta}\ (\delta - d)^2\ (2r + \delta + d) \qquad [2.20]$$

where θ_∞ is the surface coverage when $H = \infty$, Ns is the number of segments extending to the outside of the adsorbed layer, k is Boltzmanns' constant, r is the particle radius, δ is the adsorbed layer thickness and d is the distance from the particle surface to the adsorbed film contact point. Mackor's model has been extended by several other workers such as Clayfield and Lumb (1966), Bagchi and Vold (1970), and Meier (1967).

The enthalpy contribution to ΔG_s was first considered by Fischer (1958) who proposed the excess chemical potential produced by the overlap of adsorbed polymer layers would give rise to a repulsive osmotic force given as ΔG_m, the free energy of mixing repulsion, as

$$\Delta G_m = \frac{4}{3} \Pi R T B C^2 \left(\delta - \frac{H}{2}\right)\left(3r + 2\delta + \frac{H}{2}\right) \qquad [2.21]$$

where R is the gas constant, C is the adsorbed layer polymer concentration and B is the second virial coefficient of the polymer in solution. Similar relationships were obtained by Ottewill and Walker (1968) and Napper (1968). The total interactive repulsive energy due to steric stabilisation, ΔG_s, may be estimated by summing the contributions of ΔG_e and ΔG_m, although this is far from satisfactory considering the different models upon which each theory is based and single modelled calculations are to be preferred (Vincent, 1974). However, by reference to equations such as [2.20] and [2.21] it can be seen that both the osmotic and entropic repulsion models predict that an increase in the adsorption layer thickness, δ , should enhance the stability of a dispersion. Since δ is dependent upon the molecular weight of the polymer (Sato and Ruch, 1980), stability should increase with increasing molecular weight which is reflected in a decrease in particle size as seen in table 2.6.

The contribution of ΔH_s and ΔS_s to the total stabilising effect may be determined by reference to the work of Napper and Netschey (1971) who studied the temperature dependence of ΔG_s which is given by

$$\partial(\Delta G_s)/\partial T = -\Delta S_s \qquad [2.22]$$

From their results it is possible to classify sterically stabilised dispersions close to their critical flocculation temperature as summarised in table 2.7 (Napper, 1977). Heating (autoclaving) p(BCA) nanoparticle supsensions to 121^{o}C at pH 2.2 did not induce flocculation but resulted in a small increase in nanoparticle diameter from 143 to 202nm with no significant change in the polydispersity index. This increase in size is probably due to partial hydrolysis of the polymer resulting in swelling of the nanoparticle matrix. Cooling also failed to induce flocculation unless the supensions were frozen and then thawed, whereupon a flocculated system was produced. This flocculation was not reversible, however, and therefore does not comply with the restraints imposed by equilibrium thermodynamics necessary for the application of this theory (Napper and Netschey, 1971). High dextran concentrations (> 2.5%w/v) were also found to have a protective effect and these suspensions could not be flocculated even after several freeze/thaw cycles. Due to this complex behaviour it is not possible, therefore, to determine whether the nanoparticle suspensions are solely entropically stabilised or whether a combined enthalpic-entropic mechanism applies.

The theory of steric stabilisation also predicts that the steric repulsive energy governing particle size, ΔG_s, is dependent upon the concentration of stabilising polymer in the adsorbed layer, as indicated in equations [2.20] and [2.21] (Sato and Ruch, 1980). This concentration is determined by the bulk polymer concentration, as shown by the results in table 2.6, and the affinity of the

TABLE 2.7 Thermodynamic requirements and thermal methods of flocculating sterically stabilised dispersions (Napper and Netschey, 1971).

ΔH_s sign	ΔS_s sign	$\lvert T\Delta S_s\rvert / \lvert\Delta H_s\rvert$	Stabilisation type	Flocculation method
+	+	< 1	Enthalpic	Heat
+	0	0	Enthalpic	Not possible
-	-	> 1	Entropic	Cool
0	-	∞	Entropic	Not possible
+	-	$>_<$ 1	Enthalpic-entropic	Not possible

stabiliser for the particle surface. Amphiphatic block or graft copolymers are found to be the best stabilisers in dispersion polymerisation (Walbridge, 1975) since these contain anchoring moieties with a high particle surface affinity and stabilising moieties soluble in the dispersion medium. These 'dual' properties ensure the stabiliser remains firmly attached to the particle surface while maintaining an adsorbed layer thickness of sufficient magnitude to produce a strong steric repulsive interaction. Dextran, however, being a totally hydrophilic polymer does not fit into this category and would be expected to have a poor affinity for the nanoparticle surface and therefore be a poor stabiliser. Although stability by free polymer in solution could be imparted by depletion stabilisation, this is only observed at polymer concentrations higher than those required to cause the onset of depletion flocculation (Napper, 1982) and certainly greater than those employed here. Also, nanoparticles may be redispersed readily by sonication after removal of the free dextran in solution. These 'cleaned' nanoparticles were found to be partly composed of dextran which could not be removed despite repeated washing. Dextran, therefore, appears to copolymerise with the monomer, forming a covalently linked surface layer which explains their ability to act as efficient stabilisers despite having a low surface affinity. These findings are discussed in more detail in chapter 3.

2.3.3.2. Influence of β-cyclodextrin

β-cyclodextrin is a cyclic oligosaccharide, with a molecular weight of 1135, consisting of 7 glucopyranose units joined by

α-1,4-glycoside linkages forming a torus-like ring (Szejtli, 1982). As with dextran, β-cyclodextrin should, in theory, be a poor steric stabiliser due to low affinity for the nanoparticle surface. Due to the similarities in structure between these two molecules, however, copolymerisation of β-cyclodextrin with the monomer is theoretically possible. The low molecular weight and cyclic nature of the molecule would be expected to produce a relatively thin stabilising layer of low repulsive energy, as discussed above, leading to the formation of relatively large particles.

Microscopic analysis of p(BCA) particles prepared using this stabiliser revealed the system to consist of individual spherical particles approximately 3μm in diameter and loose aggregates of up to 30 particles. The aggregates were easily dispersed by addition of 0.2% w/v poloxamer 188 followed by sonication for 30 minutes. When examined by Coulter counting the system was found to have a log-normal PSD as shown in figure 2.9. The concentration range studied produced only a slight reduction in particle size and no significant change in size distribution (table 2.8). This trend is similar to that seen for the dextrans over the same range of concentrations.

2.3.3.3. Influence of type and concentration of poloxamer

The poloxamer non-ionic surfactants are a series of closely related polyalkylene oxide block copolymers classified as poly-oxypropylene (POP) polyoxyethylene (POE) condensates of the general formula

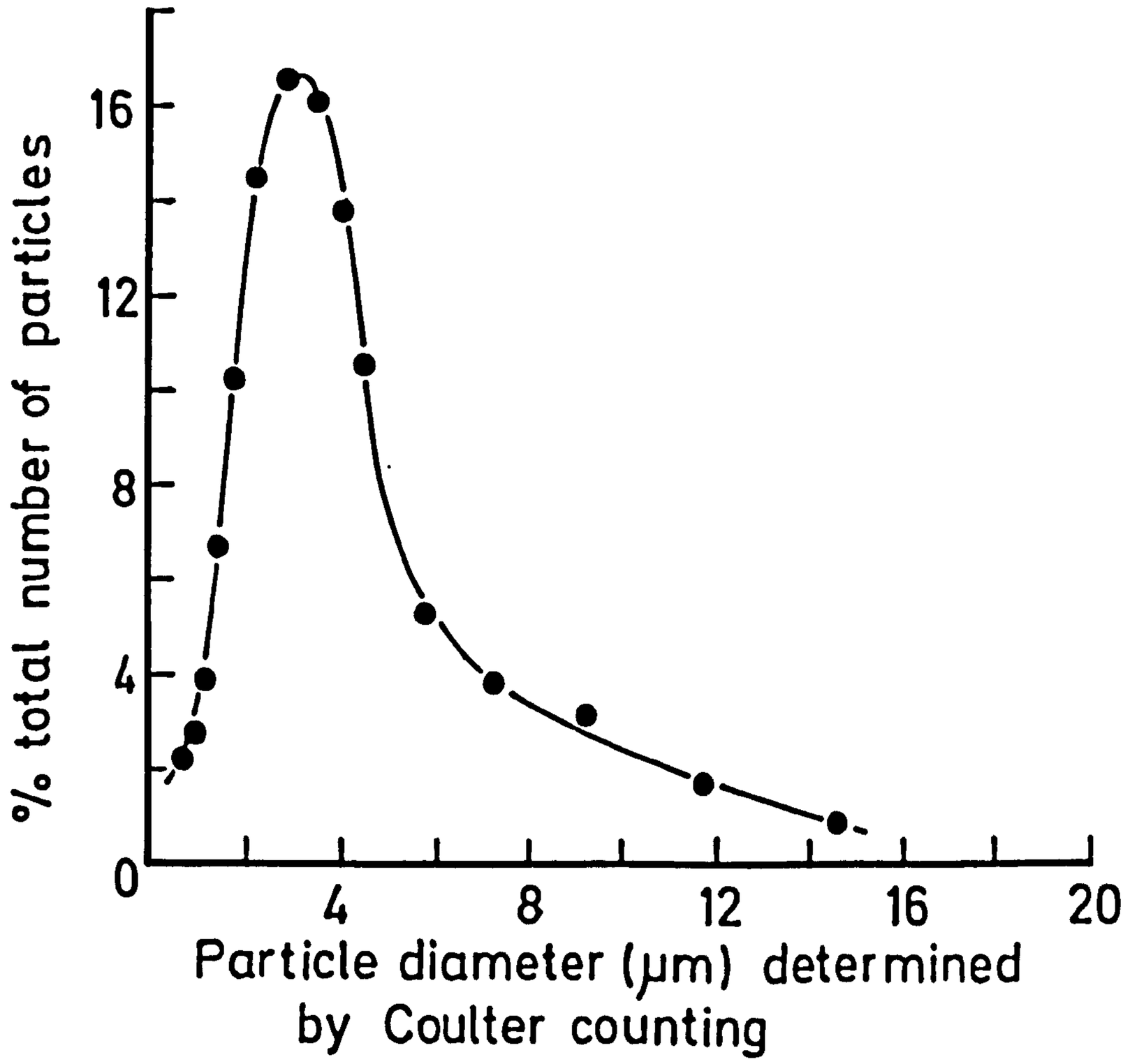

Figure 2.9. Typical particle size distribution of p(BCA) particles stabilised by β-cyclodextrin (0.75% w/v),. after addition of 0.2% w/v poloxamer 188 and sonication.

TABLE 2.8 Variation of particle size with β-cyclodextrin concentration, as determined by Coulter counting.

Conc. (% w/v)	Number average diameter (μm)	Weight average diameter (μm)	Polydispersity ratio *
0.75	3.45	4.52	1.31
1.00	3.00	3.58	1.19
1.50	2.68	3.22	1.20
1.75	2.70	3.51	1.30

* ratio of the weight / number average diameter.

$$HO(CH_2CH_2O)_a(\underset{\displaystyle CH_3}{\underset{|}{CH}}CH_2O)_b(CH_2CH_2O)_cH$$

where b is at least 15 and a and c are statistically equal.

The first two digits of the poloxamer number represent, when multiplied by 100, the approximate molecular weight of the POP moiety; the third digit represents, when multiplied by 10, the percentage by weight of the POE portion.

The influence of poloxamer 188 concentration on nanoparticle size and polydispersity index is shown in figure 2.10. The polydispersity index is seen to increase with poloxamer 188 concentration as expected, since the greater rate of poloxamer adsorption at higher concentrations leads to a more continuous and extended nucleation stage producing a wider PSD (Walbridge, 1975). The particle size shows a minimum at a concentration of 1% w/v for both dz and dn. The initial decrease in size with increasing stabiliser concentration is expected whereas the subsequent increase is indicative of a weakly anchored dispersant. This is unlikely for poloxamer 188, however, since this surfactant adsorbs strongly to the particle surface and is not totally desorbed even after extensive dialysis (Illum, 1984). The increase in average particle size with poloxamer 188 concentration may be partly due to a measurement artifact caused by the wide particle distribution. PCS measurements can be strongly affected by the presence of large particles in the sample resulting in the measured particle diameter being greater than the true value (Munro and Randle, 1976). This effect can be minimised by calculating dn from dz and Q values.

Figure 2.10. Variation of nanoparticle diameter and polydispersity index with poloxamer 188 concentration.
(•) polydispersity index, Q
(o) dz
(▵) dn

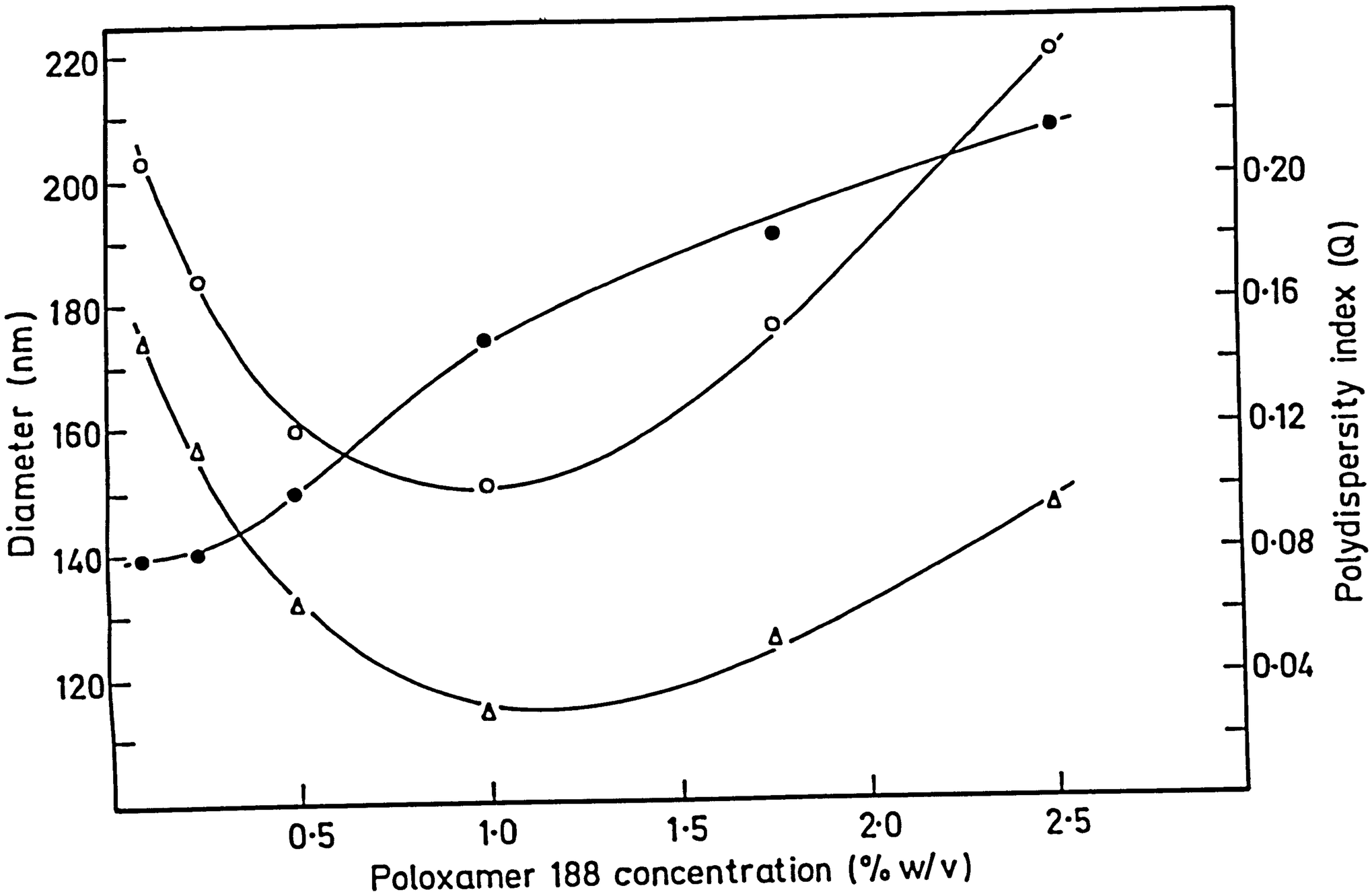
220
200
180
160
140
120
Diameter (nm)
0·20
0·16
0·12
0·08
0·04
Polydispersity index (Q)
0·5
1·0
1·5
2·0
2·5
Poloxamer 188 concentration (% w/v)

Consequently, the increase in dn is not so great compared with dz over the same poloxamer concentration range.

The influence of the type of poloxamer on nanoparticle size was investigated at a concentration of 0.5% w/v as shown in table 2.9. The approximate molecular weights of the POP and POE segments in each molecule together with the hydrophile-lipophile balance (HLB) numbers are also given. When considering the effect of the size of the POE groups on nanoparticle diameter, it can be seen that the particle size generally decreases with an increase in the average molecular weight of the POE segment. This observation may be further explained by comparing the results for nanoparticles produced in the presence of poloxamers with POP segments of the same molecular weight. Poloxamers 237 and 238 have anchoring POP groups of equal molecular weight but 238 has larger POE stabilising chains which would be expected to impart greater steric stability and so lead to smaller nanoparticles, as observed. A similar effect is seen for poloxamers 184 and 188. Rationalisation of the particle size results in terms of POP molecular weight is much more complex due to the size dependent contribution of the water soluble POE moiety to the adsorption process and final particle size. Thus, the HLB value is of little help in defining particle size effects unless the size of the stabilising group remains constant within a given series of surfactants. Nevertheless, it is clear that by employing a suitable poloxamer at an appropriate concentration it is possible to obtain nanoparticles with a controlled average diameter, and low polydispersity index, in the range 70 to 250nm.

TABLE 2.9 Variation of p(BCA) nanoparticle size and polydispersity index with poloxamer type at a concentration of 0.5% w/v.

Poloxamer	HLB	Average molecular weight of each molecular block POE	POP	dz (nm)	Q	dn (nm)
338	27	11264	3132	73	0.074	63
238	28	8536	2262	71	0.085	61
237	24	5456	2262	118	0.043	108
188	29	6600	1740	160	0.103	132
184	15	1144	1740	254	0.066	224

Also given are the corresponding poloxamer HLB numbers and average molecular weights of the POE and POP segments in each molecule (manufacturers data).

2.3.3.4. Influence of polysorbate type and concentration

The first report of nanoparticle formation (Couvreur et al, 1979a) described the use of polysorbate 20 as the stabilising agent although, somewhat surprisingly, a variation in surfactant concentration was stated to have no effect on particle size. In contrast, the results in figure 2.11 show a decrease in nanoparticle diameter as polysorbate 20 concentration was increased over the range 0.3 to 1.0% w/v, although the polydispersity index shows a slight decrease contrary to theory (Walbridge, 1975).

The influence of different polysorbate surfactants on nanoparticle size at a fixed concentration of 0.5% w/v was also investigated. The affinity of these surfactants for the particle surface would be expected to increase in the order polysorbate 20 < 40 < 60 in relation to the molecular weight increase of the hydrophobic anchoring groups. The molecular weight of the water soluble (stabilising) moieties in this series remains constant and thus a decrease in nanoparticle size should occur as the HLB number decreases as seen in table 2.10. The polydispersity index also follows the expected trend of increasing as the affinity of the surfactant for the particle surface increases.

These results show that by using suitable non-ionic surfactants at the appropriate concentration it is possible to produce nanoparticles of low average size. Other surfactants may also be used, such as Brij 96, which at a concentration of 0.5% w/v yields p(BCA) nanoparticles with dz = 28nm and Q = 0.248. When compared with the dextran systems, however, the possible disadvantages of high polydispersity values and higher toxicity for these surfactants may outweigh any advantages gained in reducing nanoparticle size.

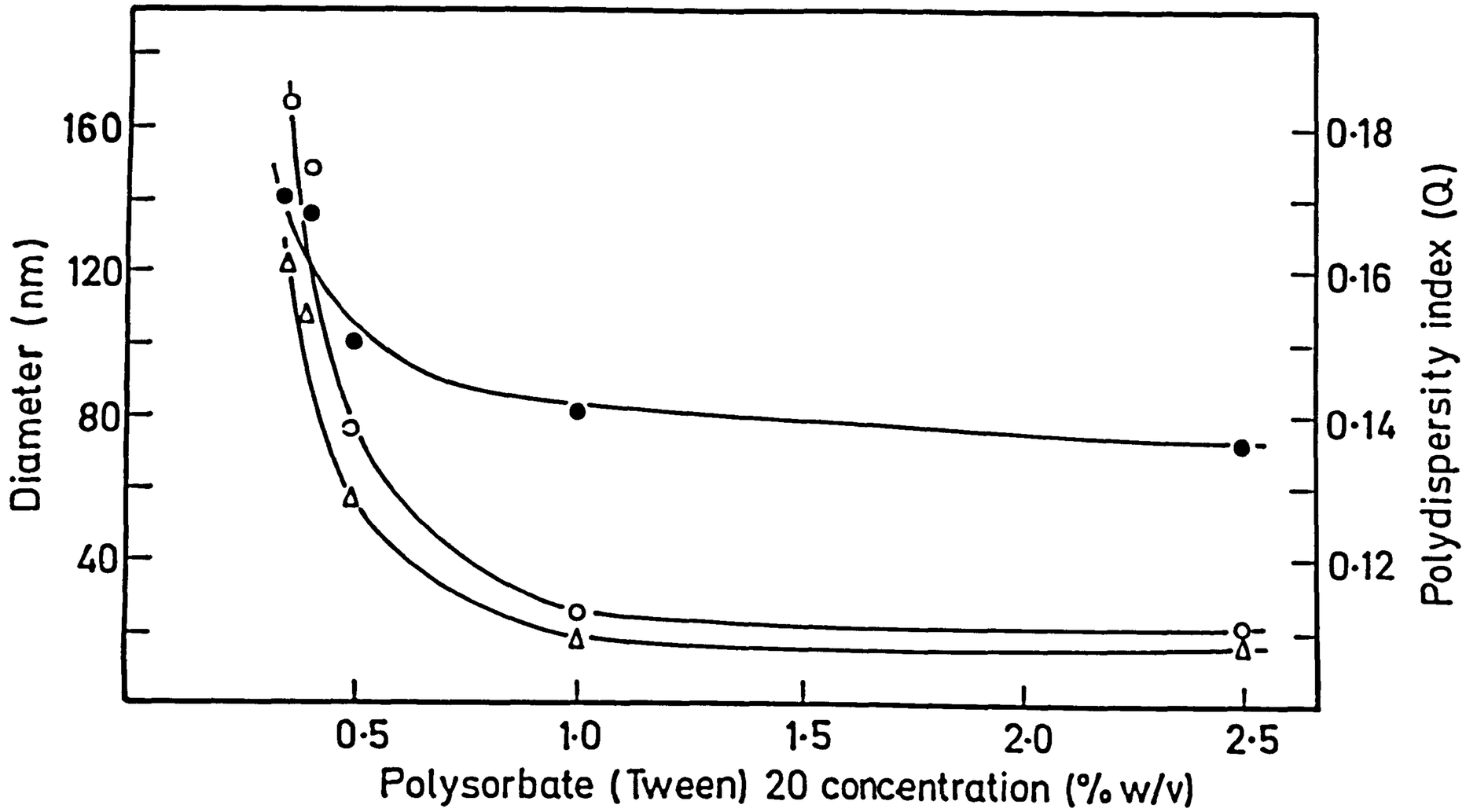

Figure 2.11. Variation of nanoparticle diameter and polydispersity index with polysorbate (Tween) 20 concentration.
(●) polydispersity index, (○) dz, (△) dn.

TABLE 2.10 Variation of p(BCA) nanoparticle diameter and polydispersity index with polysorbate type at a concentration of 0.5% w/v.

Polysorbate	HLB	dz (nm)	Q	dn (nm)
60	14.9	52	0.169	38
40	15.6	62	0.154	46
20	16.7	77	0.150	58

CHAPTER THREE

NANOPARTICLE COMPOSITION

3.1. INTRODUCTION

The need to control the particle size of p(BCA) nanoparticles for use *in vivo* requires their formation under a range of polymerisation conditions as described in the previous chapter. Such variation in the reaction medium may lead to the formation of nanoparticles composed of differing molecular weights, which could affect nanoparticle degradation, drug release rates and biodistribution of the payload (see sections 1.7.3 and 1.7.5). In addition, it would appear that certain polyhydroxyl stabilisers, such as dextrans, may copolymerise with the monomer and be incorporated into the nanoparticle matrix (section 2.3.3.1).

The composition of p(BCA) nanoparticles was determined, therefore, by examining the molecular weights and molecular weight distributions of the cyanoacrylate polymer produced under a series of different polymerisation conditions. The incorporation of dextran 70 into the nanoparticle matrix was also investigated. The data are relevant not only to the possible *in vivo* behaviour of nanoparticles, but also the elucidation of the mechanism of nanoparticle formation. The systems investigated are those for which the greatest variation in particle size was obtained in chapter 2.

3.2. EXPERIMENTAL METHODS AND MATERIALS

3.2.1. Nanoparticle Preparation and Isolation

Nanoparticles were prepared as described in chapter 2, except the preparative scale was increased from 25 to 50ml to provide sufficient polymer for extraction. The systems investigated were the effects of dextran concentration and molecular weight, polymerisation pH, monomer concentration, poloxamer 188 concentration, and polysorbate 20 concentration.

The nanoparticles were isolated by centrifugation (MSE High Speed 25; 20000 rpm for 2 hours) and then repeatedly washed with distilled water and centrifuged until no more dextran or surfactant could be removed. The samples were then freeze-dried.

Free dextran in the washings was detected according to the method of Corrigan and Stanley (1981). This involved treating 2ml of the washings with 4ml of a 0.1% w/v anthrone (Sigma) solution in concentrated sulphuric acid. This latter solution was from 4 hours to 9 days old. After 15 minutes the sample was cooled to room temperature and the absorbance read at 625nm against a suitable blank. This method had a sensitivity of approximately 5×10^{-4}% w/v.

Free surfactants were detected according to the method of Baleux (1972). This involved adding 0.1ml of an iodide/iodine solution (1g of iodine (resublimed, BDH) and 2g of potassium iodide in 100ml of distilled water, not more than 8 days old) to 4ml of the washings and, after 5 minutes, measuring the absorbance at 500nm against a suitable blank. This method had a sensitivity of

approximately $5x10^{-5}$% w/v. Absorbances were determined using an LKB Ultraspec 4050 (LKB Biochrom ,UK).

3.2.2. Polymer Extraction

Each sample was extracted three times with tetrahydrofuran (THF) (Analar, BDH) and any insoluble material removed by low speed centrifugation (3000 rpm). The combined THF fractions were evaporated under reduced pressure and the resulting oil extracted with chloroform (Analar, BDH). This solution was washed three times with distilled water and then evaporated under reduced pressure to yield an off-white foam.

The THF insoluble material from the dextran 70 samples was isolated and repeatedly washed and centrifuged with THF until no further cyanoacrylate polymer was removed (as indicated by the constancy of the infrared carbonyl stretch of the solid).

3.2.3. Molecular Weight Analysis

Although some dextran 70 samples were examined by nuclear magnetic resonance (NMR) the majority of the samples were analysed by gel permeation chromatography (GPC). This work was performed by Dr. S. Holding at the Rubber and Plastics Research Association, Shawbury, UK.

3.2.3.1. Nuclear magnetic resonance

Approximately 50mg of the polymer sample was dissolved in 1ml of deuterated chloroform (Gold Label, Aldrich, UK) containing

tetramethylsilane (NMR grade, Aldrich) as a reference. Spectra were recorded using a 90 MHz Varian EM390 spectrometer (Varian Associates, USA). The spectra were integrated a total of 5 times and the average integral value determined for each signal.

3.2.3.2. Gel permeation chromatography

The polymer samples were dissolved in THF and analysed using a polystyrene calibrated GPC system with THF as the eluant. This system consisted of two Du Pont 870 pumps, a Du Pont 834 auto-sampler, two Polymer Laboratories columns (1 x 500A and 1 x 100A columns, 60cm long, filled with 10μm packing material), a Du Pont ultraviolet detector, and a Knauer refractive index detector. The solvent flow rate was 1.0 ml/minute and an internal marker (toluene) was added to allow a flow-rate correction to be made. Data from the refractive index detector were collected and analysed using a Trivector Scientific, Trojan (level 1) data handling system. Results are quoted as the polystyrene equivalent molecular weights for the peak molecular weight (Mp) number average molecular weight ($\bar{M}n$) and the weight average molecular weight ($\bar{M}w$). The results obtained for the high molecular weight polymers (> 20000) are only approximate since these values are at the far end of the calibration range for the columns. For this reason $\bar{M}n$ and $\bar{M}w$ values are only quoted for the low molecular weight polymers.

A certain degree of column conditioning was observed for these samples so that the first set of data obtained for the effects of dextran concentration and molecular weight differ slightly from

subsequent results, although data within each set of results may be compared directly.

3.2.4. Infrared Spectroscopy

Infrared (IR) spectra were recorded on a Perkin-Elmer 257 grating spectrophotometer (Perkin-Elmer, UK) and the recording wavelength checked against a standard polystyrene film. Samples were prepared by forming potassium bromide disks containing 2mg of polymer.

3.3. RESULTS AND DISCUSSION

3.3.1. Dextran Incorporation Into Nanoparticles

Theoretically, covalent linking of dextran to the cyanoacrylate polymer is possible according to the polymerisation mechanism given in scheme 2.1. Due to the ease of polarisation of the double bond of the monomer caused by the highly electronegative nitrile and alkoxycarbonyl groups, polymerisation can be initiated by weak bases such as water and alcohol. According to this mechanism the basic initiating species is present in the final polymer as an end group (Leonard et al, 1966). Normally, under aqueous conditions, OH^- is the attacking nucleophile resulting in a hydroxyl-terminated polymer as shown by the IR spectrum of p(BCA) produced under aqueous conditions (figure 3.1a). However, when nanoparticles were formed in the presence of dextran 70 and the cyanoacrylate polymer removed by dissolution in THF, a derivatised dextran molecule was isolated. This compound possessed a reduced IR inter- and intra-molecular

hydrogen-bonded OH stretch compared with dextran and a carbonyl stretch corresponding to that of the cyanoacrylate polymer (figures 3.1b and 3.1c). Dextran appears, therefore, to act as an initiator for polymerisation and a possible mechanism for this reaction is given in scheme 3.1.

Each dextran molecule could, therefore, contain several cyanoacrylate polymer moieties covalently linked via any of the available dextran hydroxyl groups. Anchoring of the cyanoacrylate groups within the nanoparticle matrix would result in an irreversible attachment between the dextran and the nanoparticle, possibly by multipoint linkages as depicted in figure 3.2. Although most of the dextran would be expected to reside at the particle surface, some of the stabiliser could be incorporated into the nanoparticle core, producing particles analogous to the biodegradable microspheres of polyacryldextran developed by Edman et al (1980).

The degree of dextran incorporation into nanoparticles was found to increase with the concentration of dextran added to the polymerisation medium as shown in table 3.1. Thus, at a concentration of 2.5% w/v dextran 70 approximately 20% by weight of the nanoparticles are composed of the covalently linked derivatised dextran.

In considering the ability of hydrophilic polymeric alcohols to stabilise nanoparticles, the molar fraction of hydroxyl groups appears to be important. Dextran and β-cyclodextrin have a high hydroxyl content and act as efficient stabilisers, whereas PEG's possess far fewer hydroxyl groups and are ineffective stabilisers in

Figure 3.1. Infrared Spectra.

(a) Poly (butyl 2-cyanoacrylate) produced under aqueous conditions. A = OH stretch, B = ester carbonyl strecth.

(b) Dextran 70. A = broad OH stretch due to inter- and intramolecular hydrogen bonding.

(c) Derivatised dextran isolated from p(BCA) nanoparticles produced in the presence of 0.5% dextran 70. A = reduced inter- and intra-molecular hydrogen bonded OH strecth, B = ester carbonyl stretch corresponding to that of (a).

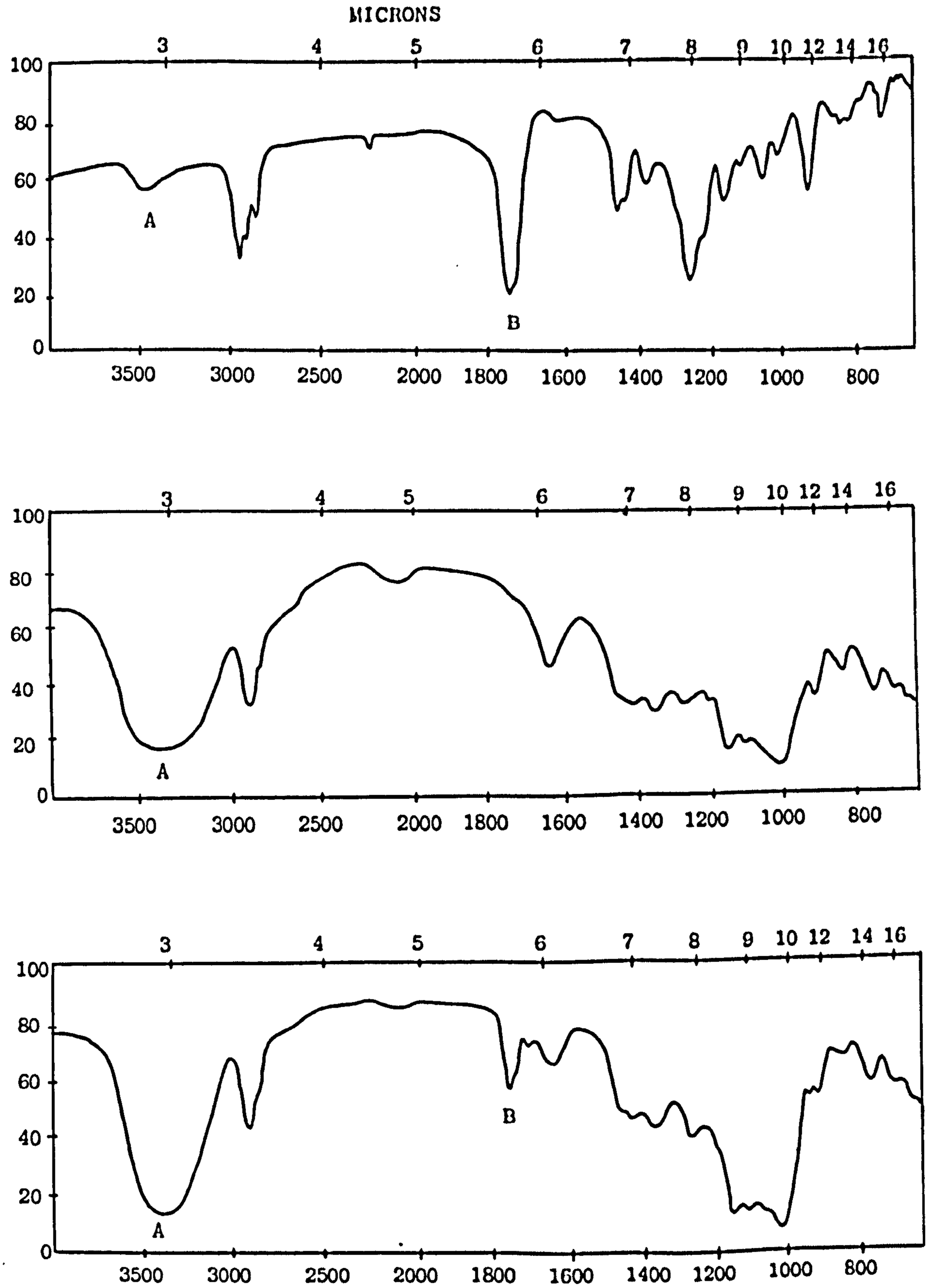
MICRONS
3
4
5
6
7
8
9
10
12
14
16
100
80
60
40
20
0
A
B
3500
3000
2500
2000
1800
1600
1400
1200
1000
800
TRANSMITTANCE(%)
WAVENUMBER(CM-1)

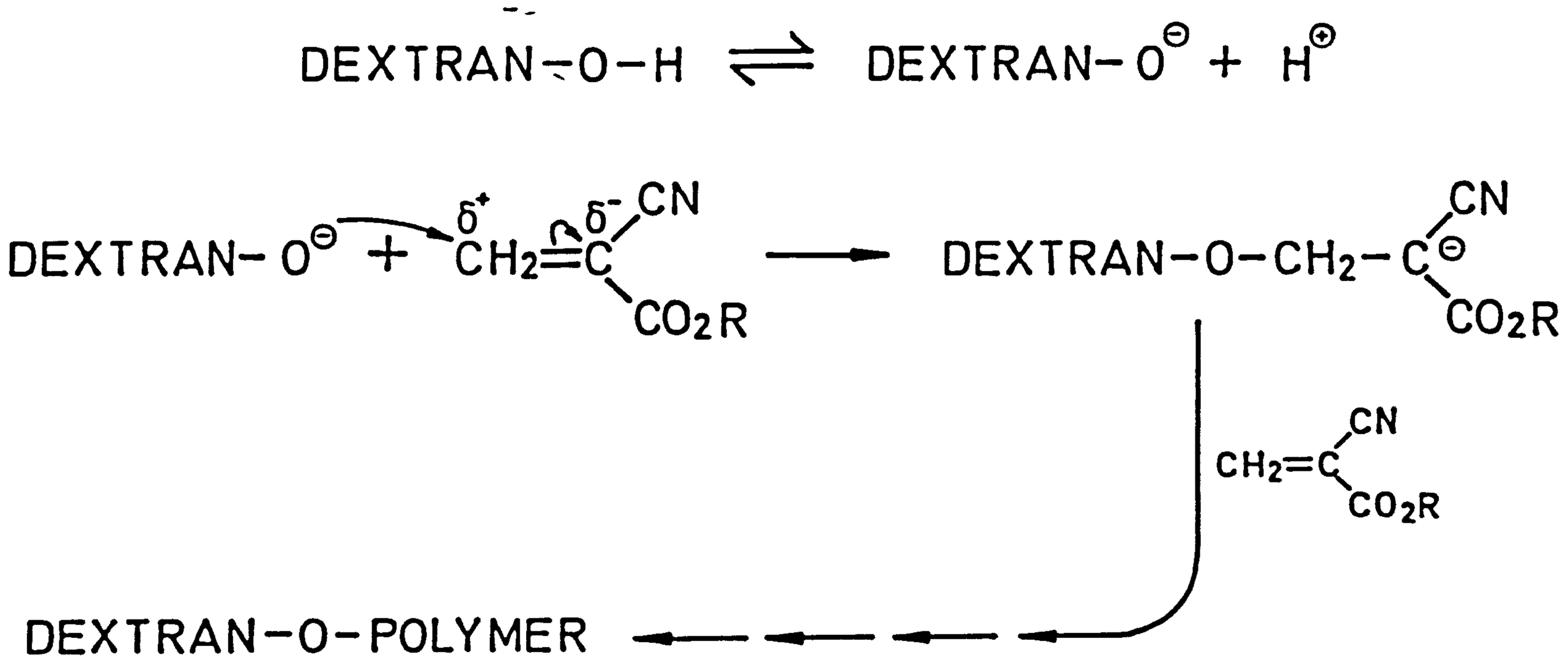

Scheme 3.1. Proposed mechanism of dextran-cyanoacrylate polymer covalent linkage (R = n-butyl).

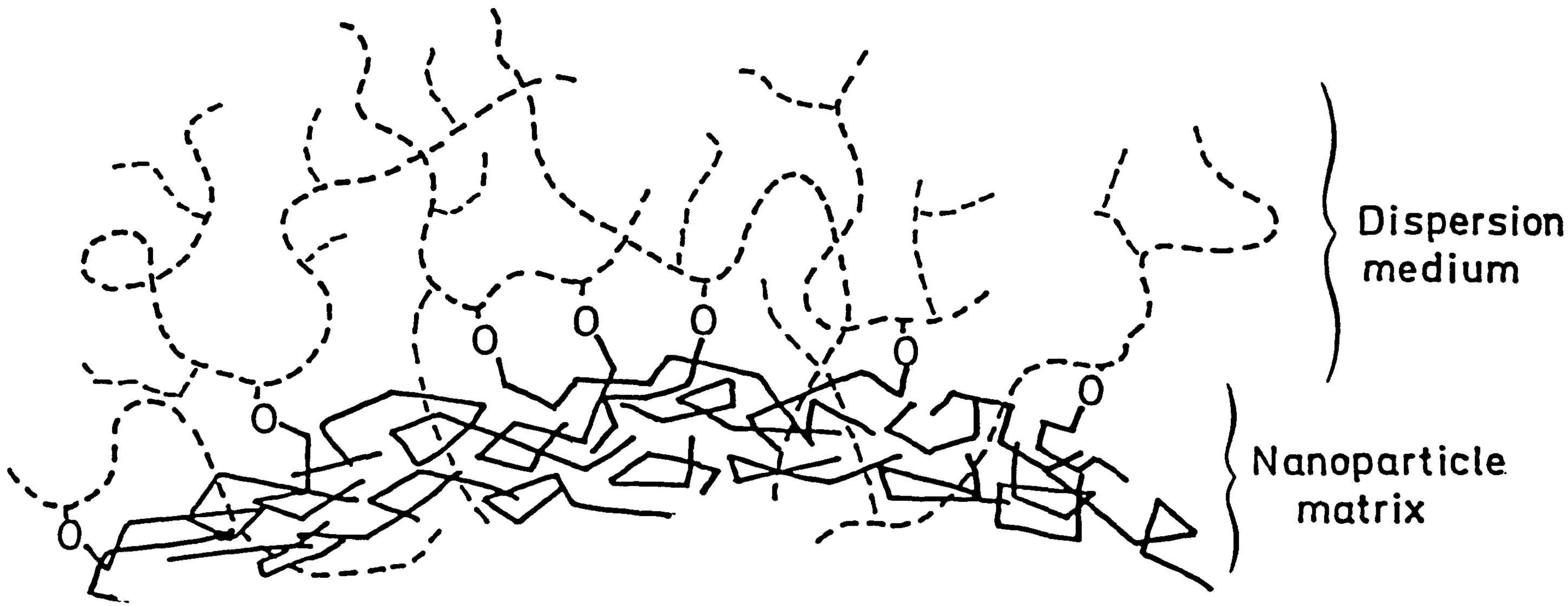

Figure 3.2. Proposed model of the nanoparticle surface when dextran is used as the stabiliser. ——— , denotes the cyanoacrylate polymer: ----, denotes the dextran molecules.

TABLE 3.1 Variation in the amount of derivatised dextran 70 incorporated into p(BCA) nanoparticles as a function of dextran 70 concentration. Monomer concentration was 1% v/v and reaction pH 2.25

Dextran 70 concentration (% w/v)	% incorporation*
0.05	1.0
0.10	1.8
0.25	5.4
0.50	8.7
1.00	16.0
2.50	20.5

* results given as the percentage of the total nanoparticle weight composed of derivatised dextran 70.

nanoparticle formation. Copolymerisation of PEG's with the monomer, therefore, occurs at a much lower frequency compared with the polysaccharides, resulting in a level of incorporation that is too low to impart effective steric stability as shown by the results in chapter 2.

3.3.2. Molecular Weight Analysis by Nuclear Magnetic Resonance

It is possible to determine an absolute number average molecular weight for p(BCA) from the NMR spectrum by comparing the ratio of the signal integrals of the repeating butyl ester protons, or the backbone methylene protons, with the terminal methylene and methine protons. NMR has also been used to study the thermal degradation of p(ACA) (Rooney, 1981).

The NMR spectrum of p(BCA) extracted from nanoparticles produced in the presence of 0.5% w/v dextran 70 may be related to its chemical structure as follows

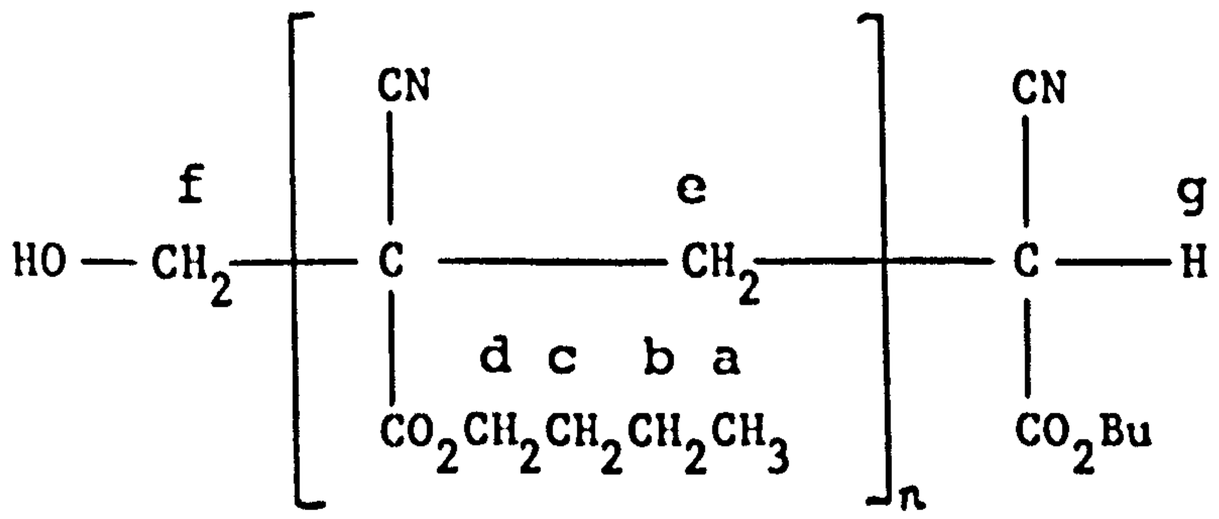

Designation	δ	Signal multiplicity	Number of protons	Integral
a	1.0	triplet	3H	66
b,c	1.25-2.0	multiplet	4H	94
e	2.62	broad singlet	2H	40
d,f,g	3.8-4.55	multiplet	5H	52

Summation of the integrals for the 7 protons of a,b, and c gives a value of 160, corresponding to 22.9 for each proton of the ester group. The integral value for the d,f, and g protons comprises 45.8 due to the d protons (2 x 22.9) and, therefore, 6.2 due to the f and g protons. This gives an integral value of 2.1 for the terminal methine proton. The ratio of the terminal methine proton to the repeating protons of the ester group is 10.9 (22.9 / 2.1) so that in the general formula above, n = 9.9 which gives an approximate average molecular weight of 1685. Alternatively, by comparing the ratio of the terminal methine with the backbone methylene protons, n is found to be 9.5, giving a molecular weight of 1625. These values were found to be in reasonable agreement with the results obtained by GPC analysis given below.

Although this technique gives an absolute value for the number average molecular weight, it is very insensitive to the presence of high molecular weight components and gives no indication of the molecular weight distribution. To determine this latter parameter GPC must be used.

3.3.3. Molecular Weight Analysis by Gel Permeation Chromatography

3.3.3.1. Molecular weights of dextran stabilised nanoparticles

Dextran molecular weight and concentration had little effect on the resulting cyanoacrylate polymer molecular weight as shown in table 3.2, although a slight trend in increasing polymer molecular weight can be seen with increased stabiliser concentration. A typical molecular weight distribution for this type of system

TABLE 3.2 Effect of dextran type and concentration on the molecular weight of p(BCA) produced at a pH of 2.25 and a monomer concentration of 1% v/v.

Conc.	Dextran 10			Dextran 40			Dextran 70		
(% w/v)	Mp	$\bar{M}n$	$\bar{M}w$	Mp	$\bar{M}n$	$\bar{M}w$	Mp	$\bar{M}n$	$\bar{M}w$
0.05	900	730	970	1050	810	1380	980	700	1090
0.10	990	880	1150	1020	820	1260	1050	790	1230
0.25	1110	980	1360	1450	1000	1670	1250	950	1660
0.50	1340	1180	1600	1020	730	1230	1080	950	1350
1.00	1820	1430	2340	1340	980	1590	1050	780	1400
2.50	1700	1190	1950	2180	1340	2460	1420	850	2890

(figure 3.3a) shows the presence of two distinct distributions which are referred to as distributions 1 (low Mp) and 2 (high Mp). The height ratio of the two peaks remained fairly constant. Dextrans 10 and 70 gave an Mp value of 27000 and dextran 40 an Mp of 29600, with these values being unaffected by concentration.

The bimodal molecular weight distribution obtained with these samples indicates the presence of two separate polymerisation reactions. The first is assumed to occur in the aqueous phase where initiation by hydroxyl ions leads to the formation of growing oligomeric chains according to the mechanism in scheme 2.1. Polymerisation is terminated rapidly, however, due to the high proton, H^+, concentration at the low pH, so producing a low molecular weight polymer (distribution 1). Aggregation of these oligomers produces particle nuclei which grow by capture of further oligomers and by sorption of monomer which subsequently polymerises within the nanoparticles. In this environment polymerisation termination occurs at a much lower frequency, due to the reduced H^+ concentration, and yields polymers of much higher molecular weight (distribution 2). The majority of the polymer, however, has a low molecular weight which implies that nanoparticle formation occurs via an aggregative mechanism as opposed to self-nucleation which would yield polymers of a much higher molecular weight (Barrett and Thomas, 1975).

The results obtained for distribution 1 are similar to those found by Van Snick et al (1985) with dextran 40 stabilised systems, although these workers did not report the presence of a second high molecular weight distribution. Direct numerical comparison of

Figure 3.3. Molecular weight distributions of the cyanoacrylate polymer extracted from p(BCA) nanoparticles prepared in the presence of various stabilisers.

(a) 0.5% dextran 70
(b) 0.5% poloxamer 188
(c) 0.5% polysorbate 20

The monomer concentration was 1.0% v/v and the polymerisation pH 2.25.

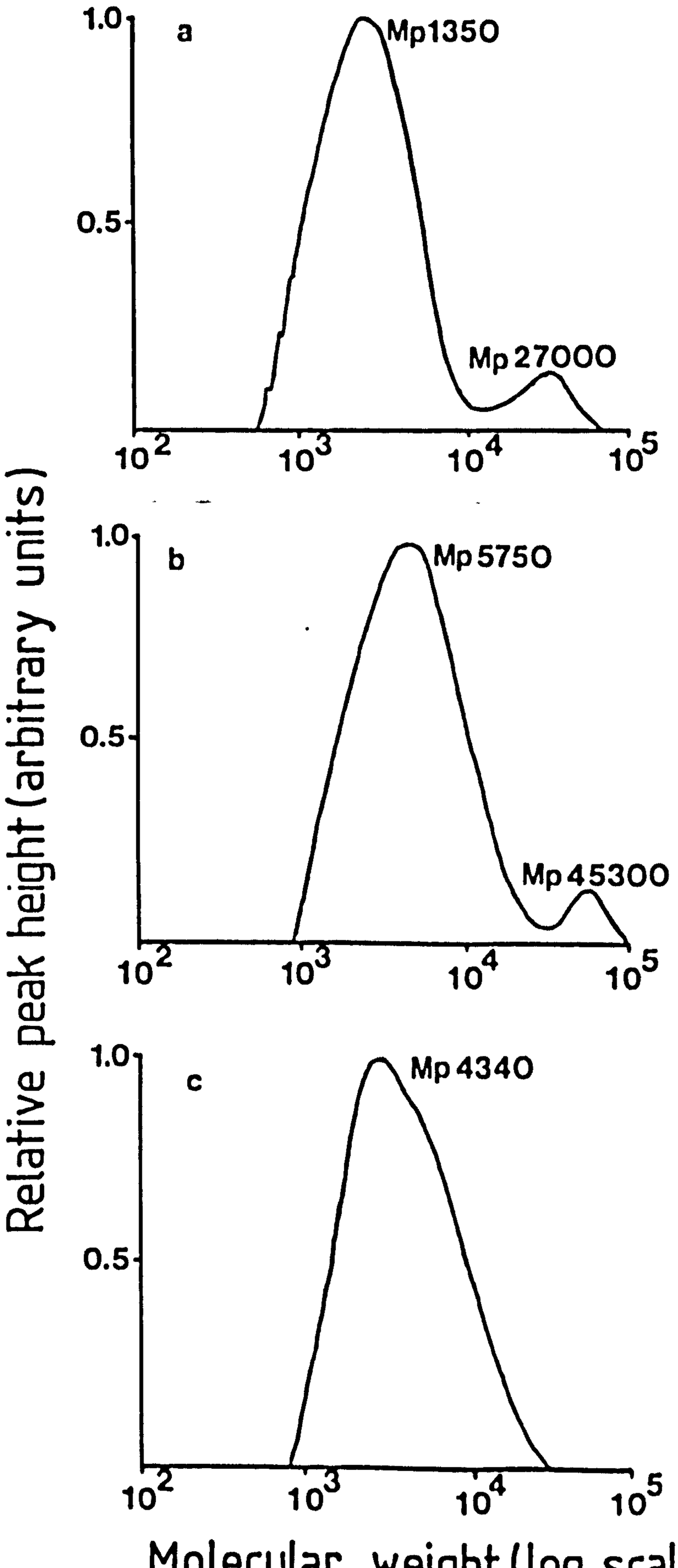
a
Mp1350
Mp 27000
b
Mp 5750
Mp 45300
c
Mp 4340
1.0
0.5
10^2
10^3
10^4
10^5
Relative peak height (arbitrary units)
Molecular weight (log scale)

results between these two studies is not possible since Van Snick *et al* used polyethylene glycol standards.

The variation of polymer molecular weight with polymerisation pH for a 0.5% w/v dextran 70 system is given in table 3.3 and shows the molecular weight values for both distributions to increase with increasing pH. These findings are similar to those of other workers (El-Egakey *et al*, 1983; Van Snick *et al*, 1985). The effect of polymerisation pH appears to be complex. Normally, as initiator concentration increases (in this case OH^-) the resulting polymer molecular weight decreases, as seen with other polymerisation processes (Goodwin *et al*, 1973). In the present system, however, the pH would also be expected to affect the termination reaction by reference to scheme 2.1. This, together with the fact that the solvent generates the initiator, may explain the anomalous behaviour observed (El-Egakey *et al*, 1983).

Increasing the monomer concentration in a 0.5% w/v dextran 70 stabilised system produced an increase in molecular weight of both distributions 1 and 2 as expected (table 3.4). The increase in the peak height ratio of distribution 2 would indicate a higher degree of polymerisation within the nanoparticles as monomer concentration increases. Excess monomer, at the higher concentrations, partitions into the growing particles and polymerises whereas at low concentrations most of the monomer is consumed forming particle nuclei via the aggregative mechanism discussed previously.

TABLE 3.3 Effect of polymerisation pH on the molecular weight of p(BCA). The system was stabilised with 0.5% w/v dextran 70 and the monomer concentration was 1% v/v.

pH	Distribution 1			Distribution 2
	Mp	$\bar{M}n$	$\bar{M}w$	Mp
1.0	1490	1410	1990	*
1.5	1700	1610	1990	28000
2.0	1490	1430	1910	27500
2.5	1700	1720	2320	29000
3.0	1820	1680	2300	30500
3.5	1910	1820	2500	32400

* no value obtained

TABLE 3.4 Variation of p(BCA) molecular weight with monomer concentration. The polymerisation pH was 2.25 and dextran 70 at a concentration of 0.5% w/v used as the stabiliser.

Monomer conc. (% v/v)	Distribution 1 Mp	$\bar{M}n$	$\bar{M}w$	Distribution 2 Mp	Peak height ratio *
0.5	1710	1630	2300	27600	0.08
1.0	1710	1630	2310	27600	0.08
1.5	1820	1760	2470	31500	0.21
2.0	1880	1720	2530	32000	0.24
2.5	1910	1590	2480	33000	0.32
3.0	2080	1790	2810	32000	0.41
5.0	1940	1840	2730	34000	0.53
7.0	2190	2030	2960	33000	0.61

* this is the peak height ratio of Mp2 / Mp1.

3.3.3.2. Molecular weights of poloxamer 188 stabilised nanoparticles

A bimodal molecular weight distribution similar to the dextran systems was obtained when poloxamer 188 was used as the stabiliser, although each peak was centred at a higher molecular weight (figure 3.3b). The effect of poloxamer concentration on molecular weight is given in table 3.5. The peak height of distribution 2 was seen to increase slightly with poloxamer 188 concentration. Similar findings have been reported by Couvreur et al (1984) and Van Snick et al (1985).

The formation of polymers with higher molecular weights in these poloxamer systems, compared with dextran, may be due to the surfactant associating with the growing oligomeric chains and particle nuclei, producing a protective layer from the acid environment and so reducing the rate of polymerisation termination. If this explanation is correct, however, then the molecular weight would be expected to show a dependence on the poloxamer concentration, which was not seen. This may be due to the concentration range investigated being greater than a certain critical maximum poloxamer concentration, above which the addition of further surfactant to the system had no effect on the molecular weight of the polymer. Concentrations of poloxamer less than 0.1% w/v were not investigated because discrete nanoparticle formation does not occur at these low poloxamer concentrations.

TABLE 3.5 Effect of the concentration of poloxamer 188 on the molecular weight of p(BCA). The monomer concentration was 1% v/v and polymerisation pH 2.25.

Conc.	Distribution 1			Distribution 2
(% w/v)	Mp	$\bar{M}n$	$\bar{M}w$	Mp
0.10	3440	2780	4360	41400
0.25	3940	3140	5030	35200
0.50	4460	3500	5750	44400
1.00	3670	3270	4930	36000
2.50	*			

* data accidentally erased from floppy disc.

3.3.3.3. Molecular weights of polysorbate 20 stabilised nanoparticles

The results obtained with polysorbate stabilised systems did not show the distinct high molecular weight distribution seen previously (figure 3.3c). These results indicate that sorption of monomer and secondary polymerisation within the nanoparticle matrix probably does not occur to any great extent. This may help to explain why nanoparticles with much smaller diameters of < 70nm are obtained with this surfactant compared with approximately 150nm for systems stabilised by dextran and poloxamer 188 at a concentration of 0.5% w/v. Although a single micellar polymerisation mechanism is proposed, a slight shoulder in the molecular weight distribution (figure 3.3c) may imply a dual polymerisation process.

Variation in the concentration of polysorbate 20 had little effect on the molecular weight of the resulting polymer (table 3.6), probably for the same reasons discussed regarding poloxamer 188. These results are similar to those obtained elsewhere (El-Egakey et al, 1983).

3.3.4. Possible Effects of Molecular Weight Differences on Nanoparticle Degradation

Despite the fact that within each system the effects of the concentration of the stabiliser on molecular weight are not very pronounced, there are marked differences in the molecular weight distributions between nanoparticles produced with different stabilisers. According to Vezin and Florence (1980) the in vitro

TABLE 3.6 Effect of the concentration of polysorbate 20 on the molecular weight of p(BCA). The monomer concentration was 1% v/v and polymerisation pH 2.25.

Conc. (% w/v)	Mp	$\bar{M}n$	$\bar{M}w$
0.1*	1980	2330	3400
0.3	2160	2590	4070
0.5	2280	2780	4340
1.0	2160	2640	4200
2.5	2160	2610	4190

* data included although the nanoparticle system was unsuitable due to gross flocculation.

degradation rates of p(ACA) appear to be approximately proportional to $\bar{M}n^{-1}$ since degradation occurs at chain ends and travels along the polymer chain (scheme 3.2). Thus polymers with high $\bar{M}n$, as produced in the systems stabilised by dextrans and poloxamer 188, would be expected to degrade slowly. However, apart from when high monomer concentrations were employed, the quantity of the high molecular weight component was small compared with the total amount of polymer.

The situation is further complicated by an alternative degradation mechanism involving ester hydrolysis (see section 1.7.3) which yields, eventually, water soluble poly (2-cyanoacrylic acid) and an alkyl alcohol (scheme 3.2). Although there is no evidence to indicate that this mechanism is dependent on molecular weight, the presence of high molecular weight polymers would be expected to retard the dissolution of the nanoparticles due to the binding effect of large molecules penetrating throughout the nanoparticle matrix. It has been found that the absence of high molecular weight components leads to increased water solubility resulting in bulk, rather than surface, polymer degradation (Vezin and Florence, 1980).

The finding that dextran stabilised nanoparticles may be composed of up to approximately 20% by weight derivatised dextran may have important implications concerning nanoparticle degradation. The presence of this hydrophilic polymer in the particles may create aqueous channels allowing water to penetrate the matrix to a greater extent and increase the rate of cyanoacrylate degradation.

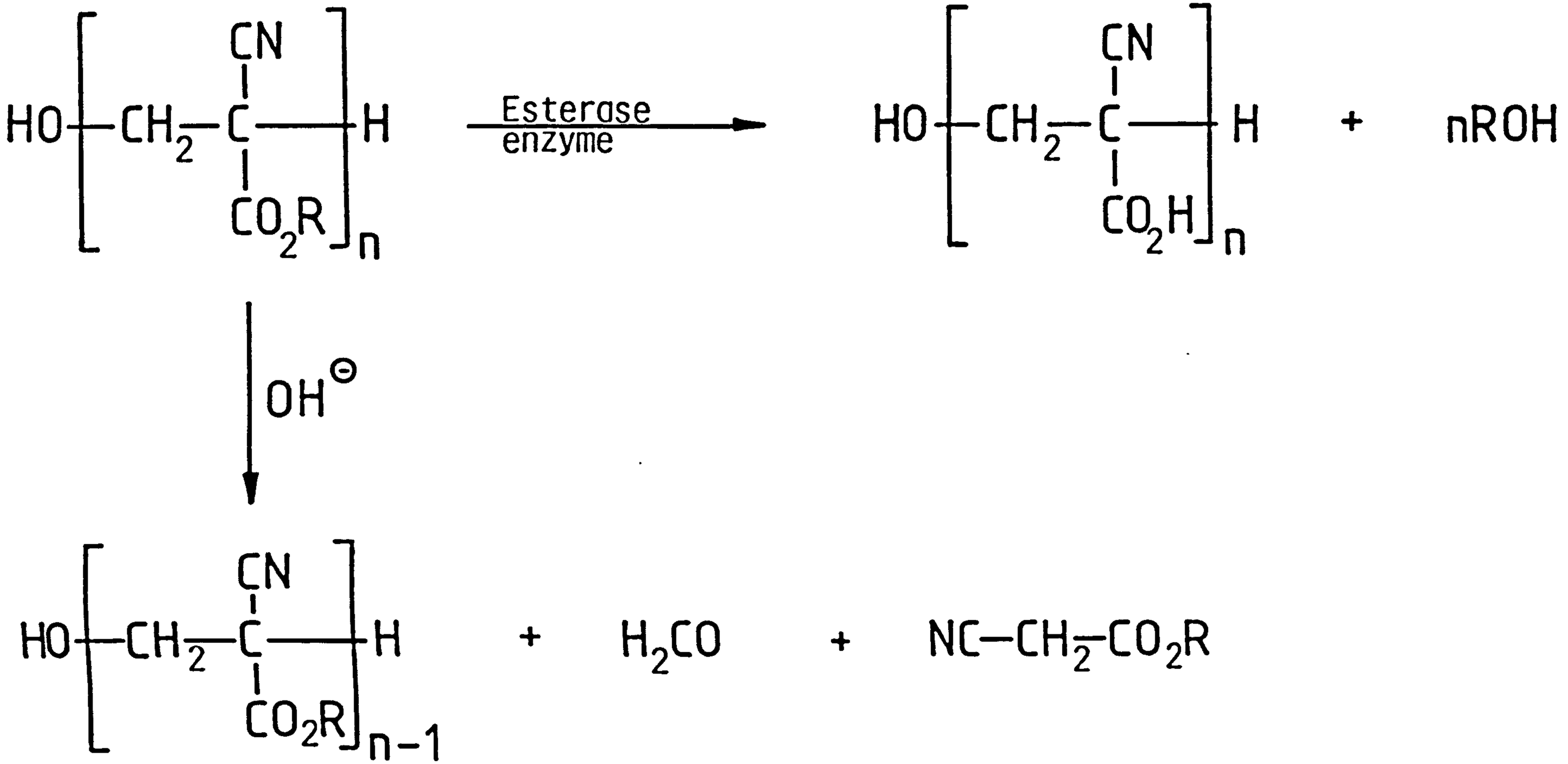

Scheme 3.2. Degradation pathways of poly (alkyl 2-cyanoacrylates). R = alkyl.

CHAPTER FOUR

CONTROL OF THE ELECTROPHORETIC MOBILITY OF NANOPARTICLES

4.1. INTRODUCTION

As already discussed (section 1.3.3), the electrophoretic properties of colloidal materials affect both their rate of clearance and site of deposition *in vivo*. These effects are complicated, however, by simultaneous changes in other surface properties, such as hydrophobicity/hydrophilicity, which can result from changes in surface charge. Thus it is probably a concurrent effect of the general surface properties of the particles on interaction with the RES that determines the fate of colloidal drug carriers in the body.

Previous chapters have shown that polyhydroxyl stabilisers, such as dextrans, can copolymerise with ACA's forming covalent linkages between the stabiliser and the cyanoacrylate polymer. This produces an interfacial layer of the stabiliser which is firmly attached to the nanoparticle surface. It should be possible, therefore, to alter the surface charge characteristics of nanoparticles by the incorporation of dextrans with charged functional groups.

This chapter describes the preparation of p(BCA) nanoparticles with high and low negative and positive surface charges using dextran 70, dextran sulphate 500, and diethylaminoethyl-dextran (DEAE-dextran) as stabilising agents. Subsequent studies *in vivo* with these nanoparticles may show differences in the tissue

distribution attributable to the variation in particle charge. Hopefully any such effects could be utilised in drug targeting.

4.2. EXPERIMENTAL METHODS AND MATERIALS

4.2.1. Nanoparticle Preparation

The dextran materials, dextran 70, DEAE-dextran and dextran sulphate 500, used in preparing the nanoparticles were purchased from Sigma. Dextran sulphate is a polyanionic derivative of dextran produced by esterification of dextran, molecular weight 500000, with chlorosulphonic acid. The sulphur content is approximately 17% which corresponds to an average of 2.3 sulphate groups per glucosyl residue. The dextran sulphate salt was converted to its free acid before use with an ion exchange resin (Amberlite IR-120, BDH). DEAE-dextran is a polycationic derivative of dextran containing diethylaminoethyl groups coupled to the glucose residues by ether linkages. The parent dextran has an average molecular weight of 500000. The nitrogen content is approximately 3.2% which corresponds to one charged group to three glucose units.

The nanoparticles were prepared by adding 0.25ml of BCA to 24.75ml of a filtered (0.2μm membrane filter, Whatman) stirred solution of dextran 70 (0.5% w/v) or DEAE-dextran (1.0% w/v) in approximately 0.01N hydrochloric acid, or dextran sulphate (1.0% w/v) in distilled water. After the polymerisation was complete the suspension was filtered through a sintered glass filter (grade 4, pore size 11-16μm) and diluted accordingly for particle size or electrophoretic mobility measurements.

4.2.2. Particle Size Analysis

Particle size measurements were performed by PCS as outlined in chapter 2. Results are quoted as the z-average particle diameter (dz) and polydispersity index (Q).

4.2.3. Electrophoretic Mobility Measurements

The determination of the electrophoretic mobility (EPM) and the related zeta potential (ZP) of the nanoparticles was performed using the technique of electrophoretic laser doppler anemometry (LDA) (Preece and Luckman, 1981). The instrument used was a commercially available Malvern Zetasizer (Malvern Instruments) and measurements were performed by Malvern Instruments.

LDA was used to determine the nanoparticle EPM since conventional measuring techniques such as microelectrophoresis and moving boundary electrophoresis (Shaw, 1969) are not suitable for the small particles under investigation here. The technique of LDA involves the application of a known electric field across a suspension of the sample contained in a cylindrical sample cell. The sample is illuminated with a laser light source (15mW helium-neon laser) which is split into two beams of equal intensity. The split beams are caused to cross at a stationary level (zero electro-osmotic flow) in the cell forming an ellipsoid measuring volume. In this region a pattern of interference fringes is formed due to the coherence of the two laser beams. The spacing of these light and dark bands is an exact function of the beam crossing angle and laser frequency. Particles moving through the fringe system will scatter

light with a frequency different from the incident beam due to the Doppler effect. This frequency shift, the Doppler frequency, Fd, is correlated with the particle velocity via the equation

$$Fd = \frac{2 \sin(\theta/2)\, v}{\lambda} \qquad [4.1]$$

where θ is the detection angle, λ the laser wavelength and v the particle velocity.

To determine the charge and velocity of the particles under investigation one of the laser beams is modulated by a frequency of 250 Hz. This causes the interference fringes to drift in a direction parallel to the particle motion. Particles with a net charge of zero will remain stationary under the applied electric field but will appear to scatter light with a Doppler frequency of 250 Hz due to the moving fringe pattern. Charged particles, however, will move either with the fringe system, thereby decreasing Fd, or against it, thereby increasing Fd, depending on the polarity of the applied electric field. Synchronisation of the modulating frequency and the field polarity with the particle movement then yields information about the sign and magnitude of the particle surface charge. The Malvern Zetasizer determines Fd by generating a correlation function of the scattered light intensity and converting this to a frequency spectrum via a Fourier transform.

For the electrophoretic measurements, a few drops of the nanoparticle suspension were added to 10ml of a 10^{-3}M potassium chloride solution and mixed thoroughly. A total of 1000 measurements were performed on each sample at 25^{o}C and the EPM and ZP calculated

from the mean result. The DEAE-dextran stabilised nanoparticle sample was adjusted to increasing pH values by adding small volumes of 0.01N sodium hydroxide and checking with a calibrated pH meter. The electrophoretic measurements were performed immediately after each pH value was set. Measurements could not be made above pH 10 due to rapid degradation of the nanoparticles.

Calculation of ZP depends upon the magnitude of the Debye-Huckel parameter, κ , and the particle radius, r. At large values of κr the Smoluchowski equation can be applied whereas at small values of κr the Huckel equation is employed (Shaw, 1969). However, for values in the range $0.1 < \kappa r < 100$ (James 1980) recourse is made to the Henry equation which for non-conducting spherical particles is given by

$$U_E = \frac{ZP\ e\ f(\kappa r)}{6\ \pi\ n} \qquad [4.2]$$

where U_E is the electrophoretic mobility, e is the permittivity of the medium, n is the solvent viscosity and $f(\kappa r)$ is a function of κr which varies between 1 (Huckel equation) and 1.5 (Smoluchowski equation). For the systems studied here with particle radii from 74nm (dextran 70) to 549nm (dextran sulphate) and κ of $0.104nm^{-1}$ (calculated for an ionic strength of 10^{-3} M), the values of κr are $7.7 < \kappa r < 59$. The corresponding function $f(\kappa r)$ may be obtained graphically (as in this case) or calculated exactly according to the expressions given by Henry (1931).

4.3. RESULTS AND DISCUSSION

4.3.1. Electrophoretic Measurements

The results for the EPM and ZP of the various nanoparticle systems are given in table 4.1. The p(BCA) nanoparticles stabilised by dextran 70 were found to bear a small negative charge and have a low EPM as reported by other workers (Kreuter, 1983d). This charge probably arises from the adsorption of anions from the aqueous phase. Cations, which are generally more hydrated than anions, have a greater tendency to remain in the bulk aqueous phase compared with the larger, more polarising and less hydrated anions which consequently are adsorbed more easily (Shaw, 1969). The magnitude of the negative charge was significantly increased by preparing nanoparticles using the highly charged anionic (SO_3^-) stabiliser dextran sulphate.

By using DEAE-dextran it was possible to form nanoparticles with a positive EPM and ZP due to the cationic tertiary and quaternary amino groups present in this polymer. The EPM of these particles was found to vary as a function of pH as shown in table 4.1. This is due to the degree of ionisation of DEAE-dextran being dependent upon pH. The ionisation behaviour is complicated by the presence of three different ionisable groups each with a different pK_a as shown below.

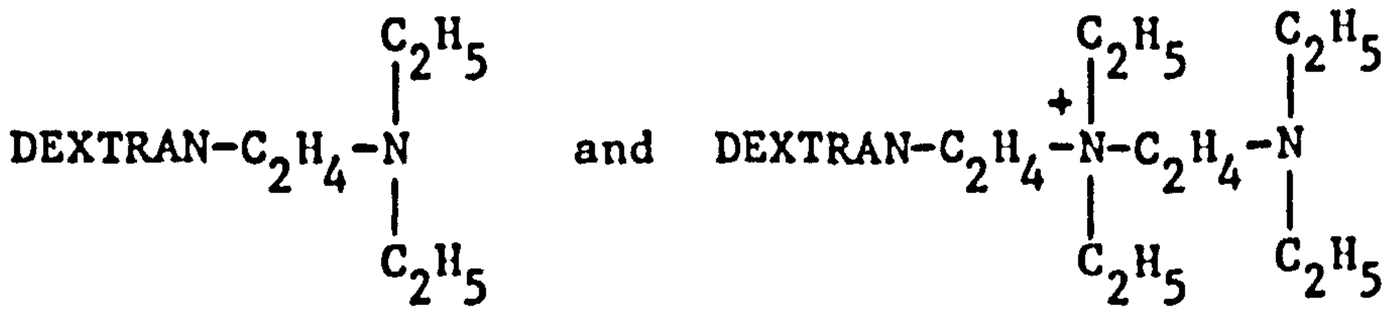

TABLE 4.1 Electrophoretic mobility (EPM), zeta potential (ZP) and K_r of p(BCA) nanoparticles produced in the presence of various stabilisers.

Stabiliser	pH	EPM ($\mu m.cm.s^{-1}.V^{-1}$)	K_r	ZP (mV)
Dextran 70	4.8	-1.72	7.7	-24.2
Dextran sulphate	3.2	-4.13	59	-49.8
DEAE-dextran	2.8	+2.93	23	+36.7
DEAE-dextran	5.0	+2.72	20	+34.5
DEAE-dextran	10.1	+2.15	9.4	+30.0

The tertiary amino group belonging to the simple DEAE substituent has a pK_a 9.5, the tertiary amino group belonging to the 'tandem' DEAE-DEAE substituent has a pK_a 5.7 and the quaternary amino group belonging to the DEAE-DEAE substituent has a $pK_a \sim 14$ (Gubensek and Lapanje, 1968). Thus, the higher the pH the less the polymer is ionised and hence a lower EPM and ZP of the nanoparticles are obtained. Due to the presence of the charged quaternary amino group it is not possible to obtain a polymer with a neutral charge, so at pH 10 the nanoparticles still have a positive EPM.

4.3.2. Particle Size Analysis

Turbidometric analysis of DEAE-dextran stabilised nanoparticles indicated the system to have an average particle diameter of less than 100nm. Analysis by PCS of the suspension diluted with distilled water (final pH = 4), however, gave an average diameter of 484nm. It was also found that the nanoparticle diameter given by PCS was highly dependent upon the ionic strength of the analysis medium (table 4.2 and figure 4.1). As the concentration of added sodium chloride was increased up to 0.5M the measured particle size decreased from 484 to 181nm. The most marked variation in size with sodium chloride concentration occurred from zero to approximately 0.35M. The polydispersity index however, remained fairly constant indicating the PSD of the system was unaltered. These results may be explained by considering the nature of the particle surface and the fact that PCS generates a hydrodynamic diameter (Pusey, 1982) which comprises the particle core plus any firmly bound surface layer that diffuses with the core as a kinetic unit.

TABLE 4.2 Variation of the PCS measured particle diameter (dz) and polydispersity index (Q) with added sodium chloride concentration at pH 4, for DEAE-dextran stabilised p(BCA) nanoparticles.

Added sodium chloride concentration (mole dm^{-3})	dz (nm)	sd	Q	sd
0.0	484	7.6	0.192	0.015
0.002	340	14.0	0.179	0.020
0.010	279	4.1	0.189	0.021
0.020	251	5.0	0.190	0.018
0.100	214	4.3	0.190	0.012
0.200	196	4.4	0.179	0.013
0.350	183	4.3	0.166	0.019
0.500	181	4.6	0.171	0.024

sd = standard deviation

Figure 4.1. The variation in size of DEAE-dextran stabilised nanoparticles as a function of ionic strength, expressed as the negative logarithm of the added sodium chloride concentration (●), and as a function of the pH of the dispersion medium at an ionic strength of 10^{-4}M (o).

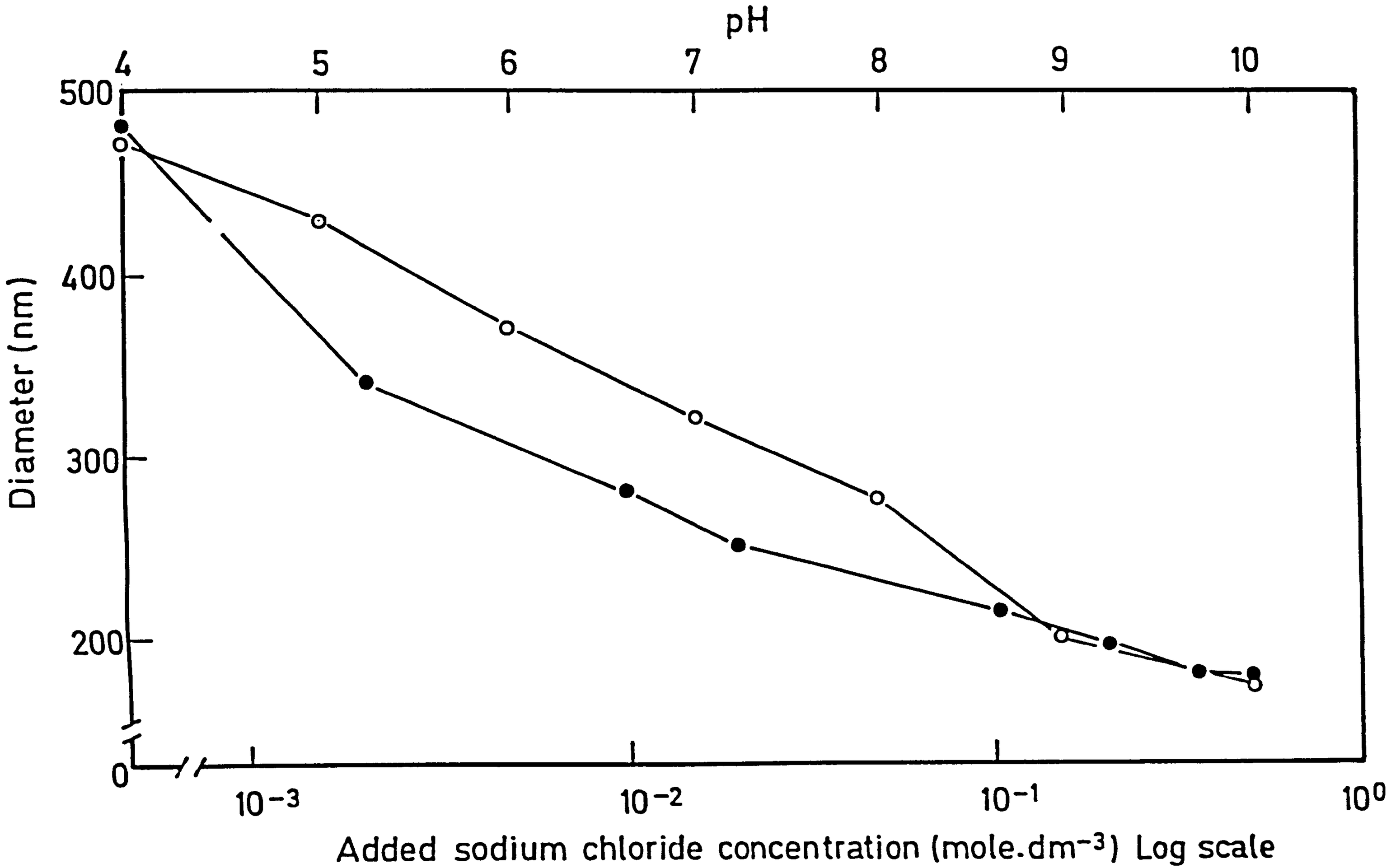
pH
4
5
6
7
8
9
10
500
400
300
200
0
Diameter (nm)
10^{-3}
10^{-2}
10^{-1}
10^{0}
Added sodium chloride concentration (mole.dm^{-3}) Log scale

Nanoparticles produced in the presence of DEAE-dextran were found to be composed of approximately 25% by weight of DEAE-dextran which was firmly bound to the nanoparticle matrix and could not be desorbed by repeated washing and centrifugation. At pH 4 and low ionic strength the amino groups of DEAE-dextran will be virtually totally ionised resulting in the polymer chains, residing in the aqueous phase, adopting an extended conformation due to electrostatic repulsion of the charged groups. This has the effect of providing a relatively large hydrodynamic diameter for the nanoparticles as measured by PCS. However, by increasing the ionic strength of the aqueous medium, charge shielding of the cationic groups reduces the electrostatic interaction allowing the polymer chains to adopt a more compact configuration as depicted in figure 4.2. A limiting size of about 180nm at pH 4 is indicated (table 4.2)

A similar effect was seen by altering the pH of the dispersion medium while the ionic strength was kept constant at 10^{-4}M as expressed in table 4.3 and figure 4.1. As already discussed, by increasing the pH the degree of ionisation of the polymer decreases. This will lead to a reduction in the inter- and intra-chain electrostatic repulsion, thereby reducing the hydrodynamic diameter of the nanoparticles. A limiting size of about 180nm is indicated at pH 10 and ionic strength of 10^{-4} M. However, when both the ionic strength and pH were increased to 0.5M and 10 respectively, the PCS diameter decreased to 158nm corresponding to the maximum collapse of the surface polymer. Similar effects have been reported for other polymer latices with strongly bound layers of water soluble polymers (Goossens and Zembrod, 1979 and 1981).

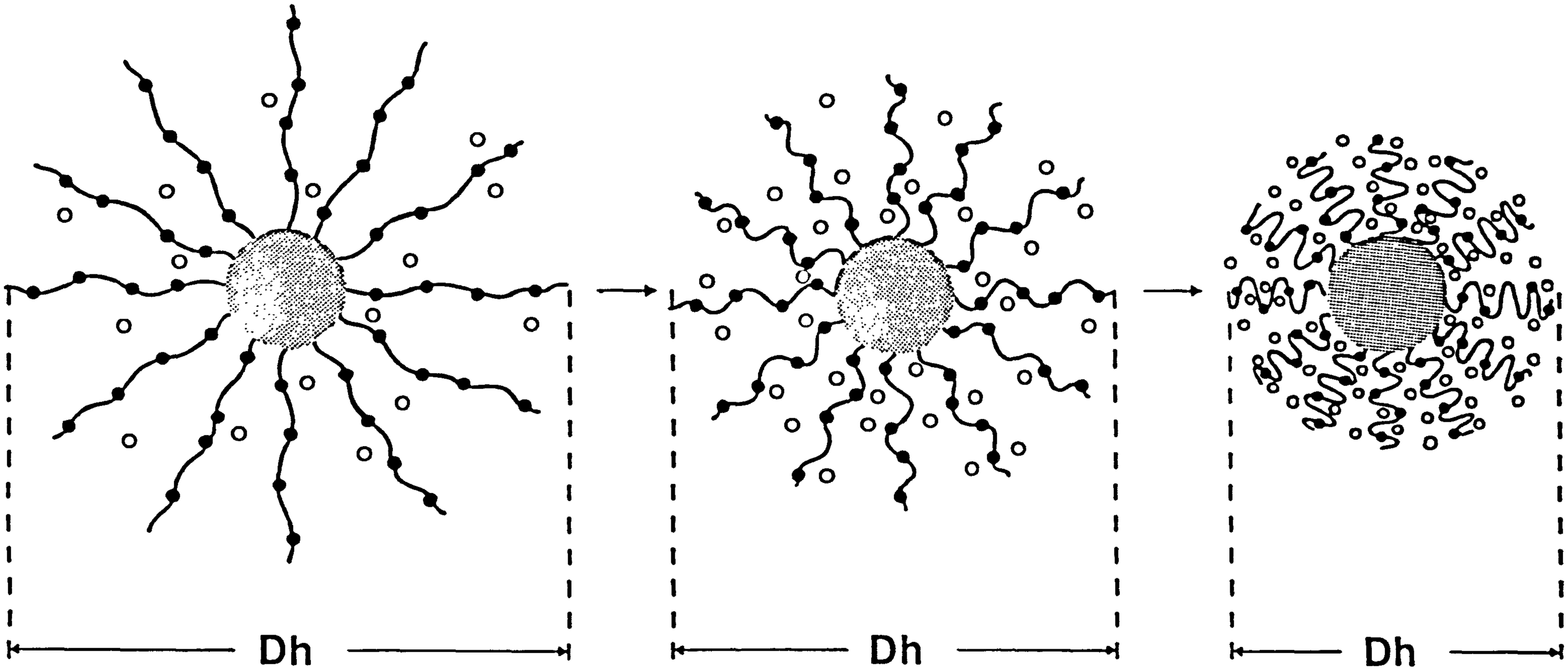

Figure 4.2. Schematic representation of the collapse of the surface DEAE-dextran with increasing ionic strength. The shaded area denotes the particle core, o denotes counterions in solution and ~•~ denotes the charged polymer chains.

TABLE 4.3 Variation of PCS measured particle diameter (dz) and polydispersity index (Q) with pH for DEAE-dextran stabilised nanoparticles at a constant ionic strength of 10^{-4}M.

pH	dz (nm)	sd	Q	sd
4.0	472	11.6	0.183	0.020
5.0	431	7.3	0.204	0.021
6.0	372	14.0	0.184	0.023
7.0	321	12.4	0.176	0.019
8.0	276	6.2	0.203	0.011
9.0	199	7.9	0.193	0.021
10.0	179	8.5	0.194	0.014

sd = standard deviation

The shape of the DEAE-dextran molecule is known to be affected by changes in the ionic strength of the medium, approximating more closely to that of a random coil as the ionic strength is raised. Even when the ionic strength is very low, however, a rigid cylindrical model for the polyion is inadequate to account for some of its properties and a certain amount of folding of the molecule must be assumed. Similar changes in shape may be expected to occur during titration of the charged groups (Gubensek and Lapanje, 1967 and 1968).

The consideration of nanoparticle hydrodynamic diameter may be important with respect to possible extravasation of the carrier. On the basis of the PCS results obtained at low pH and ionic strength there is little chance of these particles passing through fenestrae (approximate diameter 100nm) to reach target sites outside the circulation. However, only the particle core would possess a rigid structure whereas the surface polymer would be able to adapt its conformation to allow passage through pores much smaller than the hydrodynamic diameter of the nanoparticles. In addition, the high pH and ionic strength of the blood stream would result in the surface polymer adopting a collapsed configuration in vivo.

The particle diameter of dextran sulphate stabilised nanoparticles was found to be 1098nm with a polydispersity index of 0.240, as determined by PCS. This would indicate that this polymer is a poor stabiliser despite its high molecular weight which should produce a high degree of steric stabilisation. In addition, the charged nature of the polyion would be expected to impart an additional electro- static repulsive effect which could reduce

particle size still further. One explanation for the low level of stabilisation may be the high degree of substitution of sulphate groups in the glucose residues of the parent dextran; approximately 75% of the available hydroxyl groups are substituted. This would greatly reduce the ability of dextran sulphate to copolymerise with the monomer and form a firmly attached surface layer of polymer that is essential for an effective steric barrier as discussed in chapter 3. The use of a dextran with a much lower degree of substitution would hopefully overcome this problem.

CHAPTER FIVE

COVALENT ATTACHMENT OF AMINES TO NANOPARTICLES

5.1. INTRODUCTION

The potential benefits of using MCA's to achieve site specific targeting have already been illustrated in section 1.4.3.3. Utilisation of the antigen specific 'homing' action of a MCA in association with the high payload capacity and versatility of particulate carriers makes such a combination a highly attractive targeting modality for use in cancer chemotherapy.

This approach has been investigated with p(ACA) nanoparticles by Illum et al (1983 and 1984) (see section 1.7.7.3). Although these studies showed tumour-specific targeting of nanoparticles to occur in vitro this was not observed in vivo. There are several possible explanations for the lack of targeting in vivo such as RES capture, failure to extravasate and antibody displacement from the particle surface by serum proteins. This latter problem was also found to occur in vitro (Illum et al, 1983) and could be a major limiting factor to the use of MCA-nanoparticle combinations where the antibody is bound by physical adsorption. Some method is needed, therefore, of linking the MCA to the nanoparticles via an irreversible bond.

There are several ways of attaining a higher degree of association between microspheres and antibodies and these are summarised in table 5.1 (Illum and Jones, 1985). Non-covalent attachment can be enhanced by the use of ligands which interact

TABLE 5.1 Methods of attachment of monoclonal antibodies to microspheres. Reactive groups and reactions involved (Illum and Jones, 1985).

Functional group on microsphere surface	Mechanism of attachment and comments	Examples
"None"	1.Direct adsorption. Possible competitive displacement by blood proteins. No chemical reagents. Simple procedure. Hydrophobic surface required.	p(ACA) nanoparticles (1,2).
	2.Indirect adsorption via protein A. Simple efficient method. No chemical reagents.	p(ACA) nanoparticles(3). Human serum albumin microspheres(4).
	3.Indirect adsorption via avidin-biotin. Requires covalent conjugation of avidin to particles and biotin to MCA.	Methyl methacrylate microspheres(5).
Aldehyde CHO	1.Direct coupling. Simple and efficient method.	Polyacrolein microspheres (6), polyaldehyde microspheres(7) and albumin microspheres(8).
Carboxylic acid COOH	1.Coupling via carbodiimide. Simple and efficient but crosslinking of the antibody can occur.	Methyl methacrylate microsphers(9).
	2.Coupling via Woodward's reagent K. Degree of binding easy to control.	Polyacrylyl polymer-enzyme(10).
Hydroxyl OH	1.Coupling via cyanogen bromide. Not very efficient, highyl pH dependent and toxic material.	Methyl methacrylate microspheres(11).

TABLE 5.1 continued.

Amino NH_2	1.Coupling via glutaraldehyde. Efficient but derivatisation of the carrier often needed.	Ethylenediamine derivatised methacrylate microspheres (5).
	2.Coupling via SPDP*. Efficient but lengthy complicated procedure.	Liposomes(12).
Dextran	1.Introduction of aldehyde groups by periodate oxidation and imine formation with amino groups.	
	2.Coupling of amines via cyanogen bromide.	For examples see text.
	3.Introduction of a bifunctional amine using cyanogen bromide and subsequent linking via glutaraldehyde.	

* N-succinimidyl 3-(2-pyridylthio) propionate.

References. (1,2) Illum et al, 1983 and 1984; (3) Couvreur, 1984; (4) Kandzia et al, 1981; (5) Kaplan et al, 1983; (6) Margel et al, 1982; (7) Margel et al, 1979; (8) Longo et al, 1982; (9) Molday et al, 1975; (10) Patel et al, 1967; (11) Yen et al, 1976; (12) Weinstein and Leserman, 1984.

specifically with the intact or modified antibody. Staphylococcus aureus protein A (molecular weight 42000) has the capacity to bind with high affinity the Fc portion of the majority of the sub-classes of IgG (Langone, 1982), and this has been exploited for the coupling of antibodies to microspheres (Kandzia et al, 1981; Couvreur, 1984). Alternatively, the antibody may be conjugated with biotin and this specifically adsorbed onto microspheres bearing a covalently linked surface layer of avidin (Kaplan et al, 1983). The avidin then forms essentially an irreversible complex with the biotinylated protein.

Functional groups on the particle surface may be utilised for the covalent coupling of MCA's to microspheres and examples of these are given in table 5.1. Many of these techniques, however, are not applicable to p(ACA) nanoparticles. The cyanoacrylate polymer itself may be regarded as relatively unreactive with respect to derivatisation once the particles are formed. Fortunately, the surface layer of covalently linked dextran present in nanoparticles formed using dextran as a stabiliser (see chapter 3) provides an alternative means of covalent attachment.

Dextran has been widely investigated as a carrier molecule and has been coupled with a diverse range of substances such as amino acids (Barker et al, 1972), enzymes (Foster, 1975), drugs (Nuhn and Schilling, 1975; Harding, 1971) and MCA-drug conjugates (Rowland, 1977; Latif et al, 1980; Bernstein et al, 1978; Manabe et al, 1984). Molecules containing amino groups may be coupled by first activating the dextran hydroxyl groups with cyanogen bromide (Rowland, 1977; Latif et al, 1980) or by oxidising the dextran with periodate to introduce aldehyde functions which may then be condensed with amines

(Bernstein et al, 1978; Arnon and Sela, 1982). Alternatively, the dextran can be derivatised with a bifunctional amine (e.g. 1,6-diaminohexane) and this coupled to an amino containing ligand using glutaraldehyde (Rowland, 1977). Of these techniques, the periodate oxidation method is the most suitable for use with nanoparticles, being relatively simple compared with the derivatisation method and not requiring the high pH of the cyanogen bromide procedure which would cause nanoparticle degradation. The mechanism of periodate oxidation and imine formation is outlined in scheme 5.1.

This chapter describes the preliminary investigations for the application of this technique using the simple amine, aniline, as a model compound.

5.2. EXPERIMENTAL METHODS AND MATERIALS

The nanoparticles in these experiments were used in a flocculated state as obtained after lyophilisation. This allowed rapid centrifugation at low speed (3000 rpm) which was essential for the release measurements and beneficial in the other studies. All reactions were carried out in triplicate and the mean result calculated.

5.2.1. Nanoparticle Preparation and Isolation

The nanoparticles were prepared according to the standard formulation given in chapter 2, except 1% w/v dextran 70 was used as the stabiliser.

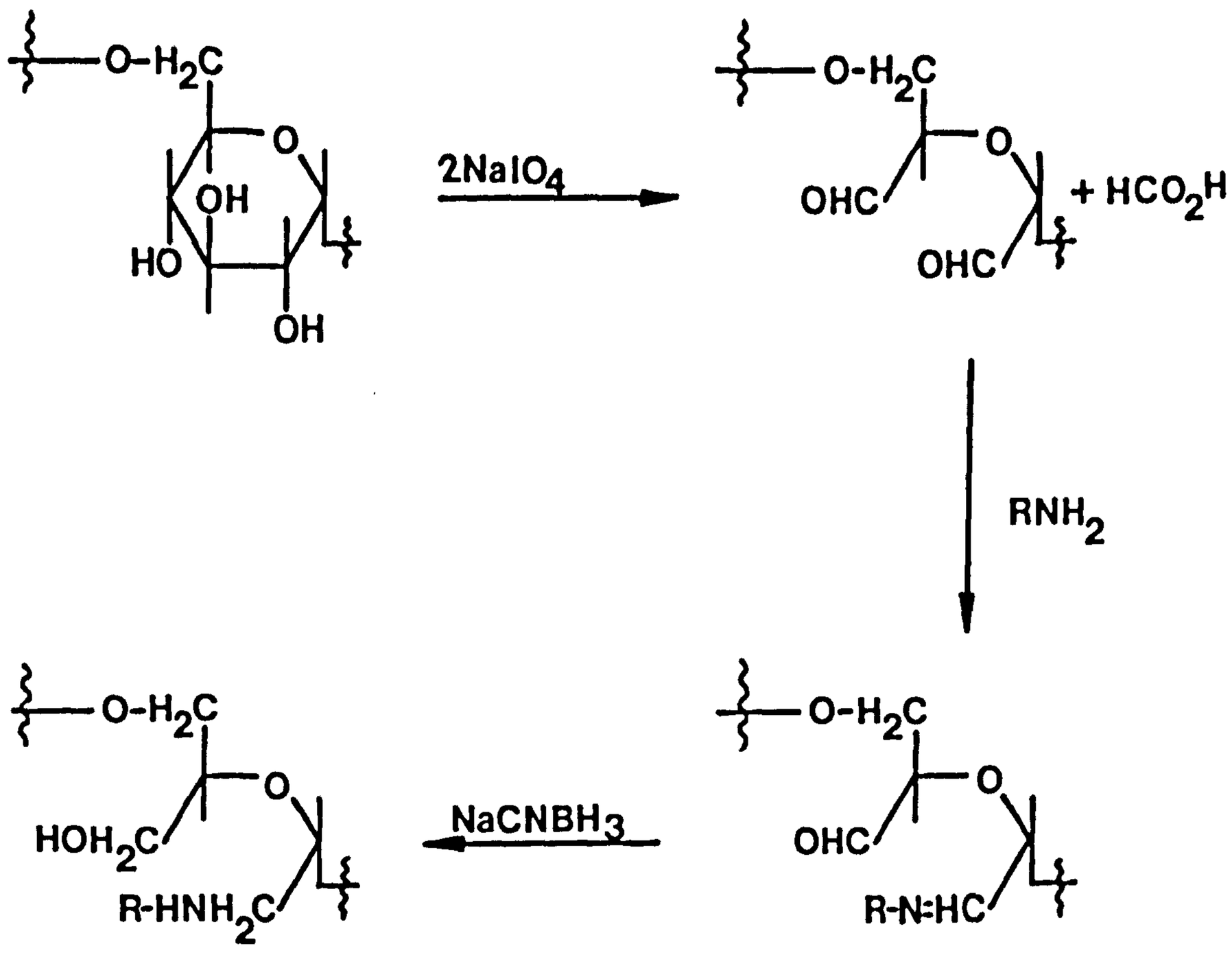

Scheme 5.1. Mechanism of periodate oxidation of dextran to introduce aldehyde groups which may then be condensed with an amine to give the corresponding imine. The imine may be reduced with borohydride to give a stable secondary amine. When R=phenyl (aniline) the intermediate imine is relatively stable and does not require final borohydride reduction.

Free dextran was removed by repeated washing and centrifugation as described in chapter 3. The 'clean' nanoparticles were isolated by lyophilisation.

5.2.2. Optimum Periodate Concentration for Dextran Oxidation

Clean nanoparticles (20mg) were suspended in various concentrations (1 to 10 mg/ml) of sodium periodate (BDH) in distilled water (2ml). These suspensions were agitated in the dark for 3 hours and then unreacted periodate removed by centrifugation and washing with distilled water 5 times. The nanoparticles were then suspended in 2ml of a 3×10^{-2}M solution of aniline (redistilled, Analar, BDH) in 0.1M McIlvaines buffer (pH 4) and agitated in the dark for 16 hours. After this time each supsension was centrifuged and the concentration of aniline remaining in solution determined spectrophotometrically by measuring the ultraviolet (UV) absorbance at 283nm against a suitable blank. Absorbance readings were carried out at alkaline pH by diluting the samples with 0.01N sodium hydroxide. This ensured the amino group was unprotonated and free to act as an auxochrome.

5.2.3. Optimum Coupling pH

Clean nanoparticles (20mg) were suspended in 2ml of a sodium periodate solution (4 mg/ml) and agitated for 3 hours in the dark. Unreacted periodate was removed by centrifugation and washing with distilled water 5 times and the nanoparticles then resuspended in 2ml of 3×10^{-2}M aniline solution in McIlvaines buffer at various

pH's (pH 3 to 7). After agitation in the dark for 16 hours the aniline uptake was determined as before.

This was repeated except periodate was not added during the initial oxidation stage. The uptake at each pH due to covalent linking was then determined by subtracting the uptake onto non-oxidised nanoparticles from the uptake onto periodate treated (oxidised) nanoparticles.

5.2.4. Adsorption of Aniline onto Oxidised and Non-oxidised Nanoparticles at pH 4 and 7

Clean nanoparticles (20mg) in 2ml of a sodium periodate solution (4 mg/ml) were agitated in the dark for 3 hours and then free periodate removed as before. The oxidised particles were then resuspended in various concentrations of aniline (5 to 100 x 10^{-3}M) in McIlvaines buffer at pH 4 or 7. After agitating for 16 hours in the dark at 20°C the degree of aniline uptake was determined as above.

To determine the uptake onto non-oxidised nanoparticles the procedure above was repeated except periodate was not added at the initial oxidation stage.

5.2.5. Release of Aniline from Oxidised and Non-oxidised Nanoparticles

Oxidised or non-oxidised nanoparticles were loaded with aniline to give an uptake of approximately 5 x 10^{-5} mole/100mg of nanoparticles and isolated from free aniline in solution by

centrifugation. These particles were then suspended in 200ml of 0.1M phosphate buffered saline (PBS) (pH 7.4), and stirred at room temperature for 24 hours. The release medium was not heated at 37°C due to the volatile nature of aniline. During this time 5ml samples were withdrawn periodically and rapidly centrifuged. The level of aniline in the aqueous phase was determined as before and the release expressed as a percentage of the total quantity of aniline added in nanoparticle form to the dissolution medium.

The release of aniline from nanoparticles into PBS containing 1% w/v bovine serum albumin (BSA) (Sigma) was also determined as above. The protein interfered with the UV assay, however, and had to be precipitated by the addition of 3ml of acetonitrile (HPLC grade, Romil Chemicals, UK) to 2ml of the centrifuged release sample. The protein was precipitated as an oil which was easily separated by centrifugation. The absorbance at 235nm was then recorded against a blank prepared from 2ml of 1% w/v BSA in PBS mixed with 3ml of acetonitrile and treated in the same way. The aniline concentration was calculated from a calibration curve prepared using the same method but with known concentrations of aniline.

5.2.6. Analysis of Polyaldehyde Dextran by NMR

Dextran 70 (80mg) was dissolved in 2.5ml of deuterium oxide (spectroscopy grade, Aldrich) containing 120mg of sodium periodate and 0.75ml of this transferred to an NMR sample tube. The NMR spectrum was recorded periodically for 6 hours and the signal observed at δ 8.2 was integrated. After this time a trace amount of trifluoroacetic acid (Aldrich) was added to the sample and the

spectrum again recorded. Details of the spectrometer are given in chapter 3.

5.3. RESULTS AND DISCUSSION

5.3.1. Effect of Periodate Concentration on Aniline Uptake

The variation of aniline uptake with the concentration of sodium periodate used during the oxidation stage is given in table 5.2. This shows the level of aniline uptake to steadily increase with periodate concentration up to approximately 4 mg/ml of periodate. Addition of further oxidising agent to the system above this concentration failed to enhance aniline uptake. There is no advantage to be gained, therefore, in using sodium periodate concentrations above 4 mg/ml since possible over-oxidation of the dextran (Dyer, 1956) could reduce the binding efficiency, although this was not seen over the concentration range studied here.

At a concentration of 4 mg/ml the molar ratio of sodium periodate to the repeating anhydroglucopyranose units of dextran 70 is approximately 1.9 (calculated assuming 100mg of nanoparticles contains 16mg of dextran 70 as found in chapter 3). On first inspection this figure is in good agreement with the mechanism proposed in scheme 5.1 where complete oxidation requires 2 moles of periodate. However, no increase in aniline uptake due to covalent linking would be expected to occur after the consumption of one molar equivalent of periodate, since the second mole of oxidising agent is involved in formaldehyde production and does not introduce further aldehyde groups. According to this theory, uptake should

TABLE 5.2 Variation of aniline uptake onto p(BCA) nanoparticles with the concentration of sodium periodate used for oxidation.

Periodate conc. (mg/ml)	Equilibrium conc. (mole dm^{-3} x 10^2)	% uptake	Loading* (mole x 10^5)
1	2.78	7.4	2.21
2	2.57	14.3	4.29
4	2.39	20.4	6.12
7	2.36	21.3	6.39
10	2.39	20.4	6.12

* loading expressed as moles of aniline per 100mg of nanoparticles.

plateau at a periodate concentration of approximately 2 mg/ml. Oxidations are seldom performed using one molar equivalent of periodate, however, and this reagent is always used in excess of that required for primary oxidation (Dyer, 1956; Rankin and Jeanes, 1954). This would agree with the finding that a periodate concentration greater than 2 mg/ml is required for optimum aniline uptake. The situation is complicated due to a number of the dextran glucose units being involved in covalent linking with the cyanoacrylate polymer, and the possible incorporation of dextran into the nanoparticle matrix. Rationalisation of the nanoparticle dextran content in terms of periodate oxidation and subsequent imine formation is, therefore, not possible.

5.3.2. Effect of Coupling pH on Aniline Uptake

The variation of aniline uptake onto oxidised and non-oxidised nanoparticles with coupling pH is given in figure 5.1. Uptake increased for both types of particles as the pH increased due to decreasing ionisation of the aniline, which has a higher affinity for the nanoparticles in its unionised form (see section 1.7.4). The uptake was higher, however, at all pH's with the oxidised nanoparticles which are capable of covalent binding. Assuming the only difference between the two types of nanoparticles is the presence or absence of aldehyde moieties in the stabilising layer of surface dextran, then the enhanced uptake must be due to covalent linking of the amine. Subtraction of the two curves generates a pH profile for aniline uptake due to covalent linking alone which showed a maximum at approximately pH 4. This behaviour is typical

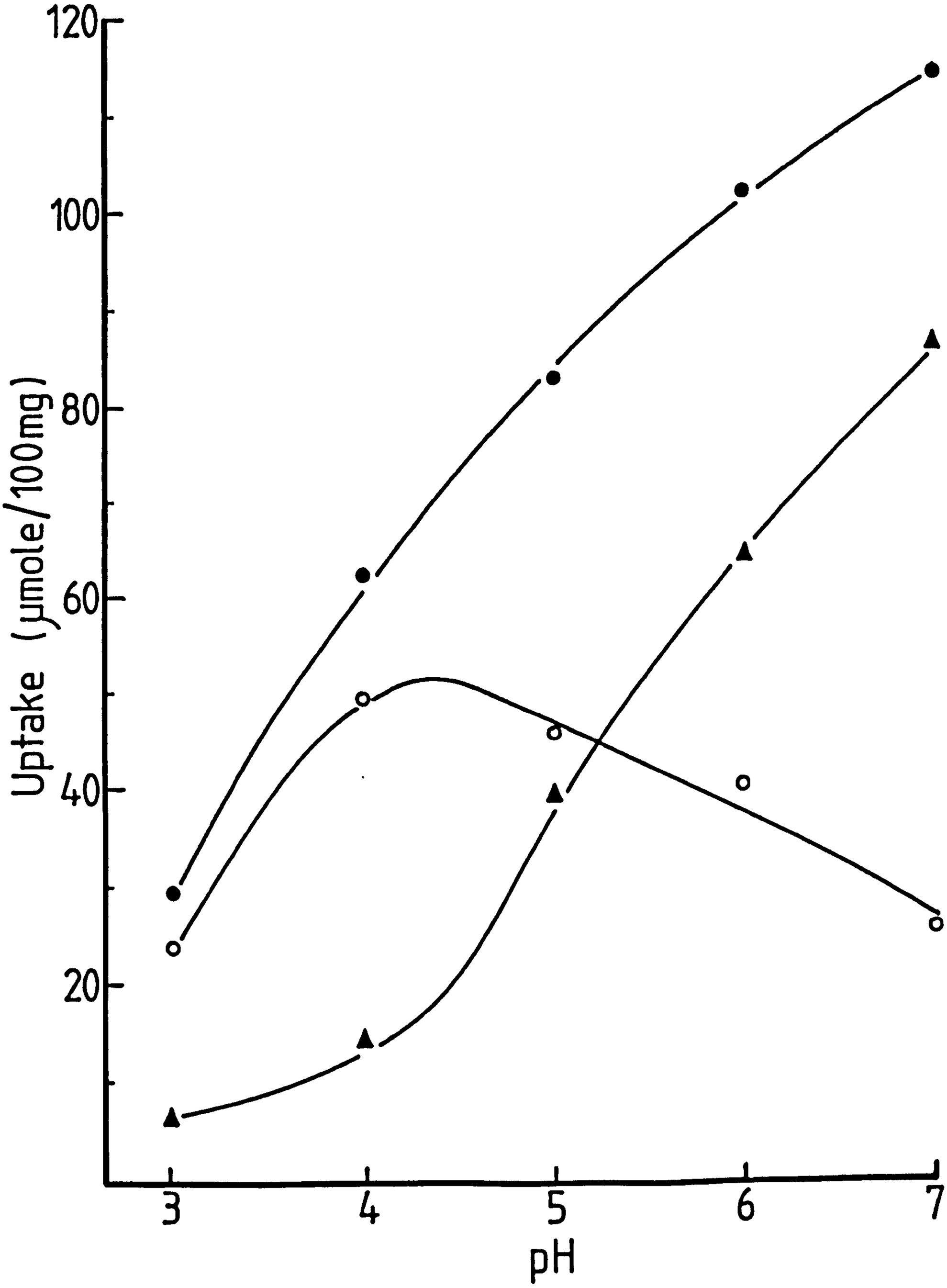

Figure 5.1. Variation of aniline uptake onto oxidised (●) and non-oxidised (▲) nanoparticles as a function of pH. Subtraction of these two curves gives the uptake due to covalent linking alone (o).

for imine formation (Roberts and Caserio, 1977) and may be explained by reference to the rates of equilibria involving aniline and the aldehyde, as well as the rate of dehydration, given by the reaction mechanisms below where Dx denotes dextran and Ph is phenyl.

$$Ph\text{-}NH_2 + H^+ \longrightarrow Ph\text{-}NH_3^+ \qquad [5.1]$$

$$Dx\text{-}CH{=}O + Ph\text{-}NH_2 \rightleftharpoons Dx\text{-}\underset{\displaystyle OH}{\underset{|}{CH}}\text{-}NH\text{-}Ph \qquad [5.2]$$

$$Dx\text{-}\underset{\displaystyle OH}{\underset{|}{CH}}\text{-}NH\text{-}Ph \overset{H^+}{\rightleftharpoons} Dx\text{-}CH{=}N\text{-}Ph + H_2O \qquad [5.3]$$

Clearly, if the unshared electron pair on the nitrogen of aniline is combined with a proton, equation [5.1], it cannot attack the carbonyl carbon to give the aminoalkanol as in equation [5.2]. At low pH the rate of equilibrium for the overall reaction is unfavourable but as pH rises the rate increases because there is more free $Ph\text{-}NH_2$ in solution. Dehydration of the aminoalkanol [5.3] is acid catalysed and this reaction is normally fast at pH values smaller than 3 to 4. At higher pH values it eventually becomes too slow to give a useful overall rate of reaction. This sequence of changes in rate and equilibria has been shown to account precisely for rate-pH profiles for imine formation (Roberts and Caserio, 1977) and is reflected in figure 5.1.

The optimum pH value for the coupling reaction with aniline appears, therefore, to be approximately pH 4. This would have to be determined separately for each amine coupled in this way since the protonation step (equation [5.1]) is dependent on the pK_a of the amine, which for aniline is 4.58. This value is much lower than the

pK_a values of aliphatic amines (typically ~10) due to sharing of the nitrogen lone pair of electrons in aniline with the aromatic ring.

5.3.3. Aniline Uptake onto Oxidised and Non-oxidised Nanoparticles

The uptake of aniline onto oxidised and non-oxidised nanoparticles was determined over a range of aniline concentrations at pH 4 and 7. The resulting adsorption isotherms are given in figure 5.2. At pH 4 the adsorption of aniline onto non-oxidised nanoparticles was minimal due to the partial ionisation of the amino function. With the oxidised system, however, uptake was much higher due to covalent linking. An increased uptake was also observed at pH 7 with the oxidised nanoparticles compared with the non-oxidised system. Uptake for both types of particles was much greater at pH 7 than at pH 4 due to the increase in non-specific adsorption of unionised aniline.

From the results obtained at pH 4 the maximum uptake due to covalent linking was approximately 5×10^{-5} mole/100mg found by subtracting the adsorption values of non-oxidised and oxidised nanoparticles. This compares with a maximum theoretical uptake of 2×10^{-4} mole/100mg calculated assuming 100mg of nanoparticles contains 16mg of dextran (see chapter 3) and each anhydroglucopyranose unit can bind two molecules of aniline. Approximately 25% of the total theoretical covalent binding capacity, therefore, is utilised by this method. This figure may be regarded as a reasonable level of incorporation since not all of the dextran would be available for reaction, as discussed earlier, and it is unlikely

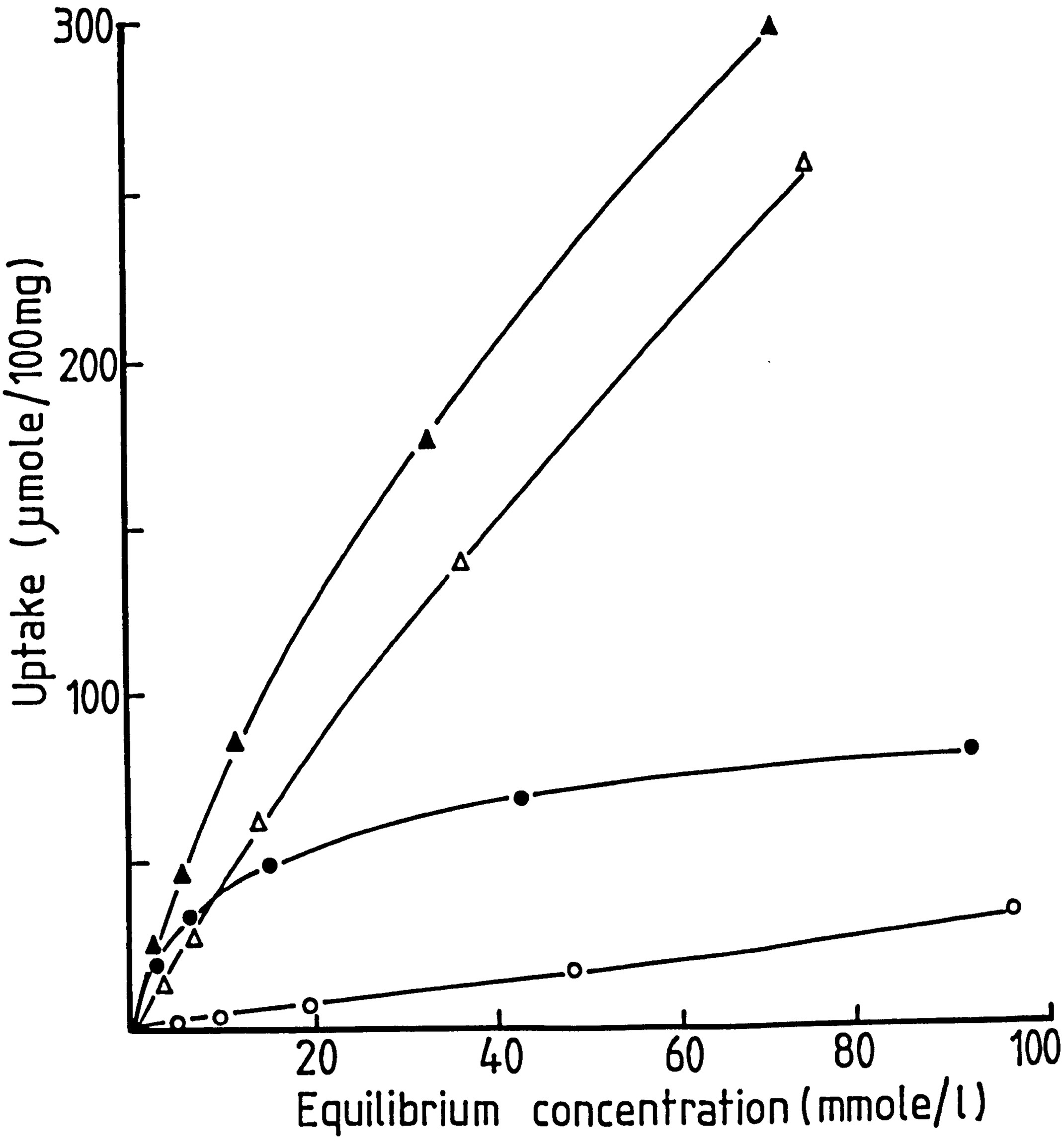

Figure 5.2. Adsorption isotherms of aniline onto oxidised (●) and non-oxidised (○) nanoparticles at pH 4 and for oxidised (▲) and non-oxidised (△) nanoparticles at pH 7 (temperature = 20°C).

that every aldehyde group could accommodate an aniline molecule due to steric hindrance.

5.3.4. Release of Aniline From Oxidised and Non-oxidised Nanoparticles

The release-time profiles of aniline from oxidised and non-oxidised nanoparticles into PBS (pH 7.4) with or without BSA are shown in figure 5.3. The release from oxidised nanoparticles was much less than the corresponding release from the non-oxidised system. For both types of particles there was a rapid 'burst effect' which has been observed for other types of microspheres (Tomlinson et al, 1984; Yapel, 1979). This initial rapid release phase was followed by a much slower rate of release over the next 24 hours. With the oxidised system approximately 16% of the total aniline content was rapidly lost. At a loading of 5×10^{-5} mole/100mg, 14% of the payload is held by non-specific adsorption, so the initial rapid release of aniline is assumed to be due to desorption of this component. With non-oxidised nanoparticles, over 40% of the payload was released initially before an adsorption/desorption equilibrium became established according to the mechanism proposed by (El-Samaligy and Rohdewald, 1982). Subsequent release of aniline in both systems occured slowly as the polymer degrades and, in the case of covalently linked aniline, as the imine broke down.

In the presence of 1% w/v BSA the release rate was enhanced with the non-oxidised nanoparticles to a much greater extent compared with the oxidised system. This indicates that covalently attached aniline is relatively unaffected by the protein interacting

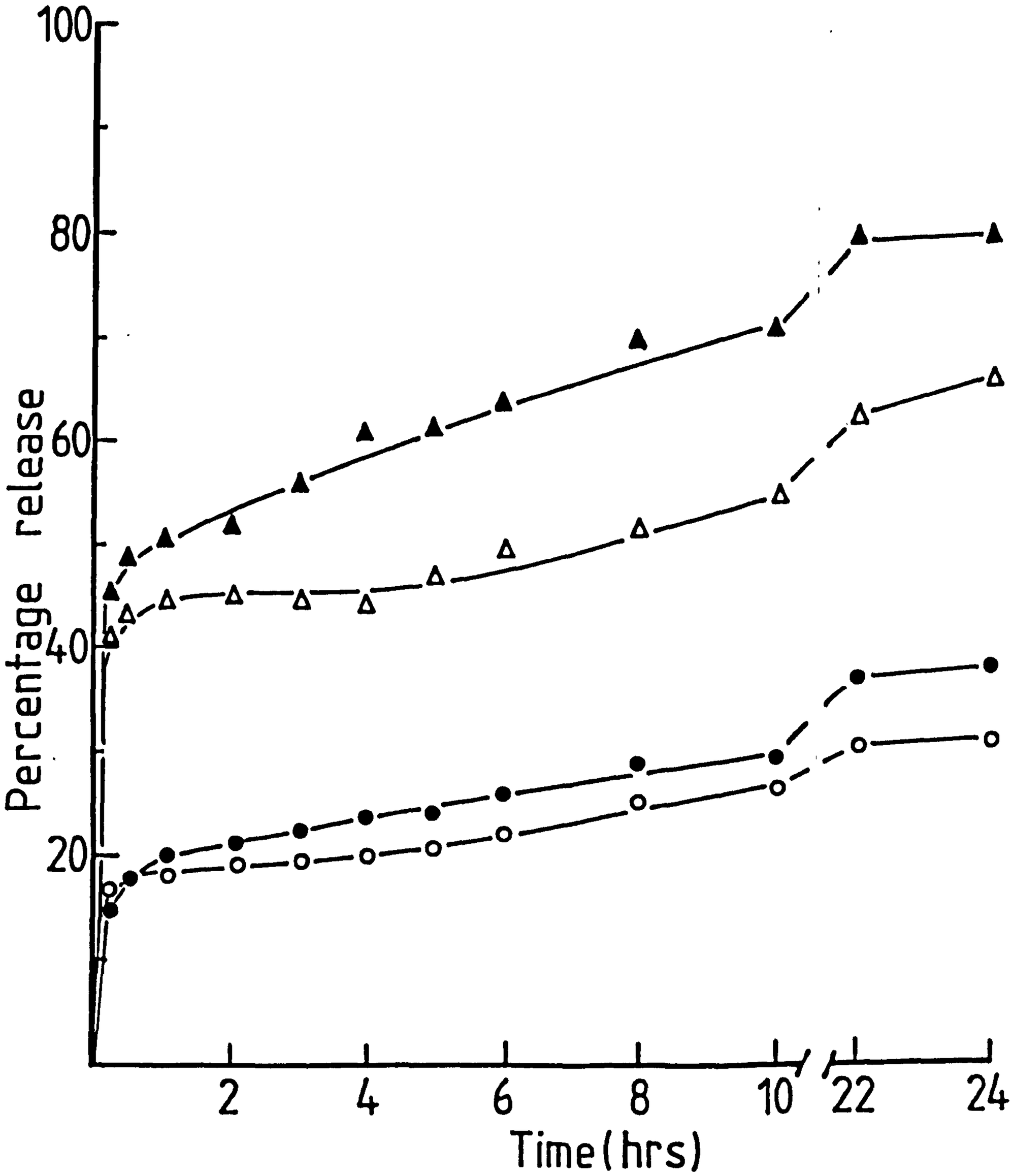

Figure 5.3. The release of aniline from oxidised (o) and non-oxidised (Δ) nanoparticles into phosphate buffered saline (pH 7.4) and from oxidised (●) and non-oxidised (▲) nanoparticles into phosphate buffered saline containing 1% w/v bovine serum albumin (pH 7.4).

with the nanoparticle surface, whereas adsorbed aniline can be displaced to some degree by the albumin.

5.3.5. Covalent Linking of Proteins to Nanoparticles

The initial studies with aniline demonstrated the feasibility of linking simple amines to the nanoparticle surface via a covalent bond. Application of this technique to the binding of antibodies should, theoretically, result in a stable linkage between the particles and the macromolecule. However, initial investigations could not differentiate between covalently attached and physically adsorbed proteins due to the high affinity of proteinaceous material for the hydrophobic nanoparticle surface.

One approach to solving this problem could be the use of NMR to follow the fate of the signal due to the aldehyde proton. This should undergo a shift in the NMR spectrum upon reaction with an amine to give a new signal due to the imine proton. The fate of this signal could also be followed during borohydride reduction as the secondary amine is formed. However, when the NMR spectrum during the formation of polyaldehyde dextran was recorded, no aldehyde signal was observed, although a peak at δ 8.2 due to the formation of formic acid was seen. The integral value for this proton steadily decreased with time as the formic acid was oxidised to carbon dioxide and water.

The absence of the aldehyde signal could be due to the proton exchanging with deuterium from the solvent, but this is unlikely since aldehydes are normally unaffected by the addition of D_2O. Alternatively, the aldehyde groups could react with free hydroxyls

present in dextran to form a hemi-acetal or acetal according to the following reaction mechanism where Dx and Dx' denote dextran aldehyde and hydroxyl moieties respectively.

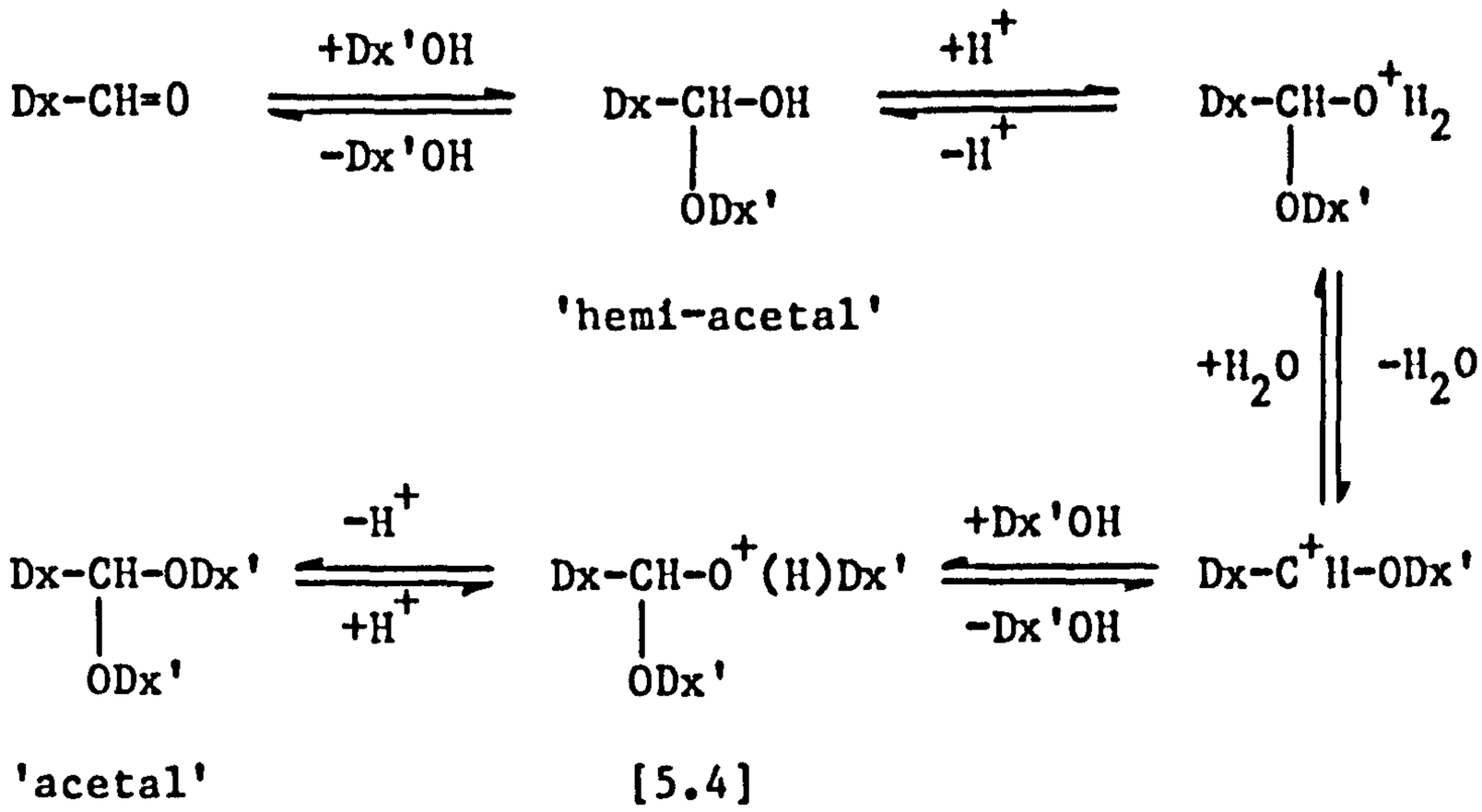

[5.4]

Normally the hemi-acetal is not isolated and the reaction proceeds to acetal formation. The proton in either of these systems could not be resolved since it occurs at a point where it is masked by other signals from the molecule. The reaction given in [5.4] is normally reversed by the addition of acid. However, when trifluoroacetic acid was added to the NMR sample the aldehyde signal failed to appear, indicating the acetal is particularly stable.

This reaction is known to occur with polyaldehyde dextran (Ishak and Painter, 1978) and may explain the behaviour observed in the NMR spectrum. Similarly, Sloan et al (1954) found polyaldehyde dextran to give only a weak IR carbonyl absorption and no UV aldehyde absorption, although these workers proposed a hydration effect to explain the anomalous spectra.

NMR does not, therefore, appear to be a suitable method for following the coupling reaction with proteins. Although a more powerful spectrometer could possibly resolve the remainder of the

spectrum, it is doubtful if the resolution would be high enough to achieve this on the nanoparticle surface and in the presence of interference from the protein.

CHAPTER SIX

RADIOLABELLING OF NANOPARTICLES

6.1. INTRODUCTION

In order to determine the _in vivo_ distribution of parenterally administered nanoparticles, the colloidal system must be radiolabelled with a suitable radionuclide. This may be achieved using a beta-emitter such as carbon-14 which has been used with p(ACA) nanoparticles (Grislain _et al_, 1983; Lenaerts _et al_, 1984b) and various other colloidal systems such as poly methyl methacrylate particles (Leu _et al_, 1984). The use of ^{14}C as a radiolabel for p(ACA) nanoparticles, however, has several problems. Initial prepration of the ^{14}C labelled monomer is a highly specialised procedure and this compound, when isolated, is prone to spontaneous polymerisation and yields systems with a wide particle size distribution (Kreuter, 1984). The _in vivo_ studies require the sequential sacrifice of a large number of animals, normally rats or mice, and subsequent time consuming liquid scintillation counting of the activity in individual organs. Interference from the degradation products of labelled particles is hard to detect and eliminate since the biodistribution of these components cannot readily be determined.

Alternatively, the nanoparticles could be radiolabelled with a gamma-emitting radionuclide and the biodistribution followed by gamma scintigraphy. This approach has several advantages over beta counting, requiring fewer animals and yet providing much more data

on kinetics concerning the dynamics of the distribution pattern. It cannot, however, resolve fine distribution detail (e.g. it is often not possible to distinguish the liver and spleen separately) nor provide information on cellular distribution within a given organ. Despite this, gamma scintigraphy has found many applications for radionuclide imaging in drug research (Wilson et al, 1982) and has been used to determine the fate of colloidal systems such as liposomes (Pro fitt et al, 1983), polystyrene latices (Kanke et al, 1980; Illum and Davis, 1984a and b) and emulsions (Davis and Hansrani, 1982) in a range of animals (rats, mice, rabbits, dogs).

Before in vivo studies can be performed it is necessary to develop a technique for radiolabelling nanoparticles with a suitable gamma-emitter. The choice of radionuclide will be governed by several factors: the gamma ray energy should be in the range 70 to 400 keV with an ideal energy of about 150 keV (McAfee and Subramanian, 1969) and the half life of the nuclide should be sufficiently long to enable imaging over a period of at least a day. Taking into account these factors, together with the practical aspects of cost and availability, there are a limited number of suitable radionuclides available (table 6.1). These may be divided into those which can be covalently bonded and the metal-ion nuclides which are mostly used in a complexed form. Of the 'covalent labels' iodine-131 is the most widely used but has the disadvantage of beta-emission, making handling hazardous. Although iodine-123 is ideal for gamma camera imaging its short half life affects availability and cost.

TABLE 6.1 Radionuclides which may be suitable for labelling nanoparticles (data taken from Kelly, 1982).

Radionuclide	$T_{1/2}$	Principle photons, keV, with abundances
'Covalent' labels		
^{75}Se	118.5 days	136 (54%), 265 (57%)
^{123}I	13 hours	159 (97%)
^{125}I	60 days	27 (138%)
^{131}I	8.05 days	360 (79%)
^{197}Hg	2.7 days	77 (20%), 69 (75%)
Metal-ion nuclides		
^{67}Ga	78 hours	93 (40%), 184 (24%), 296 (22%)
^{99m}Tc	6 hours	140 (90%)
^{111}In	2.8 days	171 (91%), 245 (94%)
^{113m}In	1.7 hours	393 (65%)
^{201}Tl	73 hours	69-83 (98%)

There are several techniques available for radioiodinating substrates (Kelly, 1982) such as exchange iodination (Hupf et al, 1978), direct iodination (Bolton, 1977), indirect iodination (Bolton and Hunter, 1973) and direct chemical synthesis (Kabalka et al, 1981). Polystyrene particles have been radiolabelled by irradiating suspensions of polystyrene latex containing ^{131}I with a cobalt-60 source at radiation doses up to 5×10^{20} eV ml^{-1} (Huh et al, 1974). Labelling was proposed to occur by the reaction of hydroxyl radicals, produced by the ionising radiation, with ^{131}I to form stable carbon-iodine-131 bonds. This technique has been used by Illum and Davis (1984a and b) when radiolabelling polystyrene particles for use in vivo.

Of the metal-ion nuclides, technetium-99m is widely used due to its chemical versatility, ideal decay energy, optimum half life and relatively low cost (Kelly, 1982). Technetium-99m is readily obtained from a generator system (Stang and Richards, 1964) in which ^{99}Mo decays to ^{99m}Tc and is eluted from the generator column as $^{99m}TcO_4^-$. In this oxidation state (+7) ^{99m}Tc will not bind to chelating agents nor to particles. Consequently it is reduced to one of its lower oxidation states usually with stannous ion. The radiochemistry of ^{99m}Tc has been extensively studied (Eckelman and Levenson, 1978) together with its applications for labelling radiopharmaceuticals (Eckelman and Levenson, 1977). Of the other metal-ion nuclides, indium-111 is highly versatile and has attracted much attention (Thakur, 1977).

Although a vast literature exists on radiolabelling techniques, the application of this technology to p(ACA) nanoparticles poses

many problems. Ideally the radiolabel should remain associated with the colloid over a sufficient period of time to allow the biodistribution to be accurately determined. If the label does dissociate *in vivo* then spurious results will be obtained. Much of the work presented in this chapter, therefore, is concerned not only with developing a simple and efficient radiolabelling technique but also with its validation for use *in vivo*. In addition, the label itself should not adversely affect such factors as nanoparticle size, stability, degradation or surface characteristics.

6.2. EXPERIMENTAL METHODS AND MATERIALS

6.2.1. Labelling of Nanoparticles Using Rose Bengal and Rose Bengal Benzyl Ester

Rose bengal was investigated as a possible radiolabel for nanoparticles since this compound readily undergoes exchange radioiodination (Hupf *et al*, 1978) and would be expected to have high affinity for p(BCA) nanoparticles due to its hydrophobic nature. In addition, this organic acid may be readily derivatised to yield less polar esters which would be expected to show an enhanced affinity for the nanoparticles.

6.2.1.1 Synthesis of rose bengal benzyl ester

The benzyl ester of rose bengal was prepared according to a modified method of Lamberts and Neckers (1983). This is outlined in scheme 6.1.

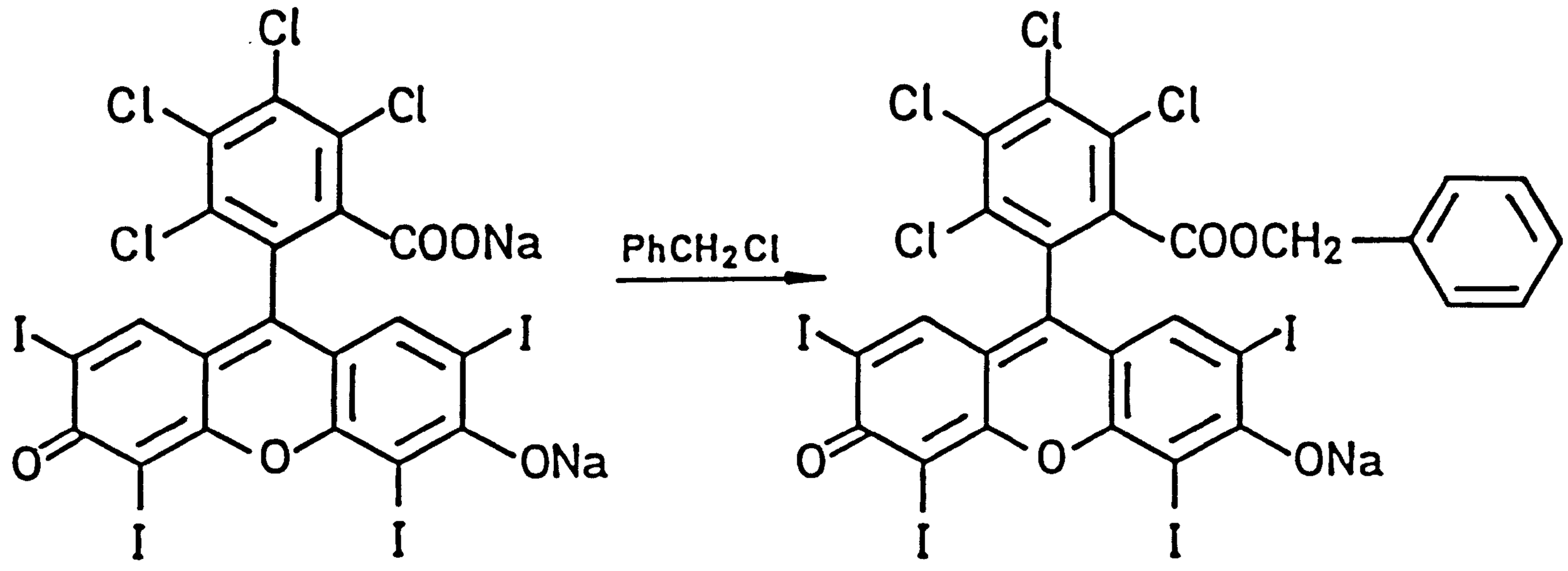

(a) (b)

Scheme 6.1. Conversion of rose bengal (a) to its benzyl ester (b).

To 500mg of rose bengal (BDH) in 10ml of dimethylformamide was added 62mg of benzyl chloride (Aldrich) and this heated at 100°C for 3 hours. After cooling, ethyl acetate (30ml) and distilled water (30ml) were added and the organic phase separated after gentle agitation. The aqueous layer was then extracted with ethyl acetate (3 x 30ml) and the combined extracts washed with distilled water (2 x 50ml). The ethyl acetate was removed under reduced pressure and dichloromethane (50ml) together with 1N hydrochloric acid (20ml) added to the residue. After vigorous shaking the organic phase was washed with water (2 x 30ml) followed by saturated sodium bicarbonate solution (1 x 30ml), distilled water (3 x 30ml), 1N hydrochloric acid (1 x 30ml), distilled water (2 x 30ml), and saturated sodium chloride solution (1 x 30ml). After drying over dried magnesium sulphate the solvent was removed under reduced pressure. The resulting solid was washed with ether (3 x 30ml) and then dried in vacuo to give a dark red solid. Yield = 57%.
^{1}H NMR, 90MHz ($CDCl_3$, Me_4Si) δ : 5.00 (2H, s, $C\underline{H}_2Ph$), 6.70-7.40 (7H, m, aromatics and xanthene 2H). UV max.,in water containing 1% w/v poloxamer 338 (E1%): 572 (635), 532 (128). IR max., wavenumber (cm^{-1}): 3420, 2920, 1735, 1610, 1560, 1505, 1250, 960.

6.2.1.2. Adsorption isotherms of rose bengal and its benzyl ester

Clean flocculated dextran 70 stabilised nanoparticles were prepared as described in chapter 5. The particles (30mg) were suspended in 3ml of various concentrations of rose bengal in PBS (pH 7) and gently agitated at 20°C for 3 hours. After this time the samples were centrifuged (3000 rpm) and the equilibrium

concentration remaining in solution determined by UV analysis at 547nm against a suitable blank. From this, the equilibrium uptake was calculated and an adsorption isotherm constructed.

This was repeated using nanoparticles stabilised with DEAE-dextran, prepared as described in chapter 4. These particles were cleaned by repeated washing and centrifugation and used in a flocculated state as obtained after lyophilisation.

The adsorption of rose bengal benzyl ester onto dextran 70 stabilised nanoparticles was determined as described above using a wavelength of 572nm for UV analysis. Due to the low water solubility of this compound, solutions had to be prepared using PBS (pH 7) containing 1% w/v poloxamer 338. To enable comparison between the uptake of rose bengal and its benzyl ester an additional adsorption isotherm was constructed for rose bengal using solutions prepared in PBS (pH 7) containing 1% w/v poloxamer 338.

6.2.1.3. Release of rose bengal and its benzyl ester from nanoparticles

Dextran 70 stabilised nanoparticles (100mg) were loaded with approximately 2×10^{-6} mole of rose bengal or its benzyl ester and isolated by centrifugation. The particles were then suspended in 200ml of PBS (pH 7.4) or in PBS (pH 7.4) containing 1% w/v BSA. These suspensions were stirred at 37°C for 24 hours and 5ml samples withdrawn periodically. The samples were rapidly centrifuged and the concentration of label in solution determined by UV analysis against a suitable blank. The release was then calculated and expressed as a

percentage of the total amount of rose bengal or its ester added to the dissolution medium.

This was repeated with DEAE-dextran nanoparticles loaded with a similar quantity of rose bengal.

6.2.2. Radiolabelling of the Nanoparticle Cyanoacrylate Polymer With Iodide-131

The polymerisation mechanism of ACA given in scheme 2.1 indicates the initiating nucleophile is present in the final polymer as an end group. This has been shown to occur during nanoparticle formation (chapter 3) and during ACA polymerisation by other workers (Leonard et al, 1966). The ability of a nucleophile to initiate polymerisation will be related to its degree of nucleophilicity which is defined as the ability to form bonds with carbon atoms (Finar, 1973). The order of nucleophilicity is dependent upon the nature of the solvent but generally may be given as

$$PhS^- > CN^- > I^- > EtO^- > OH^- > Br^- > PhO^- > Cl^-$$

This indicates that iodide is a more powerful nucleophile than hydroxyl which is normally the initiating species. Addition of $^{131}I^-$ to the polymerisation medium could result in this nucleophile being incorporated into the polymer chain, thereby providing a simple method for radiolabelling nanoparticles.

To the standard nanoparticle reaction formulation at pH 1 or 2, given in chapter 2, was added 0.01ml of sodium iodide-131 solution (Amersham, UK) containing a total activity of 1 mega-Becquerel (MBq). After addition of the monomer the mixture was stirred for 2 hours. The nanoparticles were then flocculated by a freeze/thaw

cycle and centrifuged. The activity in the solid was determined by gamma counting (IN Intertechnique CG4000 Automatic Gamma Well Counter, Intertechnique, France) and expressed as a percentage of the total added activity.

6.2.3. Radiolabelling of Nanoparticles With Iodine-131

Molecular iodine, I_2, is poorly soluble in water (0.33g dm^{-3} at 25°C) but partitions readily into non-polar solvents such as carbon tetrachloride (Cotton and Wilkinson, 1968). This species would be expected, therefore, to partition into the hydrophobic nanoparticle matrix in preference to the aqueous phase.

6.2.3.1. Incorporation of molecular iodine-131 into nanoparticles

To a solution of dextran 70 (125mg) and sodium iodide (17.3mg) in distilled water (24.4ml) was added 0.1ml of a sodium iodide-131 solution (total activity 1MBq). This was followed by 25mg of chloramine T (Sigma) and 0.31ml of 1N hydrochloric acid to adjust the pH to 2. BCA (0.25ml) was rapidly added and the mixture stirred at room temperature until polymerisation was complete (2 hours). The nanoparticles were then flocculated and centrifuged. The percentage of the total added activity incorporated into the nanoparticles was then determined by gamma counting.

The optimum chloramine T/sodium iodide ratio was determined by keeping the chloramine T concentration constant at 1 mg/ml and varying the sodium iodide concentration in the formulation given above.

6.2.3.2. Release of incorporated molecular iodine-131 from nanoparticles

Nanoparticles radiolabelled with $^{131}I_2$ were prepared as described above. This suspension was flocculated by a freeze/thaw cycle and a 10ml sample centrifuged. The solid was resuspended in 200ml of PBS (pH 7.4) or PBS (pH 7.4) containing 1% w/v BSA and stirred at 20°C for 24 hours, during which time 5ml samples were withdrawn at regular intervals and centrifuged. The activity released into solution was then determined for each sample by gamma counting and expressed as a percentage of the total activity added to the dissolution medium.

6.2.4. Radiolabelling of Nanoparticles With Indium-111-Oxine

Oxine (8-hydroxyquinoline) forms a saturated (3:1) complex with indium (Thakur, 1977). This neutral, lipid soluble complex would be expected to partition into nanoparticles with high affinity and thereby provide a simple radiolabelling procedure.

6.2.4.1. Adsorption of indium-111-oxine onto nanoparticles

Clean, flocculated dextran 70 stabilised nanoparticles were prepared as described in chapter 5. To 2.5ml of a 1% w/v nano-particle suspension in distilled water at pH 7 (adjusted by the addition of 0.01N sodium hydroxide) was added 0.1ml of an indium-111 oxine complex (Amersham) with a total activity of 1MBq. After 1 hour this mixture was centrifuged and the uptake onto the nanoparticles

determined by gamma counting and expressed as a percentage of the total added activity.

This was repeated over a range of pH's (3 to 7) with the pH being adjusted by the addition of 0.01N hydrochloric acid or sodium hydroxide and checking with a calibrated pH meter. Uptake was also determined using PBS (pH 7) as the suspending medium.

6.2.4.2. Release of the indium-111-oxine complex from nanoparticles

Nanoparticles were labelled with the indium-111-oxine complex as described above by adding 0.2ml of the complex (2MBq) to 5ml of a 1% w/v nanoparticle suspension and then isolating the solid by centrifugation. These particles (50mg) were then resuspended in 100ml of PBS (pH 7.4) or distilled water. The pH of the latter system was maintained at 7.4 by the addition of 0.1N sodium hydroxide. This was repeated with the release media containing 1% w/v BSA. The release of the complex into solution was determined at 37°C over a period of 24 hours as described for $^{131}I_2$ labelled nanoparticles.

6.2.5. Radiolabelling of Nanoparticles Using a Technetium-99m-Dextran Complex

Technetium-99m is capable of forming a complex with dextran after reduction of pertechnetate with stannous ion according to the following mechanism (Henze et al, 1982a)

$$TcO_4^- + 2[C_6H_{10}O_5] + Sn^{2+} + H_2O \longrightarrow [TcO(C_6H_8O_5)_2]^- + 4H^+ + [SnO_2(OH)_2]^{2-}$$

in which two anhydroglucopyranose units of the dextran chains form bidentate chelates with the reduced ^{99m}Tc. Two adjacent hydroxyl groups per anhydroglucopyranose unit are assumed to be involved in forming the two five membered chelate rings. The resulting complex is stable *in vitro* and *in vivo* and has been used for angiocardiography (Henze *et al*, 1982a) and lymphoscintigraphy (Henze *et al*, 1982b).

It has already been shown (chapter 3) that dextran can copolymerise with the monomer during nanoparticle formation and become incorporated into the nanoparticle matrix. It should be possible, therefore, to radiolabel nanoparticles using a ^{99m}Tc-dextran complex.

6.2.5.1. Incorporation of a technetium-99m-dextran complex into nanoparticles

Technetium-99m was attached to dextran 10 (molecular weight 9000, Sigma) after reduction with stannous ion by a modified method of Henze *et al* (1982a). This involved adding, with vigorous mixing, 10ml of a 10% w/v dextran 10 solution in deoxygenated distilled water to 0.05ml of a solution of stannous chloride (Sigma) in concentrated hydrochloric acid (6 mg/ml). 2.2ml of this solution was filtered (0.2μm membrane filter) and mixed with 1ml of the eluate from a ^{99m}Tc generator (Amersham) containing 1 MBq of activity. After 10 minutes this was diluted to 11ml with deoxygenated distilled water and 9.8ml filtered (0.2μm membrane filter) into a McCartney vial fitted with a glass covered magnetic stirrer bar. To this was added BCA (0.2ml) and the mixture rapidly stirred for 1.75

hours. After this time 1ml of 0.5M phosphate buffer (pH 7) was added and stirring continued for a further 15 minutes. 2.5ml of the suspension was then passed through a 1 x 20cm Sepharose CL 4B column (Pharmacia, Sweden) which had been pre-conditioned with 2ml of a 'cold' nanoparticle suspension flushed through with 30ml of PBS (pH 7). The labelled nanoparticles were eluted with PBS (pH 7) and the activity in each 1ml fraction was determined by gamma counting and expressed as a percentage of the total activity added to the column. The total nanoparticle elution volume was found to be 2.5ml which had a solids content of 33mg.

Thin layer chromatography was performed on the ^{99m}Tc-dextran solution prior to addition of the monomer and on the nanoparticle solutions before and after gel filtration. Silica gel impregnated glass fibre sheets (1 TLC-SG, Gelman Instruments, USA) were used with 0.9% w/v sodium chloride as the solvent. The chromatograms were scanned by a radiochromatogram scanner (Medical Physics Department, Queens Medical Centre, Nottingham).

6.2.5.2 Release of activity from ^{99m}Tc-dextran labelled nanoparticles

The labelling procedure was repeated as above and the column fractions containing a total of 50mg of labelled nanoparticles combined and flocculated (obtained from two separate column elutions). These particles were resuspended in 100ml of PBS (pH 7.4) or PBS (pH 7.4) containing 1% w/v BSA. The suspensions were stirred at 37^{o}C for 24 hours and the release of activity determined as described previously.

6.3. RESULTS AND DISCUSSION

6.3.1. Labelling With Rose Bengal and its Benzyl Ester

The high affinity of rose bengal for p(BCA) nanoparticles is shown by the adsorption isotherm for rose bengal onto dextran 70 stabilised nanoparticles given in figure 6.1. The data give a good linear relationship (correlation coefficient 0.9991) when analysed in accordance with the linear form of the Langmuir adsorption isotherm equation (Giles et al, 1974) which may be written as

$$c/(x/m) = 1/sb + c/s \qquad [6.1]$$

where x is the amount of solute adsorbed by weight, m, of adsorbant, c is the equilibrium concentration, b is a constant related to the enthalpy of adsorption, and s, which is related to the surface area of the solid, is a measure of the adsorptive capacity of adsorbent for the adsorbate.

The Langmuir constants in this case were found to be

$s = 5.37 \times 10^{-3}$ mole g^{-1} and $b = 1.06 \times 10^{2}$ dm^{-3} $mole^{-1}$

The adsorption of rose bengal was greatly enhanced (10 fold) by using nanoparticles stabilised with DEAE-dextran as shown by the adsorption isotherm in figure 6.2. The cationic groups of this surface polymer located at the nanoparticle surface are capable of ion-pairing with anionic rose bengal molecules giving a high binding capacity. The isotherm shows complete (high affinity) adsorption of rose bengal from solution up to a particle loading of approximately 3.5×10^{-4} mole solute/g of nanoparticles. This corresponds well with the theoretical maximum uptake attributable to the DEAE-dextran

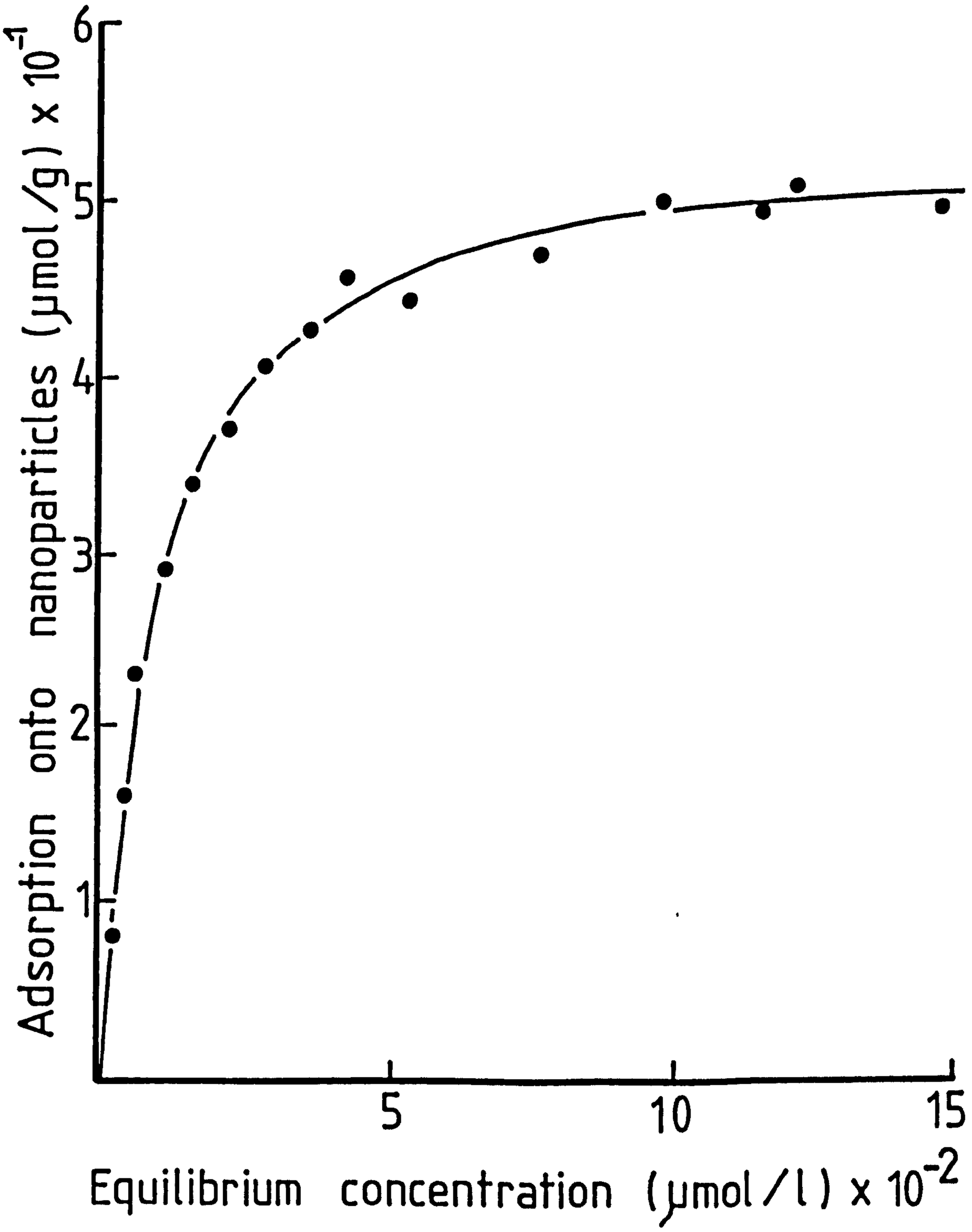

Figure 6.1. Adsorption isotherm of rose bengal onto dextran 70 stabilised nanoparticles at 20°C.

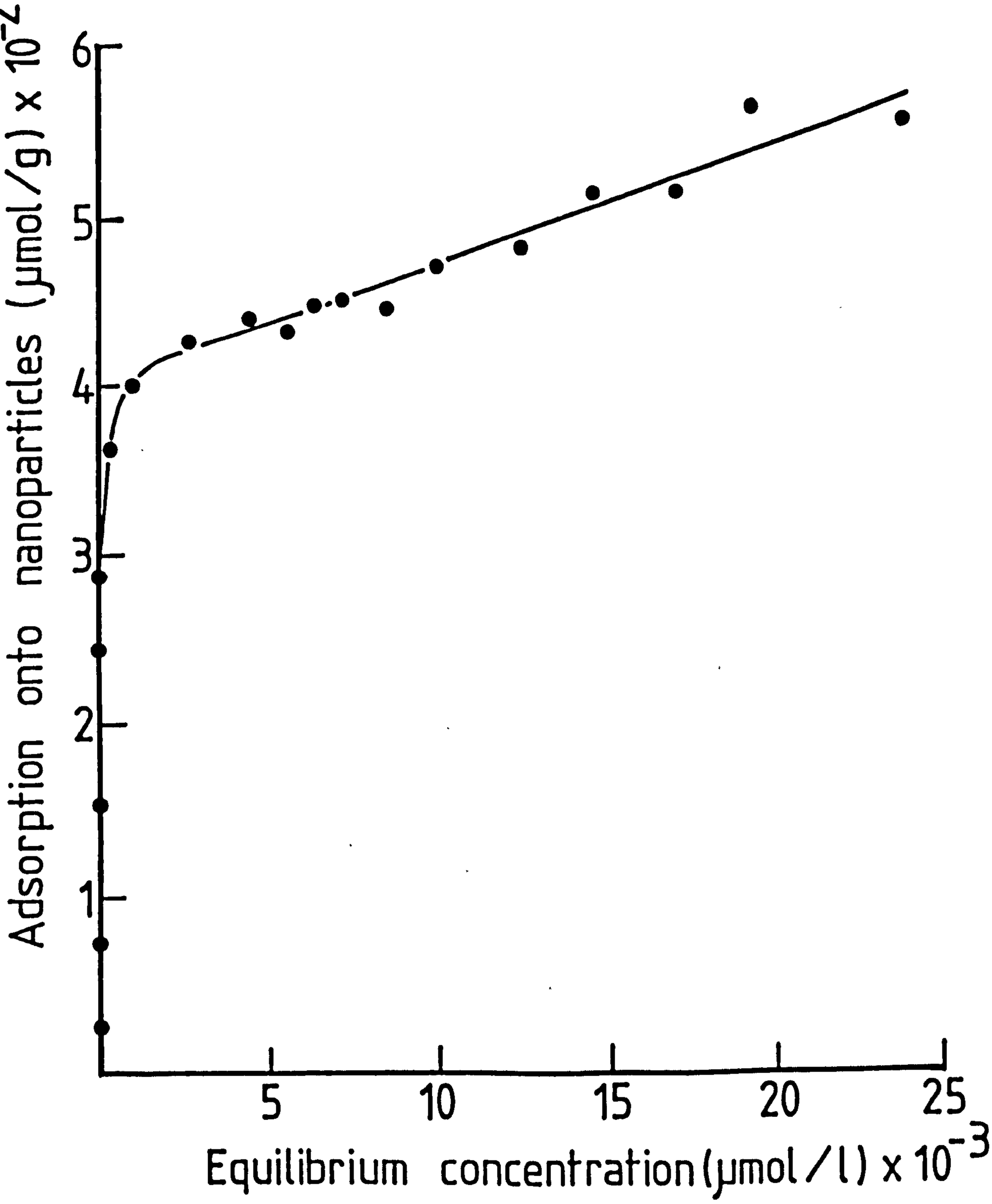

Figure 6.2. Adsorption isotherm of rose bengal onto DEAE-dextran stabilised nanoparticles at 20°C.

content, calculated assuming each cationic group will bind one molecule of rose bengal. Thus, 1g of nanoparticles containing 0.25g of DEAE-dextran with a nitrogen content of 3.2% gives a binding capacity of 5.7×10^{-4} mole. However, this assumes all amino groups will be charged, but at pH 7 the tertiary amino group of the 'tandem' DEAE-DEAE substituent (pK_a 5.7) will be mainly unionised ($\sim$3% as N^+) giving a maximum theoretical binding capacity of approximately 3.8×10^{-4} mole/g nanoparticles. The sharp inflection point in the isotherm which occurs at this loading implies, therefore, that most or all of the DEAE-dextran is situated on the nanoparticle surface.

Once the readily available surface polymer is saturated with rose bengal, a second adsorption phase is seen to occur, probably due to microporous adsorption. In this process, the solute begins to penetrate the particle pores in such a way as to provide access for following solute molecules (Giles et al, 1974). The surface available for adsorption therefore expands proportionally with solute concentration giving a linear region to the adsorption isotherm. Figure 6.2 therefore implies that DEAE-dextran stabilised nanoparticles have a high degree of porosity.

Adsorption was also enhanced by preparing the benzyl ester of rose bengal. This is shown by the adsorption isotherms of this compound and rose bengal onto dextran 70 stabilised nanoparticles suspended in PBS (pH 7) containing 1% w/v poloxamer 338 (figure 6.3). The increased uptake, compared with rose bengal, is due to the decreased ionic character and increased hydrophobicity caused by esterification of the carboxylic acid group of the parent compound.

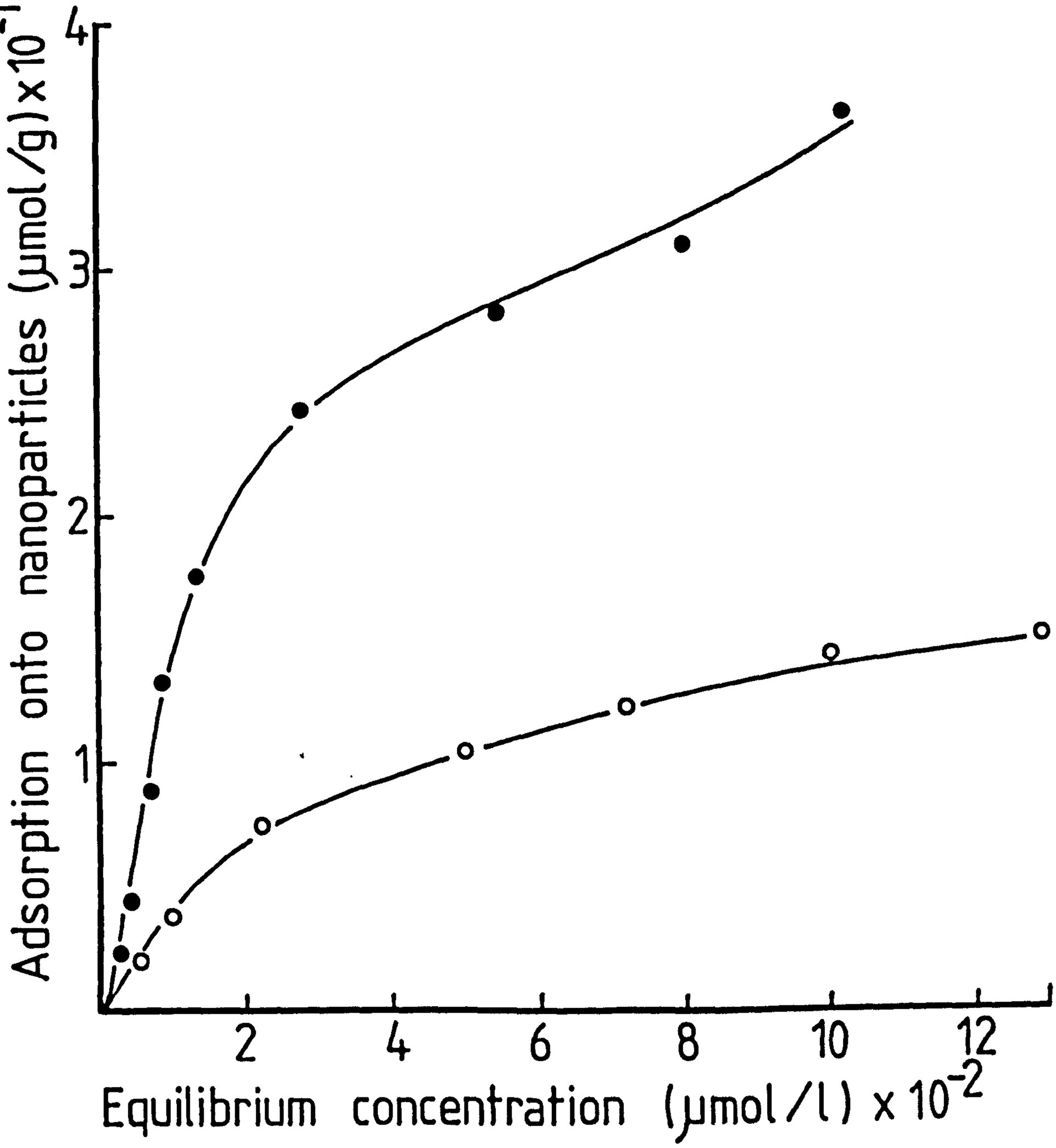

Figure 6.3. Adsorption isotherm of rose bengal (o) and rose bengal benzyl ester (●) onto dextran 70 stabilised nanoparticles in the presence of 1% w/v poloxamer 338 at 20°C.

The adsorption data, however, were obtained in the presence of 1% w/v poloxamer 338 which was needed to increase the water solubility of the ester. This surfactant causes a decrease in the uptake of the solutes by adsorbing to the nanoparticle surface, thereby displacing adsorbed solute and decreasing the effective surface hydrophobicity. This can be seen by comparing the uptake of rose bengal in figure 6.1 (maximum loading 50 μmole/g) with the diminished uptake due to the presence of the poloxamer in figure 6.3 (maximum loading 14 μmole/g). The true adsorption of the rose bengal benzyl ester in the absence of any surfactants would be, therefore, much greater than indicated here.

Despite the high affinity of rose bengal for the nanoparticle surface, the release rate from dextran 70 stabilised nanoparticles was found to be quite rapid, with a time for 50% release of approximately 30 minutes (figure 6.4). In addition, a 'burst effect' was observed in which 35% of the payload was released within 5 minutes. The release of rose bengal from DEAE-dextran nanoparticles and rose bengal benzyl ester from dextran 70 nanoparticles was, however, much slower (figure 6.4). After 24 hours, only approximately 10% of the label was found free in solution for these systems and indicates a much higher affinity of the adsorbate for the adsorbant which corresponds with the adsorption data.

When the same release studies were repeated in the presence of BSA, however, totally different release profiles were obtained (figure 6.5). In all three systems the label was rapidly released with over 80% being found in solution after only 1 hour. Despite this, differences can be seen between each system in the initial

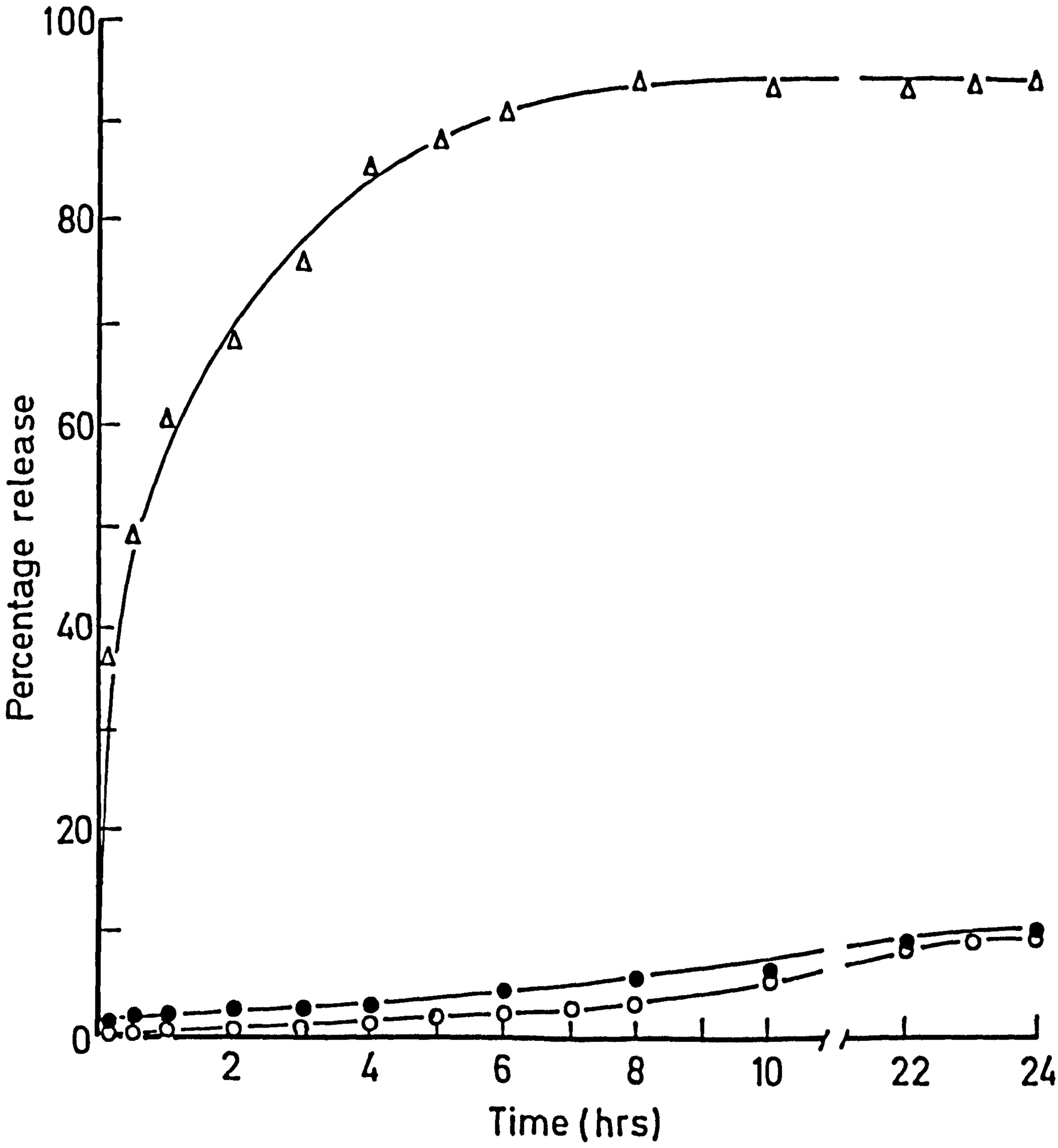

Figure 6.4. Release of rose bengal from nanoparticles stabilised with dextran 70 (Δ) or DEAE-dextran (o), and rose bengal benzyl ester from dextran 70 stabilised nanoparticles (●), at 37°C in phosphate buffered saline (pH 7.4).

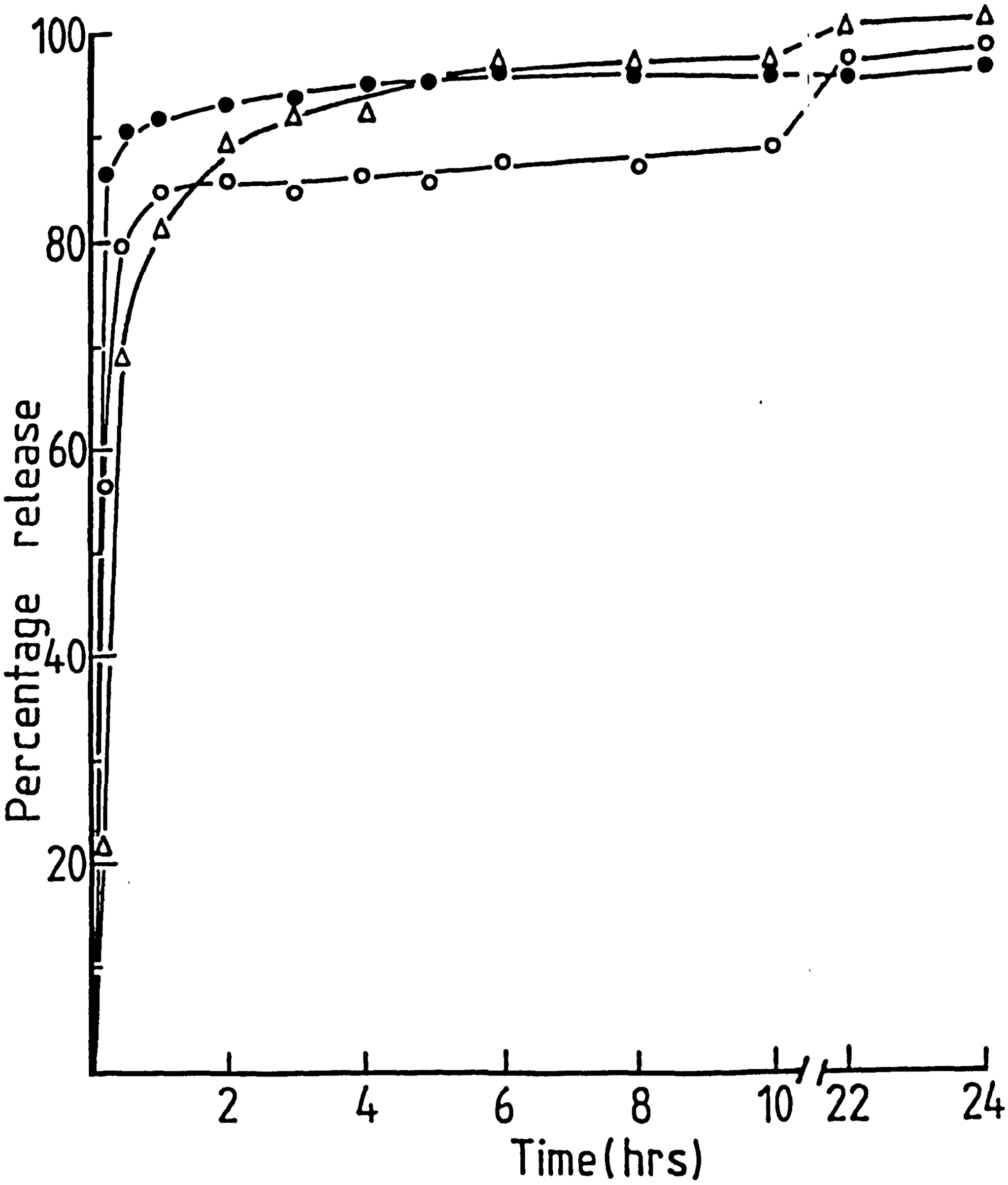

Figure 6.5. Release of rose bengal from nanoparticles stabilised with dextran 70 (●) or DEAE-dextran (O), and rose bengal benzyl ester from dextran 70 stabilised nanoparticles (Δ), at 37°C in phosphate buffered saline (pH 7.4) containing 1% w/v bovine serum albumin.

release phase of up to 30 minutes with the release rate decreasing in the order rose bengal-dextran 70 > rose bengal-DEAE-dextran > rose bengal benzyl ester-dextran 70. The enhanced release in the presence of BSA is due to the protein displacing the adsorbed label from the nanoparticle surface or exchanging with rose bengal in the ion-pair complex in the DEAE-dextran system. This is followed by subsequent binding of rose bengal or its ester by albumin in solution. These findings correlate with the known interaction of serum proteins with nanoparticles (Kreuter, 1983d) and with rose bengal (Coulson and Yonetani, 1972).

In vivo the release rates would be expected to be at least as fast as those found in vitro. Since any free label would be rapidly cleared by liver hepatocytes (Bowman and Rand, 1980) it would be difficult to distinguish between liver accumulation of the labelled nanoparticles and hepatic uptake of free label. Thus radiolabelling with ^{131}I-rose bengal or its benzyl ester is not considered a suitable method for following the biofate of nanoparticles by gamma scintigraphy.

6.3.2. Radiolabelling With Iodide-131

When nanoparticle formation was carried out in the presence of $^{131}I^-$ at pH 1 or 2, only low levels of activity (approximately 2%) were found associated with the nanoparticles. This low degree of incorporation can be accounted for by the non-specific iodide adsorption and implies that initiation by $^{131}I^-$ is occuring only at a very low frequency, if at all. The vast excess of hydroxyl ions in comparison with the trace amounts of $^{131}I^-$

effectively prevents initiation by iodide. Unfortunately, this method is unsuitable as a radiolabelling procedure due to the low incorporation efficiency.

6.3.3. Radiolabelling With Iodine-131

Iodine-131 may be readily formed by the oxidation of iodide-131 and carrier iodide using chloramine T (Millar and Springall, 1966). When this reaction was carried out <u>in situ</u> during nanoparticle formation, up to 90% of the added activity was incorporated into the nanoparticles as shown in table 6.2. This table shows the effect of various iodide/chloramine T ratios on the level of incorporation. The optimum molar ratio was found to be 1:1.3 (chloramine T:sodium iodide). This is in contrast to the theoretical optimum ratio of 1:2 for the formation of $^{131}I_2$ given by the following equations

$$CH_3C_6H_4SO_2N^-Cl\ Na^+ + HCl \longrightarrow CH_3C_6H_4SO_2NHCl + NaCl$$

$$CH_3C_6H_4SO_2NHCl + H_2O \longrightarrow CH_3C_6H_4SO_2NH_2 + HOCl$$

$$HOCl + HCl \longrightarrow H_2O + Cl_2$$

$$Cl_2 + 2NaI \longrightarrow I_2 + 2NaCl$$

Over-oxidation with excess chloramine T would yield iodate according to

$$I_2 + 5HOCl + H_2O \longrightarrow 2IO_3^- + 7H^+ + 5Cl^-$$

TABLE 6.2 Variation of iodine-131 incorporation into nanoparticles with the molar ratio of sodium iodide to chloramine T. The concentration of chloramine T was kept constant at 1 mg/ml.

Concentration of NaI (mg/ml)	Molar ratio of NaI/chloramine T	% of total added activity incorporated
0.052	0.10	14
0.133	0.25	16
0.267	0.50	54
0.532	1.00	88
0.692	1.30	92
0.852	1.60	86
1.064	2.00	76
2.128	4.00	60

and under-oxidation would leave unreacted iodide. Both of these ions would have low affinity for the nanoparticles and would therefore reduce labelling efficiency. In addition, free iodide in solution would increase the aqueous solubility of the iodine, thereby reducing nanoparticle uptake still further. The need to use a higher molar ratio of oxidising agent than theoretically required may be due to the complex nature of the reaction conditions in which strict stoichiometry may not apply.

The release of activity from $^{131}I_2$ labelled nanoparticles is shown in figure 6.6. In contrast to the rose bengal systems, addition of BSA to the release medium retarded release of the label slightly, indicating that the label would be unaffected by the presence of serum proteins. Release, however, is still fairly rapid with 50% of the label being lost in approximately 3 hours. This moderately fast release rate together with possible toxicity problems of any residual chloramine T makes this method unsuitable as a radiolabelling technique for nanoparticles.

6.3.4. Radiolabelling With Indium-111-Oxine Complex

The uptake of ^{111}In-oxine onto nanoparticles was found to be highly dependent upon pH. At below pH 4 the level of uptake fell sharply from 83% (pH 4) to 20% (pH 3) due to protonation of the basic nitrogen in oxine (pK_a 5.02) which in this form is no longer able to form a complex. Due to this effect it is not possible to incorporate the complex into nanoparticles during the polymerisation stage because of the low reaction pH. Despite this, the labelling

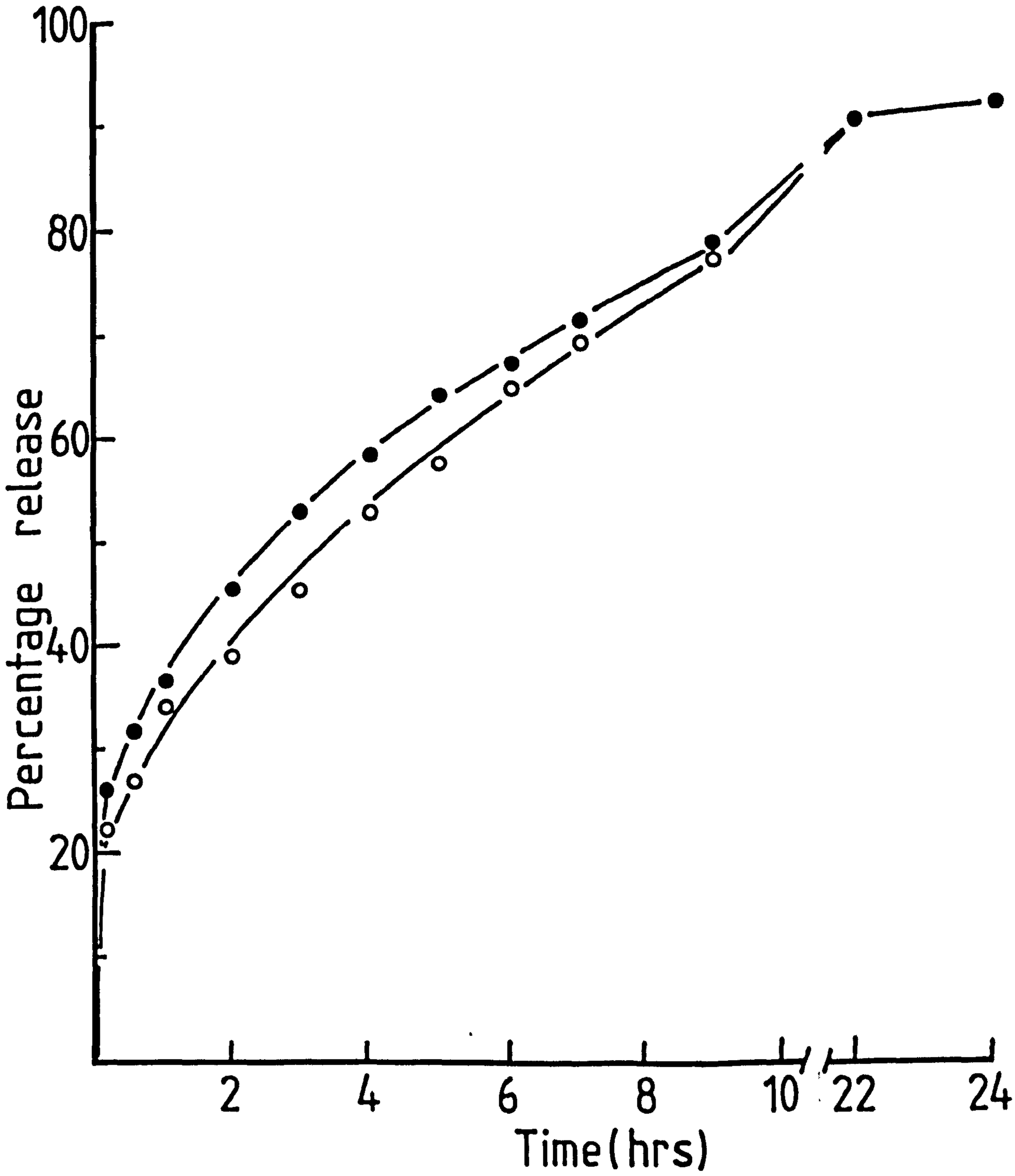

Figure 6.6. Release of radioactivity from $^{131}I_2$ labelled nanoparticles in phosphate buffered saline (pH 7.4) (●), and in phosphate buffered saline (pH 7.4) containing 1% w/v bovine serum albumin (○) at 20°C.

efficiency in water at pHs' greater than 5 was found to be high giving an uptake of 88% at pH 7. Phosphate ions were also found to interfere with the labelling efficiency. When adsorption of ^{111}In-oxine was carried out in PBS (pH 7) none of the activity was found associated with the nanoparticles. It is known that terminal phosphate groups on lipid molecules can complex with indium (Hwang, 1978) and a similar process probably occurs in PBS resulting in the formation of a water soluble ^{111}In-phosphate complex.

The indium complexing behaviour of phosphate ions can also be observed in the release profiles of ^{111}In-oxine labelled nanoparticles given in figures 6.7 and 6.8. When release studies were performed in PBS (figure 6.7) a much greater rate of release was observed compared with release into water (figure 6.8). The addition of BSA to the release media also enhanced release in both systems. This may be attributed to the ability of indium to form a complex with albumin (Hagan et al, 1978) and displacement of the oxine complex from the nanoparticle surface due to adsorption of albumin.

Despite the simple and efficient nanoparticle labelling procedure with ^{111}In-oxine this technique is not suitable for use in vivo due to rapid release of the label. Although an indium-tropolone complex would be expected to yield better results due to higher stability and lipophilicity (Dewanjee et al, 1981) this complex has been found to be taken up poorly by p(BCA) nanoparticles (Fitzgerald, 1985).

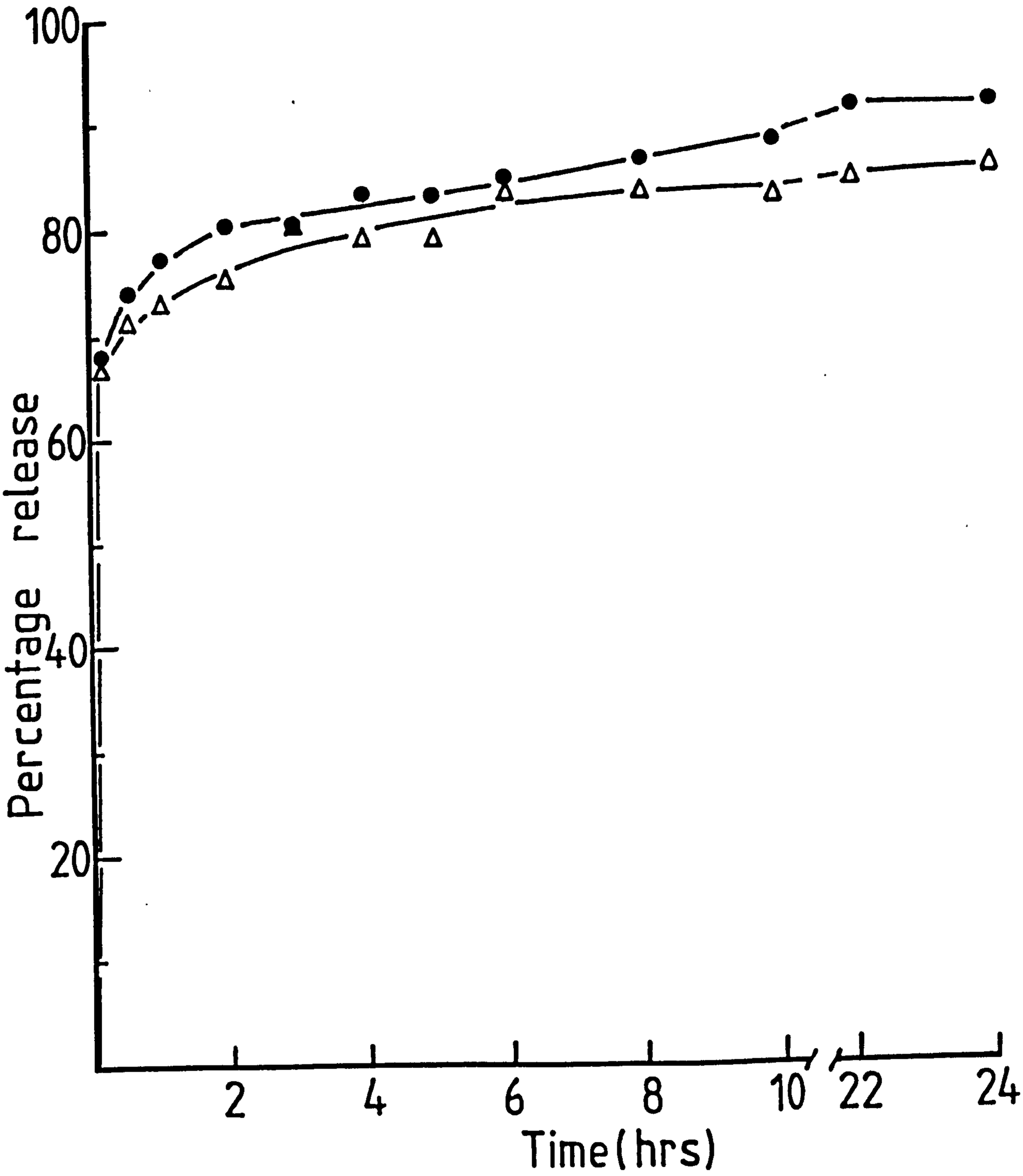

Figure 6.7. Release of radioactivity from ^{111}In-oxine labelled nanoparticles in phosphate buffered saline (pH 7.4) (Δ), and in phosphate buffered saline (pH7.4) containing 1% bovine serum albumin (●) at 37°C.

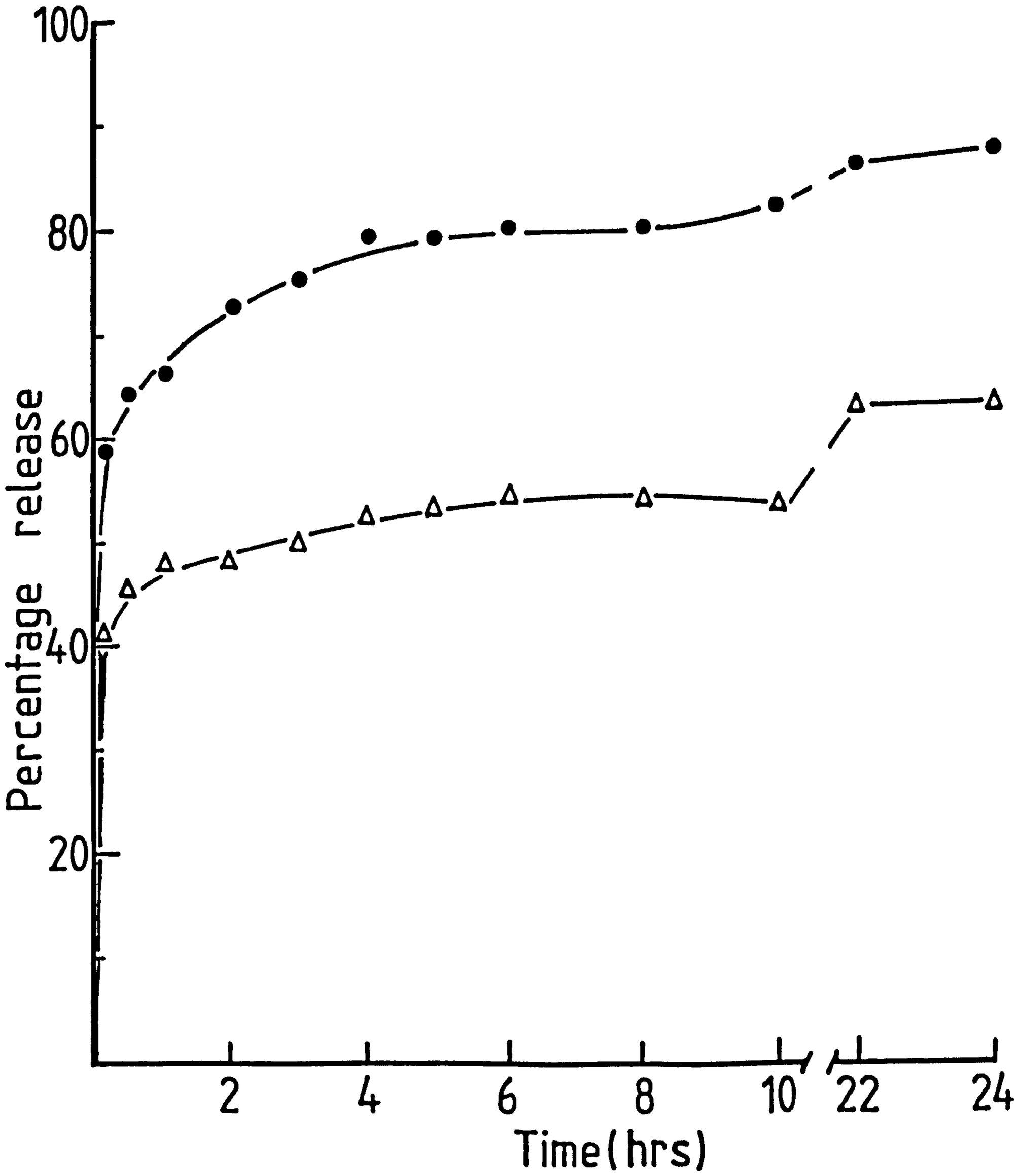

Figure 6.8. Release of radioactivity from ^{111}In -oxine labelled nanoparticles in distilled water (pH 7.4) (Δ), and in distilled water containing 1% w/v bovine serum albumin (pH 7.4) (●) at 37°C.

6.3.5. Radiolabelling With Technetium-99m-Dextran Complex

The technetium-99m-dextran 10 complex was relatively simple to prepare and could be used directly in place of ordinary dextran for nanoparticle formation. The resulting particle size and polydispersity index were unaffected (dz = 126nm, Q = 0.130). Labelled nanoparticles were readily separated from free radiolabel by gel filtration chromatography. On passing through a Sepharose CL 4B column, the small dextran molecules were retained to a much greater extent than the relatively large nanoparticles which were eluted in the column void volume. By using dextran 10 as opposed to higher molecular weight dextrans the separation was enhanced allowing the use of relatively short columns which was necessary to keep dilution of the nanoparticle fraction to a minimum. The elution-activity profile for this system is given in figure 6.9. The combined nanoparticle fractions were found to contain approximately 21% of the activity added to the column. Centrifugation (20000 rpm) of these particles indicated that 88% of this activity was firmly bound to the nanoparticles, which gives a labelling efficiency of 18.5%.

Thin layer chromatography of the ^{99m}Tc-dextran complex showed most of the activity to move at the solvent front (figure 6.10a) and indicates that ^{99m}Tc labelled tin colloid, which would remain at the origin, was not formed. Similar chromatographic analysis of the nanoparticle suspension prior to gel filtration (figure 6.10b) showed approximately 18% of the activity to remain at the origin due to incorporation into nanoparticles. This figure is in good agreement with the results obtained after centrifugation. After the

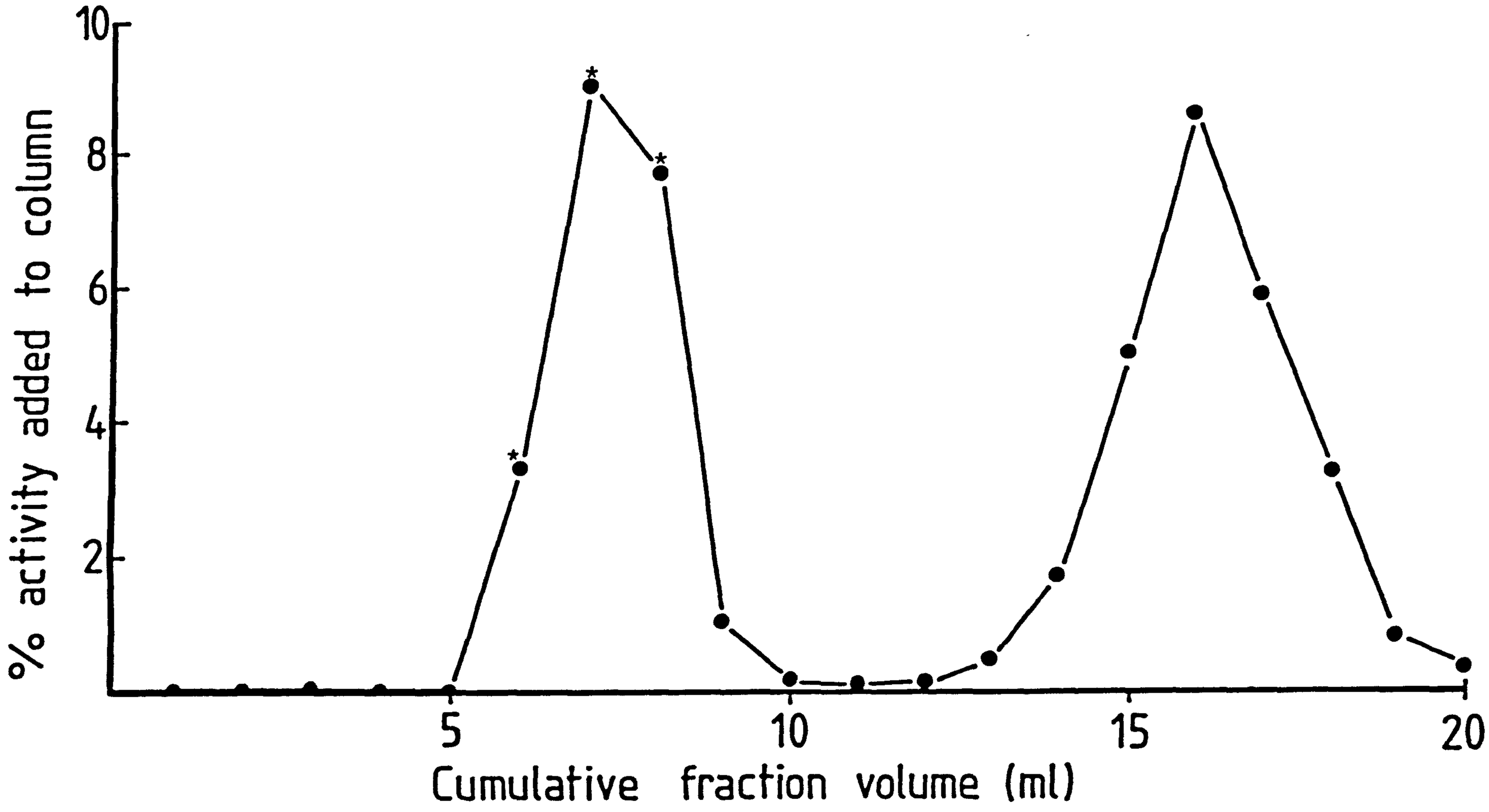

Figure 6.9. Radioactivity found in each 1ml fraction eluted from a sepharose CL 4B gel filtration column expressed as a percentage of the total activity added to the column. * denotes the major nanoparticle fractions

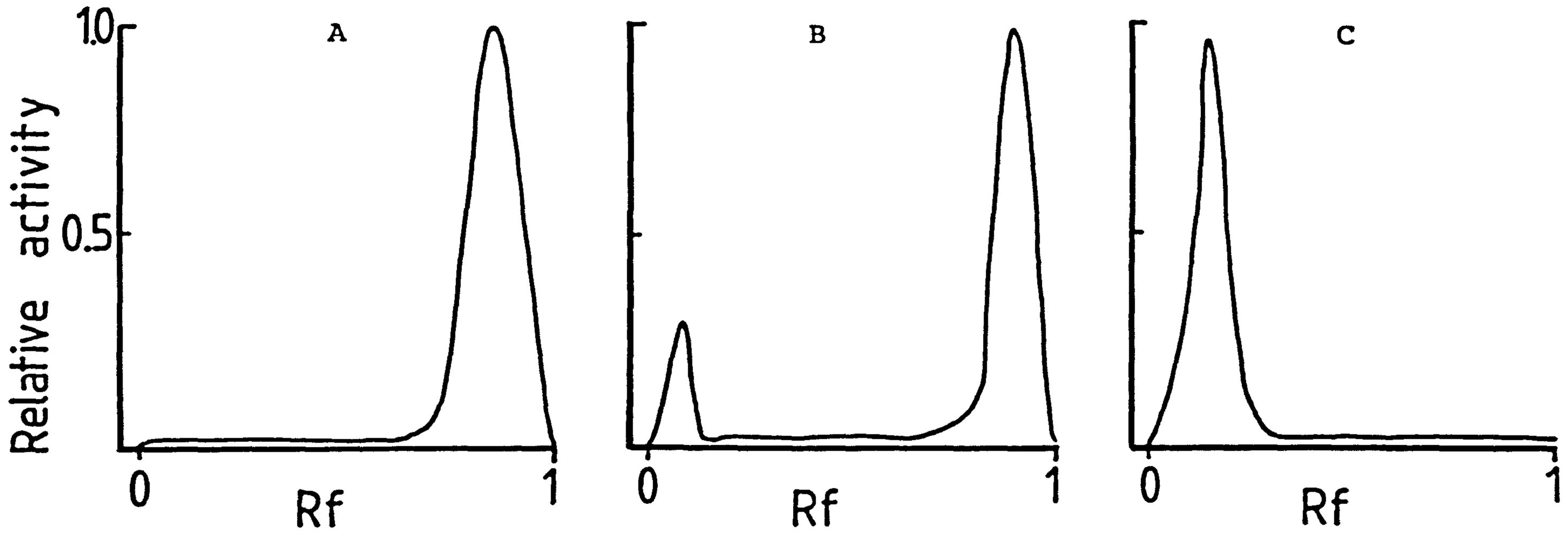

Figure 6.10. Radiochromatograms of (A) ^{99m}Tc-dextran 10, (B) the nanoparticle suspension isolated after polymerisation and (C) the nanoparticle supsension isolated from the gel filtration column.

nanoparticles were isolated from the column, most of the activity was found at the origin and no distinct band of activity due to the free complex could be detected at the solvent front (figure 6.10c).

When these radiolabelled nanoparticles were suspended in PBS or PBS containing BSA, a low but steady release was obtained over a period of 24 hours which was relatively unaffected by the presence of protein as shown (figure 6.11). Since the technetium-99m-dextran complex is known to be highly stable (Henze et al, 1982a and b) the release of activity was probably due to nanoparticle degradation.

Despite the low incorporation efficiency, this technique is regarded as a suitable method for radiolabelling dextran stabilised nanoparticles. Although the slow release of activity observed in vitro could cause interference when determining the fate of the colloid in vivo, rapid filtration by the kidneys of the free label would be expected to minimise any adverse effects.

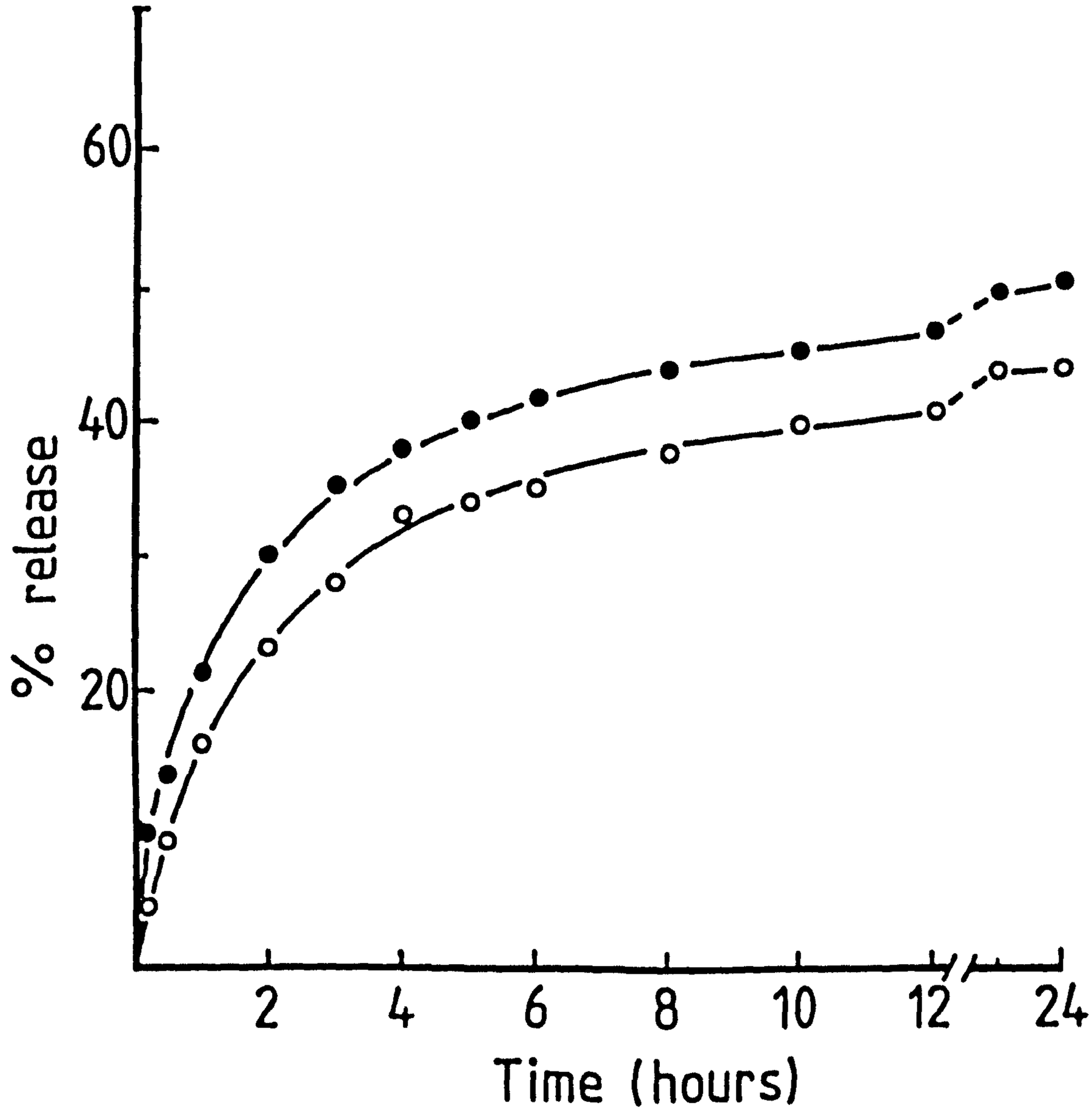

Figure 6.11. Release of radioactivity from ^{99m}Tc-dextran labelled nanoparticles in phosphate buffered saline (pH 7.4) (○), and in phosphate buffered saline containing 1% w/v bovine serum albumin (pH 7.4) (●) at 37°C.

CHAPTER SEVEN

IN VIVO STUDIES

7.1. INTRODUCTION

A major limiting factor to the systemic use of particulate drug delivery systems is the rapid clearance of the carrier from the circulation by the RES (Poste, 1985). This problem has already been discussed together with the possible solutions in chapter 1. Of these, the coating of particles with non-ionic surfactants has been shown to be highly effective in altering the pattern of RES capture (Davis et al, 1985). Although coating polystyrene particles with poloxamer 338 greatly reduced liver and spleen uptake, this system was rapidly cleared by RES cells of the bone marrow (Illum and Davis, 1984a). This may be prevented, however, by employing Tetronic 908 as the coating agent. This non-ionic surfactant has similar properties to the poloxamers (Schmolka, 1967) and can suppress RES capture throughout the body leading to prolonged circulation times (Davis et al, 1985). This approach may be applicable to p(ACA) nanoparticles which are normally deposited mainly in the liver and spleen (Grislain et al, 1983).

The previous chapter has shown that it is possible to radiolabel p(BCA) nanoparticles with the gamma-emitting radionuclide technetium-99m. This will enable the biodistribution of these labelled nanoparticles to be followed by the technique of gamma scintigraphy. This involves determining the radiation pattern due to the injected label using a scintillation detector known as a gamma

camera. Only a brief outline of the function of this system will be given here since comprehensive coverage of the subject is available by Fernando et al (1978) together with applications in drug research by Wilson et al, (1982).

A gamma camera system is depicted diagrammaticaly in figure 7.1. The scintillation detector consists of a single large thallium-activated sodium iodide crystal about 50cm in diameter and 1.2cm thick, with one face optically coupled via a clear plastic 'light pipe' to a hexagonal array of 37 photomultiplier (PM) tubes. A parallel hole collimator fitted to the other side only allows passage of gammma rays travelling in an approximately perpendicular direction. The gamma rays penetrating the collimator strike the scintillation crystal yielding photons of an energy proportional to the amount of energy dissipated within the crystal. Each scintillation event is detected by the PM array and analysed by the positioning circuitory which converts the signal into a two dimensional image. This is shown on the display unit as a brief spot of light in a position which is related to the position of the radiation source. Summation of these events over a period of time yields an image indicating the areas of more, or less radioactivity in the object of interest. If this time period is sufficiently short (a few seconds) and images recorded sequentially, then dynamic views of the distribution of the radionuclide with time are produced. Alternatively, static views can be collected at suitable time intervals which may be minutes, days or weeks.

Most gamma cameras are interfaced with a computer-controlled data acquisition, storage and analysis system. The data are

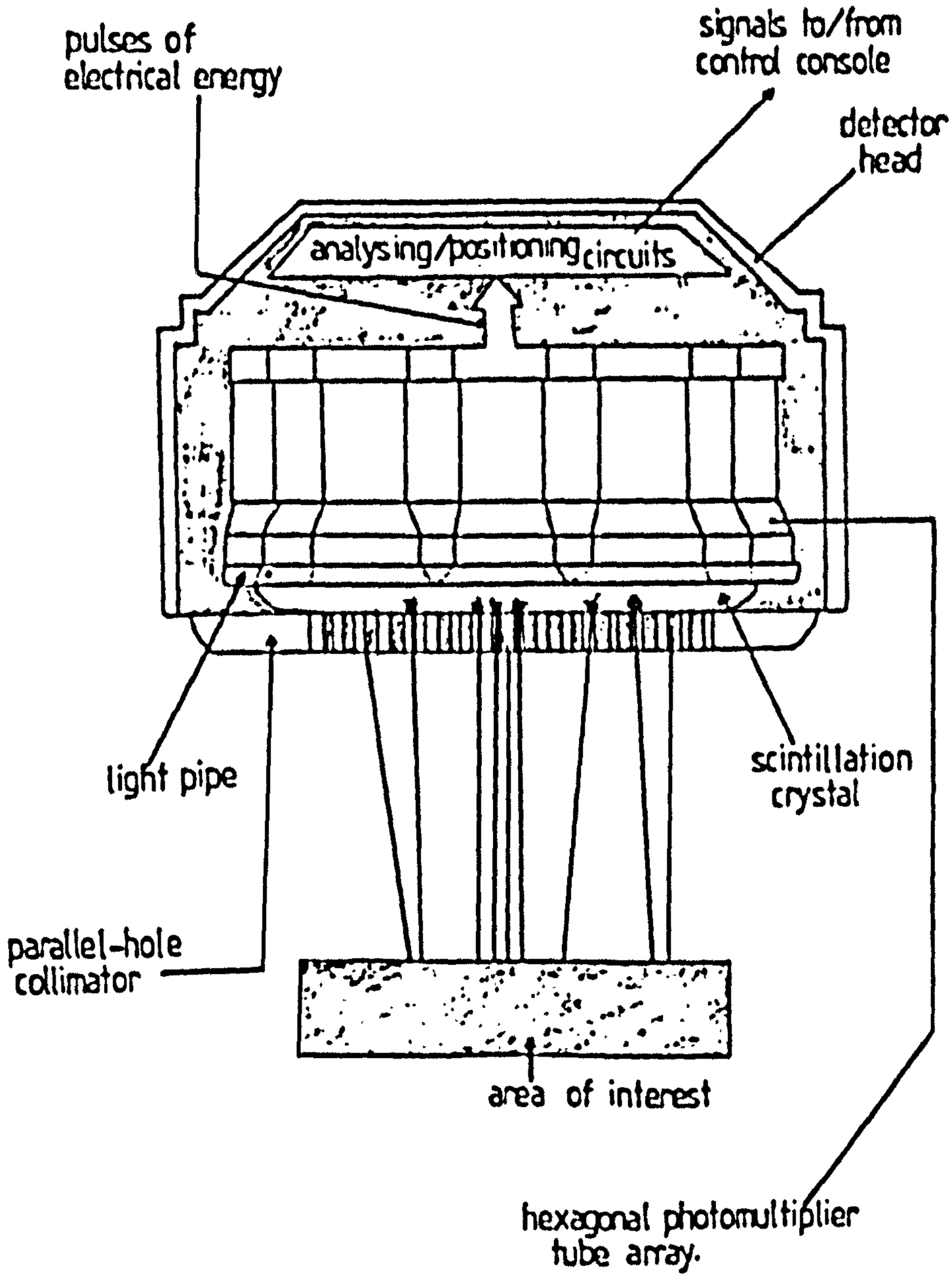

Figure 7.1. Diagram of the gamma camera detector head. Signals from the detector are passed to a control console and then to a computer system for data storage and manipulation.

digitalised into a maximum of 16384 (128 x 128) elements, with the number of gamma rays in each element denoted by up to 16 different shades of grey or colours. These data may be presented as a hard copy or scintigram, which shows the qualitative and quantitative distribution of activity. The computer allows the activity within various parts of the image to be calculated by defining a region of interest (ROI). For example, by constructing a ROI around the liver it is possible to determine the uptake of activity within this organ. ROI's may be defined for other areas allowing background correction and calculation of the total body activity.

There are, however, various errors associated with gamma scintigraphy. The relationship between the detected radiation and the quantity of radionuclide is constant only if the source-to-detector distance is kept constant, together with the thickness of any absorbing media in between. The positioning of the animal should, therefore, be reproducible. Since a two dimensional image is obtained, possible interference from superimposed organs must be taken into account. In addition, the error associated with the operator definition of the ROI is difficult to eliminate. Finally, the intrinsic variation in the gamma camera response, as a result of variations in the sensitivity across the field of view and from spatial non-linearality can lead to errors of about 6% in day-to-day measurements (Pitt and Sharp, 1981).

This chapter describes the use of gamma scintigraphy in determining the biodistribution of ^{99m}Tc-dextran labelled p(BCA) nanoparticles. The effects of coating these particles with poloxamer

338 and Tetronic 908 have also been investigated in an attempt to alter the biodistribution pattern.

7.2. EXPERIMENTAL METHODS AND MATERIALS

7.2.1. Adsorption of Poloxamer 338 and Tetronic 908 onto Nanoparticles

Nanoparticles were prepared according to the standard polymerisation formulation in chapter 2, except dextran 10 at a concentration of 2% w/v was used as the stabiliser and a monomer concentration of 2% v/v was employed. After polymerisation, the nanoparticle suspension was flocculated by freezing and the free dextran removed by repeated centrifugation (3000 rpm) and washing with distilled water as described in chapter 3. The nanoparticles were isolated by lyophilisation and fully resuspended by sonication in distilled water to give a solids content of 15 mg/ml. A series of dilutions of this suspension were prepared giving a final nanoparticle concentration of 1 mg/ml and a poloxamer 338 or Tetronic 908 (Pechiney Ugine Kuhlmann) concentration over the range 1 to 50 x 10^{-3}% w/v. These samples were gently agitated for 2 hours at 20^{o}C and then centrifuged (20000 rpm). The supernatant from each sample was analysed according to the method of Baleux (1972) given in chapter 5 and the equilibrium concentration determined. From these results adsorption isotherms were constructed.

The rates of uptake of the surfactants onto nanoparticles were determined by suspending flocculated nanoparticles (10 mg/ml) in 1 x 10^{-3}% w/v solutions of each surfactant and periodically

centrifuging samples of these suspensions. The degree of uptake of the surfactant was then determined as described above and expressed as a percentage of the amount of surfactant added to the system.

7.2.2. Preparation of Radiolabelled Nanoparticles

The nanoparticles were radiolabelled with a ^{99m}Tc-dextran 10 complex according to the method given in chapter 6. Aseptic technique was used throughout the preparation procedure. All glassware was sterilised by autoclaving (121^{o}C for 15 minutes), solutions prepared using sterile apyrogenic water and filtrations carried out using sterile 0.2μm membrane filters (Millipore, USA). The sepharose gel filtration material was sterilised by autoclaving according to the manufacturer's instructions (15 minutes at 121^{o}C). The column was pre-conditioned as before with a sterile nanoparticle suspension and flushed through with sterile PBS (pH 7).

To produce a final nanoparticle suspension of sufficient specific activity for use with the gamma camera, 400MBq of $^{99m}TcO_4^-$ in 2ml of eluate from the technetium generator was used. This was added to the 10% w/v dextran 10 solution in place of the 1MBq of activity previously used in chapter 6.

The nanoparticle fraction from the sepharose CL 4B column (2.5ml) was diluted to 3.3ml with 0.9% w/v sodium chloride, or 0.9% w/v sodium chloride containing 4.13% w/v poloxamer 338 or Tetronic 908. This gave a final activity of approximately 4 MBq/ml (Isotope assay calibrator 238, Pitman, UK), a nanoparticle concentration of 10 mg/ml and a surfactant concentration (if added) of 1% w/v. The supensions were left to equilibrate for 15 minutes

prior to injection. Adding surfactant to the nanoparticle suspension did not affect the labelling efficiency.

7.2.3. Preparation of Free Technetium-99m-dextran 10

Dextran 10 (0.5g) was dissolved in deoxygenated water (5ml) and this added to 0.025ml of a solution of stannous chloride (30mg) in concentrated sulphuric acid (5ml). 0.4ml of this was filtered (0.2µm sterile membrane filter) into a sterile vial and 0.2ml of eluate from a ^{99m}Tc generator added to this (total activity 20MBq). After 10 minutes, 3.4ml of sterile PBS (pH 7) was added to give a 1% w/v solution of ^{99m}Tc-dextran 10 with an activity of 4 MBq/ml. This solution was filtered through a sterile 0.2µm membrane filter prior to injection.

7.2.4. Animal Experiments

Male New Zealand White rabbits (NZW) (Animal House, Medical School, Nottingham University) 2.5kg in weight were randomly divided into four groups of three. Each experimental group was injected with uncoated, poloxamer 338 coated or Tetronic 908 coated nanoparticles, with each rabbit receiving 1ml of suspension via the right marginal ear vein. The control group of three animals were each injected with 1ml of the ^{99m}Tc-dextran 10 solution. Injections were flushed through with 1ml of sterile 0.9% w/v sodium chloride solution. The animals were positioned on the gamma camera (Maxi Camera II, General Electrics, USA) and data acquisition commenced immediately. Dynamic images (45 x 20 seconds) were recorded during the first 15 minutes

and static images (60 seconds) taken at 1,2,4 and 8 hours post injection. The data were stored and processed by a dedicated computer system (Micas 2020 Medical Computer System, Nodecrest, UK).

7.2.5. Data Processing

ROI's were created around the liver/spleen, lung/heart, lower kidney and bladder, and the activity within each region calculated. The data for each ROI were normalised by subtracting the background count for an equivalent sized ROI taken from an image recorded without an animal on the camera. For the dynamic data, a decay correction was applied to account for the radioactive decay of ^{99m}Tc during the dynamic phase. Results for each ROI during the dynamic phase are expressed as a percentage of the total activity in the whole animal. For the static images, the total body activity at 1 hour post injection was used to calculate the total activity at 2,4 and 8 hours, after allowing for radioactive decay. The activity in each ROI was then expressed as a percentage of this value.

Due to the image of the upper kidney (situated on the right of the image) being superimposed on the liver image, the activity in the lower, well resolved kidney was subtracted from the liver activity to give values due to liver uptake alone. In calculating the total kidney and bladder activities, the value from the lower kidney was doubled and added to that of the bladder. All activities are quoted as the mean of the three animals within each group together with the standard deviations.

7.3. RESULTS AND DISCUSSION

7.3.1. Adsorption of Poloxamer 338 and Tetronic 908 onto Nanoparticles

The adsorption of poloxamer 338 and Tetronic 908 onto p(BCA) nanoparticles was found to be rapid, with equilibrium being established in a few minutes (table 7.1). It was necessary to determine the rate of uptake for the in vivo work because the nanoparticles needed to be prepared and used on the same day due to the relatively short half life (6 hours) of ^{99m}Tc. For this reason, extensive incubation times could not be employed and it was essential to establish the minimum time needed to reach equilibrium for the uptake of the surfactants.

The adsorption isotherms given in figure 7.2 show a maximum uptake of approximately 85 mg/g of nanoparticles for poloxamer 338 and 60 mg/g for Tetronic 908. At a nanoparticle concentration of 10 mg/ml the minimum concentrations of surfactants needed to ensure full surface coverage would be approximately 0.29% w/v for poloxamer 338 and 0.36% w/v for Tetronic 908.

On the basis of these findings the nanoparticles were coated with surfactant by incubating the suspensions for 15 minutes in 1% w/v solutions of poloxamer 338 or Tetronic 908.

7.3.2. Biodistribution of Uncoated and Surfactant Coated Nanoparticles in Rabbits

Following injection into NZW rabbits via the marginal ear vein, approximately 50% of the uncoated nanoparticles were found to

TABLE 7.1 Rate of uptake of poloxamer 338 and Tetronic 908 onto nanoparticles.

Time (mins)	% taken up from solution	
	Poloxamer 338	Tetronic 908
5	88.4	83.1
15	94.5	81.3
30	96.1	84.1
60	96.3	79.2
90	97.1	-
120	98.0	80.5

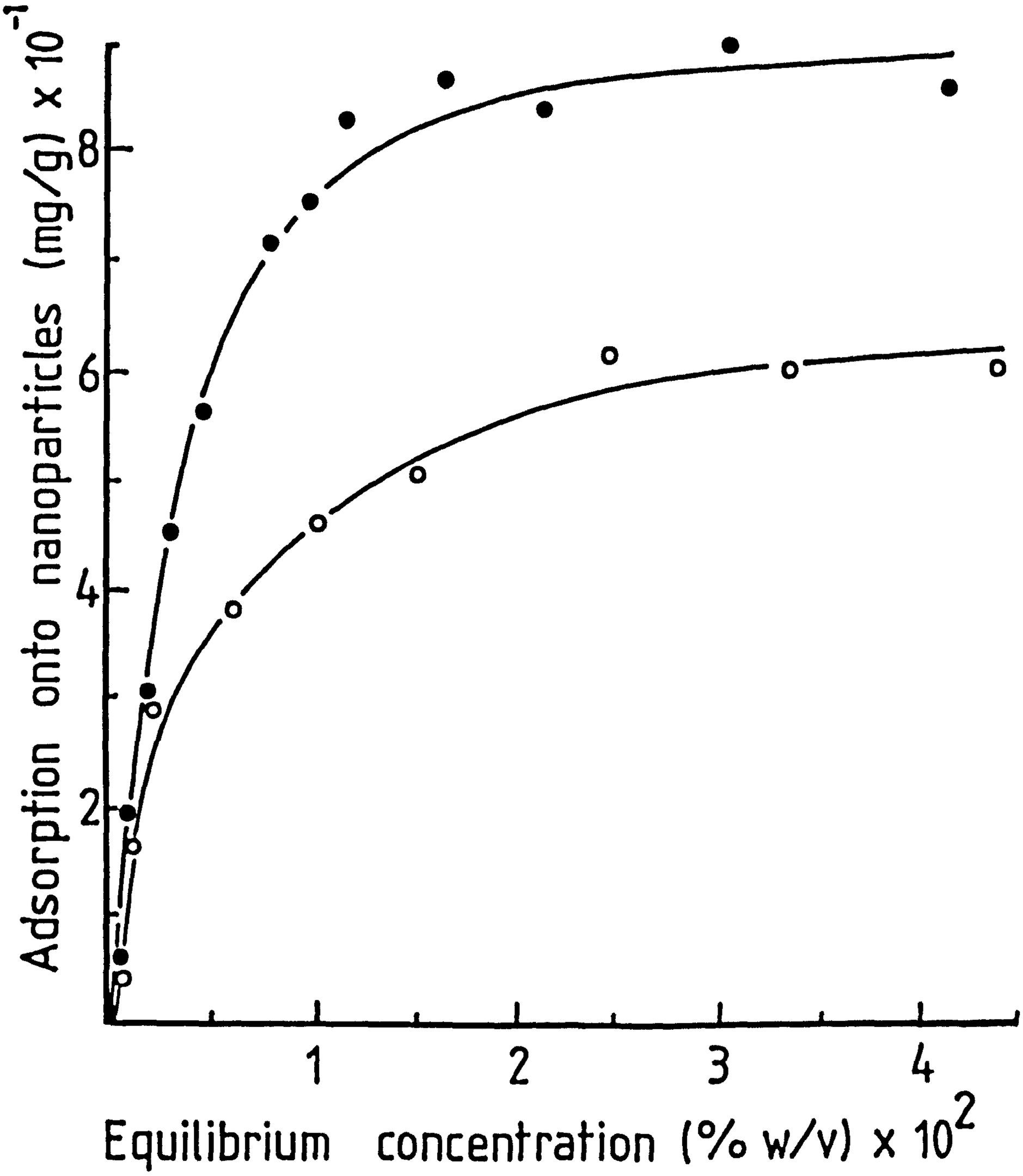

Figure 7.2. Adsorption isotherms of poloxamer 338 (●) and Tetronic 908 (O) onto nanoparticles at 20°C.

localise in the liver/spleen region within 2 minutes (figure 7.3). Coating with poloxamer 338 or Tetronic 908 caused a slight delay in liver/spleen clearance with maximum uptake occurring after 4 minutes (figure 7.3). There was no significant difference, however, in the final liver/spleen uptake between the coated and uncoated systems. The loss of activity from this region after 3 to 4 minutes is due to nanoparticle degradation resulting in the release of the water soluble ^{99m}Tc-dextran radiolabel. In contrast, non-biodegradable polystyrene particles give a constant liver/spleen activity profile over the same time period (Illum and Davis, 1984a).

As the liver/spleen activity decreased, the activity found in the kidneys and bladder steadily increased as the radiolabel was filtered by the kidneys and accumulated in the bladder (figure 7.4). The kidney activity maintained a constant level of approximately 14% as the label was filtered and discharged to the bladder, in which activity steadily increased with time. After 4 hours, between 50 and 60% of the total injected activity was found in the kidneys and bladder. This value fell sharply during the next 4 hours when the animals urinated, giving activities of approximately 25% at 8 hours post injection. No significant difference was found between the activity-time profiles for the coated and uncoated nanoparticles given in figure 7.4. The initial rapid filtration by the kidneys of about 15% of the total injected activity was due to the presence of free radiolabel which constituted 12% of the injected dose.

The activity-time profiles for the lung/heart region are given in figure 7.5. Following injection into the marginal ear vein, the suspension is delivered to the heart and then the lungs before

Figure 7.3. Activity-time profile for the liver/spleen region of interest following injection of uncoated (o), poloxamer 338 coated (•) and Tetronic 908 coated (Δ) nanoparticles labelled with ^{99m}Tc-dextran 10. Results are the mean for 3 rabbits together with the standard deviation (bar).

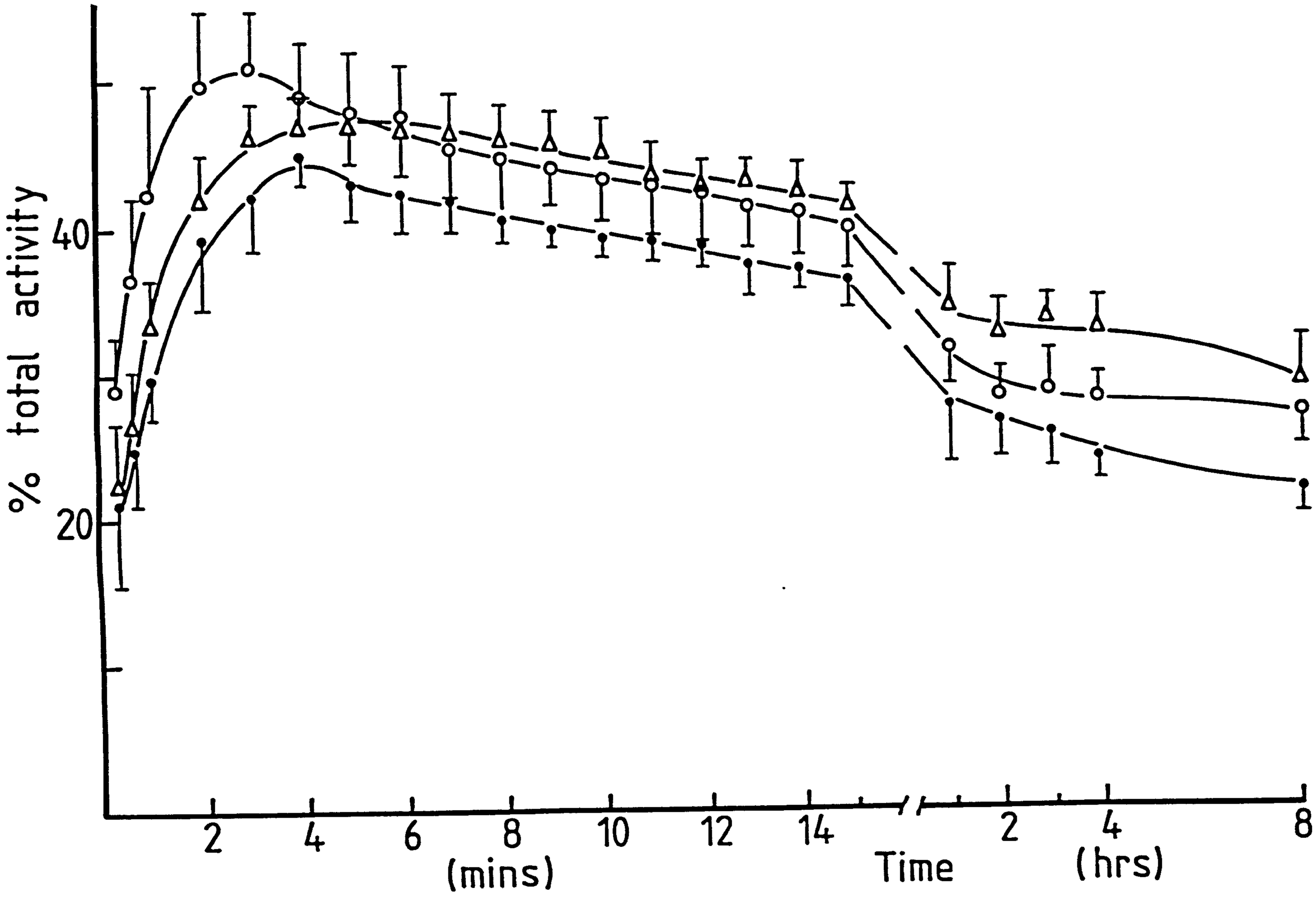
% total activity
40
20
2
4
6
8
10
12
14
(mins)
Time
2
4
8
(hrs)

Figure 7.4. Activity-time profiles for the kidney and bladder regions of interest following injection of uncoated (O), poloxamer 338 coated (●) and Tetronic 908 coated (Δ) nanoparticles labelled with ^{99m}Tc-dextran 10. Results are the mean for 3 rabbits together with the standard deviation (bar).

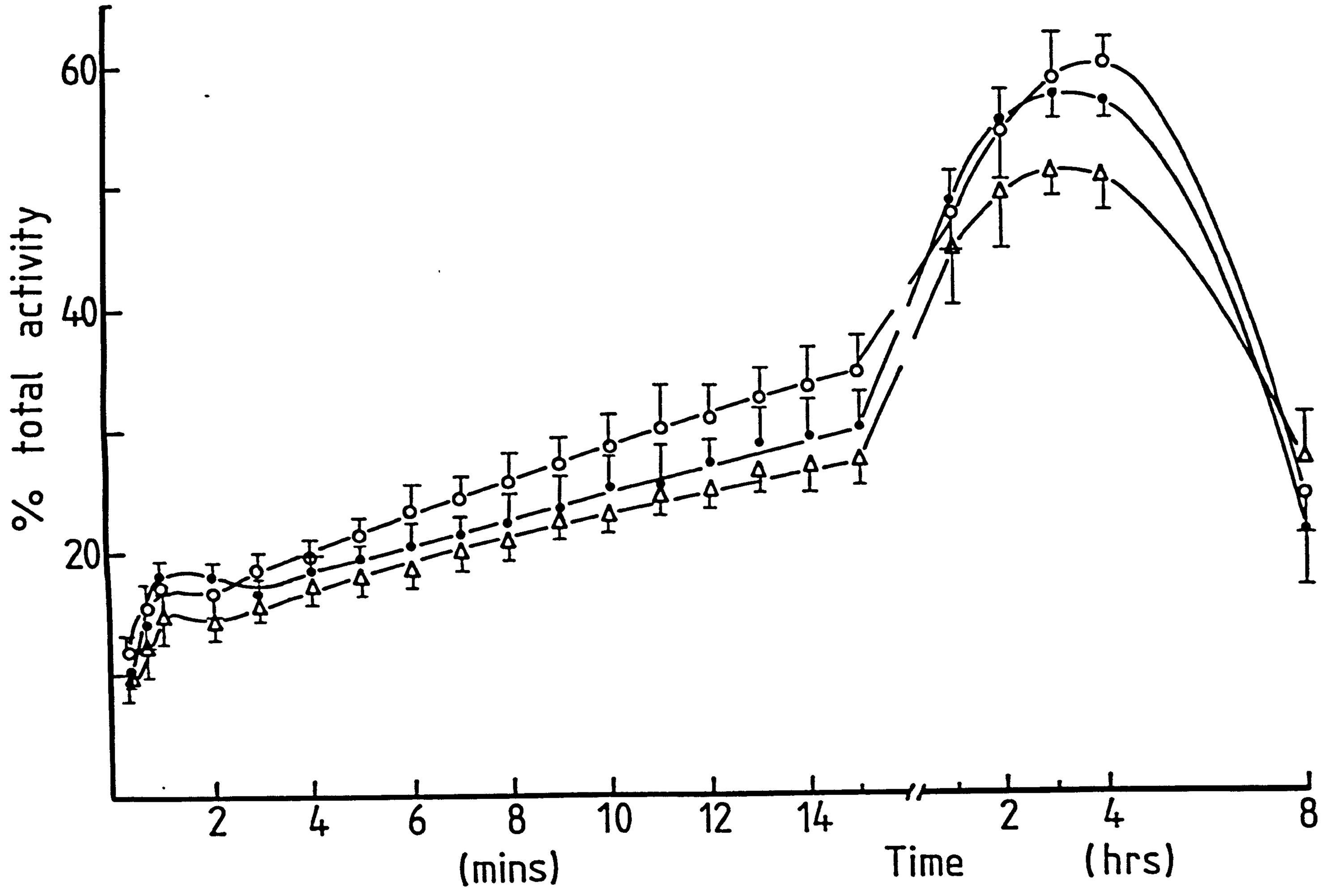
% total activity
60
40
20
2
4
6
8
10
12
14
2
4
8
(mins)
Time
(hrs)

Figure 7.5. Activity-time profiles for the lung/heart region of interest following injection of uncoated (o), poloxamer 338 coated (●) and Tetronic 908 coated (Δ) nanoparticles labelled with ^{99m}Tc-dextran 10. Results are the mean for 3 rabbits together with the standard deviation (bar).

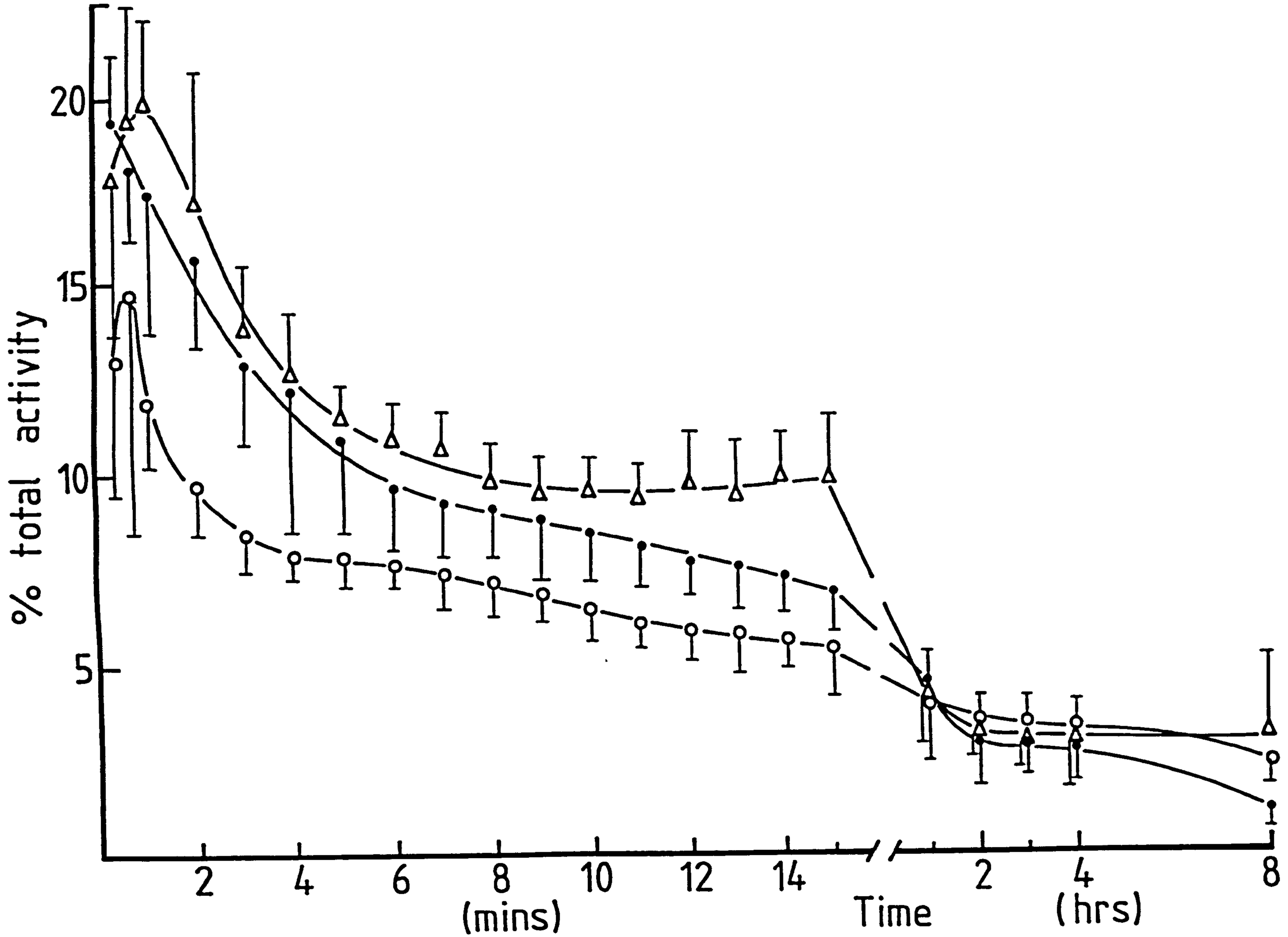
20
15
10
5
% total activity
2
4
6
8
10
12
14
(mins)
Time
2
4
8
(hrs)

returning to the heart and entering the general circulation. Hence a relatively high activity was observed initially in this region before the nanoparticles and free label were cleared by the RES and kidneys. A similar profile is observed for polystyrene particles (Illum and Davis, 1984a). Although there was a small difference between the profiles for the uncoated and Tetronic 908 coated nanoparticles, this was not significant (Mann-Whitney U test, U statistic = 200).

The distribution pattern can be observed clearly in the scintiscans given in figure 7.6 for a rabbit injected with uncoated nanoparticles. At 1 minute post injection, the localised activity in the lung/heart region could be seen. After 2 minutes, the liver was well defined and the outline of the two kidneys could be distingushed (normally the right kidney was obscured by the liver image). At 6 minutes, the bladder could be seen and by the end of the dynamic phase (15 minutes) most of the activity was in the liver, kidneys and bladder. In all these scintigrams the outline of the rabbit was well defined indicating a relatively high level of circulating activity. After 1 hour, the bladder was seen to contain most of the activity and this distribution was maintained until 4 hours post injection. The apparent increase in liver and kidney activity at 8 hours is due to the data analysis system automatically increasing the sensitivity due to loss of most of the activity in the urine. Liver activity at this stage was only about 30% of the total injected dose after allowing for radioactive decay.

Figure 7.7 gives the activity-time profiles for the control animals injected with free ^{99m}Tc-dextran 10. This compound was

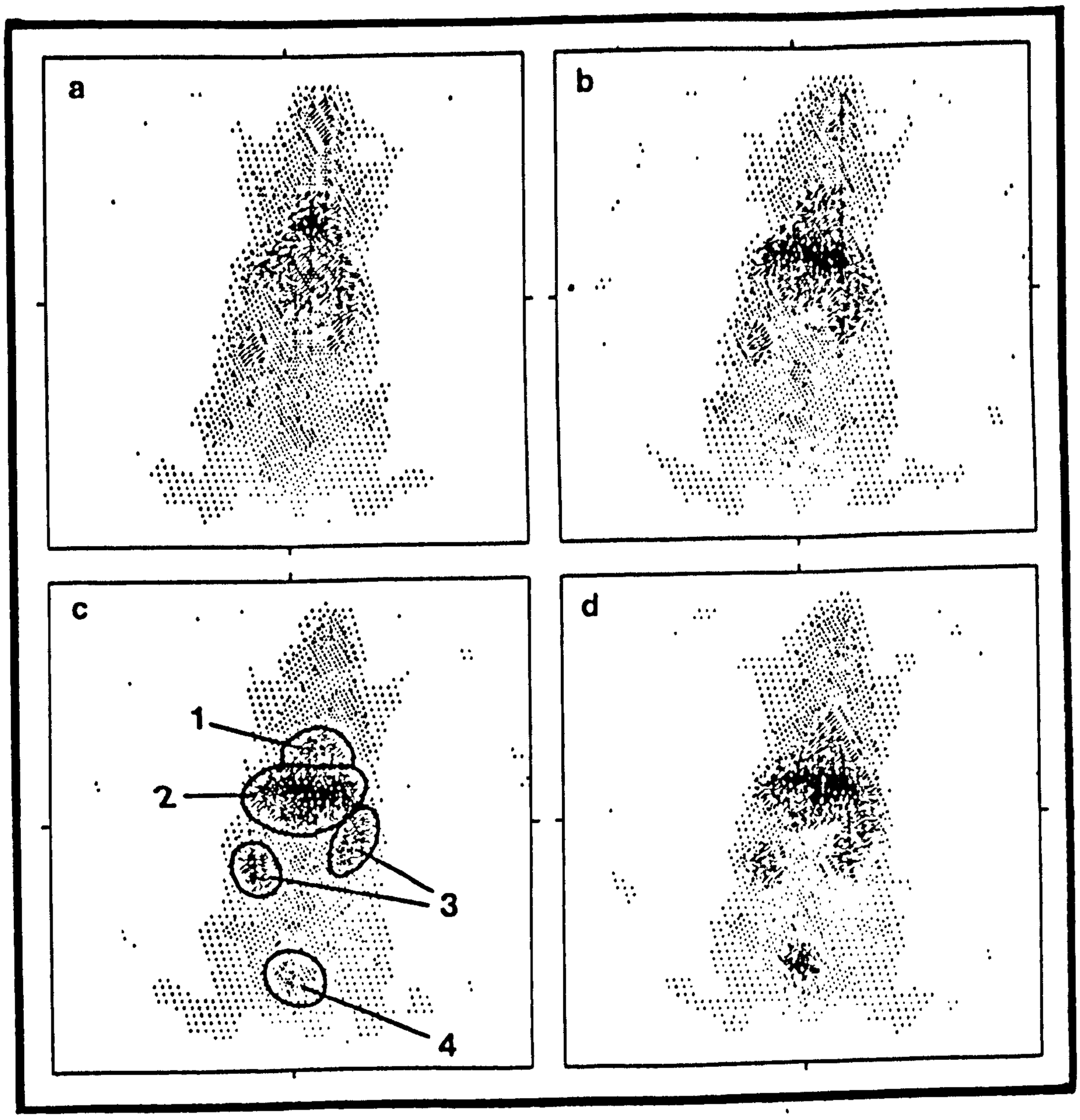

Figure 7.6. Scintiscans of a rabbit injected with uncoated nanoparticles labelled with ^{99m}Tc-dextran 10 at various times after injection.
The regions of interest are shown in the 3rd frame. Normally the kidney seen on the right was obscured by the liver/spleen image (ROI designation: 1= lung/ heart, 2= liver/spleen, 3= kidneys and 4= bladder).

Time after injection- (a) 1 minute
(b) 2 minutes
(c) 4 minutes
(d) 6 minutes

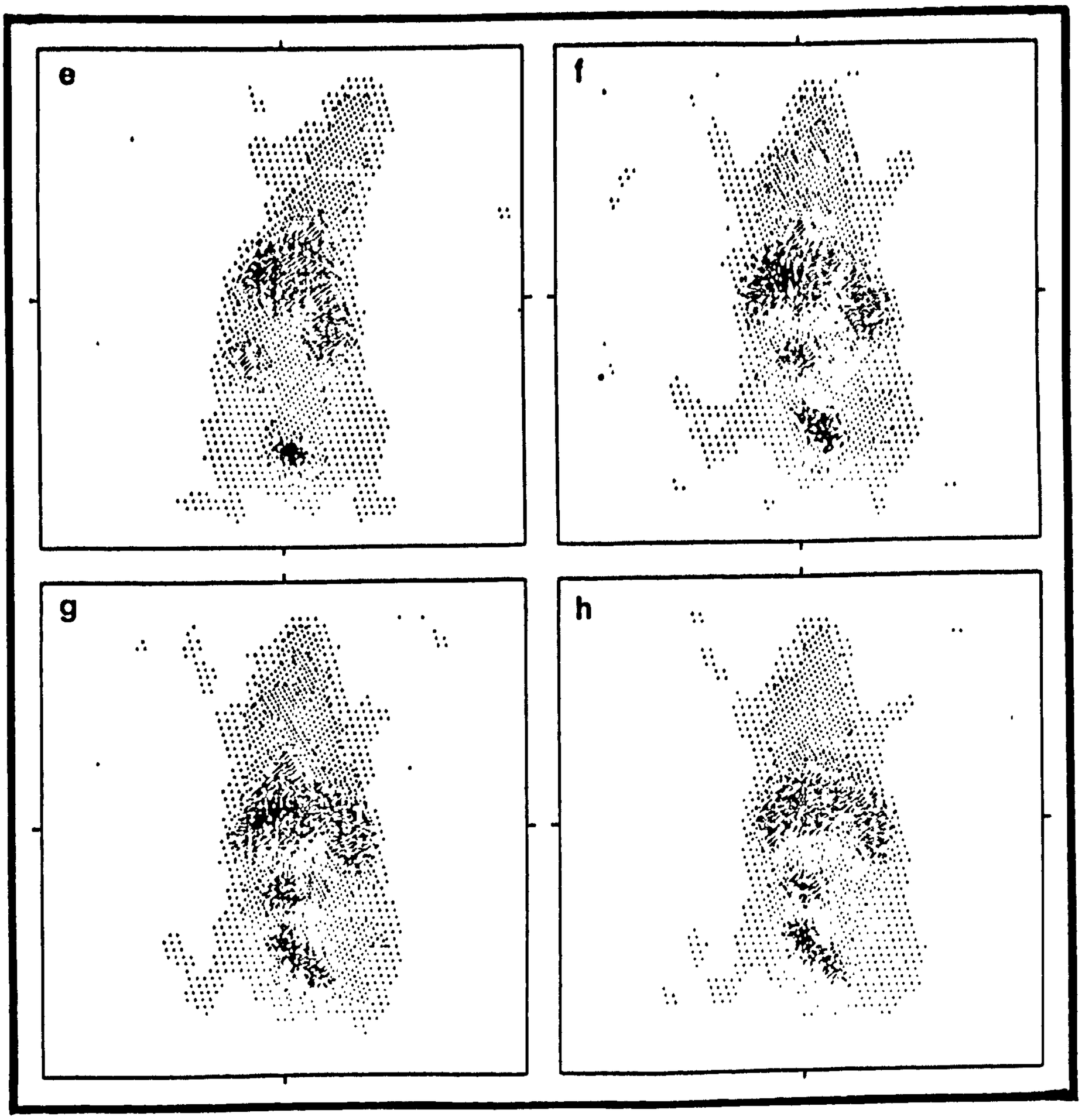

Figure 7.6. continued. Scintiscans of a rabbit injected with uncoated nanoparticles labelled with ^{99m}Tc-dextran 10 at various times after injection.

(e) 8 minutes

(f) 10 minutes

(g) 12 minutes

(h) 14 minutes

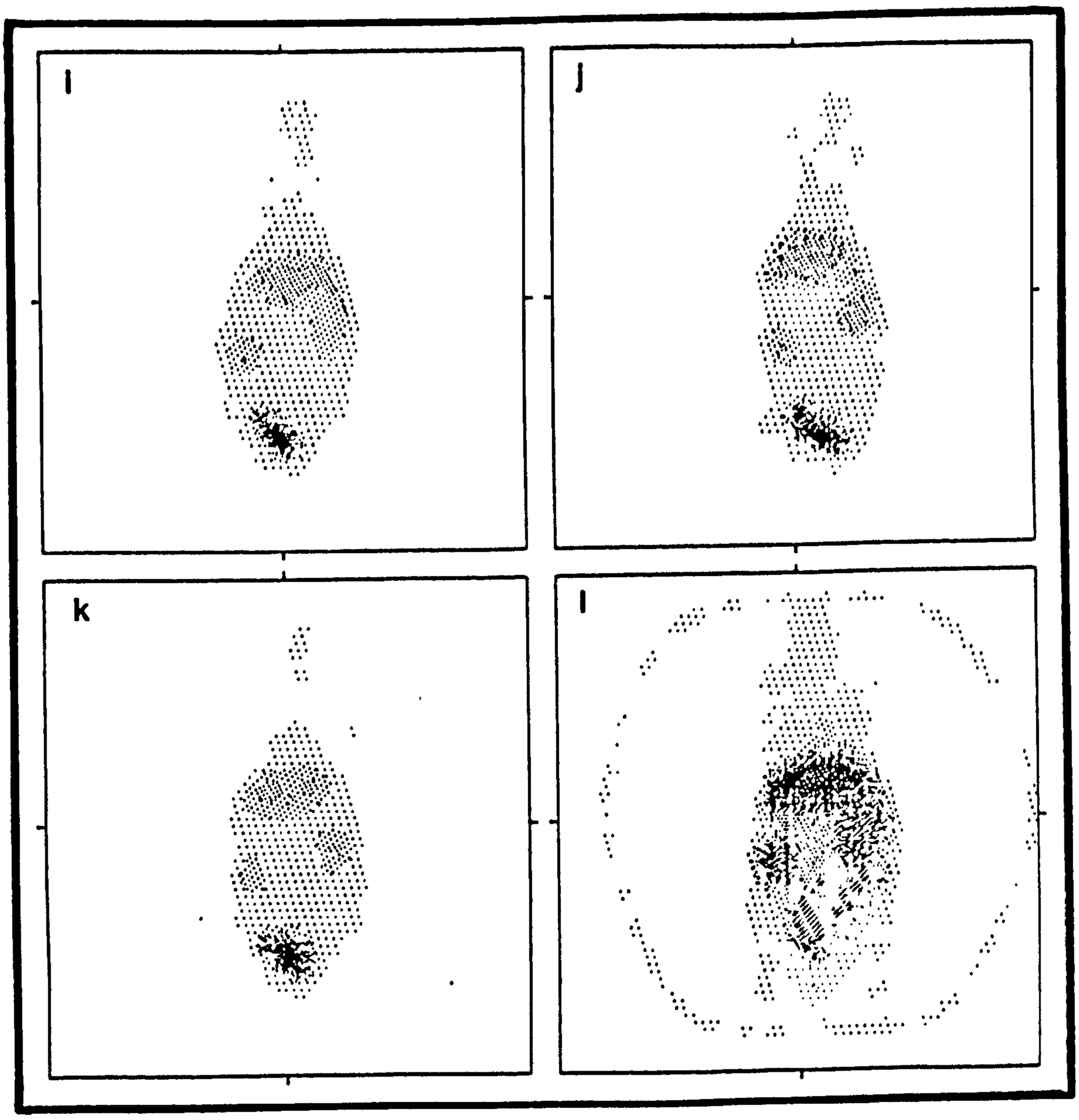

Figure 7.6. continued. Scintiscans of a rabbit injected with uncoated nanoparticles labelled with ^{99m}Tc-dextran 10 at various times after injection.

(i) 1 hour

(j) 2 hours

(k) 4 hours

(l) 8 hours

Figure 7.7. Activity-time profiles for the control animals injected with free ^{99m}Tc-dextran 10.
(Δ) liver/spleen region
(o) lung/heart region
(●) kidneys and bladder regions
Results are the mean for 3 rabbits together with the standard deviation (bar).

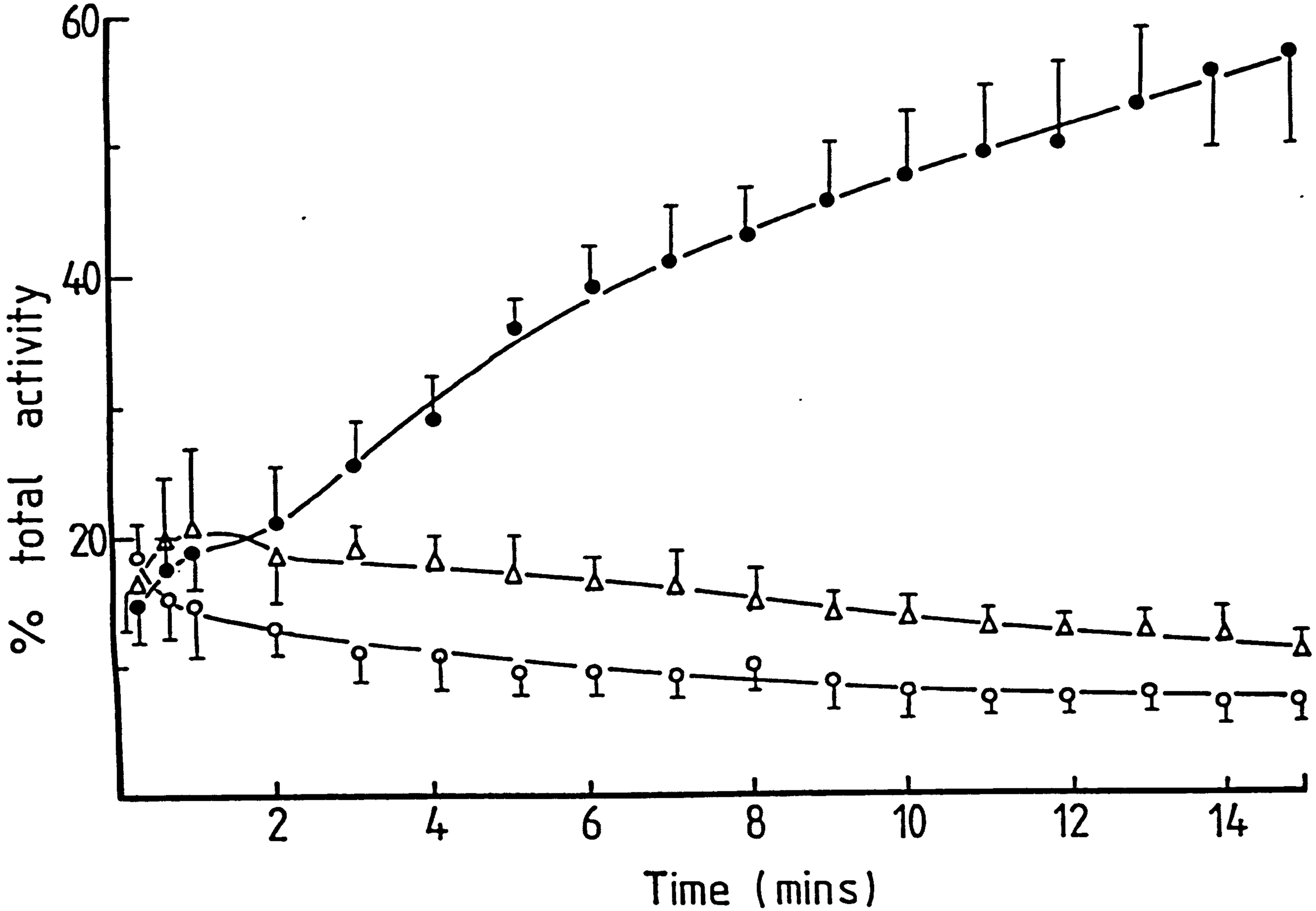
60
40
20
% total activity
2
4
6
8
10
12
14
Time (mins)

rapidly cleared by the kidneys and accumulated in the bladder. The kidney and bladder activities in these animals were much higher compared with the experimental groups, since all of the radiolabel is essentially free in the circulation and capable of being filtered by the kidneys. The low levels of activity found in the liver/spleen region are further evidence for the lack of ^{99m}Tc-tin-colloid formation during the radiolabelling procedure. Due to the very rapid clearance of the label from the circulation, data are only given for the dynamic phase. Any liver uptake of colloidal contaminants would have been observed in these first 15 minutes following injection.

Taking into account the level of free radiolabel in the uncoated nanoparticle injection (about 12%) the maximum liver/spleen uptake was of the order 60%. This figure is much lower compared with other colloidal systems (Illum and Davis, 1984a; Leu et al, 1984) and approximately 20% lower than the findings of Grislain et al (1983) for ^{14}C labelled p(iBCA) nanoparticles injected into rats. Obviously direct comparison of results between various studies is not possible due to the large number of variables which include the nature of the particles (size, surface charge, composition, hydrophobicity), radiolabelling procedures, animal species, radiation detection techniques and dosage levels. The results obtained here, however, imply that p(BCA) nanoparticles stabilised by dextran 10 are mostly cleared by the liver and/or spleen and are rapidly degraded. The coating of nanoparticles with surfactants did not significantly alter the liver/spleen uptake in contrast to other systems (Illum and Davis, 1984a; Leu et al, 1984). It has been proposed (Davis et al, 1985) that the interfacial coating of

surfactants decreases capture by macrophages of the RES due to enhanced steric stabilisation preventing close approach and particle/cell interactions. Since the nanoparticle system under investigation here already possesses a strong steric barrier provided by the surface layer of covalently linked dextran, the addition of further stabiliser to the system may fail to significantly increase the existing repulsive steric potential energy. This is reflected in the liver/spleen activity-time profiles (figure 7.3). Other factors such as particle-surfactant affinity and particle polydispersity also may be important. Clearly further work needs to be done in this area to resolve the possible mechanisms of macrophage capture in relation to particle-cell surface interactions.

CHAPTER EIGHT

GENERAL DISCUSSION

8.1. GENERAL DISCUSSION AND CONCLUSIONS

The work presented in this thesis has involved a systematic study of the characteristics of p(BCA) nanoparticles in relation to their potential use as drug carriers for site specific drug targeting. The results have yielded valuable information concerning nanoparticle formation, composition, surface properties and behaviour in vivo. Much of these data were unpublished at the outset of this project which was surprising considering the importance of such physico-chemical properties on the behaviour of particulate drug carriers. Of these, the effects of particle size are particularly well understood. The initial investigations, therefore, dealt with the control of nanoparticle size.

By varying the nature and concentration of polymeric stabilisers added to the polymerisation medium used in nanoparticle preparation, it was possible to vary particle size over a wide range. Dextrans were found to be the most versatile stabilisers and by altering the molecular weight and concentration of this polysaccharide, it was possible to prepare nanoparticles with diameters in the range of approximately 100 to 800nm. The upper size limit could be extended to about 3μm by using an oligosaccharide, β-cyclodextrin, in place of the dextran. The lower size limit was extended to approximately 20nm by using non-ionic surfactants such as polysorbate 20. Variation in other polymerisation factors such as

pH, ionic strength, temperature and monomer concentration, although producing small changes in nanoparticle diameter, did not affect particle size greatly. These results, in combination, imply that nanoparticles are stabilised by steric forces and that electrostatic stabilisation is not important in maintaining colloidal stability. This is in contrast to many other colloidal systems which are formed by a free radical polymerisation mechanism which results in the incorporation of charged initiators into the particle matrix.

The formation of very small nanoparticles (<100nm diameter) may be important with respect to the possible extravasation of the carrier *in vivo*, which was discussed in detail in the general introduction. In addition to the importance of average particle size is the consideration of particle size polydispersity. This factor is often ignored when determining the potential of particulate carriers to reach extravascular sites. The importance of polydispersity may be illustrated by considering the nanoparticles used in the *in vivo* work described in chapter 7 as a theoretical example of a carrier system loaded with drug. This system had an average diameter of 126nm and a polydispersity index of 0.13 as measured by PCS, which gives the theoretical particle size distribution in terms of particle number shown in figure 8.1. If 100nm is taken as an arbitrary diameter below which particles could escape the vascular circulation, then integration of this curve indicates that only 44% of the carrier could extravasate despite the average size (number average diameter = 98.6nm) being approximately 100nm. In terms of drug delivery, even less of the drug would be expected to reach the target site, since the payload capacity of these nanoparticles is

Figure 8.1. Theoretical particle size distributions for a nanoparticle supsension calculated from PCS measurements (dz= 126nm, Q= 0.130) according to equation 2.13.

(●) distribution given in terms of particle number.

(o) distribution given in terms of particle surface area.

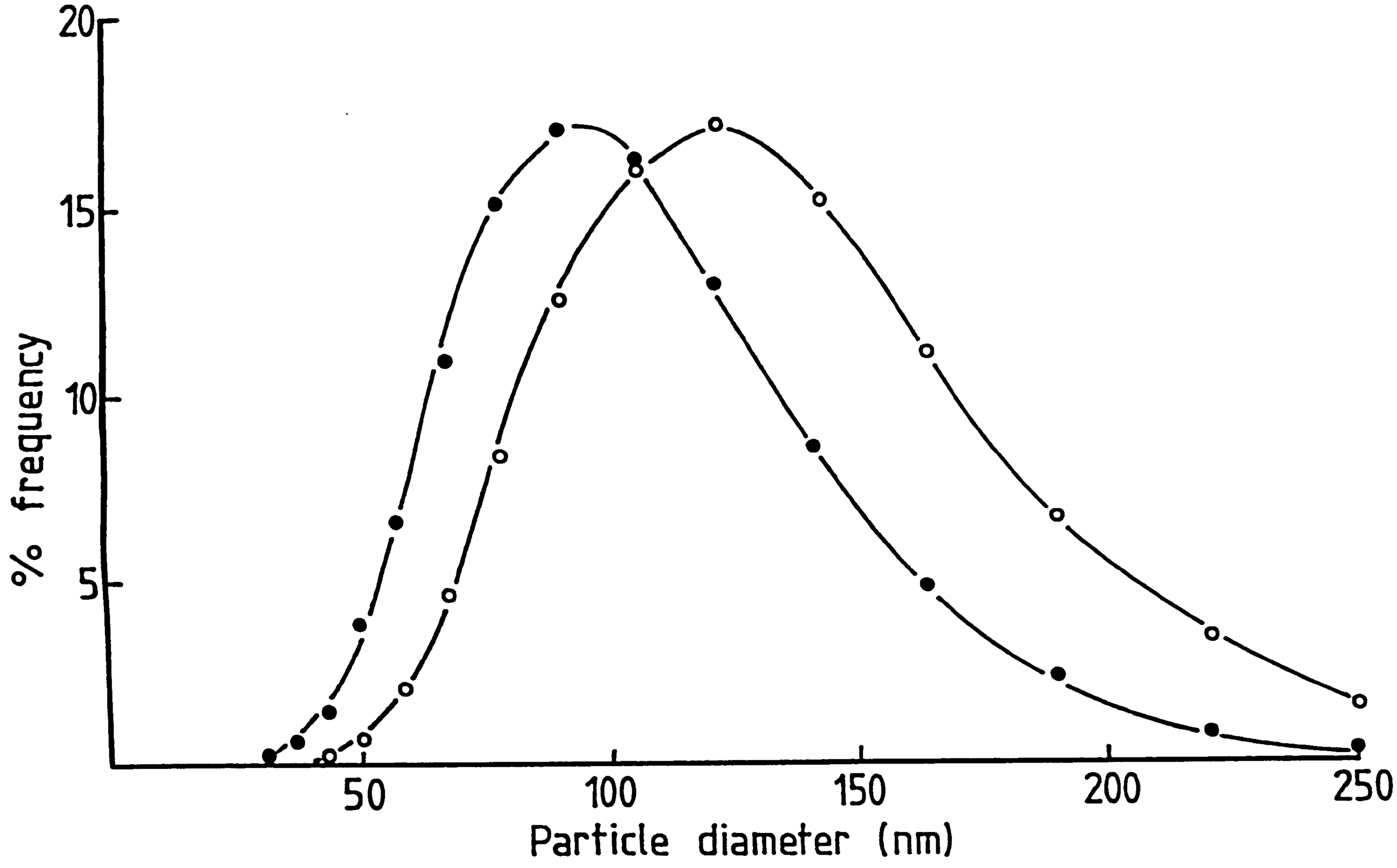
20
15
10
5
% frequency
50
100
150
200
250
Particle diameter (nm)

mainly dependent on surface sorption of the drug. Thus, if the distribution is plotted in terms of particle surface area and integrated, only 21% of the total therapeutic payload has the possibility of extravasation (figure 8.1). For carrier systems where drug loading is a function of particle volume, such as liposomes, an even smaller percentage of the total payload would be contained in carriers with diameters less than 100nm.

With nanoparticle systems a compromise has to be reached concerning the requirements for low particle size and polydispersity. Although the polysorbate stabilised nanoparticles had a very low average diameter this was associated with a wide particle size distribution. The narrowest size distributions were obtained with dextran stabilised systems, but the particle size of these carriers was generally greater than 100nm. Certain poloxamer stabilised nanoparticles, however, gave reasonably low sizes together with low polydispersity values. The situation is further complicated by the need to maximise the therapeutic payload, which can be drastically reduced in the presence of surfactants as shown in chapter 6 with rose bengal. Overall, nanoparticles stabilised with dextran 10 appear to offer the best compromise with respect to size, polydispersity and possible drug loading.

The choice of steric stabiliser was also found to affect markedly the molecular weight of the cyanoacrylate polymer which comprised the nanoparticle matrix. Although the molecular weight of this polymer theoretically may affect the rate of nanoparticle degradation and possibly drug release, this has yet to be ascertained. The copolymerisation of dextran with the monomer also

has important implications regarding degradation and release of the payload. These results, in conjunction with those obtained in controlling particle size, imply that nanoparticles are formed initially by an aggregative mechanism involving aggregation of many relatively small oligomeric polymer chains.

The great importance of the interfacial region of nanoparticles was demonstrated throughout the course of the work. In particular, the finding that dextran could be incorporated via covalent linkages and resided at the nanoparticle surface was extensively exploited to manipulate various properties.

By employing dextrans with charged functional groups, such as DEAE or sulphate, it was possible to control to a certain degree the electrophoretic behaviour of nanoparticles. In theory, it should be possible to produce nanoparticles with a range of particle charges by varying the concentration of charged stabiliser added to the polymerisation medium. However, the formation of small particles bearing a highly negative potential was not possible with the materials available. This section of work (chapter 4) demonstrated the versatility of PCS in determining particle size. PCS was used throughout the project and was invaluable for routine size analysis or the more detailed studies performed in chapters 2 and 4.

The interfacial layer of dextran was exploited still further in chapter 5 for the covalent attachment of ligands to the particle surface. Although this section of work did not realise the initial objectives, it did demonstrate the feasibility of attaching antibodies to the nanoparticle surface via dextran 'bridges'. This approach may also be used for increasing drug loading and

controlling the release of amino containing drugs. Theoretically, several cytotoxic agents such as methotrexate, daunorubicin, azaserine or mitomycin C could be linked to nanoparticles in this way.

Radiolabelling the nanoparticles for use in vivo proved to be a highly difficult task. Conventional adsorption or incorporation of radiolabels such as rose bengal, molecular iodine or indium-oxine, although giving good loading efficiencies, produced rapid release rates that were unsuitable for use with gamma scintigraphy. These findings also have relevance to the release of drugs from nanoparticles and imply that in many instances drug release could be very rapid in vivo. This was well demonstrated in the case of rose bengal. Although the release of this compound in buffer solution was steady over a period of 24 hours, in the presence of protein release was virtually complete in a matter of minutes. Despite the ion-pairing effect of DEAE-dextran stabilised nanoparticles or the use of a water insoluble ester, both of which substantially retarded release rates into buffer, the presence of albumin in the release medium lead to a rapid release in both instances. Further detailed studies are needed with a wide range of drugs before a single release mechanism, if one exists, can be proposed.

Eventually, radiolabelling was achieved by utilising the covalent attachment of dextran to the nanoparticle matrix. By preforming a technetium-99m-dextran complex and adding this to the polymerisation medium, it was possible to incorporate sufficient activity to allow imaging by a gamma camera following injection into rabbits. It may be possible to improve the labelling method by using

a higher molecular weight dextran in place of dextran 10. This would be expected to give a slower rate of release of the radiolabel due to the higher degree of association between each dextran molecule and the nanoparticle matrix.

The in vivo data given in chapter 7 represent preliminary studies into the biofate of nanoparticles. As expected, most of the carrier was found to be taken up into the liver and/or spleen, although the level of uptake was found to be lower than with many other colloidal systems. Coating the particles with surfactants which are known to reduce the uptake of other colloidal materials failed to reduce the liver accumulation of nanoparticles. This effect needs to be investigated further.

In summary, p(BCA) nanoparticles have been shown to be a highly versatile colloidal drug delivery system. This project has attempted to emphasise the possibilities and problems associated with their potential use in drug targeting, mainly from a physico-chemical perspective. Despite studies such as this, the main problems in achieving site specific drug delivery to tumour sites have yet to be addressed fully. Many of these concern processes which occur at a cellular level and are obviously outside the scope of this project. Although a detailed knowledge of the carrier system can help in resolving these problems, this type of approach in the field of drug targeting is regarded by certain workers, possibly with some justification, as merely "rearranging the deckchairs on the Titanic". It is hoped that the rearrangements presented in this thesis may eventually help 'the sinking ship'.

APPENDIX I

Listing of the computer program designed to calculate the theoretical particle size distribution from PCS data according to equation 2.13. The program is written for use with an Apple IIe microprocessor (Apple Computers, USA).

```
]LIST

50  PR£ 3
100 G1 = 0
200 G4 = 0
300  INPUT "INPUT SAMPLE NUMBER ";A$
350  PRINT ""
400  INPUT "INPUT PCS DIAMETER(NM)  ";D
450  PRINT ""
500  INPUT "INPUT PCS POLYDISPERSITY INDEX  ";Q
550  PRINT ""
600  INPUT "PRINT SIZE DISTRIBUTION? Y OR N  ";B$
700  PR£ 1
800  PRINT "SAMPLE NUMBER "A$
850  PRINT ""
900  PRINT "PCS DIAMETER(NM)="D"          POLYDISPERSITY INDEX="Q
910  PRINT : PRINT
1000  IF B$ = "N" GOTO 2800
1200  PRINT "LN(DIAM)   DIAMETER(NM)    NUMBER %   CUM.% UNDERSIZE"
1300  FOR I = 1.5 TO 500 STEP 0.15
1400 A =  - ((1 / (2 *  LOG (1 + Q))) * ((I - ( LOG (D / ((1 + Q) ^ 2.5)))
     )) ^ 2)
1500 B = 1 / ( SQR (2 * 3.14159265 * ( LOG (1 + Q))))
1600 G =  INT ((( EXP (A) * B) * 10000) + 0.5)
1700  IF G1 = 0 GOTO 1900
1800  IF G < 1 GOTO 2300
1900  IF G < 1 GOTO 2200
2000  IF Z = 1 GOTO 10000
2100 G1 = G + G1
2200  NEXT I
2300 G2 = 100 / G1
2400 Z = 1
2500 G1 = 0
2600  GOTO 1300
2700  PRINT
2800 D1 =  INT (((D / ((1 + Q) ^ 2.5)) * 10) + 0.5) / 10
2900 S =  INT (( EXP ( SQR ( LOG (1 + Q))) * 1000) + 0.5) / 1000
3000 D2 =  INT ((( EXP ( LOG (D1) + (0.5 *  LOG (1 + Q)))) * 10) + 0.5) /
     10
3100 M =  INT ((( EXP ( LOG (D1) -  LOG (1 + Q))) * 10) + 0.5) / 10
3200 C =  INT ((( SQR (Q) * 100) * 10) + 0.5) / 10
3400  PRINT "GEOMETRIC MEAN DIAMETER=       "D1"NM"
3500  PRINT "GEOMETRIC STANDARD DEVIATION= "S
3600  PRINT "LENGTH NUMBER MEAN DIAMETER=  "D2"NM"
3700  PRINT "NUMBER MODAL DIAMETER=        "M"NM"
3800  PRINT "COEFFICIENT OF VARIATION=     "C"%"
3900  PRINT : PRINT : PRINT : PRINT
4000  PR£ 0
4200  GOTO 50
10000 G3 =  INT ((G * G2 * 100) + 0.5) / 100
10100 G4 = G3 + G4
10200  IF G3 < 0.009 GOTO 10700
10300 I1 =  INT ((I * 100) + 0.5) / 100
10400 E =  INT (( EXP (I) * 10) + 0.5) / 10
10500  PRINT I1; TAB( 12);E; TAB( 28);G3; TAB( 39);G4
10600  GOTO 2200
10700  IF G4 > 50 GOTO 2700
10800  GOTO 2200
20000  END
```

Example of a typical print out of results obtained from the computer program given on the previous page. The program automatically adjusts the upper and lower limits of the size range for each set of data.

SAMPLE NUMBER EXAMPLE

PCS DIAMETER(NM)=200 POLYDISPERSITY INDEX=.15

LN(DIAM)	DIAMETER(NM)	NUMBER %	CUM.% UNDERSIZE
3.6	36.6	.02	.02
3.75	42.5	.09	.11
3.9	49.4	.31	.42
4.05	57.4	.89	1.31
4.2	66.7	2.15	3.46
4.35	77.5	4.44	7.9
4.5	90	7.78	15.68
4.65	104.6	11.63	27.31
4.8	121.5	14.79	42.1
4.95	141.2	16.01	58.11
5.1	164	14.75	72.86
5.25	190.6	11.57	84.43
5.4	221.4	7.73	92.16
5.55	257.2	4.4	96.56
5.7	298.9	2.13	98.69
5.85	347.2	.88	99.57
6	403.4	.31	99.88
6.15	468.7	.09	99.97
6.3	544.6	.02	99.99

GEOMETRIC MEAN DIAMETER= 141NM
GEOMETRIC STANDARD DEVIATION= 1.453
LENGTH NUMBER MEAN DIAMETER= 151.2NM
NUMBER MODAL DIAMETER= 122.6NM
COEFFICIENT OF VARIATION= 38.7%

REFERENCES

Akimoto, M. and Morimoto, Y. (1983) Biomaterials, 4, 49.

Alving, C.R. (1983) Pharmac. Ther., 22, 407.

Alving, C.R., Steck, E.A., Chapman, W.L., Waits, V.B., Hendricks, L.D., Swartz, Jnr., G.M. and Hanson, W.L. (1978) Proc. Natl. Acad. Sci., 75, 2959.

Armaly, M.F. and Rao, K.R. (1973) Invest. Ophthalmol., 12, 491.

Arnon, R. and Sela, M. (1982) Immunol. Rev., 62, 5.

Avila, J.L. (1983) Intersciencia, 8, 405.

Bagchi, P. and Vold, R.D. (1970) J. Colloid Interface Sci., 33, 405.

Baleux, B. (1972) C.R. Acad. Sci. Paris, 274C, 1617.

Barker, S.A., Disney, H.M. and Somers, P.J. (1972) Carbohydrate Res., 25, 237.

Barrett, K.E.J. and Thomas, H.R. (1975) in "Dispersion Polymerisation in Organic Media", (K.E.J. Barrett, ed.), John Wiley and Sons: London, p115.

Benacereff, B., Biozzi, G., Halpern, B.N. and Stiffel, C. (1975) in "Physiopathology of the Reticuloendothelial System", (B.N. Halpern, B. Benacereff and J.F. Delafresnaye, eds.), Blackwell: Oxford, p137.

Bernstein, A., Hurwitz, E., Maron, R., Arnon, R., Sela, M. and Wilchek, M. (1978) J. Natl. Cancer Inst., 60, 379.

Bolton, A.E. (1977) "Radioiodination Techniques", Review 18, The Radiochemical Centre: Amersham.

Bolton, A.E. and Hunter, W.M. (1973) Biochem. J., 133, 529.

Bowman, W.C. and Rand, M.J. (1980) "Textbook of Pharmacology" 2nd Edn., Blackwell: Oxford.

Boxer, L.A. and Stossel, T.P. (1974) J. Clin. Invest., 53, 1534.

Bradfield, J.W.B. (1984) in "Microspheres and Drug Therapy", (S.S. Davis, L. Illum, J.G. McVie and E. Tomlinson, eds.), Elsevier: Amsterdam, p25.

Brasseur, F., Couvreur, P., Kante, B., Deckers-Passau, L., Roland, M., Deckers, C. and Speiser, P. (1980) Eur. J. Cancer, 16, 1441.

Brown, J.C., Pusey, P.N. and Dietz, R. (1975) J. Chem. Phys., 62, 1136.

Chu, B. (1974) "Laser Light Scattering", Academic Press: New York.

Chu, B., Gulari, E. and Gulari, E. (1979) Phys. Scr., 19, 476.

Cikes, M. (1978) Eur. J. Cancer, 14, 211.

Clayfield, E.J. and Lumb, E.C. (1966) J. Colloid Interface Sci., 22, 269.

Collins, J.A., Pani, C., Seidenstein, M., Brandes, G. and Leonard, F. (1969) Surgery, 65, 256.

Coover, Jr., H.W. and McIntire, J.M. (1977) in "Handbook of Adhesives", (I. Skeist, ed.), Van Nostrand Reinhold: New York, p569.

Corrigan, O.I. and Stanley, C.T. (1981) Pharm. Acta Helv., 56, 204

Cotton, F.A. and Wilkinson, G. (1968) "Advanced Inorganic Chemistry" 2nd Edn., John Wiley and Sons: London.

Coulson, A.F.W. and Yonetani, T. (1972) Eur. J. Biochem., 26, 125.

Couvreur, P. (1984) J. Pharm. Belg., 39, 249.

Couvreur, P., Tulkens, P., Roland, M., Trouet, A. and Speiser, P. (1977) FEBS Letters, 84, 149.

Couvreur, P., Kante, B., Roland, M., Guiot, P., Baudhuin, P. and Speiser, P. (1979a) J. Pharm. Pharmacol., 31, 331.

Couvreur, P., Kante, B., Roland, M. and Speiser, P. (1979b) J. Pharm. Sci., 68, 1521.

Couvreur, P., Kante, B., Lenaerts, V., Scailteur, V., Roland, M. and Speiser, P. (1980a) J. Pharm. Sci., 69, 199.

Couvreur, P., Lenaerts, V., Kante, B., Roland, M. and Speiser, P. (1980b) Acta Pharm. Tech., 26, 220.

Couvreur, P., Roland, M. and Speiser, P. (1982a) United States Patent No.4,329,332.

Couvreur, P., Kante, B., Grislain, L., Roland, M. and Speiser, P. (1982b) J. Pharm. Sci., 71, 790.

Couvreur, P., Lenaerts, V., Leyh, D., Guiot, P. and Rowland, M. (1984) in "Microspheres and Drug Therapy", (S.S. Davis, L. Illum, J.G. McVie and E. Tomlinson, eds.), Elsevier: Amsterdam, p103.

Couvreur, P., Lenaerts, V., Grislain, L., Brasseur, F. and Van Snick, L. (1985) in "Targeting of Drugs With Synthetic Systems", (G.

Gregoriadis, A. Trouet, G. Poste and J. Senior, eds.), NATO Advanced Studies Institute Series A, Plenum Press: New York, in press.

Davis, S.S. (1981) Pharm. Tech., May, 71.

Davis, S.S. and Hansrani, P. (1982) in "Radionuclide Imaging in Drug Research", (C.G. Wilson, J.G. Hardy, M. Frier and S.S Davis, eds.), Croom Helm: London, p217.

Davis, S.S. and Hansrani, P. (1985) Int. J. Pharm., 23, 69.

Davis, S.S., Illum, L., McVie, J.G. and Tomlinson, E. (eds.) (1984) "Microspheres and Drug Delivery", Elsevier: Amsterdam.

Davis, S.S., Douglas, S.J., Illum, L., Jones, P.D.E., Mak, E. and Muller, R.H. (1985) in "Targeting of Drugs With Synthetic Systems", (G. Gregoriadis, A. Trouet, G. Poste and J. Senior, eds.), NATO Advanced Studies Institute Series A, Plenum Press: New York, in press.

Derderian, E.J. and MacRury, T.B. (1981) J. Dispersion Sci. Tech., 2, 345.

Dewanjee, M.K., Rao, S.A. and Didisheim, P. (1981) J. Nucl. Med., 22, 981.

Dyer, J.R. (1956) in "Methods of Biochemical Analysis", Vol.III, (D. Glick, ed.), Interscience: New York, p111.

Eckelman, W.C. and Levenson, S.M. (1977) Int. J. Appl. Radiation Isotop., 28, 67.

Eckelman, W.C. and Levenson, S.M. (1978) in "Textbook of Nuclear Medicine: Basic Science", (A. Fernando, G. Rocha and J.C. Harbert, eds.), Lea and Febiger: Philadelphia, p192.

Edman, P., Ekman, B. and Sjoholm, I. (1980) J. Pharm. Sci., 69, 838.

Ehrlich, P. (1906) "Collected Studies on Immunity", Vol.II, Wiley: New York, p442. Through Poste, G. and Kirsh, R. (1983) Biotechnol., 1, 869.

El-Egakey, M.A. and Speiser, P. (1982a) Pharm. Acta Helv., 57, 236

El-Egakey, M.A. and Speiser, P. (1982b) Acta Pharm. Tech., 28, 103

El-Egakey, M.A., Bentele, V. and Kreuter, J. (1983) Int. J. Pharm., 13, 349.

El-Samaligy, M. and Rohdewald, P. (1982) Pharm. Acta. Helv., 57, 201.

Fairbrother, J.E. (1979) Pharm. J., 223, 651 and 662.

Fernando, A., Rocha, G. and Harbert, J.C. (eds.) (1978) "Textbook of Nuclear Medicine: Basic Science", Lea and Febiger: Philadelphia.

Fidler, I.J. (1977) Cancer Res., 34, 1074.

Fidler, I.J., Sone, S., Fogler, W.E. and Barnes, Z.L. (1981) Proc. Natl. Acad. Sci. USA, 78, 1680.

Fidler, I.J., Barnes, Z.L., Fogler, W.E., Kirsh, R., Bugelski, P. and Poste, G. (1982) Cancer Res., 42, 496.

Finar, I.L. (1973) "Organic Chemisrty", Vol. 1. 6th Edn., Longman: London.

Fischer, E.W. (1958) Kolloid Z., 160, 120.

Fitch, R.M. (ed.) (1971) "Polymer Colloids", Plenum: New York.

Fitch, R.M. (1973) Br. Polym. J., 5, 467.

Fitch, R.M. (ed.) (1980) "Polymer Colloids II", Plenum: New York.

Fitzgerald, P. (1985) Pharmacy Dept. Nottingham University. Personal communication.

Fiume, L., Busi, C., Mattioli, A., Balboni, P.G., Barbanti-Bradona, G. and Wieland, Th. (1982) in "Targeting of Drugs", (G. Gregoriadis, J. Senior and A. Trouet, eds.), NATO Advanced Studies Institute Series A, Plenum: New York, p56.

Foster, R.L. (1975) Experientia, 31, 772.

Frier, M. (1981) in "Progress in Pharmacology", Vol. 2, (P.H. Cox, ed.), Elsevier: Amsterdam, p249.

Gigli, I. and Nelson, R.A. (1968) Exp. Cell Res., 51, 45.

Giles, C.H., Smith, D. and Huitson, A. (1974) J. Colloid Interface Sci., 47, 755.

Goldberg, E.P., (ed.) (1983) "Targeted Drugs", John Wiley and Sons: New York.

Goodall, A.R., Randle, K.J. and Wilkinson, M.C. (1980) J. Colloid Interface Sci., 75, 493.

Goodwin, J.W., Hearn, J., Ho, C.C. and Ottewill, R.H. (1973) Br. Polym. J., 5, 347.

Goodwin, J.W., Ottewill, R.H., Pelton, R., Vianello, G. and Yates, D.E. (1978) Br. Polym. J., 10, 173.

Goossens, J.W.S. and Zembrod, A. (1979) Colloid Polym. Sci., 257, 437.

Goossens, J.W.S. and Zembrod, A. (1981) J. Dispersion Sci. Tech., 2, 255.

Graybill, J.R., Cravin, P.C., Taylor, R.L., Williams, D.M. and Magee, W.E. (1982) J. Inf. Dis., 145, 748.

Green, D.J., Sattelle, D.B., Westhead, D.W. and Langley, K.H. (1976) in "Photon Correlation Spectroscopy and Velocimetry", (H.Z. Cummins and E.R. Pike, eds.), NATO Advanced Studies Institute Series B, Plenum: New York, p477.

Gregoriadis, G. (1977) Nature, 265, 407.

Gregoriadis, G. and Allison, A.C. (1980) (eds.) "Liposomes in Biological Systems", John Wiley and Sons: New York.

Gregoriadis, G., Senior, J. and Trouet, A., (eds.) (1982) "Targeting of Drugs", NATO Advanced Studies Institute Series A, Plenum Press: New York.

Gregoriadis, G., Poste, G., Senior, J. and Trouet, A., (eds.) (1985) "Receptor Mediated Targeting of Drugs", NATO Advanced Studies Institute Series A, Plenum Press; New York.

Grislain, L., Couvreur, P., Lenaerts, V., Roland, M., Deprez-Decampeneere, D. and Speiser, P. (1983) Int. J. Pharm., 15, 335.

Gubensek, F. and Lapanje, S. (1967) Biopolymers, 5, 351.

Gubensek, F. and Lapanje, S. (1968) J. Macromol. Sci. Chem., A2, 1045.

Hagan, P.L., Krecarek, G.E., Taylor, A. and Alazraki, N. (1978) J. Nucl. Med., 19, 1055.

Harding, N.G.L. (1971) Annals. New York Acad. Sci., 186, 270.

Hastings, G. (1984) Biomedical Unit, North Staffordshire Polytechnic, Stoke. Personal communication.

Hatch, T. (1933) J. Franklin Inst., 215, 27.

Hatch, T. and Choate, S.P. (1929) J. Franklin Inst., 207, 369.

Hearden, G. (1960) "Small Particle Statistics" 2nd Edn, Butterworths: London.

Hearn, J., Wilkinson, M.C. and Goodall, A.R. (1981) Adv. Colloid Interface Sci., 14, 173.

Heath, T.D., Montgomery, J.A., Piper, J.R. and Papahadjopoulos, D. (1983) Proc. Natl. Acad. Sci. USA, 80, 1377.

Henry, D.C. (1931) Proc. Royal Soc., 133A, 106.

Henze, E., Robinson, G.D., Kuhl, D.E. and Schelbert, H.R. (1982a) J. Nucl. Med., 23, 348.

Henze, E., Schelbert, H.R., Collins, J.D., Najafi, A., Barrio, J.R. and Bennett, L.R. (1982b) J. Nucl. Med., 23, 923.

Hnatowich, D.J. and Clancy, B. (1980) J. Nucl. Med., 21, 662.

Houston, S., Ousterhout, D.K., Sleeman, H. and Leonard, F. (1970) J. Biomed. Mater. Res., 4, 25.

Huh, Y., Donaldson, W. and Johnston, F.J. (1974) Radiation Res., 60, 42.

Hupf, H.B., Wanek, P.M., O'Brien, Jnr., H.A. and Holland, L.M. (1978) J. Nucl. Med., 19, 525.

Hwang, K.J. (1978) J. Nucl. Med., 19, 1162.

Ibrahim, A., Couvreur, P., Roland, M. and Speiser, P. (1983) J. Pharm. Pharmacol., 35, 59.

Illum, L. (1984) Royal Danish School of Pharmacy, Copenhagen, Denmark. Personal communication.

Illum, L. and Davis, S.S. (1982a) J. Parenteral Sci. Tech., 36, 242.

Illum, L. and Davis, S.S. (1982b) Int. J. Pharm., 11, 323.

Illum, L. and Davis, S.S. (1984a) FEBS Letters, 167, 79.

Illum, L. and Davis, S.S. (1984b) Proc. Second European Congress on Biopharmaceuticals and Pharmacokinetics, Salamaca, Spain, Vol.II, p97.

Illum, L. and Jones, P.D.E. (1985) in "Methods in Enzymology", in press.

Illum, L., Davis, S.S., Wilson, C.G., Thomas, N.W., Frier, M. and Hardy, J.G. (1982) Int. J. Pharm., 12, 135.

Illum, L., Jones, P.D.E., Kreuter, J., Baldwin, R.W. and Davis, S.S. (1983) Int. J. Pharm., 17, 65.

Illum, L., Jones, P.D.E., Baldwin, R.W. and Davis, S.S. (1984) J. Exp. Ther. Pharmacol., 230, 733.

Ishak, M.F. and Painter, T.J. (1978) Carbohydrate Res., 64, 189.

James, A.M. (1980) in "Surface and Colloid Science", Vol. 11, (R.J. Good and R.R Stromberg, eds.), John Wiley and Sons: New York, p121.

Jansen, F.K., Blythman, H.E., Carriere, D., Casellas, P., Gros, O., Gros, P., Laurent, J.C., Paolucci, F., Pau, B., Poncelet, P., Richer, G., Vidal, H. and Voisin, G.A. (1982) Immunol. Rev., 62, 186.

Juliano, R.L. (ed.) (1980) "Drug Delivery Systems. Characteristics and Biomedical Applications", Oxford University Press: New York.

Juliano, R.L. and Stamp, D. (1975) Biochem. Biophys. Res. Comm., 63, 651.

Kabalka, G.W., Gooch, E.E. and Sastry, K.A.R. (1981) J. Nucl. Med., 22, 908.

Kandzia, J., Anderson, M.J.D. and Muller-Ruchholtz, W. (1981) J. Cancer Res. Clin. Oncol., 101, 165.

Kanke, M., Simmons, G.H., Weiss, D.L., Bivins, B.A. and De Luca, P.P. (1980) J. Pharm. Sci., 69, 755.

Kante B., Couvreur, P., Lenaerts, V., Guiot, P., Roland, M., Baudhuin, P. and Speiser, P. (1980) Int. J. Pharm., 7, 45.

Kante, B., Couvreur, P., Dubois-Krack, G., De Meester, C., Guiot, P., Roland, M., Mercier, M. and Speiser, P. (1982) J. Pharm. Sci., 71, 786.

Kaplan, M.R., Calif, E., Bercovici, T. and Gitler, C. (1983) Biochim. Biophys. Acta, 728, 112.

Kato, T., Nemeto, R., Mori, H., Unno, K., Goto, A., Harada, M. and Homma, M. (1979) Proc. Jap. Acad., 55(B), 470.

Kato, T., Nemeto, R., Mori, H. and Kumagai, I. (1980) Cancer, 46, 14.

Kelly, J.D. (1982) in "Radionuclide Imaging in Drug Research", (C.G. Wilson, J.G. Hardy, M. Frier and S.S. Davis, eds.), Croom Helm: London, p39.

Kitao, T. and Hattori, K. (1977) Nature, 265, 81.

Kohler, G. and Milstein, C. (1975) Nature, 256, 495.

Koppel, D.E. (1972) J. Chem. Phys., 57, 4814.

Kramer, P.A. (1974) J. Pharm. Sci., 63, 1646.

Kreuter, J. (1983a) Pharm. Acta Helv., 58, 196.

Kreuter, J. (1983b) Pharm. Acta Helv., 58, 217.

Kreuter, J. (1983c) Pharm. Acta Helv., 58, 242.

Kreuter, J. (1983d) Int. J. Pharm., 14, 43.

Kreuter, J. (1984) ETH, Zurich, Switzerland. Personal communication.

Kreuter, J. and Hartmann, H.R. (1983) Oncology, 40, 363.

Kreuter, J., Mills, S.N., Davis, S.S. and Wilson, C.G. (1983) Int. J. Pharm., 16, 105.

Kulkarni, P.N., Blair, P.H. and Ghose, T. (1981) Fed. Proc., 40, 642.

Lamberts, J.J.M. and Neckers, D.C. (1983) J. Am. Chem. Soc., 105, 7465.

Langone, J.J. (1982) Adv. Immunol., 32, 158.

Latif, Z.A., Lozzio, B.B., Wust, C.J., Krauss, S., Aggio, M.C. and Lozzio, C.B. (1980) Cancer, 45, 1326.

Lenaerts, V., Nagelkerke, J.F., Van Berkel, T.J.C., Couvreur, P., Grislain, L., Roland, M. and Speiser, P. (1982) in "Sinusoidal Liver Cells", (D.L. Knook and E. Wisse, eds.), Elsevier Biomedical Press: Amsterdam, p259.

Lenaerts, V., Couvreur, P., Christiaens-Leyh, D., Joiris, E., Roland, M., Rollman, B. and Speiser, P. (1984a) Biomaterials, 5, 65.

Lenaerts, V., Nagelkerke, J.F., Van Berkel, T.J.C., Couvreur, P., Grislain, L., Roalnd, M. and Speiser, P. (1984b) J. Pharm. Sci., 73, 980.

Leonard, F., Kulkarni, R.K., Brandes G., Nelson, J. and Cameron, J.J. (1966) J. Appl. Polym. Sci., 10, 259.

Leonard, F., Kulkarni, R.K. and Nelson, J. (1967) J. Biomed. Mater. Res., 1, 3.

Leu, D., Manthey, B., Kreuter, J., Speiser, P. and DeLuca, P. (1984) J. Pharm. Sci., 73, 1433.

Lindberg, B., Lote, K. and Teder, H. (1984) in "Microspheres and Drug Therapy", (S.S. Davis, L. Illum, J.G. McVie and E. Tomlinson, eds.), Elsevier: Amsterdam, p153.

Longo, W.E., Iwata, H., Lindheimer, T.A. and Goldberg, E.P. (1982) J. Pharm. Sci., 71, 1323.

Lopez-Berestein, G., Mehta, R., Hopfer, R.L., Mills, K., Kasi, L., Mehta, K., Fainstein, V., Luna, M., Hersh, E.M. and Juliano, R.L. (1983) J. Inf. Dis., 147, 939.

Mackor, E.L. (1951) J. Colloid Interface Sci., 6, 492.

Maincent, P. (1982) "Etude Pharmococinetique et Biopharmaceutique de Vecteurs Lysosomotropes Chez L'Animal", PhD Thesis, University Paris-Sud, Paris.

Manabe, Y., Tsubota, T., Haruta, Y., Kataoka, K., Okazaki, M., Haisa, S., Nakamura, K. and Kimura, I. (1984) J. Lab. Clin. Med., 104, 445.

Margel, S., Zisblatt, S. and Rembaum, A. (1979) J. Immunol. Methods, 28, 341.

Margel, S., Beitler, V. and Ofarim, M. (1982) J. Cell Sci., 56, 157.

McAfee, J.G. and Subramanian, G. (1969) in "Clinical Scintillation Snanning", (L.M. Freeman and P.M. Johnson, eds.), Hoeber and Row: New York, p50.

McConnell, M.L. (1981) Anal. Chem., 53, 1007A.

Meier, D.J. (1967) J. Phys. Chem., 71, 1861.

Midoux, P., Maillet, T., Therain, F., Monsigny, M. and Roche, A.C. (1984) Cancer Immunol. Immunother., 18, 19.

Millar, I.T. and Springall, B. (1966) in "The Organic Chemistry of Nitrogen", (N.V. Sidgwick, ed.), Clarendon Press: Oxford, p252.

Molday, R.S., Dreyer, W.J., Rembaum, A. and Yen, S.P.S. (1975) J. Cell Biol., 64, 75.

Mori, S., Ota, K., Takada, M. and Inou, T. (1967) J. Biomed. Mater. Res., 1, 55.

Morimoto, Y., Sugibayashi, K., Okumura, M. and Kato, Y. (1981) J. Pharm. Dyn., 4, 624.

Muirhead, M., Martin, P.J., Torok-Storb, B., Uhr, J.W. and Vifetta, S. (1983) Blood, 62, 327.

Munro, D. and Randle, J. (1976) in "Photon Correlation Spectroscopy and Velocimetry", NATO Advanced Studies Institute Series B, Plenum: New York, p537.

Napper, D.H. (1968) Trans. Faraday Soc., 64, 170.

Napper, D.H. (1977) J. Colloid Interface Sci., 58, 390.

Napper, D.H. (1982) in "Colloidal Dispersions", (J.W. Goodwin, ed.), Royal Society of Chemistry: London, p105.

Napper, D.H. and Netschey, A. (1971) J. Colloid Interface Sci., 137, 528.

Nuhn, P. and Schilling, E. (1975) Pharmazie, 30, 593.

Oppenheim, R.C. (1981) Int. J. Pharm., 8, 217.

Ottewill, R.H. (1967) in "Nonionic Surfactants", (M.J. Schick, ed.), Marcel Dekker: New York, p627.

Ottewill, R.H. and Walker, T. (1968) Kolloid-Z.Z. Polym., 227, 108.

Patel, R.P., Lopiekes, D.V., Brown, S.P. and Price, S. (1967) Biopolymers, 5, 577.

Pearce, A.J. (1984) "A Kinetic Study of Emulsion Coalescence", PhD Thesis, University of Nottingham, Nottingham.

Pechiney Ugine Kuhlmann Ltd., "Pluronic Polyols Toxicity and Irritation Data", (manufacturers publication), Pechiney Ugine Kuhlmann: Paris.

Peterson, H.I. (ed.) (1979) "Tumour Blood Circulation", CRC: Boca Raton.

Pimm, M.V., Jones, J.A., Price, M.R., Middle, J.G., Embleton, M.J. and Baldwin, R.W. (1982) Cancer Immunonol. Immunother., 12, 125.

Pitt, W.R. and Sharp, P.F. (1981) Phys. Med. Biol., 26, 693.

Poste, G. (1983) Biol. Cell, 47, 19.

Poste, G. (1985) in "Receptor Mediated Targeting of Drugs", (G. Gregoriadis, G. Poste, J. Senior and A. Trouet, eds.), NATO Advanced Studies Institute Series A, Plenum: New York, p427.

Poste, G. and Kirsh, R. (1983) Biotechnol., 1, 869.

Poste, G., Bucana, C. and Fidler, I.J. (1982) in "Targeting of Drugs", (G. Gregoriadis, J. Senior and A. Trouet, eds.), NATO Advanced Studies Institute Series A, Plenum: New York, p256.

Pouton, C.W. (1985) J. Clin. Hosp. Pharm., 10, 45.

Preece, A.W. and Luckman, N.P. (1981) Phys. Med. Biol., 26, 11.

Price, L.A., Hill, B.T. and Ghilchick, M.W. (eds.) (1981) "Safer Cancer Chemotherapy", Bailliere Tindall: London.

Profitt, R.T., Williams, L.E., Presant, C.A., Tin, G.W., Uliana, J.A., Gamble, R.C. and Baldeschwieler, J.D. (1983) Science, 220, 502.

Pusey, P.N., Koppel, D.E., Schaeffer, D.W., Camerini-Otero, R.D. and Koenig, S.H. (1974) Biochemistry, 13, 952.

Pusey, P.N. (1982) in "Colloidal Dispersions", (J.W. Goodwin, ed.), Royal Chemical Society: London, p129.

Rankin, J.C. and Jeanes, A. (1954) J. Am. Chem. Soc., 76, 4435.

Ratcliffe, J.H., Hunneyball, I.M., Smith, A., Wilson, C.G. and Davis, S.S. (1984) J. Pharm. Pharmacol., 36, 431.

Rembaum, A., Yen, S.P.S. and Holday, R.S. (1979) Macromol. Sci. Chem., A13, 603.

Richardson, V.J., Jeyasingh, K., Jewkes, R.F., Ryman, B.E. and Tattersale, M.N.H. (1978) J. Nucl. Med., 19, 1049.

Ringsdorf, H. (1975) J. Polym. Sci., 51, 135.

Roberts, J.D. and Caserio, M.C. (1977) "Basic Principles of Organic Chemistry", 2nd Edn., Benjamint New Yoyk.

Roe, J.M. and Barry, B.W. (1983) Int. J. Pharm., 14, 159.

Roerdink, F., Wassef, N.M., Richardson, E.C. and Alving, C.R. (1983) Biochim. Biophys. Acta, 734, 33.

Rooney, J. M. (1981) Br. Polym. J., 13, 160.

Rowland, G.F. (1977) Europ. J. Cancer, 13, 593.

Russell, G.F.J. (1983) Pharm. Int., 4, 260.

Saba, T.M. (1970) Arch. Intern. Med., 126, 1031.

Sato, T. (1971) J. Appl. Polym. Sci., 15, 1053.

Sato, T. and Ruch, R. (1980) "Stabilisation of Colloidal Dipsersions by Polymer Adsorption", Marcel Dekker: New York.

Scheider, Y.J., Abarca, J., Aboud-Pirak, E., Baurain, R., Ceulemans, F., Deprez-DeCampeneere, D., Lesur, B., Masquelier, M., Otte-Slachmuylder, C., Rolin van Swieten, D. and Trouet, A. (1985) in "Receptor Mediated Targeting of Drugs", (G. Gregoriadis, G. Poste, J. Senior and A. Trouet, eds.), NATO Advanced Studies Institute Series A, Plenum: New York, p42.

Scherphof, G., Roerdink, E., Waite, M. and Parks, J. (1978) Biochim. Biophys. Acta, 542, 29.

Schmeissner, H. (1970) Dtsch. Zahnaerztl. Z., 25, 907.

Schmolka, I.R. (1967) in "Nonionic Surfactants", (M.J. Schick ed.), Marcel Dekker: New York, p300.

Schneinberg, D.A. and Strand, M. (1982) Cancer Res., 42, 44.

Senior, J. and Gregoriadis, G. (1982) FEBS Letters, 145, 109.

Senior, J., Crawley, J.C.W. and Gregoriadis, G. (1985) Biochim. Biophys. Acta, 839, 1.

Sezaki, H. and Hashida, M. (1985) CRC Critical Rev. Ther. Drug Carrier Systems, 1, 1.

Shaw, D.J. (1969) "Electrophoresis", Academic Press: London.

Shaw, D.J. (1970) "Introduction to Colloid and Surface Chemistry", Butterworths: London.

Sikora, K., Smedley, H. and Thorpe, P. (1984) Brit. Med. Bull., 40, 233.

Singer, J.M., Adlersberg, L., Hoenig, E.M., Ende, E. and Tchorsch, Y. (1969) J. Reticuloendothelial Soc., 6, 561.

Slack, J.D., Kanke, M., Simmons, G.H. and DeLuca, P.P. (1981) J. Pharm. Sci., 70, 660.

Sloan, J.W., Alexander, B.H., Lohmar, R.L., Wolff, I.A. and Rist, C.E. (1954) J. Am. Chem. Soc., 76, 4429.

Stang, L.G. and Richards, P. (1964) Nucleonics, 22, 46.

Stella, V.J., Mikkelson, T.J. and Pipkin, J.D. (1980) in "Drug Delivery Systems", (R.L. Juliano, ed.), Oxford University Press: New York, p112.

Stossel, T.P., Mason, R.J., Hartwig, J. and Vaughan, M. (1972) J. Clin. Invest., 51, 615.

Szejtli, J. (1982) "Cyclodextrins and Their Inclusion Complexes", Akademiai Kiado: Budapest.

Szoka, F.C. and Papahadjopoulos, D. (1980) Ann. Rev. Biophys. Bioeng., 9, 465.

Tatum, H.J. (1977) Fertil. Steril., 28, 3.

Taylor, R.L., Williams, D.M., Craven, P.C., Graybill, J.R., Drutz, D.J. and Magee, W.E. (1982) Am. Rev. Respir. Dis. , 125, 610.

Thakur, M.L. (1977) Int. J. Appl. Radiation Isotop., 28, 183.

Tomlinson, E. (1983) Int. J. Pharm. Tech. Prod. Mfr., 4, 49.

Tomlinson, E., Burger, J.J., Schoonderwoerd, E.M.A. and McVie, J.G. (1984) in "Microspheres and Drug Therepy", (S.S. Davis, L. Illum, J.G. McVie and E. Tomlinson, eds.), Elsevier: Amsterdam, p75.

Trouet, A., Masquelier, M., Baurain, R. and Deprez-DeCampaneere, D. (1981) Proc. Natl. Acad. Sci. USA, 79, 626.

Trouet, A., Baurain, R., Deprez-DeCampaneere, D., Masquelier, M. and Pirson, P. (1982) in "Targeting of Drugs", (G. Gregoriadis, J.

Senior and A. Trouet, eds.), NATO Advanced Studies Institute Series A, Plenum Press: New York, p207.

Van Oss, C.J. (1978) Ann. Rev. Microbiol., 32, 19.

Van Snick, L., Couvreur, P., Christiaens-Leyh, D. and Speiser, P. (1985) Pharm. Res., 1, 36.

Vezin, W.R. and Florence, A.T. (1978) J. Pharm. Pharmacol., 30, 5P.

Vezin, W.R. and Florence, A.T. (1980) J. Biomed. Mater. Res., 14, 93.

Vincent, B. (1974) Adv. Colloid Interface Sci., 4, 193.

Wade, C.W.R. and Leonard, F. (1972) J. Biomed. Mater. Res., 6, 215.

Walbridge D.J. (1975) in "Dispersion Polymerisation in Organic Media", (K.E.J. Barrett, ed.), John Wiley and Sons: London, p45.

Weinstein, J.N. and Leserman, L.D. (1984) Pharmac. Ther., 24, 207.

Weinstein, J.N., Magin, R.L., Cysyk, R.L. and Zaharko, D.S. (1980) Cancer Res., 40, 1388.

Weiss, L. and Greep, R.O. (eds.) (1977) "Histology", McGraw-Hill: New York.

Widder, K.J. and Senyei, A.E. (1983) Pharmac. Ther., 20, 377.

Widder, K.J., Senyei, A.E. and Scarpelli, D.G. (1978) Proc. Soc. Expl. Biol. Med., 158, 141.

Widder, K.J., Senyei, A.E. and Ranney, D.F. (1979) Adv. Pharmacol. Chemotherap., 16, 213.

Widder, K.J., Morris, R.M., Poore, G., Howard, Jnr., D.P. and Senyei, A.E. (1981) Proc Natl. Acad. Sci. USA, 78, 579.

Widder, K.J., Senyei, A.E. and Sears, B. (1982) J. Pharm. Sci., 71, 379.

Widder, K.J., Marino, P.A., Morris, R.M., Howard, D.P., Poore, G.A. and Senyei, A.E. (1983) Eur. J. Cancer Clin. Oncol., 19, 141.

Wilkins, D.J. and Meyers, P.A. (1966) Br. J. Exp. Path., 47, 568.

Wilson, C.G., Hardy, J.G., Frier, M. and Davis, S.S. (eds.) (1982) "Radionuclide Imaging in Drug Research", Croom Helm: London.

Yapel, Jnr., A.F. (1979) United States Patent No. 4,147,767.

Yatvin, M.B., Krentz, W., Horwitz, B.A. and Shinitzky, M. (1980) Science, 210, 1253.

Yatvin, M.B., Cree, T.C., Tegmo-Larsson, I.M. and Gipp, J.J. (1984) Stralentherapie, 160, 732.

Yen, S.P.S., Rembaum, A., Molday, R.W. and Dreyer, W.J. (1976) in "Emulsion Polymerisation", (I. Piirma and J.L. Gardon, eds.), ACS Symposium Series 24, American Chemical Society: Washington DC, p236.

Yoshioka, T., Hashida, M., Muranishi, S. and Sezaki, H. (1981) Int. J. Pharm., 81, 131.

Zimmerman, U. (1983) in "Targeted Drugs", (E.P. Goldberg, ed.), John Wiley and Sons: New York, p153.